Universidad
Carlos III de Madrid
www.uc3m.es

DOCTORAL THESIS

DESIGN STRATEGIES FOR ELECTRICALLY SMALL ANTENNAS, ACTIVELY MATCHED WITH NON-FOSTER ELEMENTS

Author:

Luis Fernando Albarracín-Vargas

Advisor:

Daniel Segovia Vargas

DEPARTMENT OF SIGNAL THEORY AND COMMUNICATIONS

Leganés, July 18th of 2017

DOCTORAL THESIS

DESIGN STRATEGIES FOR ELECTRICALLY SMALL ANTENNAS, ACTIVELY MATCHED WITH NON-FOSTER ELEMENTS

Author: **Luis Fernando Albarracín-Vargas**

Advisor: **Dr. Daniel Segovia-Vargas**

Firma del Tribunal Calificador:

Firma

Presidente:	Prof. Miloš Mazánek
Secretario:	Prof. Luis Enrique García-Muñoz
Vocal:	Prof. Marco A. Antoniades

Calificación:

Leganés, July 18th of 2017

A mi familia.

La vida no es la que uno vivió,
sino la que uno recuerda,
y cómo la recuerda para contarla.

What matters in life is not what happens to you
but what you remember and how you remember it.

Gabriel García-Márquez

CONTENTS

AGRADECIMIENTOS / ACKNOWLEDGEMENTS

Un muy especial agradecimiento a mi tutor y amigo, Dani Segovia, quien más que un profesor y director de tesis, ha sido un sólido apoyo en esta etapa de mi vida. Agradezco inmensamente la confianza que ha depositado en mí desde el primer día, cuando nos reunimos por primera vez en un breve paso suyo por Colombia. Es enriquecedor el conocer personas tan humanas. Agradezco también a todo el equipo docente del GREMA: LuisE, Quique, Sergio Ll., Alex G., Magdalena y Vicente, un consejo o una corrección a tiempo no tienen precio.

A mis primeros compañeros de laboratorio y amigos, el GRF-auténtico: Iván el compañero de cañas de viernes que todo lo puede fabricar; Edu el *strummeador* más inteligente que haya conocido, y mi aconsejador oficial; Javi Montero, un caballero en toda regla y el ariete del GRF en las lides de la conquista; Javi Herraiz, el superviviente de los mil "garitos;" Nachete, la autoridad de la tecnología en el lab; Adri, el tipo que más fiesta resiste sin una gota de licor; Álex, el "manitas" del equipo; y Rubén, una persona en toda regla, noble y afable como ninguno. ¡Cuántos momentazos!; ¡cuántas anécdotas entre etiles y sin ellos!; ¡cuántas risas y ocurrencias dentro y fuera del lab!; ¡cuánto espíritu URSI...!; ¡cuánta felicidad...! Inolvidable.

A la nueva sangre, la del GREMA: Gabri Galindo, Gabri "el pana," Jose, Ana, Sergio, y Kerlos (thank you, man! for all the good memories

playing football and the delicious food). Imposible olvidar los momentos *team building* CS.1.6, que hicieron del lab un espacio más alegre. Jose *in the roof*; Sergio SMA3.5; las ocurrencias de Gabri G.; los gatos y los postres de Ana; los papers *state of the art* de todo tipo que leía "el pana;" las frases "célebres" de todos apuntadas en la pared... Hay que tener mucha suerte para coincidir, en un mismo espacio, y a lo largo de una misma empresa, con dos grupos de trabajo que te hagan la vida tan alegre.

Quisiera extender el agradecimiento a aquellas personas que hicieron amena mi estancia en España, en todo sentido. A esos compañeros de Máster con quienes compartí experiencias de inmigrante: nostalgias, temores, dudas, cañas (cervezas), etc. A esos compatriotas emigrados a quienes a lo largo de estos años he conocido y reconocido como familia: Henry, Andrés Z., Doña Orfa, Ricardo, Juan Camilo. Todo cuanto viví junto a ellos: los viajes, los paseos, la comida, la fiesta y demás momentos, hacen parte de las huellas imborrables que llevo conmigo.

I would like to thank the *Parceros de Madrid* group, with whom I shared so many adventures, beers and other stunning moments across this time in Spain. Wherever you guys are right now, see you next time!

Y por supuesto, agradezco a mis amigos en Colombia, los de toda la vida, los que un día me dijeron: "vete a España, allí estarás bien, lejos, pero bien; ¡vive! que ya nos contarás lo que viviste." Sergio Manuel, Fabio, Manolo, Mónica, Diego, Chuis, Iván, Julián, Sergio, y otros, que se me quedan sin nombrar.

Finalmente, mi familia, sin ellos nada hubiera sido posible: Rita, Orlando y Duván, incansables y pacientes como nadie, ¡gracias! Al igual que mi novia, Francia, quien me ha soportado con amor todo este tiempo, y con quien comparto felizmente mi vida y mi corazón.

Hacer una tesis doctoral no te hace mejor persona, sin embargo, conocer personas valiosas en el camino te permite dar un paso más para serlo.

Fernando

RESUMEN

Durante los últimos años, algunos investigadores han venido trabajando en la inclusión de redes de adaptación tipo non-Foster en antenas eléctricamente pequeñas (*Electrically Small Antennas*, ESA). Esto en respuesta a la creciente demanda de dispositivos compactos, que funcionen a diferentes bandas de frecuencia, como parte de los modernos sistemas y plataformas multibanda. La consecución de sistemas compactos y de banda ancha, así como la obtención de múltiples frecuencias de trabajo han sido uno de los objetivos primarios de la presente tesis doctoral. La inclusión de estructuras non-Foster, que reciben éste nombre debido a que no obedecen a las propiedades establecidas por el teorema de R. M. Foster en 1924, permite el ensanchamiento de la banda de adaptación de impedancia o la obtención de una banda adicional para una misma estructura radiante. Dentro de los circuitos más representativos de las redes non-Foster se encuentran los Convertidores de Impedancia Negativa (*Negative Impedance Converter*, NIC), comúnmente implementados con transistores, a través de los cuales es posible la implementación de inductores o de condensadores "negativos". La realización de una impedancia "negativa"por medio de un NIC, es de vital importancia en la adaptación de la impedancia de antena en banda ancha que se busca en este trabajo.

En este sentido, se hace necesario establecer una metodología de diseño de este tipo de antenas, que tenga en cuenta los parámetros de funcionamiento inherentes a un elemento radiante, como son: eficiencia

y diagrama de radiación, adaptación de impedancias, factibilidad y estabilidad. Esto, a través del análisis de la sensibilidad a la ubicación de puertos (propuesto en este proyecto), análisis de estabilidad del sistema completo (antena y red de adaptación activa), análisis de distribución de corrientes etc., hace que la estrategia de diseño que se pretende desarrollar y describir pueda resultar una herramienta realmente útil en el diseño de las mencionadas antenas.

El parámetro de sensibilidad, *Sens*, introducido en este trabajo, otorga al diseñador un criterio de selección cuantitativo con respecto a qué tipo de antena puede, en efecto, ser adaptada con elementos non-Foster y la posición misma de éstos dentro de la estructura. De este modo, el parámetro *Sens* constituye una herramienta de optimización del desempeño del sistema radiante diseñado. Adicionalmente, cabe mencionar que la metodología de diseño propuesta y desarrollada en esta tesis puede ser aplicada a cualquier tipo de antena, sin importar su naturaleza ni su tamaño en términos eléctricos.

Luego de desarrollada y descrita la metodología —estrategia— de diseño, se presentan dos antenas eléctricamente pequeñas a manera de ejemplos de diseño. La primera consiste en un semilazo impreso sobre un dieléctrico, resonante a 1200 MHz, cargado con un NIC compuesto de transistores MOSFET. Como resultado, se obtiene una nueva banda de trabajo cuyo ancho de banda de adaptación relativo (FBW) es de 119 % (centrado en 117 MHz). La segunda antena ejemplo consiste en un monopolo ensanchado, tipo aleta (*blade-monopole*), en cuya estructura es embebida una red de adaptación activa, basada también en transistores MOSFET. En este segundo caso, se obtuvo una banda adicional con un FBW de 82 % (centrado en 85 MHz). Los notables resultados en términos de adaptación de impedancia y de nivel de miniaturización de las estructuras radiantes, alentaron al autor a continuar con la búsqueda de alternativas de solución a los cambios en el diagrama de radiación observados y a el nivel de ruido adicionado por la red activa embebida. Finalmente, la estrategia de diseño descrita es aplicada a arreglos (*arrays*) de antenas de pocos elementos, en busca de obtener un comportamiento multibanda en el que la banda incluida comprenda frecuencias a las que toda la estructura es eléctricamente pequeña.

ABSTRACT

During the last years, some researchers have been working on active matching or on non-Foster matching networks for electrically small antennas (ESAs), in response to the vertiginous increase in demand for compact devices working in multiband platforms. The inclusion of non-Foster networks allows broad bandwidths at lower frequencies, overcoming the inherent limitations derived from the high-quality factor (Q) property of ESAs. Thus, the development of multiband antennas with an engineered lower broadband obtained by embedding an active non-Foster matching network (MN) is one of the primary objectives addressed in this work. Such non-Foster MNs are implemented by using Negative Impedance Converters (NICs), introduced many years ago to realize negative capacitors or negative inductors that disobey the Foster's reactance theorem.

In this sense, an integral design methodology of actively matched ESAs with embedded non-Foster elements is proposed and developed. This design method takes into account the operating parameters inherent to a radiating element, such as efficiency and radiation pattern, impedance matching, realizability, and stability. A new parameter (called *Sens*) on the sensitivity of the ESA when loaded with a non-Foster form is introduced. This sensitivity analysis will allow us to choose not only the kind of antennas that can be properly matched with non-Foster networks but also the most suitable position of such networks into the antenna structure, in order to optimize the performance of the design.

The design methodology can be easily extended to any type of antenna, disregarding its electrical size.

Two electrically small antennas are presented as design examples in which the proposed design strategy is applied. First, a printed small semiloop antenna, which is resonant at 1200 MHz, is loaded with an embedded MOSFET-based NIC, resulting in a new lower-band with a fractional bandwidth (FBW) of 119% (centered at 117 MHz). Second, a blade-type monopole, whose resonant frequency is around 300 MHz, is loaded with an embedded non-Foster MN, resulting in a new working band whose FBW of 82% (centered at 85 MHz). The notable results in terms of impedance bandwidth and miniaturization level encouraged us to keep seeking for solutions for radiation pattern changes and added noise issues. Finally, the proposed design strategy is applied to few-element antenna arrays to obtain a multiband performance, keeping unchanged the natural response of the host structure (i.e. around its resonant frequency).

LIST OF TERMS

2D	Two-Dimensional
3D	Three-Dimensional
ADC	Analog to Digital Converter
AM	Amplitude Modulation
ATC	Air Traffic Control
AUT	Antenna Under Test
AWR	Applied Wave Research
BJT	Bipolar Junction Transistors
BMAA	Biomimetic Antenna Array
BWIF	Bandwidth Improvement Factor
BWv	Impedance Bandwidth related to a certain VSWR
CAD	Computer-Aided Design
CPU	Central Processing Unit
CRLH	Composite Right-and-Left-Handed
CST	Computer Simulation Technology

DAC	Digital to Analog Converter
dB	Decibels
dBi	Decibels relative to an isotropic radiator
DC	Direct Current
DRA	Dielectric Resonator Antennas
DUT	Device Under Test
EDA	Electronic Design Automation
EM	electromagnetic
ENR	Excess Noise Ratio
ESA	Electrically Small Antenna
F	Noise Factor
F/B	Front-to-Back ratio
FBW	Fractional Bandwidth
FET	Field Effect Transistor
FM	Frequency Modulation
FNBW	First Null Beamwidth
FR4	Composite material: "Fire Retardant" fiber-glass epoxy.
FSA	Functionally Small Antenna
FW	Fast Wave Propagation
GPS	Global Positioning System
GREMA	Radiofrequency, Electromagnetics, Microwaves & Antennas' Group
HF	High Frequency
HPBW	Half Power Beamwidth
HPC	High-Performance Computing
IEEE	Institute of Electrical and Electronics Engineers
LF	Low Frequency
LH	Left-Handed
LHP	Left Half-Plane
LNA	Low Noise Amplifier

MANA	Miniaturization of Airborne Antennas Project
MEMS	Micro-electromechanical Systems
MMIC	Monolithic Microwave Integrated Circuits
MN	Matching Network
MOSFET	Metal-Oxide-Semiconductor Field Effect Transistor
NDF	Normalized Determinant Function
NDR	Negative Differential Resistance
NF	Noise Figure
NFA	Noise Figure Analyzers
NFC	Non-Foster Circuits
NFRP	Near-Field Resonant Parasitic
NGD	Negative Group Delay
NIC	Negative Impedance Converter
NII	Negative Impedance Inverter
OATS	Open-Area Test Site
OCS	Open Circuit Stable
op-amp	Operational Amplifiers
PC	Personal Computers
PCB	Printed Circuit Board
PCSA	Physically Constrained Small Antenna
PIFA	Planar Inverted-F Antenna
PIN	Positive-Intrinsic-Negative Semiconductor
PSA	Physically Small Antenna
QMUL	Queen Mary University of London
RF	Radio Frequency
RFID	Radio Frequency Identification
RH	Right-Handed
RHP	Right Half-Plane
RL	Return Loss
RR	Return Ratio
RSS	Root of the Sum of Squares

RTD	Resonant-Tunneling Diodes
SA	Spectrum Analyzer
SCS	Short Circuit Stable
Sens	Sensitivity Parameter
SEP	Scan Element Pattern
SINR	Signal to Interference plus Noise Ratio
SLL	Side-Lobe Levels
SMD	Surface Mount Device
SMMW	Submillimeter Wave
SMR	Surface Movement Radar
SNR	Signal to Noise Ratio
TE	Transverse Electric
TETRA	Terrestrial Trunked Radio
THz	Terahertz
TL	Transmission Line
TM	Transverse Magnetic
UHF	Ultra High Frequency
VHF	Very High Frequency
VLF	Very Low Frequency
VNA	Vector Network Analyzer
VSWR	Voltage Standing Wave Ratio

PREFACE

Over the last years, there has been a continuous and vertiginous increase in demand for compact devices for different systems and wireless platforms such as mobile communications, vehicle navigation, and aeronautical applications, among others. This fact has encouraged the Radiofrequency, Electromagnetics, Microwaves & Antennas' Group (GREMA) to seek to transfer its acquired knowledge and expertise to alternative designs involving antennas and subsystems, active or passive ones, operating in a versatile and compact way. Likewise, GREMA has been committed to the development and implementation of new design techniques and devices for wireless communication systems, for instance in the microwave-band. Some of these devices operate in such a way they can be cataloged as metamaterials, or devices with an alternative behavior, which assure values of equivalent parameters (impedance, permittivity, or permeability) that are not present in nature.

In this way, and as a result of uninterrupted work, some Ph.D. dissertations have been developed, as they are:

- F.J. Herraiz-Martínez, "Metamaterial-Loaded Printed Antennas: Design and Applications" Ph.D. dissertation, Carlos III University, March, 2010.
- O.A. García-Pérez, "Contributions to the Development of Microwave Active Circuits: Metamaterial Dual-Band Active Filters

and Broadband Differential Low-Noise Amplifiers", Ph.D. dissertation, Carlos III University, June, 2011.

- D. De-Castro-Galán, "Aplicación de Metamateriales para el Desarrollo de Antenas Activas Autodiplexadas/Applied Metamaterials for the Development of Active and Self-Diplexing Antennas", Ph.D. dissertation, Carlos III University, June, 2014.
- E. Ugarte-Muñoz, "New Techniques for Improving Gain and Directivity Capabilities in Metamaterial Inspired Antennas and Circuits", Unpublished Ph.D. dissertation, Carlos III University.

In the first dissertation, the application to antennas of passive printed metamaterial structures is presented to improve their performance regarding bandwidth, while different radiation modes are achieved. In the second one, some new active circuit topologies are investigated, using metamaterial structures in interaction with active circuits, to develop dual-band active filters and active antenna arrays. In the third one, it was explored the bidirectional performance in wireless systems including active antennas. It was, therefore, necessary to implement the diplexing feature, either externally or within the radiating element itself. For carrying out such a feature, passive metamaterial structures were used, particularly Composite Right-and-Left-Handed (CRLH) lines, as well as resistive equalization in the amplifying stage of the active antenna, in order to obtain a flat gain response over the frequency band of design. In the fourth Ph.D. dissertation, it was investigated how to develop active metamaterial structures to mitigate the narrow-band response, characteristic of passive metamaterial structures, through the analysis and development of the Negative Impedance Converters (NIC) circuits. NICs are the most representative non-Foster networks (i.e. elements/devices that do not obey Foster's reactance theorem) developed in the literature.

Along with the development of the dissertations mentioned earlier, the GREMA group has become involved in several research projects, among which the Miniaturization of Airborne Antennas Project (MANA), granted by the Spanish Ministry under project RTC-2014-2380-4, has been part of the supporting funds, and one of the motivations for carrying out the presented work. The goal of MANA project is to design and develop a new miniaturized multi-band VHF/UHF (30-88

MHz, 225-400 MHz) airborne antenna of 22.5 cm in height. Thus, an important miniaturization level, in comparison to the typical commercial antennas for the same application, is required since the intended antenna shall be nearly 50% shorter than its commercial counterparts. Project specifications include radio-electrical, mechanical and environmental requirements that comprise challenging tasks, typically related to an industry that has greatly contributed to antenna technology.

This thesis aims at continuing the line of work mentioned above, by developing a systematic methodology for integral designing of actively-matched small antennas, in order to facilitate the successful inclusion of Non-Foster Circuits (NFC) in antennas, working at frequencies where the radiating element is electrically small. Thus, compact antennas operating in multiple bands are feasible. In this methodology, the antenna + NFC set is considered as a single entity, whose performance must be globally studied, without leaving aside crucial considerations in the development of active devices, such as noise, stability, and efficiency.

CHAPTER 1

INTRODUCTION

1.1 Description of the Problem

In addition to the size reduction of today ubiquitous wireless devices, there is an increasing demand for smaller antennas. Usually, the performance requirements are not relaxed in the same proportion as the antenna is shortened. This fact comprises an important challenge for the antenna engineer since a reduction in size significantly affects the performance of the antenna properties. Moreover, the multiplicity of today wireless platforms requires the devices to operate over multiple frequency bands, leading to further design challenges. When designing antennas that are small, related to their operating wavelength (λ), it is important to have a proper apprehension of the fundamental concepts that relate the antenna size with its electrical performance [1]. This, in order to find out alternatives to mitigate the inherent limitations, and successfully include the designed antenna in the wireless system.

During the early period of radio communications, for example, vertical monopoles were almost exclusively used in the very low (VLF, 3–30 kHz) and low (LF, 30–300 kHz) bands, built utilizing metallic towers of dozens of meters [2]. Those vertical monopoles took advantage of the unique properties that those frequency regions offer, such as very stable

propagation conditions and the ability to penetrate the sea and earth. However, with the growing use of higher frequency bands —starting in the 1930's with high (HF, 3–30 MHz) and later very-high (VHF, 30–300 MHz), ultra-high (UHF, 300–3000 MHz), and microwave (> 3 GHz)— the difficulties in Electrically Small Antenna (ESA) design have been extrapolated to new applications and other types of antennas. In this sense, different topologies, materials, and shapes are able to be involved with ESAs due to mechanical practicality, aerodynamic compatibility, lightness, and so on.

1.1.1 Definition of an Electrically Small Antenna (ESA)

Since the word "small" constitutes a comparative term, an antenna can be defined by its relative physical size related to its surrounding components, for instance into a radio transceiver, or in a Submillimeter Wave (SMMW) imaging application. Nonetheless, in antenna design, after an implicit and long-time discussion, it is possible to state that to distinguish between the physical and electrical size of the antenna, we define the antenna electrical size in terms of its occupied volume related to the operating free-space wavelength. Thus, an electrically small antenna is one whose overall occupied volume is such that the factor ka is less than or equal to 0.5; where a is the radius of the smallest sphere (*radiansphere*) enclosing all the radiating structure and k is the free-space wave-number ($k = 2\pi/\lambda$) [3]. Figure 1.1 depicts the radiansphere for a dipole-like antenna. This definition differs from some others, where the ESA's limit is, for example, considered as $ka = 1$ [4, 5]; or from other more restrictive: the definition so that the largest dimension of the antenna is no more than one-tenth of a wavelength ($\lambda/10$). Further details regarding the ESA's definition and classification are included in the next chapter.

Another important factor that must be considered when defining the electrical size of an antenna, is the presence of surrounding dielectric material and any ground plane structure. If such a dielectric material surrounds the antenna element, its dimensions must be included in the definition of the antenna's electrical size (i.e. the calculation of the radiansphere with radius a), especially if it extends beyond the radiating or conductive part of the antenna. In the presence of a ground plane

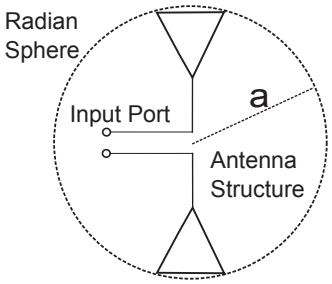

Figure 1.1: Diagram of a vertical polarized antenna, enclosed by a sphere of radius a.

structure, the antenna image must be included in the definition of a. In the case of a very large ground plane, the definition of a encompasses the physical portion of the antenna above the ground plane. Generally, if the impedance of the antenna on the finite ground plane is nearly the same as the impedance of the antenna located at the center of a very large (or infinite) ground plane, the ground plane dimension does not need to be included in the definition of a [1].

1.2 Typical Applications of ESAs

Beyond what any of us can imagine, small antennas are present in an enormous variety of systems and embedded devices involved in our routine life. Besides the conventional communication handsets (cell phones) and similar transceivers, it is possible to mention lots of others devices such as wireless computer and multimedia links, remote control units (i.e. keyless entry, garage door openers —Fig. 1.2a— wireless doorbells, remote reading thermometers etc.), satellite mobile phones, wireless Internet, AM and FM receivers for home and vehicle entertainment (Fig. 1.2c), aeronautical control and communications (Fig. 1.2d), Radio Frequency Identification (RFID) devices, and so on. The typically involved antennas (loops and short monopoles or dipoles) rarely are "full-size" resonant antennas at the frequencies they are designed to work. For instance, a 3 cm square RFID tag (see Fig. 1.2b) will have an antenna that is considered electrically small at any frequency below 1.15 GHz when the RFID systems typically work bellow 960 MHz. Only the largest form factors in modern smartphones, which have integrated Bluetooth™, GPS

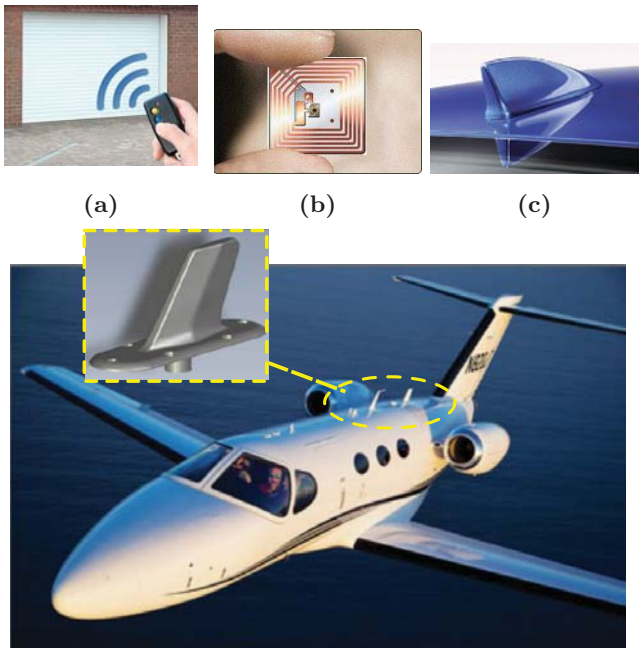

(a) **(b)** **(c)**

(d)

Figure 1.2: Some examples of typical ESAs applied to day-to-day life systems such as (a) a garage keyless door opener [6], (b) a RFID tag antenna [7], (c) a vehicular multifunction antenna [8], and (d) an airborne monopole for control and communications [9].

and other radio systems, can support antennas that are large enough for not to be considered within the *electrically small* definition.

Indeed, the rapid development in the chip industry over the last three decades, that has allowed a dramatic size reduction in microelectronics and CPU computing, has led to develop terminals that must be light, small, and energy-efficient, at the same time. On the other hand, miniaturization of the RF front-end has been a more recent focus (the last fifteen years) and has presented us with unavoidable challenges due to small antenna limitations (see Chap. 2). Some prominent researchers like H. A. Wheeler [10], H.W. Bode [11], R.M. Fano [12] and L.J. Chu [13], among others, noted that antenna size limits the values of radiation resistance, efficiency and impedance bandwidth. In other

words, ESA design is a compromise between capital factors like size, bandwidth, gain, and efficiency. It is possible to state that for the case of passively-matched small antennas, the best *tradeoff* is usually attained when most of the available volume is excited for radiation [4].

1.3 Fundamental Performance Properties of an ESA

As mentioned above, in general, when designing a small antenna, the most important performance characteristics are its input impedance, gain, and impedance bandwidth. In many of the typical wireless applications, both the radiation pattern shape and the polarization performance are relevant, but they may become of less concern in environments with significant local scattering and multipath fields since the incoming signals arrive at the device antenna from many different angles and polarizations, and also with varying axial ratio. Additionally, in many cases, the antenna engineer cannot state or control the relative position or orientation of the receiver device during use. A more detailed description of the ESA characteristics is provided in the following chapter.

In this sense, the feed point impedance —or **antenna impedance**— of any antenna can be defined as

$$Z_A(\omega) = R_A(\omega) + jX_A(\omega), \tag{1.1}$$

where $R_A(\omega)$ is the antenna's frequency-dependent total resistance, comprised of a radiation resistance term, $R_r(\omega)$, and a loss resistance term, $R_l(\omega)$, and $X_A(\omega)$ is the antenna's frequency-dependent total reactance. ω is the radian frequency $2\pi f$, where f is the frequency in hertz (Hz). The radiation resistance is primarily determined by antenna overall height or length relative to the operating wavelength. The loss resistance of the small antenna is determined by both conductor and dielectric losses —and the losses inserted afterward by a possible embedded Matching Network (MN). The total reactance at the antenna feed point is primarily determined by the self-inductance and self-capacitance, depending on the nature of the radiating structure [1].

The **radiation efficiency** of the antenna, $\eta_{\text{rad}}(\omega)$, is determined by

the ratio of the antenna's radiation resistance to its total resistance as follows:

$$\eta_{\text{rad}}(\omega) = \frac{R_r(\omega)}{R_A(\omega)} = \frac{R_r(\omega)}{R_r(\omega) + R_l(\omega)}. \tag{1.2}$$

Since the impedance performance of an antenna establishes the amount of accepted power from a transmitter (in the transmitting mode) or the amount of power delivered to a receiver (in the receiving mode), this is typically the first performance property to characterize. If any antenna is 100% efficient and conjugately matched to the transmitter or receiver, it will accept or deliver the maximum possible power, respectively. While no antenna is 100% efficient (η_{rad} never reaches 1), the small antenna can be designed to exhibit very high efficiency ($\eta_{\text{rad}} > 90\%$), even at very low values of ka.

One significant difficulty in achieving efficient radiation at low frequencies is the necessity of having antenna dimensions comparable to radiation wavelength in the air, as mentioned above. For the case of an antenna geometry like the vertical monopole of height h, the radiation efficiency drops down with the ratio $(h/\lambda)^2$ as the wavelength increases. Maximum efficiency is obtained if the antenna height is $h = \lambda/4$, provided a proper impedance matching to a low-impedance transmission line (e.g. 50 Ω).

Then, the antenna's frequency-dependent input reflection coefficient, $\Gamma_{\text{IN}}(\omega)$, is given by

$$\Gamma_{\text{IN}}(\omega) = \frac{Z_A(\omega) - Z_0}{Z_A(\omega) + Z_0}, \tag{1.3}$$

where $Z_A(\omega)$ is the impedance of the antenna under design and Z_0 is the characteristic impedance of the system. In (1.3), Z_0 is assumed to be real and constant as a function of frequency. The *realized gain*, G, of the small antenna can be computed as a function of its radiation efficiency, reflection coefficient, and directivity, D, and is given by

$$G(\omega) = \eta_{\text{rad}}(\omega) \cdot (1 - |\Gamma_{\text{IN}}(\omega)|^2) \cdot D(\omega), \tag{1.4}$$

where the term $(1 - |\Gamma_{\text{IN}}(\omega)|^2)$ represents the mismatch loss between the antenna and transmitter/receiver when Z_A is not equal to Z_0, and Z_0 being real. The first two terms of (1.4) are often combined to define the overall —or the realized— efficiency of the antenna, $\eta_0(\omega) = \eta_{\text{rad}}(\omega)(1 - |\Gamma_{\text{IN}}(\omega)|^2)$. Note that the definition of η_0 assumes that the antenna is perfectly placed with respect to the incident electromagnetic (EM) signal, in receiving mode, or the wanted radiated EM signal, in transmitting mode. Otherwise, (1.4) must include a term accounting for polarization mismatch loss. A small antenna expected to be vertically polarized will have less gain than that given by (1.4) if it simultaneously radiates (or receives) a substantial portion of horizontal polarization. With decreasing values of ka, the directivity of the small antenna approaches a constant value of 1.5, or approximately 1.8 dB. In some structures, like the short monopole over a finite ground plane, the maximum directivity reaches a value up to 4.8 dBi as some lobes appear in the pattern as frequency increases; however, in the horizontal plane, the directivity is not greater than 1.8 dBi. For small values of ka, the maximum gain that can be achieved with the small antenna is therefore about 1.8 dBi. This gain cannot be achieved in practice (assuming $D = 1.8$ dBi) because it requires that the small antenna be 100% efficient and perfectly matched to the transmitter or receiver ($\Gamma_{\text{IN}} = 0$) [1]. Achieving high radiation efficiency is a function of the antenna configuration, dielectric losses, conductor diameter and thickness, and of course, the impedance MN we include in the antenna system.

Figure 1.3a shows a short dipole antenna. At 100 MHz, the $\lambda/10$ dipole, with a 1 mm conductor diameter (30 cm in length; $ka \approx 0.31$), has an impedance at the center feed-point of $1.95 - j1750\ \Omega$, as determined by numerical modeling. A "doughnut-shaped" pattern is expected from the Transverse Magnetic (TM) mode [4] —the fundamental mode of a dipole-like antenna— which exhibits omnidirectional radiation in the horizontal plane (orthogonal to the dipole) and a figure of eight shaped pattern response in the elevation plane (or any plane containing the dipole axis), as it is depicted in Fig. 1.3b. A homologous radiation pattern is presented by the small loop antenna, radiating at its fundamental

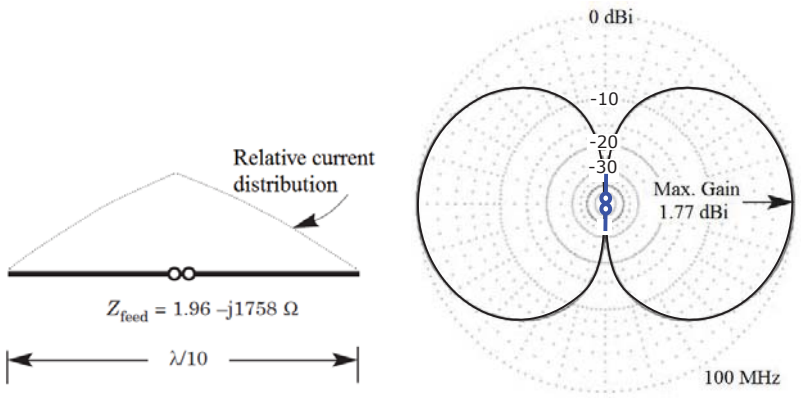

Figure 1.3: Short dipole example. (a) Dimensions, impedance, and current distribution. (b) Radiation pattern and gain.

Transverse Electric (TE) mode, but the omnidirectional projection relies on a plane containing the loop.

An intrinsic quantity of interest for an ESA is the Q factor, defined by Harrington in [14] as

$$Q = \frac{2 \cdot \omega_0 \cdot max(W_E, W_M)}{P_A}, \tag{1.5}$$

where W_E and W_M are the time averaged stored electric and magnetic energies, and P_A is the antenna received power. The radiated power is directly related to the received power through $P_{\text{rad}} = \eta_0 P_A$, where η_0 is the antenna total efficiency, defined in (1.2). It is assumed in (1.5) that the small antenna is tuned to resonance at the frequency ω_0, either through self-resonance or by using a lossless reactive tuning element (an inductor or a capacitor). Antenna Q is a quantity of interest and can be also evaluated using equivalent circuit representations of the antenna. Another important characteristic of Q is that it is inversely proportional to antenna impedance bandwidth (approximately). A commonly used approximation between Q and the 3 dB Fractional Bandwidth (FBW) of the antenna, according to [2] is given by

$$Q \approx \frac{1}{FBW_{3\,\mathrm{dB}}} \quad for \;\; Q \gg 1. \tag{1.6}$$

There is a fundamental relation between the antenna size and the Q of the antenna, expressed through the well-known equation $Q = 1/(ka)^3$ [13], however, significant corrections and modifications have been made as the result of an opened debate, which has taken place for many years [2, 4, 5, 15]. A more detailed description of this relation is presented in Chapter 2; nevertheless, what is important to notice here is the fact that as the more the antenna size decreases, the more difficult is to match the antenna over an arbitrary bandwidth, because this latter itself is limited, at the same time, by the antenna Q-factor. The high-Q inherent to small antennas can be mitigated by including losses in the antenna structure, or in the impedance matching, but at the expenses of reducing the radiation efficiency. Then, an ESA can be matched with a lossless MN, but only over very narrow bandwidths, according to the Bode [11], Fano [12], and Youla [16] gain-bandwidth criterion, limiting the performance of the transmitting/receiving system.

It is precisely at this last point where one of the most challenging issues rises up, such as to achieve broadband impedance performance on ESAs. It is, perhaps, the one that most interest has risen in ESA design since, in general, an antenna always needs an impedance matching network in practical use. As it is well-documented in the literature [1–4], achieving impedance matching at the feed terminals of an ESA is a crucial problem, because of the need to compensate its highly reactive impedance with low loss, and to transform its low resistive impedance to the load/system characteristic impedance (e.g. 50 Ω).

1.4 Active Circuits Applied to Impedance Matching

In the last decades, a notable improvement in circuit technology has been evidenced throughout the race in increasing integration and availability of electronic components. What if somehow the same technology could be applied to antennas? This inquisitiveness has led to an alternative way of designing ESAs, as it is the case of the varactor-based tunable antennas and the even more attractive: antennas matched with active non-Foster networks.

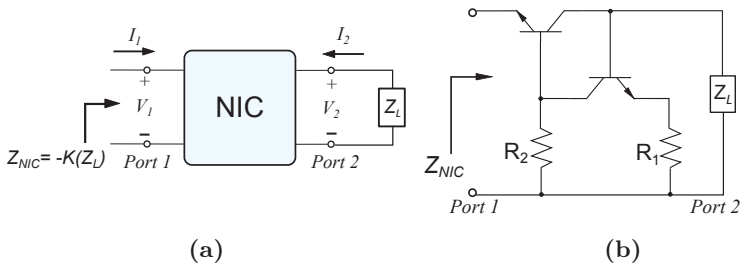

Figure 1.4: (a) Block scheme of a NIC. (b) A typical grounded topology of a BJT-based NIC proposed by Linvill [19].

Since the passive matching approach in an ESA is strongly limited by the gain-bandwidth constraint, mentioned above, and by the maximum achievable bandwidth constraint for a small-size antenna (imposed by Wheeler [10], Chu [13] and Thal [17] criteria), active-matching technique has become a very active topic during the last years. All the authors have taken advantage of the negative-slope property of the reactance response in non-Foster elements, and have tried to use it in order to compensate the natural reactance of the antenna, not only at one single frequency but over larger bandwidths. A non-Foster network/circuit (NFC) is a two-terminal device which has an impedance function that does not obey any of the three consequences of Foster's reactance theorem [18]. This theorem states that for a lossless passive two-terminal device, the slope of its reactance (and susceptance) plotted versus frequency must be strictly positive. The consequences derived from the theorem can be used to classify an element or a circuit as Foster or non-Foster, by analyzing its impedance function in the Laplace domain ($s = \sigma + j\omega$). These consequences, besides a more detailed description of the theorem itself, are given in Chapter 2.

NFCs have to be implemented with active devices; thus, they are themselves active devices also, in the sense that they consume energy from a power supply other than the signal source.

Non-Foster elements (called negative capacitors or negative inductors) are implemented using two-port active circuits called Negative Impedance Converter (NIC) [19], or Negative Impedance Inverter (NII) [20], according to their set-up or topology, as it will be shown later. A NIC

circuit implements negative impedance, $Z_{\text{NIC}} = -k \cdot Z_L$, for $k > 0$ with Z_L being the impedance to be converted, as it is depicted in Fig. 1.4a. In the case of a NII, the input impedance, Z_{NII}, results in a negated version of the *admittance* associated to the load Z_L, thus, $Z_{NII} = -k \cdot Y_L$, for $k > 0$. NFCs have been considered since the 1950s when Linvill [19] and Yanagisawa [21] introduced the first tested NIC topologies, like the one depicted in Fig. 1.4b. A NIC is a two-port network implemented via a combination of active devices (amplifiers or tunneling diodes), lumped loads (capacitors and inductors) and supportive elements (resistors, RF chokes, connections, etc.).

As mentioned before, the unique NIC/NII characteristic exploited to obtain broadband impedance matching for ESAs, is the negative slope of its impedance response, looking into the port connected to the antenna. In this way, the reactive part of the antenna impedance can be compensated over a wider frequency range. This concept is depicted comparatively in Fig. 1.5a. and b.

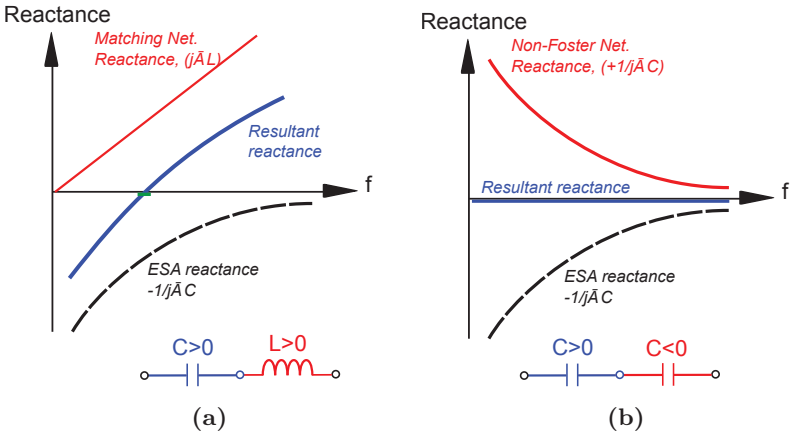

Figure 1.5: Comparative concept of (a) passive and (b) active matching for an ESA, modeled as a series capacitor.

On the other hand, the inherent conditional stability of a NIC constrains the magnitude of the impedances that can be connected to its input port [19, 22]. In general, the transistor-based NIC topologies comprise positive feedback that limits their working frequency upper-bound to up to 1 GHz. The Monolithic Microwave Integrated Circuits (MMIC)

can help but make the design process expensive and complicated [23]. Therefore, an exhaustive analysis of the stability is more than welcome. It must take into account not only the transistor model but parasitics and the antenna itself.

Further considerations should be considered, regarding, for example, the added noise. Antennas with embedded non-Foster networks, in this context, while using in receiving mode, have added noise due to the active elements composing the NFCs. This noise degrades the Signal to Noise Ratio (SNR), in addition to the bandwidth improvement of the antenna system (NFC + Antenna). The SNR improvement (or possible decrease) in the non-Foster matched antenna has to be measured in order to characterize its performance completely when included in a receiver system.

In most of the work reported, a cascade NIC + Antenna configuration has been used. This condition implies a significant inconvenient in using the active circuit, as this sort of transistor-based circuits are unidirectional in some configurations, whereas an antenna is bidirectional. Moreover, in transmitting mode, the NIC shall drive all the voltage and current levels, which can derive in saturation or damage. Hence, the classical application is limited to either transmitting or receiving. Thus, any approach that allows the engineer to unify the design process will be advantageous since other drawbacks in active matching design can be addressed such as realizability, DC biasing and stability of the whole antenna system (Antenna + NIC). This is the case of small antennas embedded with NFCs (active-MNs), according to the approach developed in this dissertation.

1.4.1 Possible Applications of Actively Matched Small Antennas

In general, ESAs with embedded active MNs can be applied to any application where a wide instantaneous impedance bandwidth is needed, as well as when a reduction in the RF power needed from the system at the radiation stage.

One interesting area to apply new designs and advances in antenna miniaturization is the aeronautical industry. Airborne navigation and

communication systems need for wideband, light and low-drag (short) antennas in their front-end. Currently used systems operate at the VHF and the lower bound of the UHF bands, where the typical sizes associated to the utilized antennas comprises some conventional blade-type monopoles with around 45 cm in height (see Fig. 1.2d), for the lower work frequency bands (down to 30 MHz). Those antennas correspond to a factor ka between 0.19 and 0.22 for the Air Traffic Control (ATC) band, or down to 0.05 for the radio links in the 30-88 MHz range. In these aeronautical systems, two different strategies have been implemented to overcome the performance limitations inherent to the involved ESAs. The first one consists of a passive and lossy MN based on lumped elements such as toroidal ferrites, resistors, and capacitors, connected somehow inside the antenna structure as a distributed MN. The second strategy consists of implementing an electronically-tuned antenna (also called *active antenna* in aeronautical jargon), typically by means of solid-state switching devices (e.g. PIN diodes). This latter alternative implies some extra control units to switch between one channel to another with up to 10 MHz per channel bandwidth, unlike the instantaneous wideband achievable with actively-matched ESAs, in which no extra control units are needed.

Some other applications can be listed, such as civil security equipment (e.g. the Terrestrial Trunked Radio (TETRA) band) and vehicle communications, where embedded active matching designs allow the development of VHF/UHF wideband antennas. In these antennas, an effective-gain improvement can be provided by connecting an active MN. Furthermore, other advantages can be obtained like better coverage, compact size and reduced power consumption, by requiring less transmission power for achieving the same coverage, compared with the current passive antennas.

1.5 Motivation, Objectives and Contribution

As mentioned earlier, the limited electrical performance of ESAs, aggravated by the rapidly developing communications world, has encouraged the antenna engineers' community to propose alternative paths to tackle the physical limitations of this type of radiating structures. Active devices have been found to be a possible solution in some of those

alternative paths. In that sense, this dissertation is focused on contributing to the antenna community with some additional observations, and a systematic design methodology for ESAs loaded with NFC. As a major contribution, a novel parameter for the proper location of the NFC within the antenna structure, called *Sensitivity Parameter (Sens)*, is introduced and applied to real designs. The entire work is intended to serve as an additional source of considerations for actively-matched ESAs loaded with non-Foster elements.

Some specific objectives, associated to this dissertation, can be listed as follows.

- To develop a strategy for the efficient and systematic design of electrically small antennas with a multiband or broadband operation.
- To establish a technique of impedance matching, based on active non-Foster-type networks embedded in the antenna structure itself.
- To explore the possible improvement of critical antenna parameters such as radiation efficiency and stability of the small actively matched antennas.
- To implement, by prototyping, such antenna systems comprising antenna + active-MN with non-Foster elements.

1.6 Organization of the Dissertation

This thesis offers firstly a brief introduction to the ESA characteristics, its applications and the description of the active impedance matching strategy as a smart miniaturization technique. This, alongside some motivation and organization words in Chapter 1. The fundamental characteristics of antennas are presented at the beginning of Chapter 2, as part of an overview of the definition, and the main characteristics, of the most typical ESA structures as radiators. The most relevant limitations and the methods conventionally used to match its impedance over wider bandwidths are also shown. A review of the literature concerning the most remarkable reported work in active matching alternatives and techniques applied for antennas is included as well.

Chapter 3 deals with relevant criteria and design considerations involved with the active impedance matching of an ESA, using such a non-Foster networks, by means of a novel parameter, introduced by the author, called sensitivity (***Sens***). This new parameter is analytically developed and applied to different antenna types, aimed at finding the most advantageous location for a NFC. Relevant considerations regarding the realizability of the analytically-found impedances needed to have wider impedance bandwidth are presented. Those analytically derived impedances have a behavior inherently non-Foster that must be addressed with active circuits.

Chapter 4 is devoted to present a complete design strategy of small antennas, actively loaded with non-Foster elements. This strategy aims at proposing a systematic methodology which includes: analytical finding of both the NFC location and the required non-Foster impedance for wideband matching, active-device selection to implement the NFC, a statistical analysis about the effect of tolerance in components and other manufacturing parameters over the global impedance and stability performance. Current distribution analysis and the analysis of stability, through the Normalized Determinant Function (NDF) approach, are also contemplated by the proposed strategy.

Chapter 5 presents, as a prospective of future work, the effect of the inclusion of an active non-Foster network in the impedance matching of a phased array. Finally, the main conclusions and future working lines are presented in Chapter 6. The list of contributions resulting from the development of this dissertation is shown in the Publications section at the end of this document.

CHAPTER 2

IMPEDANCE MATCHING TECHNIQUES FOR ESAS: BACKGROUND

2.1 Fundamental Parameters of Antennas

To begin, in this section, the main parameters of antennas are briefly reviewed. These parameters are explained in a simplified way, but there exists a huge amount of books where the reader can go into further detail of any of them [1, 24–26].

2.1.1 Radiation Pattern

A radiation pattern is a representation of the radiated field by an antenna as a function of the different directions of the space at a fixed distance. Normally, spherical coordinates (r, θ, ϕ) are used and the representation is referred to the electric field. As the electric field is of vectorial type, two orthogonal components at each point of the constant radius sphere, defined by the spherical coordinates, must be calculated (usually θ and ϕ). Field radiation pattern or power radiation pattern have the same information since power density (in the far field) is proportional to the square of the electric field module, and when they are represented in dB they are equal.

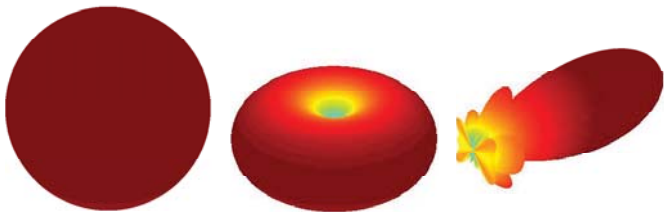

(a) **(b)** **(c)**

Figure 2.1: 3D radiation patterns. (a) Isotropic, (b) Omnidirectional, and (c) Directive.

The radiation pattern is commonly represented by using a Three-Dimensional (3D) plot but also a Two-Dimensional (2D) one showing different cuts of the radiation pattern. In linearly polarized antennas (see polarization in Section 2.1.6) an E-Plane and H-Plane can be defined. E-Plane is the plane containing both the Poynting vector (which represents directional energy flux) and the E-vector, while H-Plane is the plane containing the Poynting vector and the H-vector. These planes are mutually perpendicular and its intersection represents a line which defines the direction of propagation.

Depending on the shape of the radiation pattern three types of radiation patterns can be identified: isotropic (Fig. 2.1a), omnidirectional (Fig. 2.1b) and directive (Fig. 2.1c).

Bi-dimensional cuts of the radiation pattern can be represented either in Polar or Cartesian coordinates. An example of both of them can be seen on Figs. 2.2a and 2.2b. In the first case, the radius represents the intensity of the radiated electric field or the power density, while the angle represents the space direction. In the second case, the angle is represented in the abscissa axis while electric field or power density is represented in the ordinate axis. Field or power density can be represented on an absolute or on a relative way (normalized to the maximum), with natural or dB scales.

From a radiation pattern representation, several parameters can be extracted. The radiation lobe containing the direction of maximal ra-

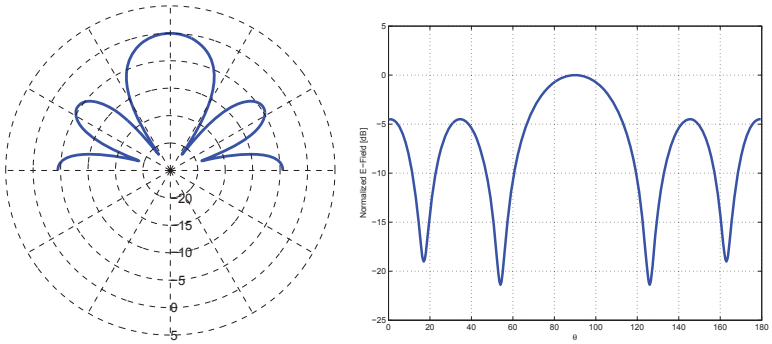

(a) **(b)**

Figure 2.2: 2D radiation pattern. (a) Polar and (b) Cartesian representation.

diation level is called the **main lobe** [25] while the lobe with more amplitude, among the rest of the lobes, is the **secondary lobe**.

2.1.2 Directivity

Directivity of an antenna is defined as the relationship between power density radiated in a direction at a fixed distance (in the far field) and the power density that would be radiated at that distance by an isotropic antenna that radiates the same power as the antenna:

$$D(\theta,\phi) = \frac{S(\theta,\phi)}{P_r/(4\pi r^2)}, \tag{2.1}$$

where $S(\theta,\phi)$ is the power density, and P_r is the radiated power.

If no angular distribution is specified, it is understood that the directivity refers to the maximum radiation direction:

$$D = \frac{S_{\max}}{P_r/(4\pi r^2)}. \tag{2.2}$$

The directivity can be obtained from the expression:

$$D\left(\theta,\phi\right)=\frac{4\pi}{\iint_{4\pi}t\left(\theta,\phi\right)\mathrm{d}\Omega},\tag{2.3}$$

where

$$t\left(\theta,\phi\right)=\frac{S\left(\theta,\phi\right)}{S_{\max}},\tag{2.4}$$

is the normalized radiation pattern.

In directive antennas, a good approximation to calculate the directivity is:

$$D=\frac{4\pi}{\Delta\theta_1\cdot\Delta\theta_2},\tag{2.5}$$

where $\Delta\theta_1$ and $\Delta\theta_2$ are the Half Power Beamwidth (HPBW) in the two main planes of the radiation pattern.

Once the maximum directivity D and the normalized radiation pattern $t\left(\theta,\phi\right)$ are known, then it is easy to obtain the directivity at any direction:

$$D\left(\theta,\phi\right)=D\cdot t\left(\theta,\phi\right).\tag{2.6}$$

2.1.3 Gain

The gain, frequently denoted as the *antenna gain* (G_A), is directly related with directivity. Its definition is the same as the directivity one, but instead of comparing with the radiated power, the actual delivered power is used. Then, it is possible to take into account the losses of the antenna ($\eta_{rad}(\omega)$ in Eq. (1.2)). The directivity and the gain are related by radiation efficiency (η_{rad}) as follows:

$$G_A(\theta,\phi) = \frac{P(\theta,\phi)}{P_{\text{delivered}}/(4\pi r^2)} = \frac{P_r}{P_{\text{delivered}}} \cdot \frac{P(\theta,\phi)}{P_r/(4\pi r^2)}$$

$$= \eta_{\text{rad}} \cdot D(\theta,\phi) \tag{2.7}$$

When other parameters are desired to be included in the calculation of the antenna gain, such as the mismatching factor $(1 - |\Gamma_{in}(\omega)|^2)$, polarization efficiency and aperture efficiency [27], Eq. (2.7) has to be complemented to become the *Realized Gain*, where all the efficiencies are still a proportionality factor between Directivity and Gain, for a real antenna. Thus, the *realized gain* is given by

$$G(\theta,\phi) = \eta_{\text{rad}} \cdot \eta_{\text{apert}} \cdot \eta_{\text{pol}} \cdot (1 - |\Gamma_{\text{in}}|^2) \cdot D(\theta,\phi)\,. \tag{2.8}$$

3 dB Beamwidth ($\Delta\theta_{3dB}$) or HPBW is the angular distance between the directions where the power density radiation pattern is equal to half the maximum.

Beamwidth Between Zeros ($\Delta\theta_c$) or First Null Beamwidth (FNBW) is the angular distance between the directions at which the main lobe has a minimum.

Side-Lobe Levels (SLL) is the relation between the value of the radiation pattern, in the direction of maximum radiation, and the value of the radiation pattern in the direction of the secondary lobe. It is normally expressed in dB.

Front-to-Back ratio (F/B) Radiation is the relation between the value of the radiation pattern, in the direction of maximum radiation, and the value of the radiation pattern in the opposite direction.

2.1.4 Effective Aperture Area and Aperture Efficiency

The effective aperture or effective area (A_{eff}) is defined as the relation between the power that the antenna delivers to its load (in a matched

case, suppose antenna working in reception) and the power density of the incident wave. It is related to the directivity by the following formula:

$$\frac{A_{\text{eff}}}{D} = \frac{\lambda^2}{4\pi}. \tag{2.9}$$

Effective aperture cannot be higher than the antenna physical aperture, so an aperture efficiency (η_{aperture}) that relates the effective area (A_{eff}) and the physical area (A_{phy}) of the antenna can be defined:

$$\eta_{\text{aperture}} = \frac{A_{\text{eff}}}{A_{\text{phy}}}. \tag{2.10}$$

2.1.5 Phase Pattern and Phase Center

Under some circumstances it is desirable to plot not the amplitude of the electric field (as in the radiation pattern) but the phase of the electric field. Such representation is called the phase pattern.

When observing an antenna at a great distance (i.e. in the far field), its radiation can be seen as coming from a single point. In other words, its wave front is spherical. This point, center of curvature of the surface aperture with constant phase, is called the phase center of the antenna.

2.1.6 Polarization

Polarization represents the electric field vector orientation in a fixed point as a function of time. It can be identified by the geometric figure described, as time goes, by the end of the electric field vector in a fixed point of the space in the perpendicular plane to the propagation direction. Three figures can be generated: an ellipse (which is the most generic one), a segment (linear polarization) and a circumference (circular polarization).

The direction of rotation of the electric field vector, either in circularly polarized waves or elliptically ones, it is called right-hand polarization if it is clockwise and left-hand if it is counterclockwise, looking from the source of radiation.

Axial ratio of an elliptically polarized wave is defined as the ratio between the major and minor axis of the ellipse. It takes values between 1 and infinity. For a circularly polarized wave the axial ratio is 1.

2.1.7 Input Impedance

The input impedance of an antenna is the relation between the voltage and the current at the feed point of the antenna. It is normally a complex number that depends on the frequency:

$$Z_{\text{IN}}(\omega) = R(\omega) + jX(\omega). \tag{2.11}$$

If $X(\omega) = 0$ at some specific frequency, it is said that the antenna is resonant at that frequency. Knowing the input impedance of an antenna is a key factor because the antenna is usually connected to a transmission line or to an active device (transistor, diode, etc.). If a mismatch occurs between the antenna and the device, then not all the power transmitted through the device will be delivered to the antenna (in transmitting mode) or not all the power received by the antenna will be delivered to the device (in receiving mode).

2.1.8 Radiation Resistance

When delivering power to an antenna, a part of it is radiated through the free-space. This quantity can be defined by a radiation resistance R_r which is defined as the equivalent resistance value that will dissipate the same amount of power than that is radiated by the antenna:

$$P_r = I^2 \cdot R_r. \tag{2.12}$$

Not all the power delivered to an antenna is radiated through the free-space. Associated to this, the loss resistance (also called *ohmic losses*), R_l, can be defined. This resistance refers to the losses that appear in

the antenna and is defined as the resistance value that will dissipate the same amount of power as the one not radiated by the antenna.

$$P_{\text{delivered}} = P_r + P_{\text{losses}} = I^2 \cdot R_r + I^2 \cdot R_l. \tag{2.13}$$

This is related to the radiation efficiency (η_{rad}) defined previously:

$$\eta_{\text{rad}} = \frac{P_r}{P_{\text{delivered}}} = \frac{P_r}{P_r + P_{\text{losses}}} = \frac{R_r}{R_r + R_l}. \tag{2.14}$$

2.1.9 Bandwidth

Bandwidth represents the frequency interval where one particular property is satisfied. For the antenna case, two different kinds of parameters can be considered: impedance parameters or radiation parameters. Then, the antenna bandwidth would be defined as the frequency margin at which the impedance, or the reflection coefficient, is kept under some value and the shape radiation pattern is kept constant. It can be represented as the absolute value ($f_{\text{max}} - f_{\text{min}}$) or as a relative one, FBW, as follows:

$$FBW = \frac{f_{\text{max}} - f_{\text{min}}}{f_0}. \tag{2.15}$$

For broadband antennas, it is common to represent the bandwidth in the form:

$$BW = \frac{f_{\text{max}}}{f_{\text{min}}} : 1. \tag{2.16}$$

The criteria used to determine the bandwidth of an antenna are related to the radiation pattern (directivity, polarization purity, beamwidth, SLL) or to the impedance (input impedance, reflection coefficient or Voltage Standing Wave Ratio (VSWR)).

2.2 A Brief History of Electrically Small Antennas

The broadest accepted, but not unique, definition of the term "electrically small antenna" (ESA), first introduced by H. A. Wheeler in 1947 [10], directly relates the performance of the antenna, in receiving or in transmitting mode, with the size of a radian sphere in which the antenna could be enclosed. The radian sphere was a sphere of radius equal to $\lambda/(2\pi)$ where λ is the wavelength. In spite of their huge physical size, the radiant structures used by the early telegraphy systems —reported by Marconi and Fessenden— were small compared to the wavelength (often greater than 3000 m), associated with working frequencies around 100 KHz. Those early electrically small antennas often involved massive mast of dozens of meters, guy-wires, inverted metallic cones, among other structures inserted to improve the antenna performance.

The purpose of the insertions (inverted fan or cones) was to increase the antenna capacitance, and thus, reduce the capacitive reactance, one of the most representative characteristics in the impedance response of small monopoles and dipoles. Wheeler (Fig. 2.3) introduced a model for a short dipole for both magnetic and electric nature, through discrete reactances (see Fig. 2.4), a parallel plate capacitor and a cylindrical inductor, stating an elegant illustration of duality for electric and magnetic dipole parameters, offering at the same time, a practical insight to the physical limitations of ESAs.

Figure 2.3: Harold Alden Wheeler (1903-1996). One of the most noted engineers in analyzing and developing small antennas, and its fundamental limits.

Wheeler related the antenna height and the cylindrical volume to a radiation power factor, p, a ratio of the actual antenna circuit power to the reactive energy stored in the cylindrical volume. It can be calculated as the ratio of the radiation resistance to the reactance of the antenna, according to (2.17) and (2.18), respectively. For the solenoid loop antenna

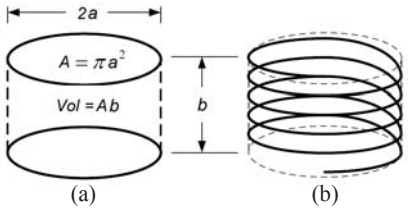

Figure 2.4: Reactive antenna model introduced by Wheeler [10] for (a) a capacitor and (b) an inductor, occupying equals cylindrical volumes

—the short magnetic dipole— $R_m = 320N^2\pi^6(a/\lambda)^4$ is the associated radiation resistance, where N is the number of turns of the solenoid, and a and b are the dimensions according to Fig. 2.4. The inductance of the solenoid loop antenna is $L = \mu_0 N^2(\pi a^2/b)$, where μ_0 is the permeability of free-space. For the parallel plate capacitor —the short electric dipole— the radiation resistance is given by $R_e = 80\pi^2(b/\lambda)^2$. The capacitance, in this case, can be calculated by $C = \epsilon_0\pi a^2/b$, where ϵ_0 is the permittivity of free-space.

$$p_m = \frac{R_m}{\omega L} = \frac{4}{3}\frac{\pi^3 a^2 b^3}{\lambda}\ , \tag{2.17}$$

$$p_e = R_e\omega C = \frac{4}{3}\frac{\pi^3 a^2 b^3}{\lambda}\ . \tag{2.18}$$

The radiation power factor for an ESA is very small, since it is inversely related with the third power of the wavelength [2]. For example, in the short dipole shown in Fig. 1.3a, whose length is 30 cm and its diameter is 1 mm; the radiation factor p_e drops down to $3.7 \cdot 10^{-7}$, approximately.

An additional definition, given by King in 1956 [28], referred to an ESA as an antenna having the length and size in terms of the product $ka \leq 0.5$, where a is the radius of the smallest sphere enclosing all the radiating structure, as it was depicted in Fig. 1.1, and k is the free-space wave-number ($k = 2\pi/\lambda$). Thus, $a = (1/2)(\lambda/2\pi)$, differs from the radiansphere described by Wheeler, where $a = \lambda/2\pi$, by a factor of 2. In this sense, it is possible to say that the minimum enclosing sphere

where the factor $ka \leq 0.5$ is a reasonable bound for an ESA, in terms of the free space wavelength, although several authors still use the classical Wheeler's condition. A value of $ka = 0.5$ represents an overall spherical volume equal to $\lambda^3/48\pi^2$.

2.3 Classification and Most Typical ESA Structures

Some authors have preferred some elaborated, but not very extended, classification of small antennas with categories depending, for example, on the situation of the practical application. These categories include: Electrically Small Antenna (ESA), when the classification parameter is exclusively the wavelength at the working frequency; the Physically Constrained Small Antenna (PCSA), when the antenna, does not have dimensions of ESA, but a part of which has dimensions corresponding to an ESA. Then, the Functionally Small Antenna (FSA), when the antenna is engineered to enhance some performance toward lower frequencies but with its size kept unchanged. This last one is the case of those antennas in which the engineer tries to expand down in frequency, for example, the impedance matching by including slots, near field parasitics, resonators, metamaterial particles etc. Finally, the Physically Small Antenna (PSA), applicable specially to millimeter wave and Terahertz (THz) applications, where manufacturing and characterizing such small structures are challenging tasks [3].

In a more classical sense, with a conventional understanding of antennas, it is possible to divide ESAs into two types. First, an electric element, which couples to the electric field and is referred to as a capacitive antenna, as the one analyzed by Wheeler in Fig. 2.4a. Second, the magnetic element (electric loop), which couples to the magnetic field and is referred to as an inductive antenna, as the one analyzed by Wheeler in Fig. 2.4b. H. Hertz utilized a sort of those structures, shown in Figs. 2.5a, and 2.5b, respectively, for his first radio wave transmission experiment [29].

However, many practical antennas are some combination of these two types, where we can include short monopoles, loaded dipoles, patch antennas with inverted insertions, loop antennas with magnetic cores, Dielectric Resonator Antennas (DRA), multi-blended conductors with

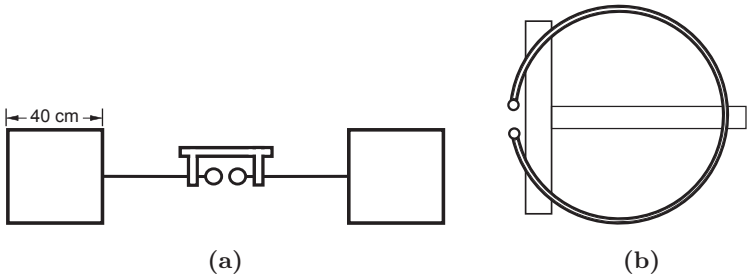

Figure 2.5: Hertz antennas used for his first radio wave transmission experiments [29]. (a) Dipole. b) Loop resonator.

exotic shapes, and antennas with metamaterials inclusions. Many of these structures have been implemented in practice, in spite of how exotic or complicated their form might be. In most cases, a compromised performance is achieved, in special when a broad impedance bandwidth or high radiation efficiency is intended [30]. Some examples of different structures, frequently performed as ESAs, are depicted in Fig. 2.6.

The re-engineering and creation of small antennas, as those mentioned above, have been accelerated rapidly in response to a global trend of urgent demands, that has been raised by the growth of mobile phone and wireless deployed systems. These constantly modified systems take the electronics components to almost its highest performance limit, nonetheless, the ESAs involved with them, in many cases, are working without a well-optimized design. Thus, it is possible to say that only the antenna can further improve the overall system performance.

Although the wide use of ESAs in current wireless systems, there are still several remaining issues to deal with concerning the design methodology, efficiency, and practical applications. There is a duality in this sense: the implementation of an ESA is a big and challenging problem for engineers, and at the same time, engineers are called to gain new skills and methods to develop useful and practical ESAs.

2.4 Performance Characteristics of ESAs

Despite of the multiple definitions and classifications for small antennas, it is possible to state some characteristics intimately linked with the

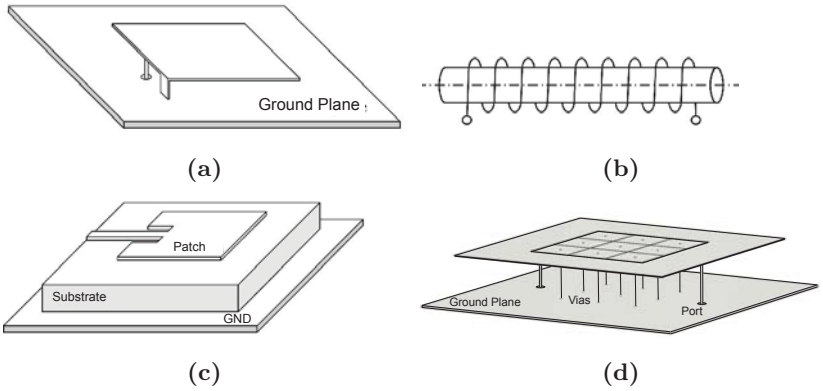

Figure 2.6: Some examples of typical structures of ESAs [3]: (a) a Planar Inverted-F Antenna (PIFA), (b) a ferrite loaded coil, (c) a conventional patch antenna, and d.) a patch antenna with metamaterial inclusions (mushrooms).

electrical size, once the operating frequency decreases. Those characteristics are common to any of the radiating structures used as an ESA, and comprises a major challenge for the designer.

2.4.1 Antenna Impedance of an ESA

As previously mentioned, the antenna impedance in an ESA, well in a small electric element (small dipole), well in a magnetic element (small loop or magnetic dipole), is highly reactive. This antenna impedance shows a capacitive nature for the electric element or an inductive nature for the magnetic one, while its resistive component is very small in both cases. This property states the first difficulty to find a perfect matching, for example, to a 50 Ω based system, in cases where the matching condition is intended to be reached over a significant bandwidth, other than a single frequency. In other words, the inverse relation between the bandwidth and the ratio reactance/resistance in the ESA impedance states a fundamental limit. That constrain is explained later, with more detail.

The input impedance of a small electric dipole with a radius d and a length $2a$ (see Fig. 2.7a), can be expressed in the form $Z_a = R_a + jX_a$ [3], where:

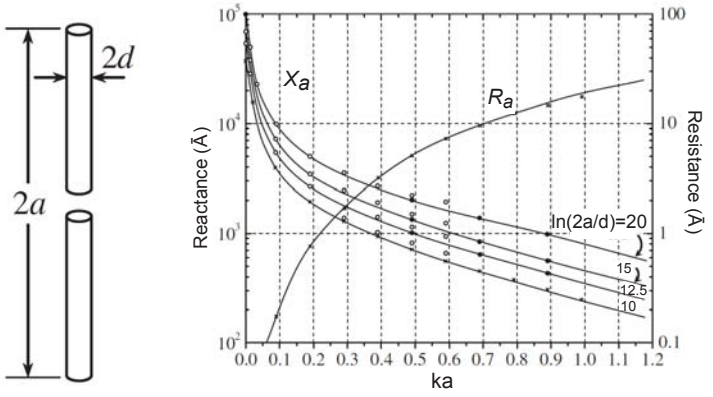

Figure 2.7: (a) Small electric dipole. (b) Impedance Z_a as a function of the size factor ka [3]

$$R_a = 20(ka)^2, \tag{2.19}$$

$$X_a = 60\left(\ln\left(\frac{2a}{d}\right) - 3.39\right)(1/ka)\,. \tag{2.20}$$

Some curves, representing the reactance X_a for different values of $\ln(2a/d)$, are shown in Fig. 2.7b. An important difference between the real and the imaginary parts of Z_a is observed (up to six magnitude orders) as the antenna size decreases.

A similar response is observed for the small magnetic element, represented by a small loop antenna with radius a and wire radius d, as the one depicted in Fig. 2.8. The inductance of the small loop can be computed as (2.22) [25], and can be depicted as a function or the ratio a/d, as shown in Fig. 2.9a. The radiation resistance of the antenna, which can be computed as (2.21), is depicted in Fig. 2.9b. Resistance values lower than 10 Ω are observed for $ka \leq 0.5$. For example, a loop with radius $a = 10$ cm, and a wire radius $d = 1$ mm ($a/d = 100$), will show an inductance of 0.59 μH. This loop antenna can be considered small up to 238 MHz since the ka factor equals 0.5 at this frequency.

$$R_a = 20(\beta^2 A)^2, \tag{2.21}$$

$$L = a\mu_0\mu_r \left[\ln(8a/d) - 2\right], \tag{2.22}$$

where $A = \pi a^2$ is the area of the loop, and $\beta = k$ for the lossless case ($\alpha = 0$), in $k = \alpha + j\beta$. The radiation resistance decreases much faster for a small loop ($R_a \propto f^{-4}$) than for a small dipole ($R_a \propto f^{-2}$), as frequency decreases.

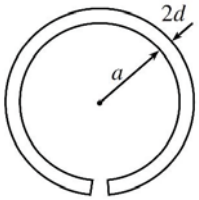

Figure 2.8: Antenna sketch of a single-turn small loop.

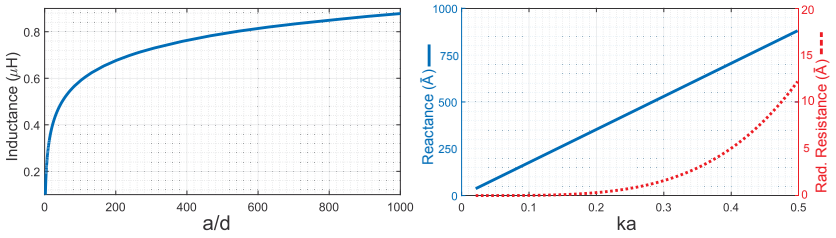

(a) **(b)**

Figure 2.9: (a) Inductance L as a function of the ratio a/d [3].
(b) Resistive and reactive response of a small loop with $a/d = 100$.

2.4.2 Quality factor Q

As introduced earlier, another important characteristic of a small antenna is described by the quality factor Q concept. This term was first introduced by K.S. Johnson in 1920, to represent the ratio of the inductive reactance to the resistance of a coil, $Q = \omega L/R$, and afterwards, the analogous quantity (in lower-case) for a capacitor, $q = \omega C/G$. If a capacitor and an inductor are connected in parallel, in order to set a

tuned circuit, the power response decreases as a factor of $1/\sqrt{2}$ when the circuit is detuned by a fractional quantity $\delta\omega/\omega = 1/2Q$. Then, $1/Q$ is the 3 dB bandwidth of the circuit. In a tuned radio terminal, for example, the higher values for parameter Q were preferred to avoid interferences with adjacent channels. By the beginning of the second half of the past century, the factor Q became important to characterize the resonance curve of resonators in radar and communications systems.

If over a resistor R, associated with the equivalent series resistance of an inductor in a tuned parallel LC circuit, with a resonant frequency given by $\omega_0 = 1/\sqrt{LC}$, is flowing a current I, then the average power dissipated in the resistor, P_L, is $I^2R/2$. The average energy stored in the magnetic field around the inductor is given by $W_m = I^2L/4$. In addition, it is known that at resonance the time-averaged energy stored in the capacitor is equal to that in the inductor. If we now use these into the definition of Q by Johnson, it is possible to derive an expression for Q as follows [2]:

Figure 2.10: Lan Jen Chu (1913-1973). Remarkable Professor and IEEE Fellow.

$$Q = \frac{\omega L}{R} = \frac{2\omega(I^2L/4)}{I^2R/2} = \frac{2\omega W_m}{P_L} = \frac{\omega(W_m + W_e)}{P_L}$$

$$Q = \frac{\omega(average\ energy\ stored\ in\ resonant\ circuit)}{average\ energy\ dissipated\ per\ second}. \tag{2.23}$$

Equation (2.23) is a very commonly used definition for the Q of a resonant circuit, and it can be extended for antennas in terms of the antenna impedance around the resonant frequency [28], as follows:

$$Q \cong \frac{\omega dX/d\omega}{2R}. \tag{2.24}$$

However, this last definition is not an easily computed expression in a real design, where the designer has to meet requirements regarding either radiation, bandwidth, and above all in ESA applications: a strong size restriction. In this sense, one of the most relevant contributions was made in 1948 by L.J. Chu [13] (see Fig. 2.10). Chu established a direct relation between antenna size and the minimum achievable Q, by using the definition given by (2.23), in order to find a lower bound for the Q of an ESA, whose radiated fields could be expressed in terms of spherical waves. The results obtained by Chu provide a more accurate measure of the limitations of ESA than Wheeler's power factors do. McLean [31] followed Chu's analysis to derive an expression for the Q of the lowest order mode in terms of the antenna electrical size:

$$Q \cong \frac{1 + 2(ka)^2}{(ka)^3[1 + (ka)^2]}. \tag{2.25}$$

Collin and Rothschild [32] approached the problem by subtracting the energy associated with radiation from the total energy of each mode. They gave the value for the lowest order spherical mode, based on the field rather than the equivalent circuit, by calculating Q for cases where both TE and TM modes are used for excitation, as follows:

$$Q = \frac{1}{ka} + \frac{1}{(ka)^3}. \tag{2.26}$$

McLean [31] described the propagating and non-propagating fields, calculated Q from the ratio of these terms, arriving at the same result as the one by Collin, above. He also found that the Q for circularly polarized antennas involving both TM and TE modes together is given by

$$Q = \frac{1}{ka} + \frac{1}{2(ka)^3}. \tag{2.27}$$

Thal [17] contributed with an additional criteria related to the calculation of Q, given new formulas to express Q for the lowest order TM and

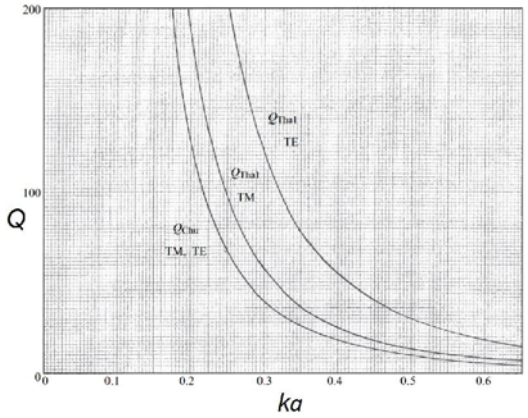

Figure 2.11: Q for lowest order modes in an ESA [2].

TE modes, computed as (2.28), by treating the reactive power inside the sphere circumscribing the antenna, whereas Chu's calculation did not include that. Thus, the Q is given by the Q_{Chu} plus an additional term which corresponds to the internal reactive energy. According to Thal, the value of Q with respect to the ka factor is depicted in Fig. 2.11, comparing his approach with the Chu's limit [2].

$$\begin{aligned} TM : Q &= \frac{1}{\sqrt{2}ka} + \frac{1.5}{(ka)^3}, \\ TE : Q &= \frac{3}{ka} + \frac{3}{(ka)^3}. \end{aligned} \tag{2.28}$$

2.4.3 Bandwidth and Passive Matching

Despite the fact that factor Q has become one of the most representative limits in ESA design, the quantity that is of most interest to antenna engineers is the frequency bandwidth, BW. As mentioned before, some authors stated a direct relation between the relative bandwidth, FBW, and the Q of a resonant circuit ($FBW = 1/Q$). This relation was associated to antennas with $Q \gg 1$ (by Geyi [33]). However, the antenna

bandwidth cannot simply be defined in the same way as in circuitry, due to the existence of some limiting factors which limits the functional bandwidth of the antenna. Among these factors it can be included, for example, the change of the radiation pattern shape or direction, variation in the impedance characteristics, near field parasitics, change in size, etc. In general, it is possible to define the bandwidth BW of an antenna as a frequency range within which the antenna meets a given set of specifications, typically based on the impedance or antenna gain characteristics. For the ESA case, either the antenna input impedance or the power spectra can be considered as the parameter to specify the bandwidth [3].

It is possible to calculate the absolute BW as the difference between the upper and the lower frequency bounds $(f_1 - f_2)$; both specified to meet certain value for parameters such as the VSWR or the Return Loss (RL), which stands for the antenna impedance (Z_a) performance. Some useful and well-known relations are given as follows:

$$\Gamma_{\text{IN}} = (Z_a - Z_0)/(Z_a + Z_0), \tag{2.29}$$

$$VSWR = (1 + \Gamma_{\text{IN}})/(1 - \Gamma_{\text{IN}}), \tag{2.30}$$

$$RL = -20\log|\Gamma_{\text{IN}}|, \tag{2.31}$$

where Γ_{IN} is the reflection coefficient looking into the driving point of the antenna. Z_a and Z_0 are the antenna and the characteristic impedances, respectively.

The FBW is defined as the ratio of BW to the central frequency (f_0) of the band, that is: $FBW = (f_2 - f_1)/f_0$. This last expression is widely used in antenna design. There is an important relation between bandwidth and the Q factor for ESAs, as it was described by Yaghjian and Best [15], who derived such relationship through the maximum allowable VSWR, or s, as follows:

$$FBW \approx \left(\frac{1}{Q}\right)\left(\frac{(s-1)}{\sqrt{s}}\right). \tag{2.32}$$

2.4.4 Radiation efficiency

As aforementioned, as the antenna size decreases to ka-factor levels much lower than 1, the resistive part of its input impedance drops to levels of a few Ohms, or even less (see Figs. 2.7b and 2.9b). This condition comprises a high difficulty in the impedance matching process, as it will be shown below. If we now take in mind the losses in the antenna structure, like those associated with lossy conductors or dielectric materials (e.g. in printed antennas), an additional issue arises as the decrease in the antenna radiation efficiency.

The radiation efficiency η_{rad} is given by

$$\eta_{rad} = P_{rad}/P_{acc} = R_{rad}/(R_{rad} + R_l), \tag{2.33}$$

where P_{rad} and P_{acc} are the radiated and the accepted powers, respectively, and R_l represents both the losses in the antenna structure and the added losses through a possible MN. In any antenna design, radiation efficiency can be understood as the constant of proportionality between directivity and gain, on account of the relation: $G_{\max} = \eta_{rad} \cdot D_{\max}$. Thus, special attention must be paid to the added losses in the design of any kind of matching or tuning network for an ESA. Therefore, any lossy material, lossy reactive element, or resistive equalization included to fulfill the impedance matching of an ESA will degrade the radiation efficiency.

2.5 Passive Impedance Matching Constraints

Considering the aforementioned characteristics of ESAs, a statement can be claimed regarding that as the antennas reduce in size, the bandwidth tends to be narrower and the gain and the efficiency will degrade. Then, the question is: how small can an antenna be designed while still being practical? From the radiation point of view, J. D. Kraus [26] showed that a small antenna could have an effective aperture as high as 98 percent of that of a half-wave dipole antenna, if the antenna could perfectly match the load. In fact, for both short dipoles and small loops,

the directivity remains at 1.5 as the dimensions decrease. It suggests that any ESA can transmit/receive almost the same amount of power (only a small percent less) as a half-wavelength dipole does. In other words, there would seem to be no limitation in reducing the antenna size so far as the antenna could be perfectly matched.

It is precisely at this point where the big challenge rises up, the perfect matching is impossible when an antenna becomes extremely small, because it is well known that large capacitive reactance in short dipoles and large inductive reactance in small loops are hard to match. In addition, losses existing in the antenna and the matching circuit will exceed the radiation resistance, resulting in a significant reduction of the effective aperture, that corresponds to a reduction of the radiation power and degradation of the radiation efficiency.

Figure 2.12: Roberto Mario Fano (1917-2016). Remarkable Professor and IEEE Fellow.

The performance of a passive impedance MN is intimately bounded up to the antenna input impedance (Z_a) behavior with the frequency. Z_a becomes the load to the matching network itself (in the conventional cascade/series approach). If the intended design comprises a small dipole-type antenna, the input impedance can be modeled as a series connection of a resistor and a capacitor, as depicted in Fig. 2.13a. If a lossless passive MN is used, there is a fundamental Gain-Bandwidth constraint limit derived by H. Bode [11] and complemented by R.M. Fano [12] (see Fig. 2.12), and years later by Youla [16]. This limit states a relation between a purely resistive generator and a complex and arbitrary passive load. Given a maximum reflection coefficient magnitude, Bode-Fano integral criterion can be expressed as the Gain-Bandwidth restriction on the load within a flat pass-band. In others words, there is a tradeoff between the achievable bandwidth and the maximum tolerable reflection coefficient magnitude. The analytical expression, for the small dipole (series RC circuit), is [34]:

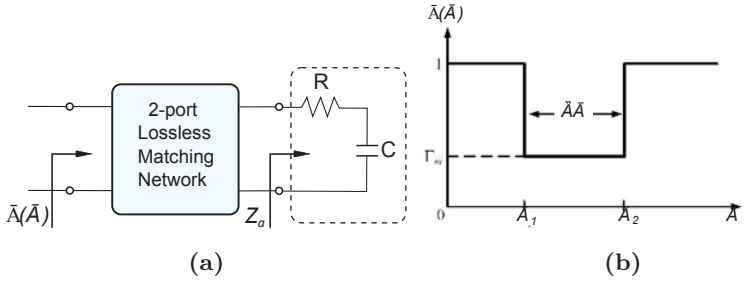

Figure 2.13: (a) Small dipole-like model loading a lossless MN. (b) A possible response for $\Gamma(\omega)$, within a limited band $\Delta\omega$, given the value Γ_m for a series passive RC [34].

$$\int_0^\infty \frac{1}{\omega^2} \ln \frac{1}{|\Gamma(\omega)|} d\omega < \pi RC. \tag{2.34}$$

Once the maximum reflection coefficient magnitude is established, the bandwidth is limited, and vice versa. Figure 2.13b shows this maximum tolerable reflection coefficient, Γ_m, over the bandwidth $\Delta\omega = \omega_2 - \omega_1$, which is governed by the Bode-Fano limit. A mathematical expression for the limit can now be written as [34]:

$$\int_{\omega_1}^{\omega_2} \frac{1}{\omega^2} \ln \frac{1}{|\Gamma_m|} d\omega = \Delta\omega \ln \frac{1}{|\Gamma_m|} \leq \pi \omega_0^2 RC, \tag{2.35}$$

where ω_0 is the central frequency of the band of interest.

If the quality factor $Q_a = 1/(\omega RC)$, associated with the antenna model in Fig. 2.13a, is included in (2.35), it is possible to re-write this expression as:

$$\Delta\omega \ln \frac{1}{|\Gamma_m|} \leq \pi \omega_0 / Q_a. \tag{2.36}$$

It is clear that a smaller Q factor results in a larger achievable bandwidth. On the other hand, antenna miniaturization implies, as expected, further limitations on the reflection coefficient, within the intended band.

A simplification of (2.36) lead us to a more convenient expression:

$$\exp\left(\frac{-\pi\omega_0}{\Delta\omega Q_a}\right) \leq |\Gamma_m| \tag{2.37}$$

This equation demonstrates that the allowable reflection coefficient can be lowered at the expense of the smaller bandwidth.

The equality in (2.35) can be satisfied by ideally including infinite lossless sections in the matching network (MN). This fact leads, for example, to a Bandwidth Improvement Factor (BWIF) of 3.8128, once added the MN, if $|\Gamma_m|$ is intended to be 0.33 (VSWR = 2). Nonetheless, when including three sections of lossless reactive components, the BWIF reaches an acceptable value of 3.1435 [2]. Hansen in [35], complementing the Bode's theory, introduced a useful expression to calculate the BWIF in terms of Γ (or VSWR by using (2.30)), as follows:

$$BWIF = \frac{1-\Gamma^2}{2\Gamma}\frac{\pi}{\ln(1/\Gamma)}. \tag{2.38}$$

This last estimation for the improvement in bandwidth by the action of a multi-section MN does not take into account the introduced losses, unavoidable in real applications, but provides the designer with some theoretical criteria to be considered when a ESA is to be performed.

2.6 Impedance Matching Using Active & non-Foster Networks

In this section, the most relevant characteristics and the evolution of the concept of active matching applied for antennas is presented. The two most important approaches are described as well as some relevant work reported in the literature.

As described in the previous section, because of the natural constraints associated with their small size relative to their operating wavelength, the impedance bandwidths associated with the most common

ESA structures are quite limited [13, 17]. Nevertheless, if it were possible, it would be highly desirable to achieve an ESA design working over a wide instantaneous frequency interval, even when this task might imply the use of active devices.

The main idea of adding active devices to a MN for an ESA is to expand the impedance bandwidth of the antenna as much as possible, beyond the bandwidth limits mentioned before, while maintaining the fundamental performance expected from an antenna. Thus, besides the intended wide impedance bandwidth, other basics characteristics such as a practical gain value, a practical radiation pattern, and a moderate difficulty in manufacturing, among others, are preferred. There are two different approaches to carry out an active MN in ESAs: the tunable realization and the non-Foster MN addition. Each of these approaches can be implemented in two ways: embedded into the antenna structure or in series/parallel configuration at the feed point of it. It is precisely the embedded alternative the one developed in the most part of this work.

In the first approach, the impedance matching of the ESA have exploited the tunability property of the antenna itself to perform it as a *tunable antenna*, by means of some reconfigurable technology. For this purpose, variable reactances —like varactor diodes— or a metamaterial particle with the possibility of varying its shape or size have been used. Those inclusions compensate the reactive part of the antenna impedance, at a certain frequency, and modify the radiating element response. It is worth noting that tunability —or reconfigurability— can be applied to the frequency of operation, direction of the main beam, beamwidth, and in general to one or more of the antenna parameters [36, 37].

In fact, the tunability property in an ESA is often checked out as a preliminary stage of an active non-Foster MN design process, the second approach mentioned above, especially in cases where the non-Foster circuit (NFC) is intended to be embedded in the antenna structure. In those cases, the tunability is checked with the purpose of observing the antenna response to a change in the reactance/susceptance, at the selected point where the active non-Foster form is going to be connected. By using this technique, it is possible to prove, in an experimental way, the need for a non-Foster element to compensate the antenna reactance

over a significant frequency range [36, 38]. This fact leads us to a more interesting alternative: the non-Foster implementation.

In this second approach, a variety of active circuits, called Negative Impedance Converters (NICs), have been used as a smart alternative to tackle the narrowband problem in ESA impedance matching. These circuits where first proposed in the 1950's by Linvill [19], but only have been widely studied and applied to ESAs in the last years, as it will be shown later. The behavior of the reactance presented by the NIC versus the frequency —its negative slope— is the cornerstone in developing non-Foster MNs and applying them to match ESAs. Many authors have reported encouraging results by placing the NFC in the antenna feed point [39–41]. Some others have reported practical designs by embedding the NFC in the radiating element itself, well in a printed or planar ESA [42, 43], well in a near-field structure or parasitic [38, 44], or in some ground plate or chassis containing the radiating element [45, 46].

Embedded or not, when an active non-Foster element acting as impedance MN is added to an ESA, the basic idea remains as to overcome the bandwidth restrictions of passive matching. These restrictions are evidenced even when reconfigurable technologies are used, as it will be shown below. Thus, the non-Foster MN approach stands for a way of achieving wide instantaneous bandwidths in size-limited applications.

2.6.1 Tunable Antennas Technique

The tunable-antenna approach takes advantage of one important property in some radiating structures: frequency agility (or tunability). Tunability consist of obtaining additional narrow bands (even additional radiating modes) by including variable reactances or by modifying other parameters such as physical dimensions, substrate permeability or substrate permittivity. Most of the reported work have been carried out utilizing varactor-type diodes inserted in the antenna itself [36], or in some parasitic [47] or metamaterial inclusion [48]. In many other cases frequency-agile antennas using varactors have been proposed including PIFAs [49–51], planar monopoles [36], slot dipoles [52], slot rings [53], printed bow-ties [54] or quasi-Yagi [55], among others, making the varactor one of the most versatile devices for implementing frequency agility.

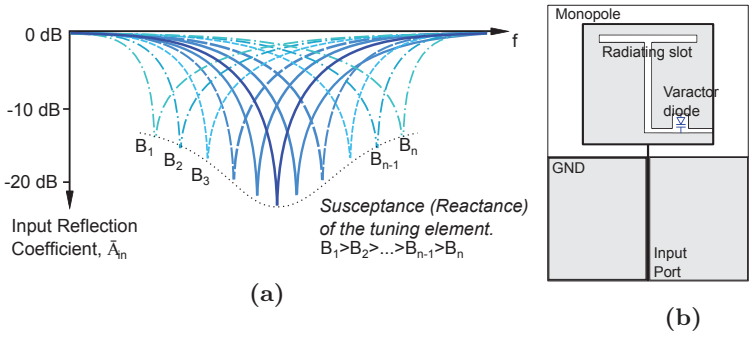

Figure 2.14: (a) Frequency agility characteristic at the antenna input (Γ_{in}) for different susceptance values of the tunning-element. (b) Printed monopole antenna sketch, with a varactor diode as tunning element [36].

It is worth mentioning other reconfigurability approaches, where switching elements are involved —Metal-Oxide-Semiconductor Field Effect Transistor (MOSFET)s, Micro-electromechanical Systems (MEMS) switches, or Positive-Intrinsic-Negative Semiconductor (PIN) diodes— in order to reconfigure the antenna structure itself, for example by extending the length or some internal conductor or radiating cavity [56]. Unlike these last types, tunable antennas try to perform a tuning process dependent on a single parameter (e.g. varactor's control voltage), allowing a non-discretized number of possible inserted narrow bands. Further specific characteristics as well as a review of the various methods for designing frequency agile antennas is presented in [57].

The underlying idea in designing tunable antennas, in terms of impedance matching, is depicted in Fig. 2.14, [36]. In most cases, especially when the intended added narrowband operates at lower frequencies at which the antenna is an ESA, an additional radiating mechanism is needed. For the monopole in Fig. 2.14b, there is a new scheme for the uniplanar feeding of the inset slot radiator. This type of feeding is made possible by loading the slot with a series capacitor —a varactor diode. In turn, by tuning the value of this capacitance, it is possible to tune the resonant frequency of the entire structure, at the lower band, and the antenna can be made frequency-reconfigurable.

At this point, one interesting phenomenon arises, when the suscep-

tance associated to the variable capacitor is analyzed, a decreasing behavior is observed as the frequency increases. This is the experimental confirmation of the non-Foster nature of the admittance needed to match the antenna all along the tuning range, which shall be placed at the slot. As the needed susceptance decreases with frequency, according to the relations $B_1 > B_2, ..., B_{n-1} > B_n$ in Fig. 2.14a, a regular passive capacitor cannot fulfill the reactance compensation because its susceptance function, $B = \omega C$, is directly proportional to the frequency. Thus, only a *negative capacitor* would show the observed non-Foster behavior. Then, the non-Foster susceptance should be $B_{\text{NF}} = \omega C_{\text{NF}} = -\omega C$. Identical phenomenon is observed in a magnetic-type ESA, like a small loop, where the reactance needed to match the antenna has a negative-slope inductive nature, implying the necessity of implementing a *negative inductor*, with a reactance function given by $X_{\text{NF}} = j\omega L_{\text{NF}} = -j\omega L$.

Among the limitations of tunable antennas, it can be mentioned their losses and the non-linearity introduced by the tuning devices. As mentioned above, some authors carry out a tunable antenna design as a previous stage for applying a non-Foster MN, replacing the reactance-variable element for a NFC which presents the same behavior of reactance versus frequency.

2.6.2 Non-Foster Impedance Matching: Concept

As mentioned before, in cases where the application demands a broad instantaneous bandwidth, the tunable approach does not fit this requirement. Then, a new dimension for ESA design field relies in the use of non-Foster circuits, whose application arises from the necessity to overcome the limitations in broad bandwidth matching shown in previous sections.

The very basic idea of non-Foster matching for an electrically small antenna is illustrated in Figs. 2.15(a, b). Figure 2.15a shows the conventional first-order passive-matching approach, which looks for canceling the reactive part of the load to reach the condition of resonance ($\text{Im}\{Z_{\text{IN}}\} = 0$) at a unique frequency. In this first example, the load consists of a mathematical model of a monopole-like ESA, as the one depicted in the upper part of Fig. 2.15a. The single frequency of resonance occurs when the resultant reactance (dash-dotted blue curve)

equals zero in the frequency domain in Fig. 2.15a. On the other hand, the non-Foster MN approach looks for compensating the load reactance, not only at one frequency but over a wide frequency range, leading to the possibility of broadband impedance matching. In theory, this *broadband resonance* can be implemented independently on the nature of the antenna impedance. Such condition can be reached, as depicted in Fig. 2.15b, for all the frequencies within the interval where the resultant reactance equals zero (dash-dotted blue curve) due to the non-Foster nature of the *negative capacitor* —the active MN— connected at the input port of the ESA model.

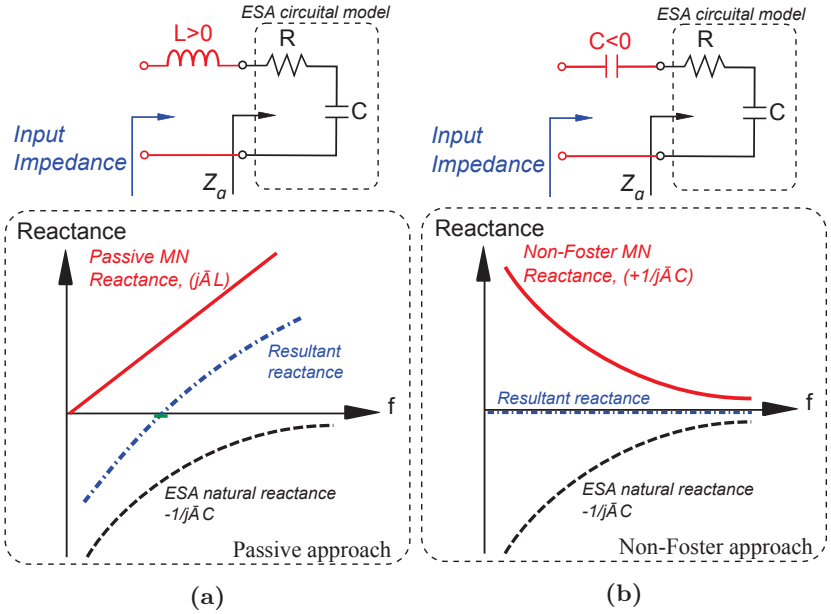

Figure 2.15: Reactance response of the input impedance for (a) a conventional passive matching network, and (b) a Non-Foster matching network, connected to a small dipole model.

In the case of ESAs with a magnetic nature, the non-Foster MN strategy can also be applied, but by means of a *negative inductor*. Thus, the added reactance shall be $X_{NF} = -\omega L$, compensating the positive one of the antenna, $X_{\text{ant}} = \omega L_{\text{ant}}$.

Once an ideal non-Foster matching network is connected to the an-

tenna, the overall input reflection coefficient (see Fig. 2.15b) will be mapped over the horizontal axis in the Smith chart, leading to a possibly conjugate matching between the generator and the antenna, provided equality in their impedance resistive parts, and therefore, the maximum power transfer to the antenna [34]. It is important to note that the inclusion of an ideal non-Foster matching network itself does not imply maximum power transfer to the antenna, however, this can be partially fulfilled by matching two different resistive parts only, then an improvement in the antenna gain and total efficiency can be expected afterward.

2.6.3 Foster's Reactance Theorem and non-Foster Elements

Foster's reactance theorem [18] is a consequence of the conservation of energy principle. It states that for a lossless passive two-terminal device, the slope of its reactance (and susceptance) plotted versus frequency must be strictly positive. In other words, the frequency derivatives of both the reactance and the susceptance are related to the total stored energy, and therefore, are positive, i.e.:

$$\frac{\partial X(\omega)}{\partial \omega} > 0 \qquad and \qquad \frac{\partial B(\omega)}{\partial \omega} > 0. \tag{2.39}$$

Now, by using the conventional definition that defines an *active device* as the one that is capable of providing power gain, or those which needs an external power supply to fulfill its function in a circuit while generating noise other than thermal [34], it is possible to state a definition for *passive device* that will be useful to explain the Foster's reactance theorem.

A device is called *passive* if it is not connected to a power supply, other than the signal source, and do not need that power supply for operating properly. Such a device (considered also as a one-port network) can be realized by resistors, ideal inductors, ideal capacitors, or a combination thereof. It turns out that a corollary that follows from Foster's reactance theorem is even more important than the theorem itself [58]. The corollary states that the poles and zeros of the reactance (and susceptance) function must alternate with the increase of frequency. We

can generalize this corollary of Foster's reactance theorem to state the following consequences about immittance functions (impedance or admittance), for a one-port network comprising passive lumped elements:

1. The immittance function can be written as the ratio of two polynomial functions of the Laplace variable $s = \sigma + j\omega$:

$$Z(s) = \frac{N(s)}{D(s)}. \tag{2.40}$$

2. The coefficients of the polynomials $N(s)$ and $D(s)$ are positive and real.

3. The difference in the orders of $N(s)$ and $D(s)$ is either zero or 1.

A simple capacitor and a series RLC circuit can be used as examples of the above. For the capacitor, the impedance function is given by:

$$Z(s) = \frac{1}{sC}, \tag{2.41}$$

and for a series RLC circuit, the impedance function is given by:

$$Z(s) = R + sL + \frac{1}{sC} = \frac{s^2LC + sRC + 1}{sC}. \tag{2.42}$$

If a two-terminal device has an impedance function that does not obey any of the three consequences of Foster's reactance theorem listed above, is called a "non-Foster" element. A non-Foster element must be an active component in the sense that it consumes energy from a power supply other than the signal source. The basic two non-Foster elements are the *negative capacitor* and the *negative inductor*, which violate the second consequence listed above.

A.) *Negative capacitor.* The impedance function of a negative capacitor of value -C (with $C > 0$) is:

$$Z(s) = \frac{-1}{sC}. \tag{2.43}$$

B) *Negative inductor*. The impedance function of a negative inductor of value -L (with $L > 0$) is:

$$Z(s) = -sL. \tag{2.44}$$

As a result, two important characteristics of the non-Foster networks, that make them attractive for several applications, can be written as:

- The negative slope (or rate of change) of its reactance or susceptance response as frequency increases.

- The counter-clockwise direction of its reflection coefficient (Γ) locus in the Smith chart, with increasing frequency.

2.7 Transistor-based Non-Foster Elements: Realizations

2.7.1 Negative Impedance Converters (NICs)

As aforementioned, performing a non-foster impedance implies the use of active components, such as transistors or, less commonly used, Resonant-Tunneling Diodes (RTD) [59, 60], configured in a variety of topologies that allow a negated version of the loading element: a conventional resistor, an inductor, a capacitor, or a combination thereof. Such attributes have let them take the name of *Negative Impedance Converters*, NICs. The first circuit topology devised for a NIC is attributed to M. Latour about the year 1920, as mentioned in [61]. In fact, is Merrill in 1951 [61] who performed a practical negative impedance converted, based on vacuum tubes, called negative impedance repeater, to increase transmission gains on telephone lines. Afterward, in 1953 Linvill [19] presented the first practical NIC comprised of solid-state devices (i.e.

transistors). Linvill designed some versions of both balanced and unbalanced voltage inversion NICs, implementing a negative resistance. He also stated relevant considerations on stability conditions of NICs, including concepts that are still used in nowadays designs.

Additional experimental results were presented by Larky [62] and Yanagisawa [21] whose topologies carried out, unlike the Linvill's, a current inversion configuration, as will be shown later. It is worth mentioning that there have been many proposed NIC topologies [63,64], but just a few percent have been implemented in practice, as stable prototypes, to be applied in microwaves circuits. This confirms the presumption of difficulty in developing this kind of circuits.

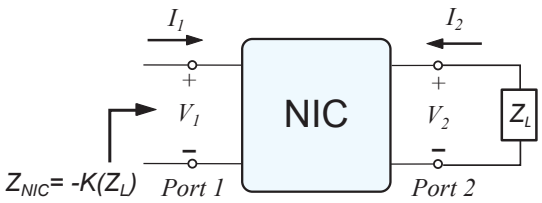

Figure 2.16: Scheme of an ideal NIC.

A NIC can be understood as a two-port network, as can be seen in Fig. 2.16, in which the input current (voltage) equals the output current (voltage), and the input voltage (current) equals the negative of the output voltage (current), with the purpose of presenting, at one input port, a negated version of the impedance loading the other port. Then, an impedance behavior that disobey the Foster theorem for passive circuit elements, is eventually possible. In an ideal NIC, the constant K, in Fig. 2.16, is positive and real.

In order to describe concisely the properties of a NIC, the hybrid h-parameters of a two-port network are used, as shown in Fig. 2.17 [65], where the network under study can be represented by two dependent sources. The first one, on the port 1 side, is a voltage source ($h_{12}V_2$) whose value depends on the output voltage, at port 2. This voltage source is connected in series with the h_{11} parameter, which is also known as the short-circuit input impedance [66]. On the output side, the model shows a dependent current source, $h_{21}I_1$, whose value depends on the input current at port 1 (I_1), in parallel with the h_{22} parameter. This

latter is also known as the open-circuit output admittance. The term h_{12} is also known as the open-circuit reverse voltage gain, and the h_{21} as the short-circuit forward current gain.

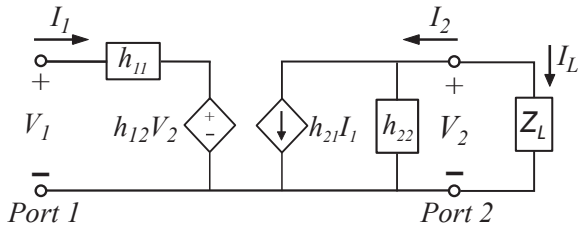

Figure 2.17: h-parameter model for and ideal NIC characterization, with an arbitrary load Z_L.

The conventional notation for the h-parameters is as follows:

$$V_1 = h_{11}I_1 + h_{12}V_2, \tag{2.45}$$

$$I_2 = h_{21}I_1 + h_{22}V_2, \tag{2.46}$$

where

$$h_{11} = \left.\frac{V_1}{I_1}\right|_{V_2=0} \qquad h_{12} = \left.\frac{V_1}{V_2}\right|_{I_1=0} \qquad h_{21} = \left.\frac{I_2}{I_1}\right|_{V_2=0} \qquad h_{22} = \left.\frac{I_2}{V_2}\right|_{I_1=0}.$$

Then, from the circuit shown in Fig. 2.17, it can be stated that $V_2 = Z_L(-I_2)$, and provided that Z_L is connected at port 2, the input impedance (looking into the port-1) is given by

$$Z_{\text{IN}} = \frac{V_1}{I_1} = h_{11} - \frac{h_{21}h_{12}Z_L}{1 + h_{22}Z_L}, \tag{2.47}$$

where the product $h_{21}h_{12}$ is designated as the parameter K, mentioned above, and referred to as the conversion ratio. If the ideal relation, $Z_{\text{IN}} = -Z_L$, is intended; the following equalities had to be satisfied:

$$h_{11} = h_{22} = 0, \qquad h_{21}h_{12} = 1. \tag{2.48}$$

Depending on whether voltage or current inversion occurs, the NIC can be classified into two types, verified through the sign of both h_{21} and h_{12} parameters, as voltage inversion or current inversion.

The **voltage inversion** occurs when both h_{12} and h_{21} are -1, provided the ideal condition: $h_{11} = h_{22} = 0$, then, (2.45) and (2.46) become:

$$V_1 = -V_2 \qquad I_1 = -I_2. \tag{2.49}$$

Hence, at port 1, we can relate voltage and current as

$$V_1 = -I_L Z_L \quad I_1 = I_L,$$

so, the input impedance (at port 1) is

$$\frac{V_1}{I_1} = \frac{-I_L Z_L}{I_L} = -Z_L. \tag{2.50}$$

As can be observed, both the input and the load currents have the same direction, unlike the voltage, which polarity across the NIC is inverted. The h-parameter matrix, $[H]$, in this case is given by

$$[H_{\text{Vinv}}] = \begin{bmatrix} h_{11} & h_{12} \\ h_{21} & h_{22} \end{bmatrix} = \begin{bmatrix} 0 & -1 \\ -1 & 0 \end{bmatrix}$$

On the other hand, the **current inversion** occurs when both h_{12} and h_{21} are 1, provided again the ideal condition: $h_{11} = h_{22} = 0$, then (2.45) and (2.46) become:

$$V_1 = V_2 \qquad I_1 = I_2. \tag{2.51}$$

Hence, at port 1, we can relate voltage and current as

$$I_1 = -I_L,$$

so, the input impedance is

$$\frac{V_1}{I_1} = \frac{I_L Z_L}{-I_L} = -Z_L. \tag{2.52}$$

In this case, the voltage at port 1 is the same as the voltage across Z_L (see Fig. 2.17), while the directions of the input current and I_L are opposed. The $[H]$ matrix in this case is given by

$$[H_{\text{Iinv}}] = \begin{bmatrix} h_{11} & h_{12} \\ h_{21} & h_{22} \end{bmatrix} = \begin{bmatrix} 0 & 1 \\ 1 & 0 \end{bmatrix}$$

Thus far, an idealized model for analyzing the principle of operation of a NIC has been presented. Nonetheless, in a more realistic sense, the most part of the reported NIC topologies comprise more than one active device, at least two transistors, to be specific. In [64], a catalog of all known two-transistor NIC designs is presented.

The principle of operation of a NIC, configured in one of the earlier topologies by using two cross-coupled Bipolar Junction Transistors (BJT), is shown in Fig. 2.18a. The red arrows showing V_{be} (base to emitter voltage), and blue arrows showing I_{ce} (collector current) generate an impedance $Z_{\text{NIC}} = -Z_L$, as seen across emitter terminals. This phenomenon is possible due to a voltage inversion at the load impedance (Z_L) terminals, which is opposed to the conventional current flux for a passive element. The sketched NIC became a very appropriate option for active non-Foster MNs in the feeding-point connection approach, described before, since it can implement a *floating NIC* to be connected in series to the ESA feed point, as it is shown in Fig. 2.18b.

For a NIC to operate, according to the current/voltage inversion principle described above, its transistors must be connected in a positive feedback configuration. This condition, according to the amplifiers basics

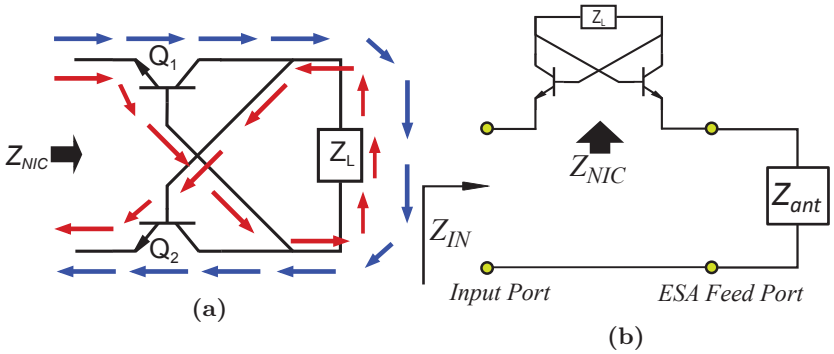

Figure 2.18: (a) Basic NIC sketch showing V_{be} (red arrows) and I_{ce} (blue arrows) [40]. (b) Typical active MN, in series and floating configuration, following the feed-point approach [39].

rules, can derive in several stability issues and makes NICs conditionally stable structures [11].

With the sake of completeness, two classical topologies in the reported work, one of each type of NICs —voltage and current inversion types— are represented in Figs. 2.19(a, b). Both of them are configured as a *grounded NIC* since the load impedance, Z_L, is connected to the ground node. Figure 2.19a shows the topology proposed by Linvill [19], where input impedance of the NIC, Z_{NIC}, is ideally $-(R_2/R_1)Z_L$. Figure 2.19b shows a current inversion type NIC, proposed by Larky [62], where Z_{IN} is expected to be $-(R_1/R_2)Z_L$.

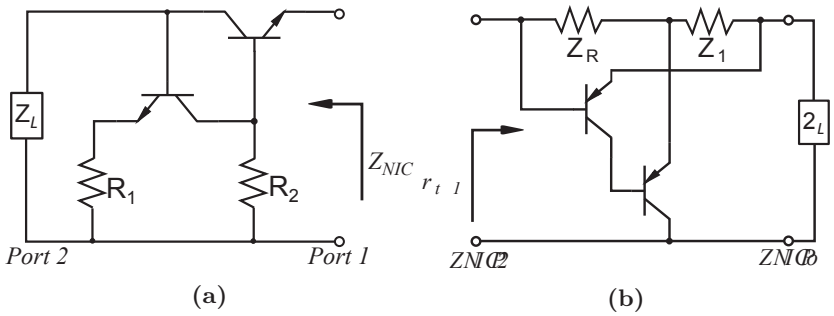

Figure 2.19: Classical topologies for (a) Linvill's voltage inversion NIC, and (b) Larky's current inversion NIC.

2.7.2 Negative Impedance Inverters (NIIs)

It is worth mentioning another useful and versatile kind of non-Foster devices: the Negative Impedance Inverter (NII), which has not been explored as widely as its dual-part —and predecessor— the NIC. NIIs are also named with the acronym *NIV* by some authors [20]. Referring to Fig. 2.20a, when an ideal NII is terminated at one port with a load impedance, Z_L, the input impedance at the other port, Z_{NII}, is the negative and inversely proportional version of Z_L, as follows

$$Z_{\text{NII}} = -K/Z_L = -KY_L, \tag{2.53}$$

where $K > 0$ (ideally $K = 1$). Hence, the input impedance Z_{IN} results in the negative dual of Z_L, so the NII realizes negative network elements in a dual way as the NIC does.

Nonetheless, a general description of the NII operation can be summarized as follows. With a variant in the relation between immittance at the input and the output port, with respect to the conventional NIC shown above, the basic block-diagram of a NII is depicted in Fig. 2.20a. For convenience, a two-port Z-parameter model can be extracted for characterizing an ideal NII, as shown in Fig. 2.20b. The model equation is given by:

$$V_1 = z_{11}I_1 + z_{12}I_2, \tag{2.54}$$

$$V_2 = z_{21}I_1 + z_{22}I_2, \tag{2.55}$$

where:

$$z_{11} = \left.\frac{V_1}{I_1}\right|_{I_2=0}, \quad z_{12} = \left.\frac{V_1}{I_2}\right|_{I_1=0}, \quad z_{21} = \left.\frac{V_2}{I_1}\right|_{I_2=0}, \quad z_{22} = \left.\frac{V_2}{I_2}\right|_{I_1=0}.$$

In a similar way as with the NIC, it is possible to describe a NII in terms of these Z-parameters. Then, the input impedance, Z_{NII} (looking into the port-1), can be expressed as:

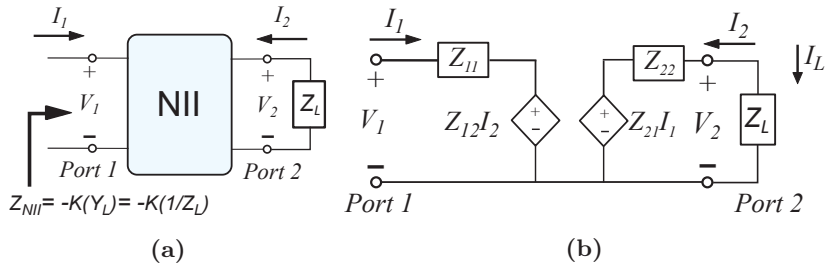

Figure 2.20: (a) Overview of an ideal NII. (b) Z-parameter model for a two-port network loaded with a load Z_L.

$$Z_{\text{NII}} = Z_{\text{IN}} = \frac{V_1}{I_1} = z_{11} - \frac{z_{21}z_{12}}{Z_L + z_{22}}. \tag{2.56}$$

Provided the ideal conditions: $z_{11} = z_{22} = 0$ and $z_{12}z_{21} = K$, the relation: $Z_{\text{NII}} = -KY_L$ with $K > 0$, shown in Fig. 2.20a, can be satisfied. Unlike NICs, the NII cannot be generally divided into a voltage or a current inversion because the property of a NII is different depending on the load (Z_L) and the sign of z_{12} and z_{21}. If a resistor is connected to the port 2, in Fig. 2.20a, the simultaneous sign of z_{12} and z_{21} can lead to a current inversion, when both equal -1, or to a voltage inversion when both z_{12} and z_{21} are positive unity. For practical applications, Z_L is commonly a reactive element, then, the sign of the impedance phase at the port 1 is not changed, relative to that at port 2, due to the fact that the NII negates the corresponding load admittance.

Figure 2.21 shows a classical NII topology, proposed in [23]. The circuit consist of two Field Effect Transistor (FET) whose drain and gate terminals are connected in a positive feedback loop. The load Z_L could be either a capacitor or an inductor. If Z_L consist in an inductor, a negative capacitor will be obtained at the input, while if Z_L is a capacitor, the obtained element will be a negative inductor.

The small signal equivalent circuit is shown in the Fig. 2.22 so that, it can be divided in two sub-circuits to be analyzed, as the ones shown in Fig. 2.23.

Some relations can be easily obtained from the sub-circuits in Fig.

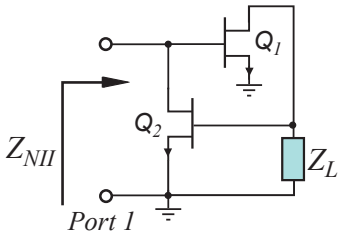

Figure 2.21: Grounded NII based on FET transistors, proposed by Kolev in [67].

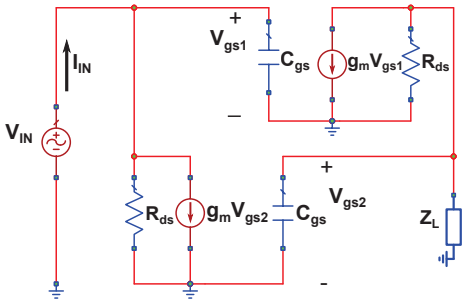

Figure 2.22: Kolev's NII small signal model.

2.23, respectively in (2.57) and (2.58).

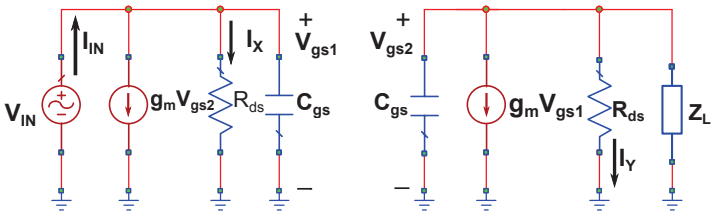

Figure 2.23: Kolev's NII small signal model, after divided in two sub-circuits.

From the first sub-circuit in Fig. 2.23, it is possible to relate V_{IN} and I_{IN} with V_{gs2}

$$V_{\text{IN}} = I_x R_{ds} = \left(I_{\text{IN}} - \frac{V_{gs1}}{Z_{cgs}} - g_m V_{gs2} \right) R_{ds}.$$

Assuming $V_{gs1} = V_{\mathrm{T}}$, in some point in the active region of the FET, then

$$V_{\mathrm{IN}} = \left(I_{\mathrm{IN}} - \frac{V_{\mathrm{T}}}{Z_{cgs}} - g_m V_{gs2} \right) R_{ds}. \tag{2.57}$$

From the second sub-circuit in Fig. 2.23,

$$\begin{aligned} V_{gs2} = I_y R_{ds} &= \left(\frac{-V_{gs2}}{Z_{cgs}} - g_m V_{gs1} - \frac{V_{gs2}}{Z_L} \right) R_{ds} \\ \rightarrow V_{gs2} &\left(1 + \frac{R_{ds}}{Z_{cgs}} + \frac{R_{ds}}{Z_L} \right) = -g_m V_{\mathrm{IN}} R_{ds}, \end{aligned}$$

then

$$\frac{V_{gs2}}{V_{\mathrm{IN}}} = \frac{-g_m R_{ds}}{\left(1 + \frac{R_{ds}}{Z_{cgs}} + \frac{R_{ds}}{Z_L} \right)}. \tag{2.58}$$

Now, combining (2.57) and (2.58)

$$\begin{aligned} V_{\mathrm{IN}} &= I_{\mathrm{IN}} R_{ds} - \frac{V_{\mathrm{IN}} R_{ds}}{Z_{cgs}} + \frac{(g_m R_{ds})^2}{\left(1 + \frac{R_{ds}}{Z_{cgs}} + \frac{R_{ds}}{Z_L} \right)} V_{\mathrm{IN}} \\ V_{\mathrm{IN}} &\left(1 + \frac{R_{ds}}{Z_{cgs}} - \frac{(g_m R_{ds})^2}{1 + \frac{R_{ds}}{Z_{cgs}} + \frac{R_{ds}}{Z_L}} \right) = I_{\mathrm{IN}} R_{ds}. \end{aligned} \tag{2.59}$$

Finally, the obtained input impedance is:

$$\begin{aligned} Z_{\mathrm{NII}} = \frac{V_{\mathrm{IN}}}{I_{\mathrm{IN}}} &= \frac{R_{ds}}{1 + \frac{R_{ds}}{Z_{CS}} - \frac{(g_m R_{ds})^2}{\left(1 + \frac{R_{ds}}{Z_{cgs}} + \frac{R_{ds}}{Z_L} \right)}} \\ &= \frac{1}{\frac{1}{R_{ds}} + \frac{1}{Z_{cgs}} + \frac{1}{\frac{-1}{R_{ds} g_m^2} + \frac{-1}{Z_{cgs} g_m^2} + \frac{-1}{Z_L g_m^2}}}. \end{aligned} \tag{2.60}$$

Depending on the nature of Z_L, either a negative inductor or negative capacitor can be obtained. If $Z_L = j\omega L$, Z_{NII} behaves as the circuit in Fig. 2.24, and can be computed as (2.61).

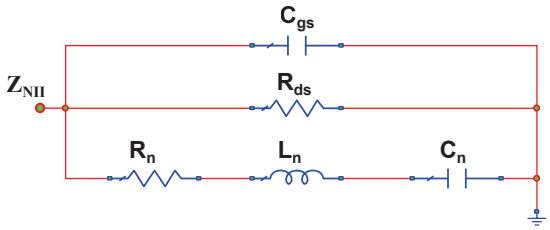

Figure 2.24: Equivalent input impedance of the Kolev's NII model, when Z_L is an inductor.

$$Z_{\text{NII}} = \frac{1}{\frac{1}{R_{ds}} + \frac{1}{Z_{cgs}} + \frac{1}{\frac{-1}{R_{ds}g_m^2} + \frac{-1}{g_m^2}(j\omega C_{gs}) + \frac{-1}{j\omega L g_m^2}}}, \tag{2.61}$$

where

$$R_n = -\frac{1}{g_m^2 R_{ds}};\ L_n = \frac{-C_{gs}}{g_m^2};\ C_n = -g_m^2 L. \tag{2.62}$$

So, the total input impedance can be modeled as

$$Z_{\text{NII}} = -\frac{1}{R_{ds}g_m^2} - j\omega\frac{C_{gs}}{g_m^2} - \frac{1}{j\omega L g_m^2}. \tag{2.63}$$

If the FET is carefully selected, the effect of C_{gs} and R_{ds} can be negligible (at least at low frequencies), and the circuit will work as a series combination of a negative capacitor, proportional to the load inductor L, with a parasitic negative inductor and resistor. These last ones should be compensated with a corresponding series resistor and inductor at the input.

In that way, the response over the operation frequency interval can be approximated as

$$Z_{\text{NII}} \approx -\frac{1}{j\omega L g_m^2} \approx -\left(\frac{1}{g_m^2}\right) Y_L. \tag{2.64}$$

In a similar way, it is possible to model the response of the NII when it is loaded by a capacitor. By using (2.60), and applying the procedure showed before, it can be obtained a negative inductor, whose impedance can be approximated as $Z_{\text{NII}} \approx -j\omega C/g_m^2$.

It is possible to find specific methods for designing NIIs with solid-state circuits, as the one described in [20] as well as several topologies to implement them in [68]. Nonetheless, the similarity in the principle of operation between the NII and the NIC allows the designer to categorize both of them as a key alternative when an active non-Foster element is required.

2.8 Negative Impedance Converters for ESAs

In recent years, NIC applications have been diversified towards targets other than loss compensation or matching networks. These rising applications comprise, among others, filter improvement (e.g. increasing of the Q factor by means of negative resistors) [64], the increase of the voltage range in varactor diodes [23, 67], enhancement of cloaking structures [69], Fast Wave Propagation (FW) in planar technologies [70], performing of thinner high-impedance surfaces [71], increase of the bandwidth of metamaterial structures [72], [44], performing squint-free beams in antenna arrays [73], and so on. Furthermore, the nature of the circuits utilized to implement negative impedances has evolved to include discrete-time signal processing devices, like analog-digital converters (ADCs and DACs), as in the approach proposed in [74]. Much of these work is still ongoing and appear to provide clever alternatives for the near future in microwave systems development.

2.8.1 Cascade and Series Topologies

Small antenna impedance matching has been one of the most active topics in applying negative impedance converters (or inverters). Noteworthy approaches have been performed since the first work presented

by Harris and Myers in 1968 [75]. In that work a transistor-based NIC (comprising both FET and BJT) was connected to the feed point of a couple of small monopoles: a 2.5" (6.35 cm) in height with a 2.5" diameter top hat, and other with 10" (25.4 cm) in height with a 10" diameter top hat, for comparing them with a 16 Foot (4.87 m) untuned whip. None of the antennas had an incorporated ground-plate other than the ground of the test site, which was located 1.8 m below them. The experiment was carried out from 200 KHz to 10 MHz, so the electrical size —for the 2.5" antenna— in terms of the ka factor is from $ka = 2.6{*}10^{-}4$ (at 200 KHz) to $ka = 0.01$ (at 10 MHz). Thus, an important degree of miniaturization was obtained. For the same interval of frequencies, the reference whip antenna presents a ka factor within the interval 0.02 to 1.

The voltage inversion NIC was made by performing an amplifier with a gain $A_v = 2$, as depicted in Fig. 2.25a. The feedback element, Z_L, is precisely the capacitor to be converted, in order to compensate the capacitive nature of the small monopole impedance, modeled as a capacitor in shunt with the radiation conductance (G_{rad}), as depicted in Fig. 2.25b.

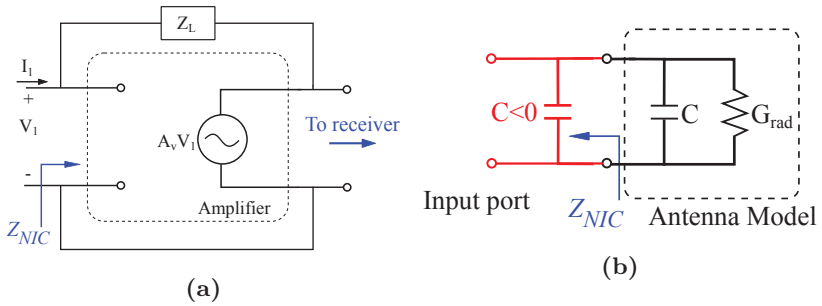

Figure 2.25: (a) NIC scheme used in [75] and (b) its application as a negative capacitor C, connected to a small monopole model.

The input voltage in Fig. 2.25a can be written as:

$$V_1 = I_1 Z_L + A_v V_1, \tag{2.65}$$

then, it is easy to express Z_{NIC} as:

$$Z_{\text{NIC}} = \frac{V_1}{I_1} = \frac{Z_L}{1 - A_v}. \tag{2.66}$$

As mentioned before, if A_v is set equal to 2, then $Z_{\text{NIC}} = -Z_L$, and the ideal impedance conversion is possible. The reported results showed that the antenna gain of the miniature (monopole + NIC) antenna, relative to the reference one (16 Foot whip), is higher for frequencies up to 10 MHz and deteriorates as frequency increase. Some comments about noise were made, pointing that the noise performance of the antenna with a negative capacitor was restricted by external noise rather than by the negative capacitor, for those frequencies ranges where the receiver is "natural noise limited" rather than "device-noise limited", as in the measured frequency range (up to 10 MHz). Some issues regarding linearity of the actively matched antenna were discussed, for different power levels in the receiver signals. As larger power was received at the NIC-loaded antenna, the non-linear effects of the active circuit become severe.

Perry in 1968 [65], also presented fabricated active MNs, connected in shunt with a small monopole, 3" in height (7.62 cm), and compared the results with those of a 12 Foot (3.65 m) untuned whip antenna. He used the term *broadband conjugate impedance matching* to designate the technique of reactance compensation with NICs. Of the three active networks he proposed, two of them utilize Operational Amplifiers (op-amp) as those depicted in Fig. 2.26. Provided two op-amp networks (dotted box in Fig. 2.26), connected as of two inverting amplifiers, the ratio of the output voltage V_2 to the voltage V_1 is:

$$\frac{V_2}{V_1} = \frac{\sqrt{2}R}{R} \cdot \frac{\sqrt{2}R}{R} = 2. \tag{2.67}$$

Therefore, this configuration allows implementing a generator with a voltage gain of 2, in a similar way as with the model in Fig. 2.25a. A second model was developed, based on op-amp was derived from nodal admittance synthesis, with a similar topology to the one shown in Fig. 2.26. One additional active network was implemented which consisted in a current inversion NIC, based on BJT transistors. In spite of the

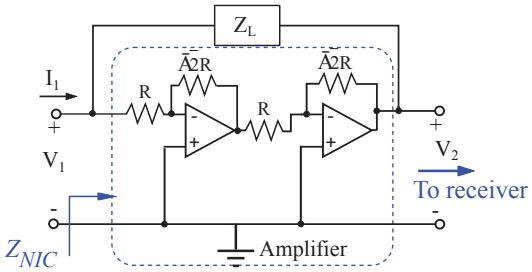

Figure 2.26: Voltage inversion negative impedance converter, based on operational amplifiers, utilized by Perry in [65].

remarkable improvement of the antenna gain with Non-Foster impedance MNs achieved by Perry (up to 35 dB relative to the unloaded whip), the active networks only worked below 5 MHz, and no noise measurements was performed.

A patent by Skahill et al. [76] provides, in addition to the reactance compensation, a frequency-squared transformer NIC that converts the short dipole radiation resistance to a constant value. The negative impedance converter is based on FET transistors.

One more important advance in active MNs for ESAs, was carried out by Sussman-Fort in 2009 [39], summarizing his previous work in [77–80]. He fabricated Non-Foster impedance MNs, working from 20 to 120 MHz, for a 6" (15.2 cm) monopole and a 12" (30.5 cm) dipole antennas and compared them with the unmatched and the passively matched cases. Taking into account the image theory, applied for monopoles, it is possible to state that for both the 6" monopole and the 12" dipole the ka factor is within the interval $[0.06 \sim 0.37]$. Unlike the authors in the previously mentioned work, Sussman-Fort performed negative capacitors connected to the antennas following a series configuration, as depicted in Fig. 2.27a. Provided a small monopole-like antenna and its capacitor-resistor parallel model (as the one depicted in Fig. 2.25b), the series connection of the NIC still compensates the reactive response of the antenna impedance at lower frequencies, while mitigates deterioration in the obtained overall performance at higher frequencies.

By using the balanced Linvill's NICs in [19], comprising BJT tran-

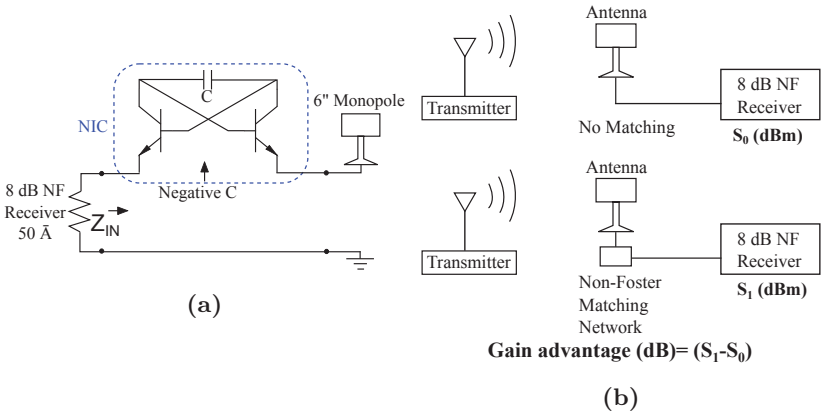

Figure 2.27: (a) Sussman-Fort's series approach for active matching of an ESA. (b) Measurement scheme of the improvement in received signal by using non-Foster matching vs. no matching. [39]

sistors, as shown in Fig. 2.19a, Sussman-Fort performed measurements to find improvement in both antenna gain and SNR from 20 MHz to 120 MHz, when compared to antennas without MNs, in reception. Figure 2.27b shows the scheme used by him to measure the gain and noise. To assess the SNR of a receiving actively matched antenna, he introduced a straightforward method [39]: The received signals of the actively matched antenna, S_1, and the unmatched antenna, S_0, were first recorded. Thus, the difference $S_1 - S_0$ (in dB scale), is the gain improvement due to the active MN.

In a similar way, the noise measurements were performed while the transmitter antenna is turned off. The difference $N_1 - N_0$ (in dB scale) is the added noise of the MN, where N_1 and N_0 are the received signals with and without the active MN, respectively. Therefore, the improvement in SNR can be written as:

$$SNR_{\text{adv.}} = (S_1 - S_0) - (N_1 - N_0). \tag{2.68}$$

The measured improvement ($SNR_{\text{adv.}}$) was within the range 6 to 9 dB, better in lower frequencies. Sussman-Fort claimed that the Op-Amp

alternative to implement non-Foster MN, in the same small monopole, resulted in at least 10 dB more generated noise due to the NIC than with the BJT-based topology. In [80], the highest effective frequency range obtained by means of the active MN, to a 20" x 2" lossy dipole antenna, is from 60 MHz to 400 MHz. It is also shown an antenna gain improvement.

Additionally, his earlier work [77], [81] laid the foundation for non-Foster transmitting matching networks. Besides the design of circuits delivering a few milliwatts to an ESA, were developed both class A- and class B-biased NICs which included a strategy for tackling the high-voltage problem, inherent to transmitting mode in active loaded ESAs. In this sense, it was suggested that a negative LC matching could be applied to an electrically small antenna to mitigate that problem. It was shown that the resonance of the antenna caused by the negative LC network forces to transfer the maximum power to the antenna (for a narrow bandwidth). He also pointed out that the power efficiency —including Direct Current (DC) biasing for transistors— should be taken into account in applications of Non-Foster matching for transmitting antennas. With this idea, class C-biased NICs in [39] were introduced to improve the power efficiency of transmitting antennas, achieving a factor-of-two improvement in power efficiency over the best passive match to an ESA model (at 20 MHz). Across 5% bandwidth, an average signal power of over 1 W can be delivered to the radiation resistance. In spite of the fact that nor the linearity of the active circuits, neither the stability analysis for the prototyped designs were presented in his papers, Sussman-Fort made remarkable contributions to the field of active MN applied to electrically small antennas.

Following the aforementioned results, other authors in [41], [82] and [83] presented active and transistor-based matching networks, connected to the driven point of some canonical small antenna structures (e.g. small monopoles or loops). The effort in these work was mostly focused on the implementation of a stable and fully characterized active MN, more than in studying the performance of the whole antenna system (antenna plus NIC). It is possible to conclude that unavoidable issues arise from the parasitics well in the selected active devices well in the manufacturing technology.

Another worthy contribution to mention was made by O. Tade et al. in 2012 [45], in which an active non-Foster MN was performed and measured, and then, applied to the driving point of a chassis antenna with a base of 50 mm X 50 mm. A customized stability analysis technique was developed and applied to show how to design a NIC for stable operation at frequencies up to 1.5 GHz, using the BFS-17 BJT transistor. Acceptable matching results were reported for the 595 MHz to 1.5 GHz band. It is important to note that the upper bound of operation for the active MN presented by Tade reached 1.5 GHz, unlike all the NIC-based MNs showed thus far, reported to work up to 200 MHz. One possible reason can be the symmetry in the component placing and the carefully designed feedback paths as well as the feed lines used to couple the measured signal.

Linearity measurements were also conducted by Tade, by means of the third order intermodulation product (OIP_3) [45], resulting in a measured OIP_3 comparable with other typical front-end components using similar transistors. A SNR advantage ($SNR_{adv.}$) between 2 dB and 12 dB compared to the resistively equalized passive antenna was also reported. However, because of a disruption on the antenna ground plane (where the active MN is placed) that disturbs the surface current and causes the antenna impedance to change, neither the noise analysis nor the linearity analysis could be undertaken in the proposed antenna. Instead, an additional NIC connected to an equivalent passive circuit, designed to generate the same antenna impedance, was studied. This fact made impractical the initially proposed structure for carrying out the whole antenna performance analysis.

2.8.2 Embedded non-Foster Matching Networks

Subsequently, additional work has been developed and implemented by other authors in the past few years, including clever approaches in sophisticated antenna structures. One of these approaches consists in embedding a non-Foster element into a resonant antenna [38, 42, 44, 84]. These antennas try to eliminate the external MN by substituting the external circuit with an internal one, intrinsically matched to a particular antenna providing a reasonable radiation resistance.

Two different strategies have been followed in this line. The first one

consists on including the non-Foster network inside the antenna itself to obtain a broadband matched antenna. A re-shaping of the current distributions over the antenna structure takes place, as in the work proposed by Mirzaei and Eleftheriades in [42]. Their strategy included a printed and slotted monopole, like the one depicted in Fig. 2.14b, in which the tunability was first checked by means of a variable capacitor —a varactor diode— leading to the synthesis of a non-Foster circuit, needed to obtain broadband matching.

The second one consists on putting the non-Foster network in a parasitic element, that modifies the antenna near-field components, inspired in a metamaterial structure, like the model proposed by Barbuto et al. in [44]. In this sense, other work has been developed by loading a Near-Field Resonant Parasitic (NFRP) with a non-Foster form, as Zhu and Ziolkowski describe in [38] and [84]. In all these works, the design procedure departs from a metamaterial-inspired antenna, followed by the inclusion of a variable reactance (i.e. conventional capacitance or inductance) in order to verify the frequency-agility (or tunability) of the antenna, as mentioned in previous sections. From the frequency-agile antenna, the needed reactance can be fulfilled by the inclusion of a non-Foster MN.

The embedded active MN approach is the one selected to be developed along this work. The fact that the active MN is embedded into the antenna structure allow the designer to use the NIC-loaded ESA in both receiving and transmitting modes, provided the consideration of the high voltage condition in transmitting mode, as mentioned before.

Additionally, it is very important to note that in none of the reported work, where the embedded MN approach was applied, the possibility of exploring the effect of changing the NFC location has been observed. This exploration leads to additional considerations which are part of a complete design strategy for ESAs, actively loaded with non-Foster elements, that will be developed across the subsequent chapters.

CHAPTER 3

EMBEDDED NON-FOSTER MATCHING NETWORKS FOR ESAs

3.1 Introduction

In the previous chapter, the basic idea of active matching for electrically small antennas (ESAs) was described. Thus, by means of the inclusion —or the connection at the feed point— of a non-Foster network, it is possible to achieve broader bandwidths at lower frequencies, compared to the counterpart: the passive lumped matching networks (MNs). It was also shown how active-matching technique has become a very active topic during the last years. Since the passive matching approach in ESAs is strongly limited by the gain-bandwidth constraint — the Bode [11], Fano [12] and Youla [16] criterion— and also by the maximum achievable bandwidth constraint for small-sized antennas — imposed by Wheeler [10], Chu [13] and Thal [17] criteria— all the authors have taken advantage of the reactance properties in non-Foster elements to neutralize the ESA reactance.

In particular, as mentioned earlier, the negative-slope property of the reactance response in non-Foster circuits (NFCs) has been used to emulate the resonance condition in the antenna, not only at one single frequency but over larger bandwidths. In this sense, all the reported

work so far has taken the assumption of a fixed and predictable characteristic of the ESA impedance: its larger reactance and its small resistive part. Additionally, most of the effort has been targeted to design a properly performed NIC to be connected at the feed point of the antenna, without paying any special attention to the location of such active non-Foster network. Even in the cases where a NIC circuit is placed inside the antenna structure, the reported work does not take in mind any consideration about the best possible location for the intended active MN.

Some analytical exploration was carried out by the author, regarding the influence on the needed impedance —to be fulfilled through the active MN— that is produced by changing the location of such active MN, within the antenna structure itself. These explorations derived in finding two crucial parameters related to the non-Foster MN location. First, the sensitivity of the obtained impedance matching —at the antenna input port— due to the difference between the analytical impedance and the one implemented through the non-Foster MN. Second, the realizability of the needed analytical impedance at that point, in terms of quantity of non-Foster elements and its values, to obtain the intended broadband impedance matching.

The two-port antenna approach, first proposed by Koulouridis in [85] and [86], has demonstrated to be a suitable starting point in the strategy to obtain the aforementioned parameters — the sensitivity to the MN location, and the analytical non-Foster impedance— at a certain point. The two-port antenna approach consists of including an additional —and fictitious— port inside the antenna, by means of a Computer-Aided Design (CAD) software suite for full-wave simulation. The idea is to extract some two-port network parameters, for example, the S- or the $ABCD$-parameters matrices. Once the network parameters have been extracted for each two-port combination, according to the number of locations to be analyzed, the analytical procedure takes place. The orientation of the analysis is to control, in somehow, the internal impedance of the network, which is an indicator of how difficult —or even possible— the active impedance matching is going to be. The detailed method will be shown in the subsequent sections.

In other words, the present chapter aims at explaining and analyt-

ically finding a suitable location for the active non-Foster MN into the antenna, by means of the two-port antenna approach. In addition, a one-port antenna using internal MN can also be considered as two-port antenna, where the second port represents the non-Foster circuit. The effects on the antenna performance when changing the position of the NFC, are also investigated. The author introduces a sensitivity parameter in this chapter, which shows the effect on the matched antenna input impedance, associated with the variations of the loading non-Foster impedance. This new parameter has been shown to be critical during the design procedure. Finally, alongside the sensitivity analysis, the type of non-Foster form is also analyzed to take into account the efficiency, and its effect on the radiation pattern.

3.2 Two-Port Antenna Approach for Active Impedance Matching

Treating an antenna as a multiport network is an interesting approach based on simple circuit theory principles [86]. By adding one or more ports to the antenna structure is possible to obtain a multiport microwave device in which one of the ports corresponds to the initial feeding port. Surely, the original input impedance —at the input port— is reproduced by letting all the added ports open circuited. It is possible to relate the antenna impedance, Z_{ant}, with the impedance connected at the fictitious port, Z_{P2}, through the extracted network parameters ([**S**] or [**ABCD**]), as it is shown in Fig. 3.1.

The initial idea tried to internally increase the real part of the antenna impedance to reach, ideally, the system reference value (Z_0). To do so, Koulouridis proposed the use of passive-lumped or possibly negative elements (NFCs). Then, a series non-Foster network is connected outside the antenna, for compensating the remaining antenna's reactance. Nonetheless, no especial attention is paid to the location of the added port-2, and no considerations are given to the possible changes that can occur in the input impedance due to possible changes in such port-2 location either.

Now, as mentioned before, the two-port antenna approach is applied to the active non-Foster matching strategy, presented in this work. The

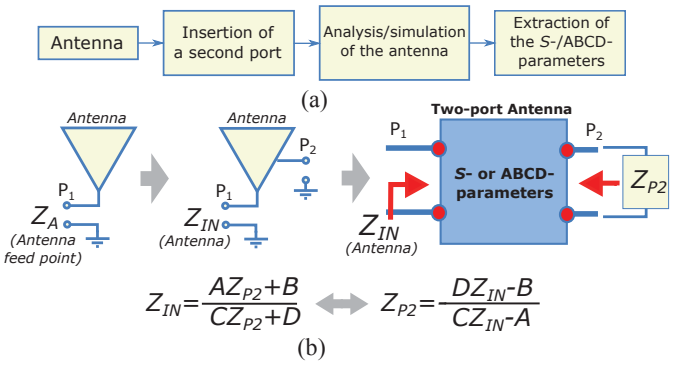

Figure 3.1: (a) Block diagram explaining the two-port antenna approach. (b) The relation between Z_{IN} and Z_L through the $ABCD$-parameters [86].

basic scheme of the active matching for two-port antennas is shown in Fig. 3.2. It consists of loading the introduced analytical port-2 of the antenna with a non-Foster impedance, Z_{NIC} (implemented by the use of a NIC), in such a way that the input impedance at the other port equals some reference value, Z_0. To introduce the fictitious port — generally called *lumped port* or *discrete port* in most electromagnetic CAD simulators— can be added inside the antenna 3D-model. The added excitation can be connected in both a grounded or a floating configuration, according to the nature of the radiating element or some constraints imposed by the application. This procedure is described in more detail throughout the design examples.

It is worth noting that there is no need for a lumped-elements model of the antenna, difficult to extract in practice. The S-parameter matrix can be easily obtained by modeling the structure in an electromagnetic CAD software. This fact facilitates and generalizes the design process to a massive variety of antenna types while takes advantage from the increasing computational power of the actual Personal Computers (PC), and High-Performance Computing (HPC) servers.

The input impedance, Z_{IN}, in Fig. 3.2 is

$$Z_{\text{IN}} = Z_0 \frac{1+\Gamma_{\text{IN}}}{1-\Gamma_{\text{IN}}}. \tag{3.1}$$

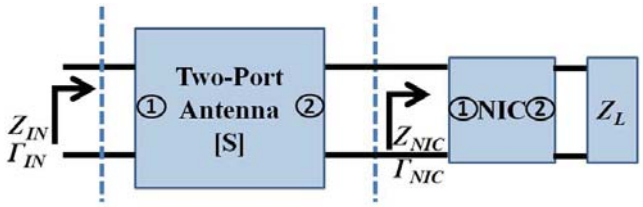

Figure 3.2: Active Matching of Two-Port Antenna.

Then, the reflection coefficient of this loaded two-port network at its input, Γ_{IN}, is given by

$$\Gamma_{\text{IN}} = S_{11} + \frac{S_{12} \cdot S_{21} \cdot \Gamma_{\text{NIC}}}{1 - S_{22} \cdot \Gamma_{\text{NIC}}}. \tag{3.2}$$

Since the goal is to have a matched antenna over a desired bandwidth (theoretically it could be at all the frequencies), the input reflection coefficient should be zero along this bandwidth. After some straightforward calculations and equating (3.2) to zero, we can obtain the optimum and analytical reflection coefficient that the non-Foster network should provide, $\Gamma^{\text{an}}_{\text{NIC}}$, as in (3.3). The superscript "*an*" stands for *analytical* and represents the ideal value or condition that should be meet to obtain the ideal result in the parameter under design.

$$\Gamma^{\text{an}}_{\text{NIC}} = \frac{S_{11}}{S_{22} \cdot S_{11} - S_{12} \cdot S_{21}}. \tag{3.3}$$

Therefore, the non-Foster analytic impedance, $Z^{\text{an}}_{\text{NIC}}$, which is related with the reflection coefficient, Γ^{an}_{NIC}, is given by

$$Z^{\text{an}}_{\text{NIC}} = Z_0 \frac{(1 + \Gamma^{\text{an}}_{\text{NIC}})}{(1 - \Gamma^{\text{an}}_{\text{NIC}})}, \tag{3.4}$$

and can also be expressed in terms of the two-port S-parameters of the antenna as:

$$Z_{\text{NIC}}^{\text{an}} = Z_0 \cdot \left(\frac{S_{22} \cdot S_{11} - S_{12} \cdot S_{21} + S_{11}}{S_{22} \cdot S_{11} - S_{12} \cdot S_{21} - S_{11}} \right). \tag{3.5}$$

When this analytical impedance $Z_{\text{NIC}}^{\text{an}}$ is placed at port-2, the reflection coefficient at port-1, Γ_{IN}, would ideally equal 0 at all frequencies and, hence, large bandwidths can be obtained.

In this point, it is important to note the dependence of $Z_{\text{NIC}}^{\text{an}}$ on the extracted S-parameters, and therefore on frequency as the [**S**] matrix is also a function of frequency. This condition implies a dependence of the input impedance, Z_{IN}, on the S-parameters. This last dependence can be deduced by the relation of Z_{IN} with Γ_{IN} in (3.1), then, in the relation between Γ_{IN} and Γ_{NIC} through (3.2), and finally in the expression of $Z_{\text{NIC}}^{\text{an}}$ in (3.5), in terms of the S-parameters only, which aims at meeting the goal $\Gamma_{\text{IN}} = 0$.

In other words, Z_{IN} is directly related to Z_{NIC}, but this relation can only be observed through the S-parameters calculation —or other network parameters— when the non-Foster matching for two-port antenna approach is used. The role of $Z_{\text{NIC}}^{\text{an}}$ is to assure the matching condition over the intended frequency band, according to the mathematical reasoning shown so far. Thus, the implementation of $Z_{\text{NIC}}^{\text{an}}$ with real circuits is a key factor in this strategy, and some additional consideration which allows us to observe the influence of the differences between the analytical $Z_{\text{NIC}}^{\text{an}}$ and a real NIC impedance is welcome.

3.3 The Sensitivity Parameter *Sens*: Definition

Till now, it has been shown how a zero reflection coefficient at the input port is possible by calculating the impedance $Z_{\text{NIC}}^{\text{an}}$, needed at port-2, only by means of the S-parameters of a simple two-port network. However, due to the fact that the NIC impedance is quite sensitive to parasitics and variations on its load impedance (Z_L in Fig. 3.2) [19], [87], it is also very important to analyze how these changes affect to obtain the goal. Then a new parameter, called *Sens*, can be defined such as the sensitivity of this solution, which is given by

$$\Delta\Gamma_{\text{IN}} = \underbrace{\left.\frac{\partial\Gamma_{\text{IN}}}{\partial\Gamma_{\text{NIC}}}\right|_{\Gamma_{\text{NIC}}=\Gamma_{\text{NIC}}^{\text{an}}}}_{\text{Sensitivity: } Sens} \cdot\Delta\Gamma_{\text{NIC}} = Sens \cdot \Delta\Gamma_{\text{NIC}}. \tag{3.6}$$

This sensitivity parameter provides information about how potential variations in the impedance of the NIC (represented by Γ_{NIC}) with respect to the analytic one, given by (3.3), affect the input reflection coefficient, Γ_{IN}. In order to deduce the expression for *Sens*, we can apply the quotient rule for derivatives in (3.2) as:

$$\frac{\partial\Gamma_{\text{IN}}}{\partial\Gamma_{\text{NIC}}} = \frac{\partial}{\partial\Gamma_{\text{NIC}}}\left(S_{11} + \frac{S_{12}\cdot S_{21}\cdot\Gamma_{\text{NIC}}}{1 - S_{22}\cdot\Gamma_{\text{NIC}}}\right), \tag{3.7}$$

that leads to

$$\begin{aligned}\frac{\partial\Gamma_{\text{IN}}}{\partial\Gamma_{\text{NIC}}} &= \frac{(1 - S_{22}\Gamma_{\text{NIC}})(S_{12}S_{21}) - (S_{12}S_{21}\Gamma_{\text{NIC}})(-S_{22})}{(1 - S_{22}\Gamma_{\text{NIC}})^2} \\ &= \frac{(S_{12}S_{21})(1 - S_{22}\Gamma_{\text{NIC}} + S_{22}\Gamma_{\text{NIC}})}{(1 - S_{22}\Gamma_{\text{NIC}})^2} \\ &= \frac{S_{21}S_{12}}{(1 - S_{22}\Gamma_{\text{NIC}})^2}.\end{aligned}$$

Then, if we evaluate the derivative for $\Gamma_{\text{NIC}} = \Gamma_{\text{NIC}}^{\text{an}}$, and take the absolute value:

$$Sens = \left|\left.\frac{\partial\Gamma_{\text{IN}}}{\partial\Gamma_{\text{NIC}}}\right|\right|_{\Gamma_{\text{NIC}}=\Gamma_{\text{NIC}}^{\text{an}}} = \left|\frac{S_{21}S_{12}}{(1 - S_{22}\Gamma_{\text{NIC}}^{\text{an}})^2}\right|. \tag{3.8}$$

Now, by applying the expression in (3.3) into (3.8), the parameter *Sens* can be obtained as follows

$$
\begin{aligned}
Sens &= \left| \frac{S_{12}S_{21}}{\left(1 - \frac{S_{11}S_{22}}{S_{11}S_{22}-S_{12}S_{21}}\right)^2} \right| \\
&= \left| \frac{S_{12}S_{21}}{\left(\frac{-S_{12}S_{21}}{S_{11}S_{22}-S_{12}S_{21}}\right)^2} \right| \\
&= \left| \frac{S_{12}S_{21}\left(S_{11}S_{22} - S_{12}S_{21}\right)^2}{\left(-S_{12}S_{21}\right)^2} \right|.
\end{aligned}
$$

Finally:

$$
Sens = \left| \frac{\left(S_{11}S_{22} - S_{12}S_{21}\right)^2}{S_{12}S_{21}} \right|. \tag{3.9}
$$

As in the case of $Z_{\text{NIC}}^{\text{an}}$, this last expression for *Sens* depends on the S-parameters, and therefore, on frequency also. Thus, it is possible to observe how difficult is to match the ESA —or any other antenna— all along the frequency interval of design.

If the two ports are symmetrically placed (S_{11}= S_{22} and S_{12}= S_{21}), equation (3.9) can be rewritten as:

$$
Sens = \left| \frac{\left({S_{11}}^2 - {S_{21}}^2\right)^2}{{S_{21}}^2} \right| = \left| \frac{\left((S_{11}+S_{21}) \cdot (S_{11} - S_{21})\right)^2}{{S_{21}}^2} \right|. \tag{3.10}
$$

In the symmetric case the sensitivity still depends on the S-parameters of the two-port antenna only. The two ports must be placed in such a way that the sensitivity is minimized. Otherwise, any small change in the impedance, provided by the NIC, will dramatically affect the antenna performance in terms of the impedance bandwidth.

The *Sens* parameter is an indicator of how the difference between the actual Z_{NIC} —from a real NFC— and the ideal one, $Z_{\text{NIC}}^{\text{an}}$ —computed

as (3.5)— actually influences the input impedance: Z_{IN}. Thus, *Sens* should be computed at every single point where port-2 is placed into the antenna. At each port-2 location, calculation of *Sens* describes such influence all along the frequency interval from which the S-parameters have been extracted. In this sense, according to the designs carried out by the author, which will be shown later, a *Sens* lower than 10 dB is considered as a reasonable value to obtain an impedance bandwidth wide enough to be implemented with an active MN. $Sens_{\text{dB}}$ is calculated as $20\log(|Sens|)$ where $|Sens|$ is given by (3.9) or (3.10), and for simplicity, in this work it will be referred as *Sens*. Therefore, once *Sens* is calculated at different points over the antenna structure, those at which *Sens* is lower than 10 dB can be considered as appropriate to place the active MN. Those low-sensitivity points represent robustness against the inherent changes and deviations proper of the implementation of $Z_{\text{NIC}}^{\text{an}}$ with active devices.

From the previous expressions, it can also be concluded that the sensitivity will be smaller when the transmission parameter (S_{21}) equals, in magnitude, the reflection parameter (S_{11}). This provides an idea about what kind of antennas are more suitable to be used in non-Foster active matching designs, as it will be shown below. The *Sens* parameter will be approximately flat for non-resonant antennas while will present different magnitude peaks for resonant ones. In general, very resonant antennas will present higher values of *Sens*, and hence, will be harder to match along a broad bandwidth since S_{21} is very small and would only agree with the S_{11} across very small frequency bands. Then, if high levels of coupling can be engineered for a high-Q two-port antenna (or even a multiport one), the return and insertion losses can be similar over larger bandwidths, and the sensitivity can be kept low over those bandwidths, enabling a broadband active matching design. In other words, if S_{21} is low, in comparison with S_{11}, the non-Foster element connected to port-2 has not much influence on the port-1. Other way, in terms of the antenna size, when it decreases in electrical terms (i.e. in an ESA), the quality factor Q of the antenna increases dramatically, as it was shown in previous sections. However, we could find a low sensitivity point over its structure, so a broadband active matched antenna design would be feasible, as we will see below devoted to a loop antenna.

3.4 The *Sens* parameter and the Bandwidth

In a similar way, as for the input reflection coefficient Γ_{IN} in the two-port antenna model, it is possible to relate the *Sens* parameter in (3.9) with changes in the resulting impedance (or VSWR) bandwidth.

So, we can obtain a minimum allowable value for the magnitude of Γ_{IN} in (3.11); (e.g. $|\Gamma_{\text{IN min}}| = 0.316$ for the typical $|S_{11}| = -10$ dB) and relates its changes with the changes in VSWR.

$$VSWR_{\max} = \frac{1 + |\Gamma_{\text{IN min}}|}{1 - |\Gamma_{\text{IN min}}|}. \tag{3.11}$$

The Impedance Bandwidth related to a certain VSWR (BWv), obtained at the input (port-1 in Fig.3.2), can be defined as the frequency interval, around a frequency ω_0, at which the VSWR equals a maximum bound (e.g. $VSWR_{\max} = 1.92$ for $|S_{11}| = -10$ dB) [88]. BWv is one of the most relevant properties to describe the performance of an ESA after a MN —active of passive— is added, and also used to compare the results between different designs. Thus, BWv can be computed as a function of VSWR, as follows:

$$BW_V \approx \frac{2 \cdot \omega_0 \left(VSWR_{\max} - 1\right)}{Q \cdot \sqrt{VSWR_{\max}}}. \tag{3.12}$$

In [89], expressions similar to (3.12) are derived for planar antennas with linear and circular polarizations.

Hence, by applying the chain rule for derivatives, an expression relating BWv with the *Sens* parameter and with the changes in the Γ_{NIC} can be devised utilizing (3.2), (3.11), and (3.12), under the assumption that $|\Gamma_{\text{IN}}|$ must equal zero. Moreover, for the following expressions, a tuned ESA is assumed to work around a frequency ω_0, which is far away from the natural antiresonant frequency, associated with the radiating structure itself, according to the work presented in [88].

First, taking the derivative of (3.2) with respect to Γ_{NIC}, and evaluating it at $\Gamma_{\text{NIC}} = \Gamma_{\text{NIC}}^{\text{an}}$, results in the expression shown before as *Sens*, in (3.9), modified here as

$$\begin{aligned} \left| \frac{\partial \Gamma_{\text{IN}}}{\partial \Gamma_{\text{NIC}}} \right| \Big|_{\Gamma_{\text{NIC}}=\Gamma_{\text{NIC}}^{\text{an}}} &= Sens \\ \rightarrow \Delta\Gamma_{\text{IN}} &= Sens \cdot \Delta\Gamma_{\text{NIC}}. \end{aligned} \tag{3.13}$$

Second, by taking the derivative in (3.11) with respect to the magnitude of Γ_{IN}, and evaluating it at zero ($|\Gamma_{\text{IN}}| = 0$), provided the condition $\Gamma_{\text{NIC}} = \Gamma_{\text{NIC}}^{\text{an}}$, an expression arises as follows

$$\frac{\partial VSWR}{\partial |\Gamma_{\text{IN}}|}\Big|_{\substack{\Gamma_{\text{NIC}}=\Gamma_{NIC}^{an} \\ |\Gamma_{\text{IN}}|=0}} = \frac{(1-|\Gamma_{\text{IN}}|)+(1+|\Gamma_{\text{IN}}|)}{1-2|\Gamma_{\text{IN}}|+|\Gamma_{\text{IN}}|^2}\Big|_{|\Gamma_{\text{IN}}|=0} = 2. \tag{3.14}$$

Third, by taking the derivative in (3.12) with respect to VSWR, and evaluating it at $VSWR = VSWR_{\max} = 1$ —the ideal condition, consequence of connecting $\Gamma_{\text{NIC}}^{\text{an}}$ at port-2— an expression arises as follows (for briefness in the expression, the variable $VSWR_{\max}$ is replaced by s, as in [88])

$$\begin{aligned} \frac{\partial BW_V}{\partial VSWR_{max}}\Big|_{\substack{\Gamma_{\text{NIC}}=\Gamma_{NIC}^{an} \\ |\Gamma_{\text{IN}}|=0 \\ VSWR_{max}=s=1}} &= \frac{2\omega_0}{Q}\left[\frac{\sqrt{s}-\frac{s-1}{2\sqrt{s}}}{s}\right]\Big|_{s=1} \\ &= \frac{2\omega_0(s+1)}{Qs^{3/2}}\Big|_{s=1} = \frac{4\omega_0}{Q}. \end{aligned} \tag{3.15}$$

Finally, by applying the chain rule for derivatives, and using (3.13), (3.14), and (3.15), the complete expression to relate changes in BW_V with respect to those in Γ_{NIC} can be given as follows

$$\left.\frac{\partial BW_V}{\partial \Gamma_{\text{NIC}}}\right|_{\substack{\Gamma_{\text{NIC}}=\Gamma_{\text{NIC}}^{an} \\ |\Gamma_{\text{IN}}|=0 \\ VSWR=1}} = \frac{\partial BW_V}{\partial VSWR} \cdot \frac{\partial VSWR}{\partial |\Gamma_{\text{IN}}|} \cdot \frac{\partial |\Gamma_{\text{IN}}|}{\partial \Gamma_{\text{NIC}}}. \tag{3.16}$$

Then, taking the corresponding expressions in (3.13), (3.14), and (3.15), and replacing them in (3.16) we find:

$$\Delta BW_V \approx \frac{8\omega_0}{Q} \cdot Sens \cdot \Delta\Gamma_{\text{NIC}}, \tag{3.17}$$

where the ratio $8\omega_0/Q$ is a constant of proportionality, for a certain antenna structure, between the parameter *Sens* and the bandwidth change factor ΔBW_V. High values of *Sens* imply that very small changes in Γ_{NIC} will result in very large changes in $|\Gamma_{\text{IN}}|$ and, hence, in the antenna impedance bandwidth BWv.

Once the sensitivity has been analyzed and the placement of the two ports has been chosen, an additional constraint on the antenna efficiency has to be considered. If the $Z_{\text{NIC}}^{\text{an}}$ presents a real part (resistive part) different from zero, the radiation efficiency would decrease dramatically at frequencies lower than resonant ones because of the lower radiation resistance, as mentioned in the previous chapter. Therefore, the energy would be mostly dissipated in heat and not radiated. That is an important constraint in active matching design. For that reason, once a low sensitivity value for a certain non-Foster circuit location has been found, a further adjustment on the obtained $Z_{\text{NIC}}^{\text{an}}$ —which presents a non-zero real part— will be done over the desired frequency range in order to have both broad bandwidth and good efficiency. This is analyzed below throughout the proposed design examples with different antenna structures.

Although this chapter has been focused on the introduced sensitivity analysis, other factor such as the feasibility of $Z_{\text{NIC}}^{\text{an}}$ (the number of non-Foster elements needed which should be implemented $Z_{\text{NIC}}^{\text{an}}$, and their values) is also described. The stability of the whole design, that is, the NIC integrated with the two-port antenna, along with the NIC topology selection are also crucial stages in an actively matched antenna design process, and will be shown in the following chapters.

3.5 Design Examples Using *Sens* Parameter

In this section, three different antennas are analyzed: a small-loop antenna, a conventional rectangular patch, and a metamaterial-inspired multi-frequency patch antenna. According to the previous section, it will be shown how the first and the second cases are suitable choices for active matching with non-Foster forms, in terms of sensitivity, while the third one presents an extremely high *Sens* value, hence, it should not be recommended for active matching.

3.5.1 Small Loop Antenna

The first antenna under test is a small-loop antenna (i.e. the factor $ka \leq 0.5$ for frequencies up to 400 MHz), with a diameter $D = 15$ cm, over a 0.5 mm thick substrate, with 0.035 mm thick metal layer; the width of the wire is 3 mm and the substrate relative permittivity, ϵ_r, is 4.5. As it is shown in Fig. 3.3a, the antenna has two ports. The first one is the feeding port, and the second one is the added one loaded with a non-Foster element.

A parametric study has been undertaken by varying the position of the second port (through the angle Φ) in order to obtain the sensitivity at each point. In this point of the analysis, the electromagnetic CAD software plays an important role. The port-2 is swept all over the loop, in discretized steps equally distributed, and the software is set to extract a S-parameter matrix for each position. Thus, one full-wave simulation runs for each position set in the parametric swept. Fig. 3.3b shows the averaged parameter *Sens* at each point. It can be seen how the averaged sensitivity is maximum when $\Phi = 90^\circ$ ($\overline{Sens} = 30$ dB) and minimum when Φ is around 0° or 180° ($\overline{Sens} = 5$ dB). Therefore, the non-Foster element should be connected at these positions of lower sensitivity. It is important to remark that, in 3.3b, the sensitivity has been averaged over the interest bandwidth 350-600 MHz.

Fig. 3.4 shows the variation of the sensitivity with the frequency for different values of Φ. The optimum placement of the non-Foster is at $\Phi = 0^\circ$, for the proposed bandwidth.

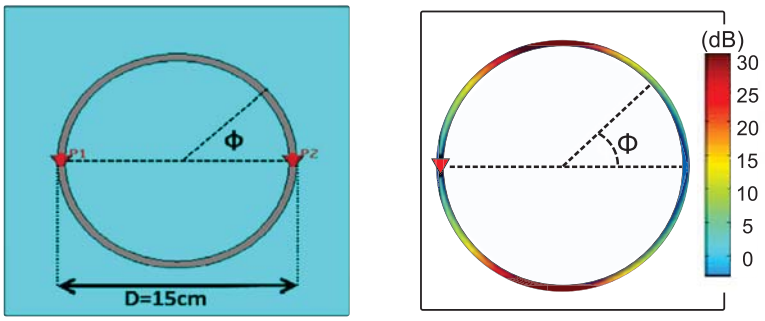

(a) (b)

Figure 3.3: Small loop antenna. (a) Sketch of the two-port loop antenna. (b) Averaged $\overline{Sens}$-parameter over the antenna vs. location of the port-2.

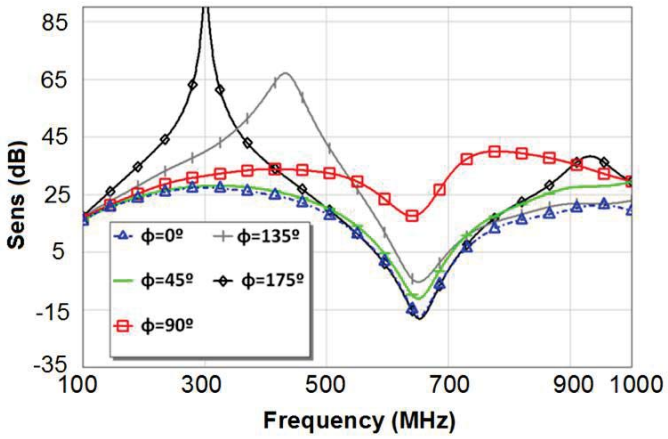

Figure 3.4: Parameter *Sens* vs. frequency for different values of Φ.

Once the position of the NIC has been chosen, according to the sensitivity criterion, a second analysis concerning the efficiency should be undertaken. The S-parameters, and the real and imaginary parts of $Z_{\text{NIC}}^{\text{an}}$ when port-2 is at $\Phi = 0^{\circ}$ are depicted in Figs. 3.5a and 3.5b, respectively.

From Fig. 3.5b it can be seen that, in the desired frequency range, the real part of the non-Foster network is small, but different from zero. Then, in order not to reduce the antenna efficiency, the analytic impe-

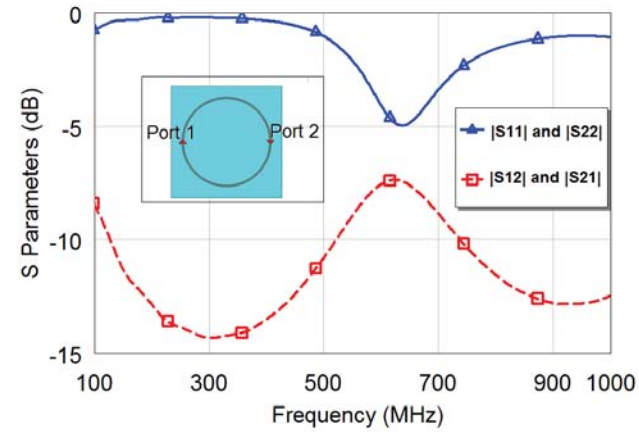

(a)

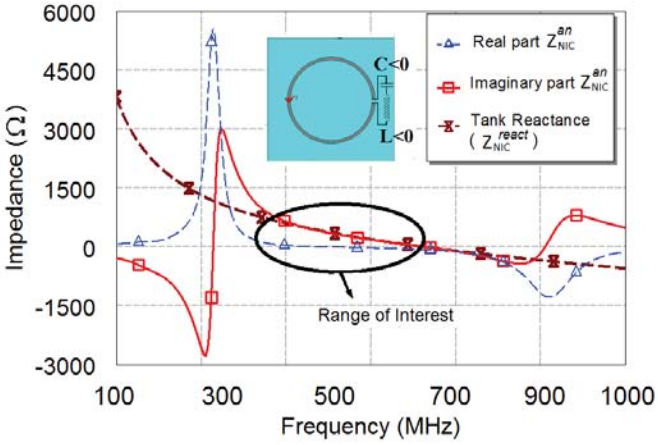

(b)

Figure 3.5: (a) Simulated S-parameters vs. Frequency of the two-port small loop-antenna. (b) Impedance response of the analytic $Z_{\mathrm{NIC}}^{\mathrm{an}}$, and its approach with a purely reactive series tank: $Z_{\mathrm{NIC}}^{\mathrm{react}}$, connected at the lowest sensitivity point in the antenna.

dance, $Z_{\mathrm{NIC}}^{\mathrm{an}}$, is modified by rejecting its real part and keeping an imaginary one (e.g. $Z_{\mathrm{NIC}}^{\mathrm{react}}$ in Fig. 3.5b), as close as possible to that of $Z_{\mathrm{NIC}}^{\mathrm{an}}$, across the intended frequency range, and close to the lowest sensitivity point. This can be achieved with an ideal non-Foster series reactive tank

($L < 0$ and $C < 0$) —a suboptimal impedance, $Z_{\text{NIC}}^{\text{react}}$— that gets a wider bandwidth in the desired frequency range, as it will show below.

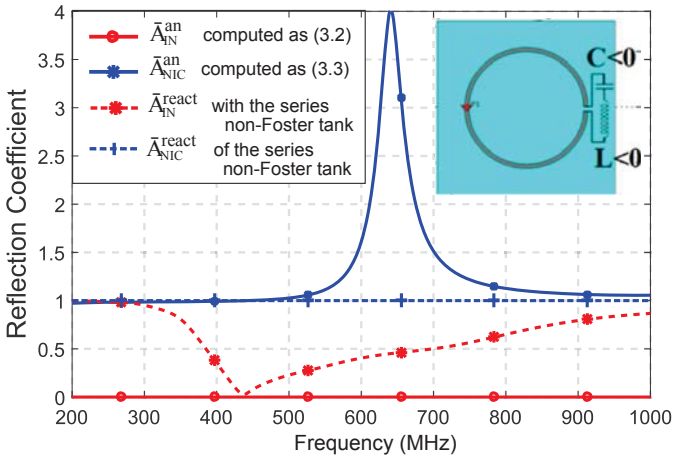

Figure 3.6: Reflection coefficient for both the analytic and the reactive load impedances ($\Gamma_{\text{NIC}}^{\text{an}}$ and $\Gamma_{\text{NIC}}^{\text{react}}$), and their corresponding overall input reflection coefficient (Γ_{IN} and $\Gamma_{\text{IN}}^{\text{react}}$), for the small-loop antenna.

In addition to the curves representing $Z_{\text{NIC}}^{\text{an}}$ and the tank impedance $Z_{\text{NIC}}^{\text{react}}$, it is useful to represent their corresponding reflection coefficients (Γ_{NIC} plane in 3.2) as well as the resulting Γ_{IN} (Γ_{IN} plane in 3.2), for each case. Figure 3.6 shows these curves. Then, if the two-port antenna is loaded with the ideal $\Gamma_{\text{NIC}}^{\text{an}}$, it can be seen that the corresponding Γ_{IN} is always 0 according to (3.2). However, when paying attention to $\Gamma_{\text{NIC}}^{\text{an}}$, it can be appreciated that after the resonance in Fig. 3.6, its magnitude is higher than 1, so that it is potentially unstable. Thus, a stability analysis has to be done to avoid that risk. Secondly, if the $\Gamma_{\text{NIC}}^{\text{an}}$ is replaced with the proposed $\Gamma_{\text{NIC}}^{\text{react}}$, it can be seen that its magnitude is 1 across the desired frequency margin (due to its purely reactive components); this yields better performance from the stability point of view. Then, when seeing the input reflection coefficient in Fig. 3.6, $\Gamma_{\text{IN}}^{\text{react}}$, it can be observed that broad matching condition can be achieved.

On the other hand, when the non-Foster element is placed at $\Phi = 90°$ it is not possible to match the antenna, neither with purely reactive elements nor with the analytic NIC impedance, due to the high sensitivity. The sensitivity is so high that very small variations (even using ideal

elements, as it is the case) in the impedance of the non-Foster element —$Z_{\mathrm{NIC}}^{\mathrm{an}}$ or $Z_{\mathrm{NIC}}^{\mathrm{react}}$— results in very large variations of Γ_{IN} and, hence, in the bandwidth as depicted in Fig. 3.7.

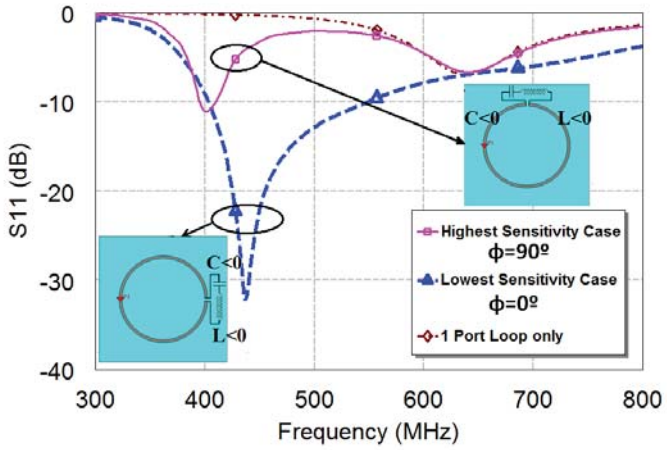

Figure 3.7: Reflection parameter, S_{11}, at the input port of the small loop-antenna, for the two designs.

The results are summarized in Table 3.1: when the port is placed at the lowest sensitivity point $\Phi = 0^{\circ}$, the obtained relative bandwidth is 30.7%. On the other hand, when the port is placed at the high sensitivity point $\Phi = 90^{\circ}$, the maximum relative bandwidth that can be obtained degrades to values lower than 5%. With these two very basic examples it has been shown that the *Sens* parameter plays an important role when designing antenna active MN based on non-Foster circuits. Then, the NIC must be connected at low sensitivity points in order to obtain feasible and robust designs.

Finally, one comment should be done concerning the current distribution along the loop with the NIC in order to check if the radiation pattern is affected by the inclusion of the NIC. The analysis that has been done to see the current distribution, once the proposed tank impedance $Z_{\mathrm{NIC}}^{\mathrm{react}}$ is inserted, at $\Phi = 0^{\circ}$ and at $\Phi = 90^{\circ}$, is shown in Fig. 3.8a. From this figure it can be seen that, at a frequency in the range of interest, there is no change in the current distributions along the loop when the NIC is inserted, in comparison when no NIC is added. In this

Antenna	***Absolute (-10 dB) Bandwidth (MHz)***	***Relative Bandwidth***
Lowest Sens value ($\Phi = 0^{\circ}$)	146	30.7%
Highest Sens value ($\Phi = 90^{\circ}$)	15	3.8%

Table 3.1: Resulting impedance bandwidth (BWv) after loading a small loop with a non-Foster MN, placed in two different locations.

way, no change occurs in the radiation pattern as can be seen in Fig. 3.8b, provided that no resistive part, through the active MN, is added.

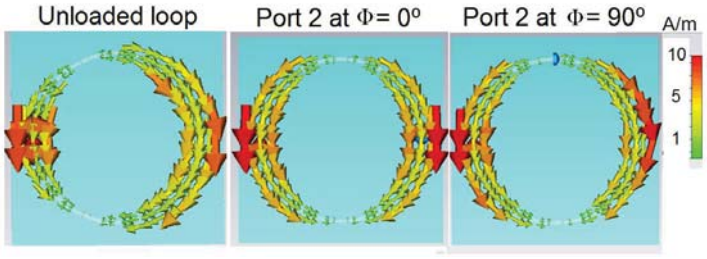

(a)

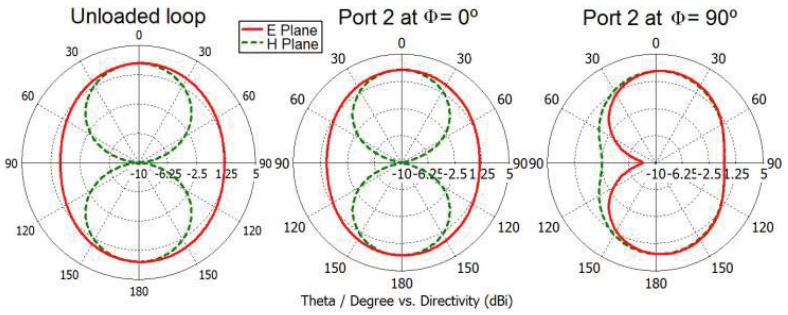

(b)

Figure 3.8: (a) Current distributions along the loop and (b) simulated radiation pattern when the ideal NIC ($Z_{\mathrm{NIC}}^{\mathrm{react}}$) is placed at $\Phi = 0^{\circ}$ and $\Phi = 90^{\circ}$, respectively, at 500 MHz.

3.5.2 Conventional Patch Antenna

For a two-port conventional patch antenna working at 300 MHz, as the one depicted in Fig. 3.9 over an FR4 ($\epsilon_r = 4.35$) substrate of 40 mm thick; a parametric study has been performed in order to evaluate the averaged sensitivity $\overline{Sens}$ (i.e. averaged over the band of interest, chosen from 150 MHz to 300 MHz) as a function of the position of the two ports. Figure 3.9 shows the results when the port-1 (referred to a $Z_0 = 50\ \Omega$) is placed at $x = -85$ mm, $y = 0$ mm, and the port-2 moves throughout the patch.

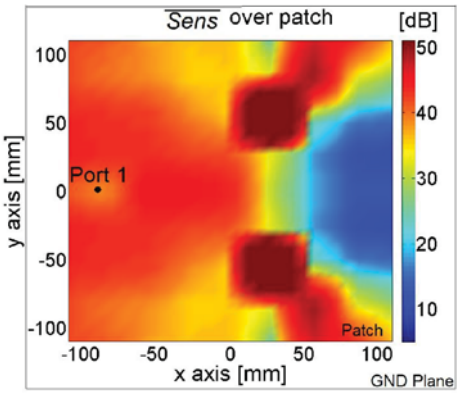

Figure 3.9: Averaged Sensitivity $\overline{Sens}$ (dB) of the patch antenna vs. placement of the analytical port-2.

It can be seen how the averaged sensitivity presents the desired low values (blue color), when port-2 is placed at positions bounded by the area around the point $x = 90$ mm, and $y \approx 0$ mm. For this situation both ports excite non-orthogonal modes so the coupling, $|S_{21}|$ or $|S_{12}|$, is large and more similar to $|S_{11}|$ and $|S_{22}|$. Hence, the denominator of the second part in (3.11) is larger while the numerator is lower so the sensitivity is minimized. When the ports are placed in other region the sensitivity is very large (red colors). The largest sensitivity is obtained when the ports are placed in an orthogonal way. In that case, the ports excite orthogonal modes being the coupling $|S_{21}|$ very small and very different from $|S_{11}|$ and $|S_{22}|$. The numerator of (3.11) is very large while the denominator is very small resulting in huge sensitivities.

Considering the value of $Z_{\mathrm{NIC}}^{\mathrm{an}}$ and its feasibility of implementation, the lowest sensitivity point ($x = 110$ mm, $y = 0$ mm, $\overline{Sens} = 4.02$ dB) has to be discarded, because of the need of three non-Foster elements to fulfill $Z_{\mathrm{NIC}}^{\mathrm{an}}$, as it is depicted in Fig. 3.10 with a series combination of a negative inductor with a negative parallel LC tank.

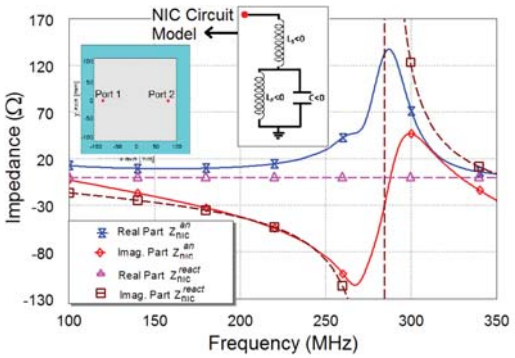

Figure 3.10: $Z_{\mathrm{NIC}}^{\mathrm{an}}$ and an ideal non-Foster realization of $Z_{\mathrm{NIC}}^{\mathrm{react}}$ at $x = 100$ mm, $y = 0$ mm.

Another possible design is studied for the point $x = 27$ mm, $y = 0$ mm, $\overline{Sens} = 20$ dB. Figure 3.11a shows the analytic impedance, $Z_{\mathrm{NIC}}^{\mathrm{an}}$, and the approximation obtained using ideal non-Foster elements when connected at this last point. It can be seen that this is the most feasible design since it only needs a negative parallel LC tank comprised of two non-Foster elements —instead of three of them— to realize $Z_{\mathrm{NIC}}^{\mathrm{react}}$. It is important to remark, as mentioned in previous sections, that the sensitivity *Sens* depends on the frequency as the S-parameters do, as shown in Fig. 3.11b. Moreover, the magnitude of *Sens* keeps lower than 12 dB —a reasonable value— over the desired bandwidth (150 MHz to 300 MHz) when the port-2 is located at $x = 27$ mm, $y = 0$ mm.

The obtained reflection parameter (S_{11}) for both the loaded and the NIC-loaded antenna is shown in Fig. 3.12.

The planar nature of the patch antenna structure requires an analysis of the current distribution, after including the non-Foster network at port-2, to see if the active matching modifies the radiation pattern. Fig. 3.13a shows a change in the current distribution at 200 MHz for the

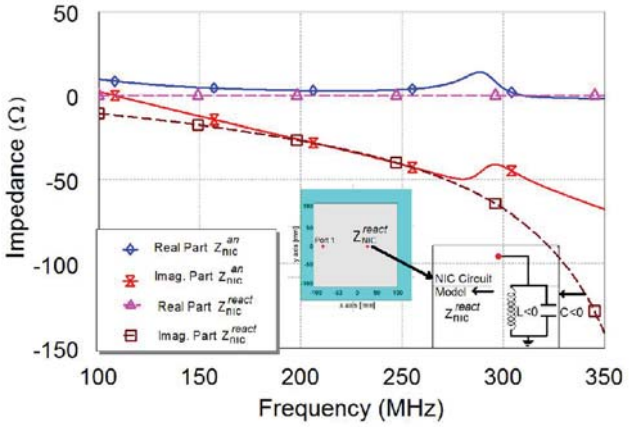

(a)

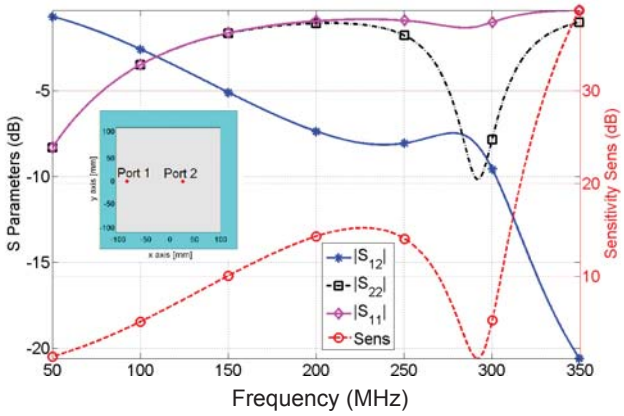

(b)

Figure 3.11: (a) $Z_{\mathrm{NIC}}^{\mathrm{an}}$ and an ideal non-Foster approximation, $Z_{\mathrm{NIC}}^{\mathrm{react}}$, at $x = 27$ mm, $y = 0$ mm. (b) Sensitivity *Sens* and $|S|$-parameters vs. Frequency when the port-2 is located at $x = 27$ mm, $y = 0$ mm.

conventional patch antenna when it is loaded with $Z_{\mathrm{NIC}}^{\mathrm{react}}$. It can be seen that for the loaded case there is a maximum of current in the middle of the patch what leads to the monopolar-like radiation pattern seen in Fig. 3.13b, different from the one expected in a frequency away from resonance one, for a conventional patch antenna (i.e. a magnetic dipole-like pattern).

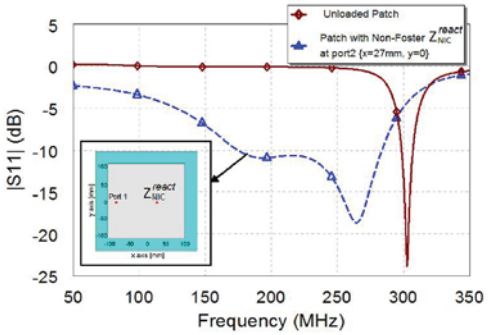

Figure 3.12: $|S_{11}|$ for the unloaded and 2-port patch with $Z_{\text{NIC}}^{\text{react}}$.

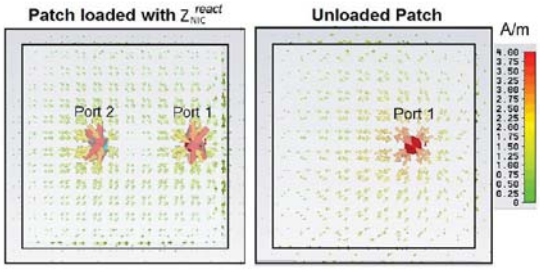

(a)

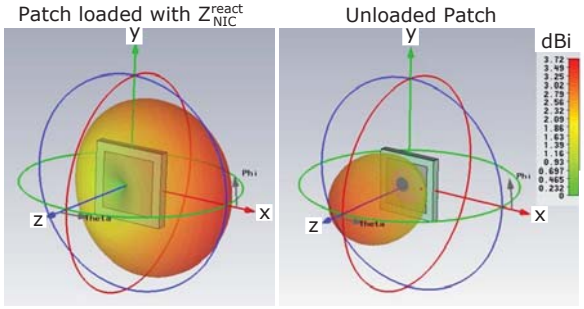

(b)

Figure 3.13: (a) Current distribution at 200 MHz for the conventional patch antenna. (b) Simulated radiation patterns for both the loaded with $Z_{\text{NIC}}^{\text{react}}$ patch with the unloaded case, respectively, with a small ground plane.

3.5.3 Multi-frequency Patch Antenna Based on Metamaterials

The third antenna under study is a patch antenna loaded with a 3X3 array of mushroom-like meta-material particles, as it is shown in Fig. 3.14a and 3.14b [90]. The antenna is fed through two coupled ports. As in the previous case, one of the ports is used to feed the antenna, while the other one is loaded with a non-Foster element, as a try to improve its bandwidth.

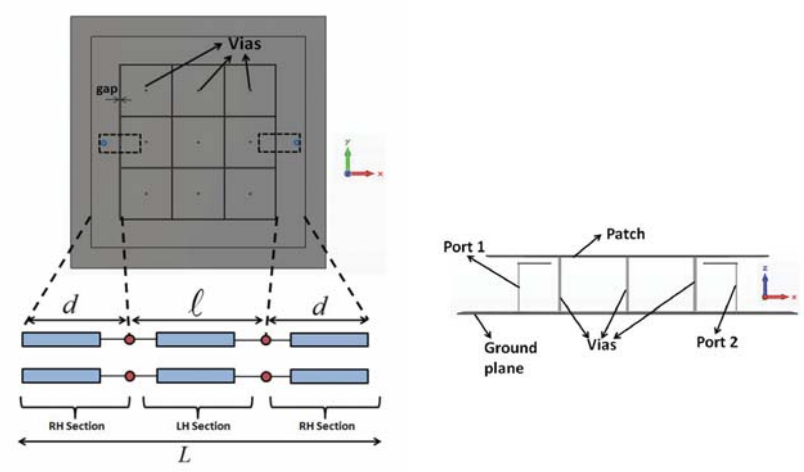

(a) **(b)**

Figure 3.14: Multi-frequency antenna based on metamaterials. (a) Top-view, (b) Lateral view. $L = 25$ cm x 25 cm, $l = 18.3$ cm x 18.3 cm. $h = 5$ cm.

The equivalent Transmission Line (TL) model of the antenna consists of a Left-Handed (LH) section between two Right-Handed (RH) ones, as shown in Fig. 3.14a. The propagation constant in the LH section, β^{LH}, is negative so, according to the resonant condition given by (3.18), it is possible to obtain additional modes to the fundamental one.

$$\beta_n L = \beta_n^{RH} d + \beta_n^{LH} \ell = k_1 f_n d - \frac{k_2}{f_n} \ell = n\pi. \tag{3.18}$$

This antenna has been chosen since the miniaturization degree that can be achieved is significant [90]. The new low-frequency mode is inherently narrowband, as it is provided by the meta-material structures [69] so, as in the previous cases, it will be studied if it is possible to improve the bandwidth by using active matching. The antenna is designed to work in the -1 mode at 150 MHz. The patch is a square one, 25 cm side, the side of the mushrooms is 18.3 cm, the gap between mushrooms is 1 mm, the diameter of the vias is 1 mm and, finally, the antenna is designed on a 5 cm thick substrate with unity permittivity ($\epsilon_r = 1$), over a squared ground plane with 30 cm side.

First, the sensitivity parameter is studied to see whether this antenna is suitable to be used with non-Foster forms. Then, the sensitivity has been computed for different placements of the second port. An average value of the sensitivity in the desired bandwidth (140 MHz-170 MHz) has been obtained. The results of this parametric analysis are shown in Fig. 3.15. It can be seen how the sensitivity is extremely large for all the possible positions for the second port.

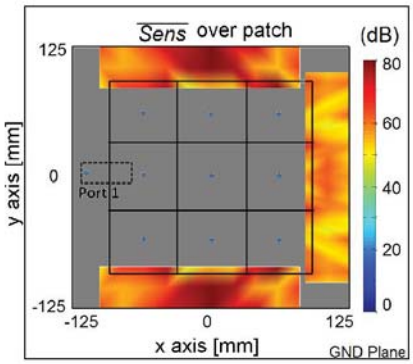

Figure 3.15: Averaged Sensitivity $\overline{Sens}$ (dB) of the antenna vs. port-2 placement.

The S-parameters of the two-port antenna can help us to understand why the sensitivity is so large for this antenna. Figure 3.16 shows the S-parameters as well as the computed sensitivity using (3.9). From that figure, it can be seen that the coupling between the two ports is very low. When this happens, $|S_{21}|$ is very low and the sensitivity is very large according to (3.9). For this reason, the sensitivity is only relatively

small at very narrow frequency bands where the $|S_{21}|$ is larger: 144 MHz, 151 MHz, and 156 MHz. For this reason, this antenna, or any antenna with similar performance, cannot be used in two-port active matching designs.

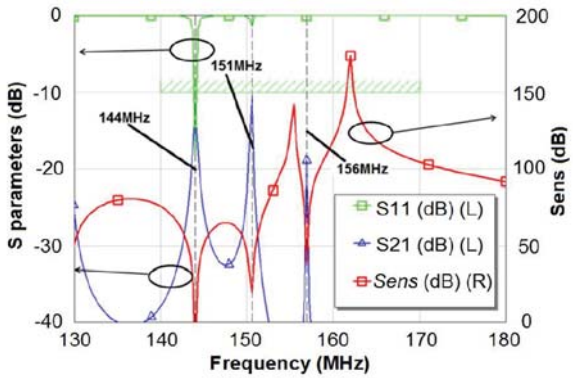

Figure 3.16: *S*-Parameters and Sensitivity *Sens* of the patch loaded with metamaterial forms.

In order to obtain low sensitivities and thus, feasible designs, the antenna should present large $|S_{21}|$ values, which is logical, because if the magnitude of S_{21} were very small, the influence at port-1 of the non-Foster element connected at port-2 will be also very small.

As aforementioned, very resonant antennas such as the patch antenna loaded with meta-materials presented in this section, are not appropriate for active non-Foster matching, since the magnitude of S_{21} is very small and only agrees with the magnitude of S_{11} for very small frequency bands. It should be emphasized that the quality factor is not directly proportional to the sensitivity. Then, for any proposed two-port antenna, a high quality factor Q does not necessary imply a high sensitivity value for a certain port distribution over the antenna, and a low quality-factor does not necessarily imply a low sensitivity level. In spite of the Q value over the frequency interval of interest, the sensitivity will have to be studied to find out the best position where the NIC can be included. As the value of the sensitivity is not suitable, the integration of non-Foster forms in this two-port antenna will not be feasible either, and larger bandwidths will not be achieved.

Although from the sensitivity analysis it has already been concluded that it is not possible to integrate a non-Foster network with this antenna, a final analysis on the current distribution and on the corresponding radiation pattern is also presented. Figure 3.17a shows the comparison between the simulated current distributions at 144 MHz when the patch is loaded with $Z_{\text{NIC}}^{\text{react}}$, at the symmetrically located port-2 (with respect to port-1), and the unloaded patch. It can be seen that for the case of loading with the non-Foster element (reactive case) there is a maximum of current in the middle of the patch which leads to a monopolar-like radiation pattern, instead of the typical dipolar-like one associated to the metamaterial patch with no loading, seen in Fig. 3.17b.

3.6 Conclusion

Finally, it can be concluded that in intervals of frequency at which the antenna is non-resonant, as in the case of the small loop and the conventional patch antenna presented in sections 3.5.1 and 3.5.2, respectively, the active non-Foster matching is feasible. These antennas present similar values of S_{11} and S_{21} over larger bandwidths so that the sensitivity is also kept low over such bandwidths, making broadband designs possible. The level of degradation in the antenna efficiency is intimately related to the real part of $Z_{\text{NIC}}^{\text{an}}$, therefore, this parameter should be kept low over the frequency range of interest.

It has been shown that the sensitivity *Sens* is a very important design parameter that can be stated as the starting point of a complete design procedure for actively matched antennas, loaded with non-Foster forms. Then, a procedure for carrying out the sensitivity analysis can be listed as follows:

1. Draw or model the desired antenna structure for extracting a two-port S-parameters matrix, for different point inside the antenna.
2. Compute the sensitivity parameter, as in (3.9), over the frequency interval of interest, at each port-2 location in the previous step, in order to see whether the proposed antenna presents suitable points to integrate a non-Foster form. In case so you can go ahead with the following points (this happens, for instance, for the loop and for the conventional patch but not for the metamaterial patch).

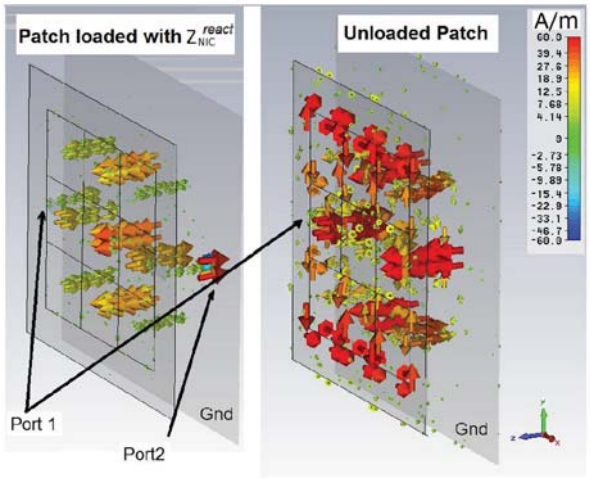

(a)

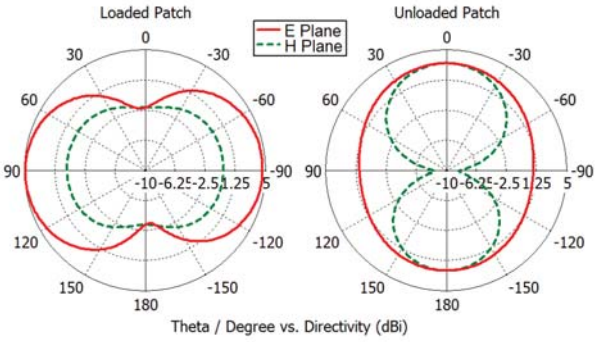

(b)

Figure 3.17: (a) Current distribution in both the loaded with $Z_{\text{NIC}}^{\text{react}}$ and the unloaded metamaterial patch. (b) Simulated radiation patterns for both cases (with a small ground plane).

3. Compute and observe the nature of the needed NIC impedance $Z_{\text{NIC}}^{\text{an}}$, as in (3.5), at locations around the lowest sensitivity point(s), looking if possible for both a "smooth shape" of the reactance and lower values of the resistive responses, respectively, since the trade-off between $Sens$ and realizability of the non-Foster element.

4. Choose a suitable active non-Foster MN that does not greatly af-

fect the efficiency of the antenna. For that reason, the impedance chosen is a suboptimal one with reactive performance.

5. Study the current distribution in order to see that the radiation modes are the same as in the original antenna (this happens for the loop, loaded with $Z_{\text{NIC}}^{\text{react}}$, but not for conventional patch or the patch loaded with metamaterial particles).

In relation to previously reported works in literature, other authors have implemented the embedded active non-Foster matching without checking any influence on Z_{IN} due to the location of the engineered non-Foster MN. No especial concerns have been taken in relation with the NIC location. In this sense, when embedding an active MN well in the antenna structure itself —as in [42]— well in some parasitic/metamaterial structure in the near field —as in [38, 84] and [44]— the *Sens* parameter can be helpful for finding the more suitable location for the non-Foster form.

The introduction of the sensitivity parameter, *Sens*, allows us to see the dependence of the input impedance on the variations of that from the NIC, with respect to the analytic one. The ports must be placed at points of low sensitivity. In this way, small variations of the non-Foster element, (variations in the NICs) will not degrade the matching performance. Then, once a low sensitivity location is chosen, the design must be made over a frequency range where the real part of $Z_{\text{NIC}}^{\text{an}}$ has low values in order not to degrade the antenna efficiency. If the ports are placed in such a way that high sensitivities are obtained, the design will not work properly, since any small variation in the implemented non-Foster element (which are unavoidable in practice) will yield in high variations of the input impedance, and hence, in the bandwidth.

Moreover, the feasibility must also be taken into account; because in some placements the needed analytical impedance (specifically the optimum reactance) is very difficult to achieve using practical NICs. For this reason, a trade-off between sensitivity and feasibility should be studied for each particular case. These last considerations have to be included in the global design procedure, alongside the stability analysis, as it will be shown in the next chapter with manufactured NIC circuits embedded in real ESAs.

CHAPTER 4

DESIGN METHOD FOR NON-FOSTER ACTIVELY MATCHED ESAs

4.1 Introduction

The current demand on more compact and broader bandwidth devices makes necessary to improve the performance of small antennas. A smart strategy for integrating non-Foster networks with ESAs, optimizing its placement into the radiating structure while considering the stability and radiation performance of the whole antenna system, will always be welcome in communication systems.

As mentioned in Chapter 2, most of the previously reported works include the use of non-Foster components at the terminals of dipole- or monopole-like antennas. Even when some other authors have considered embedding the non-Foster circuit (NFC) in the antenna structure, most of the effort has been focused in optimizing and characterizing the NFC —indeed one of the most challenging tasks— more than in analyzing the complete antenna system.

In this sense, the present chapter aims at proposing a global methodology for the design of actively matched antennas. In this way, the antenna and the non-Foster networks are considered a whole system. In

addition to the impedance bandwidth improvement, the stability and tolerance of the components, the current distributions, and the corresponding radiation patterns are also considered.

4.2 An Integral Design Method

In this section, the proposed strategy is described. First, the antenna to be integrated with a NFC undergoes the sensitivity analysis (devised and described in the previous chapter) to see whether the antenna is suitable for it or not. Additionally, this sensitivity analysis will also determine the most appropriate place for the NIC. Second, not all the non-Foster networks are valid for being integrated with the antenna, so some remarks on the non-Foster network are provided in order to choose the most suitable one. Third, a trustworthy stability analysis of the overall structure (NIC + antenna) shall be done.

It is important to emphasize that the stability analysis has to be done in the overall structure since the antenna loading can modify the overall performance of the NIC stability. Fourth, the radiation pattern of the integrated antenna has to be studied; this analysis is undertaken by studying the variations of the current distributions in the original antenna. Finally, since any change in the actual value of the components in the NIC can modify the performance, well the stability well the sensitivity of the overall structure, a tolerance analysis is welcome in order to predict potential and uncontrolled variations. Figure 4.1 shows a sketch of the previously described design strategy.

4.2.1 Step 1: Sensitivity Analysis

For the sake of conciseness and clarity, the complete deduction of the *Sens* parameter is omitted in this chapter since it was presented in Chapter 3. Nonetheless, it should be mentioned that as the first step in the design strategy, it is necessary to add an analytical second port to the antenna itself, where the active MN is to be placed. Figure 4.2 depicts the CAD model of the patch antenna, previously described in Section 3.5.2, in which the fictitious port-2 is added. The swept sketched in Fig. 4.2 indicates those port-2 locations over the patch from which

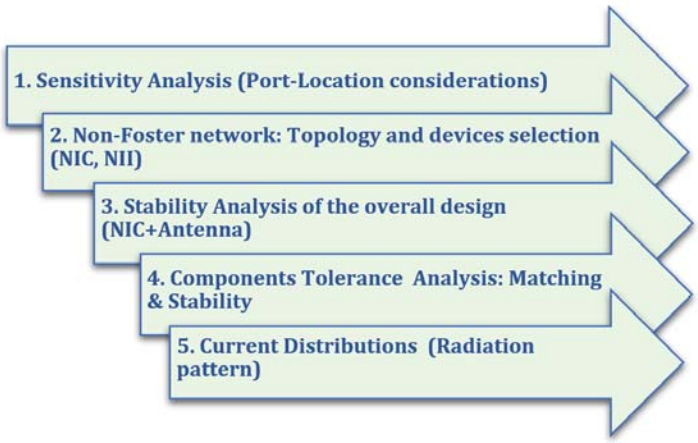

Figure 4.1: Summary of the proposed strategy.

a number n of S-parameters matrices will be extracted, after the full-wave simulation. Thus, each point of the swept gives a two-port network version of the patch that can be analyzed under the non-Foster matching approach, depicted in Fig. 4.3. Once the S-parameters matrices have been extracted, it is possible to compute the *Sens* parameter as in (3.9), whose expression is shown here again, as follows:

$$Sens = \left| \frac{S_{21}S_{12}}{(1 - S_{22}\Gamma_{\text{NIC}})^2} \right| \Bigg|_{\Gamma_{\text{NIC}}=\Gamma_{\text{NIC}}^{\text{an}}} = \left| \frac{(S_{11}S_{22} - S_{21}S_{12})^2}{S_{21}S_{12}} \right|. \quad (4.1)$$

As mentioned in Chapter 3, the *Sens* parameter only depends on the S-parameters of the two-port antenna. Not only the suitability of the proposed antenna is inferred by computing *Sens* at different points over the structure, but also the most convenient port location for the resulting two-port network. It should be pointed out that there is no need of an analytical circuit model for the antenna, difficult to extract in practice; this fact facilitates and generalizes the design process to many types of antennas since they just have to be drawn in an electromagnetic CAD software. In addition, it is possible to extend the active non-Foster MN approach of two-port antennas to any other actively embedded-matched antenna approaches, like the ones reported in the literature [38,42,44,91].

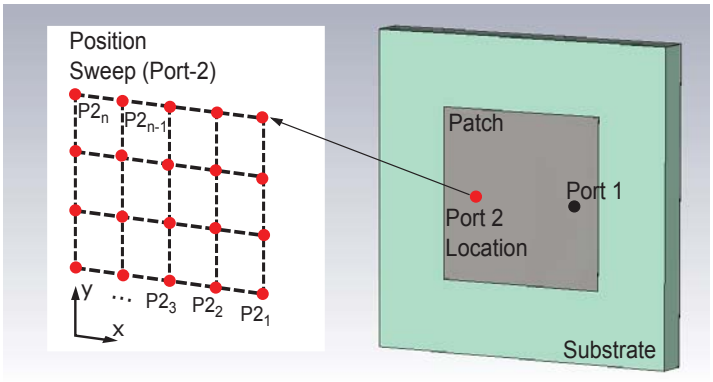

Figure 4.2: CAD Antenna model of a squared patch in which a fictitious second port is added to extract the S-parameters, for the *Sens* computation, following the sketched swept pattern.

Thus, by replacing the embedded NIC for an analytical second port, and by applying the procedure shown before, it is possible to observe the *Sens* parameter over the radiating structure, including any near-field element or parasitic around it. This alternative enables a generalization in the design process as well as a possible optimization of the broadband ESA performance, previously obtained.

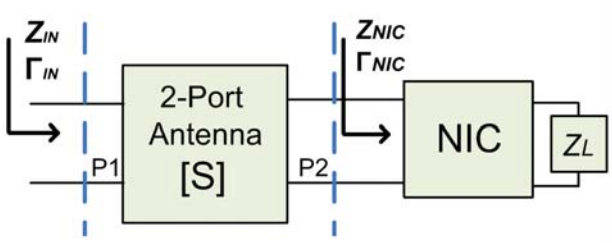

Figure 4.3: Active matching with the two-port antenna approach proposed in [86]. Z_L is the reactive load to be inverted by the NIC.

Figure 4.4 shows a printed monopole, like the one reported by Mirzaei in [42], in which a non-Foster MN was added into an antenna by embedding a BJT-based NIC. Such an active MN is acting as a negative capacitor and is located in a point close to the ground plate of the antenna, and is working at frequencies where the whole antenna system

is electrically small since the *ka* factor is lower than 0.5. Experimental results are also reported. The colored area in the monopole depicts the *Sens* parameter, computed as (4.1), averaged over the same frequency interval used by the authors in [42] at which the NIC is working (250 MHz to 500 MHz). Then, in order to extend our approach to the described work, the NFC in [42] is replaced here by an analytical second port. Thus, once the one-port monopole is treated as a two-port antenna, the port-2 location sweep takes place over several points in the antenna, leading to the observation of *Sens*. It is possible to infer that the closer the NIC is located to the bottom edge of the monopole, the lower the *Sens* parameter is. Then, the point located by the authors in [42] can be considered as a good option to embed the non-Foster MN.

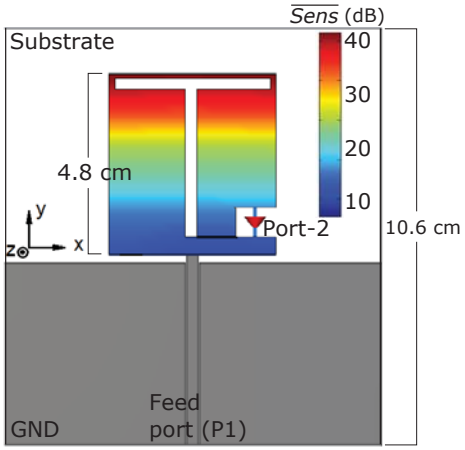

Figure 4.4: Averaged $\overline{Sens}$ parameter depicted over the printed slotted monopole proposed in [42]. The blue area represents the lower sensitivity points to embed the NIC.

Figure 4.5 shows a similar type of antenna —a printed monopole— reported in [38], but with the non-Foster MN acting as a negative inductor, and embedded in a near field resonant parasitic (NFRP) element: an Egyptian-Axe-shaped parasite. The NFRP is located on the bottom face of the substrate, opposite to the one of the monopole. At the resonant frequency added by the NFRP (300 MHz), the antenna size is such that a *ka* factor of 0.49 is checked. The reported NIC is a BJT-based one, working from 200 MHz to 400 MHz, added to broaden the resonance of the overall antenna, according to the reported simulations. That is, the

frequency interval over which the *Sens* parameter is calculated, by using again the sensitivity analysis proposed here, over the line connecting the ground plane and the parasite.

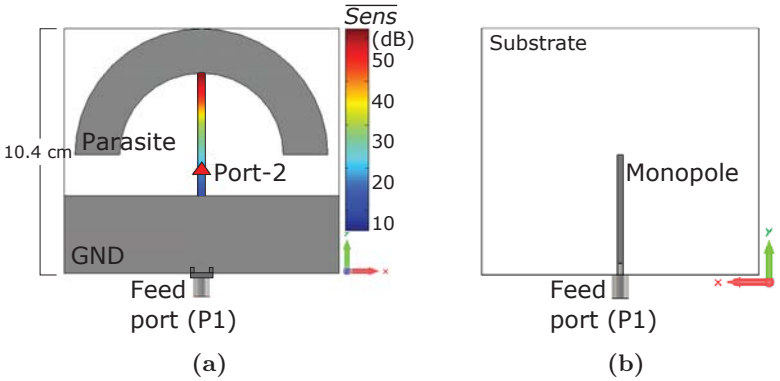

Figure 4.5: Sketch of the averaged $\overline{Sens}$ parameter, computed over the line connecting the ground plane and the NFRP, in one models presented in [38]. (a) Bottom view. (b) Top view.

The result of the swept and the computation of the averaged *Sens* is depicted in Fig. 4.5a. For this case, it is possible to state that the closer the NIC is located to the ground plate of the antenna, the lower the *Sens* parameter is. The authors in [38] decided to place the non-Foster MN at a point 9.5 mm away from the ground plane. From the point of view of the sensitivity, it is not the best option. Nonetheless, in practice, to implement an active MN to be added into the antenna, some considerations on the realizability of the non-Foster impedance at the lowest *Sens* point must be accounted for, as mentioned in Chapter 3.

It is also useful to recall the analytical impedance, $Z_{\text{NIC}}^{\text{an}}$ (deduced previously as (3.5)), that can be extracted from the S-parameter matrix at the lowest *Sens* point (or around it) in the antenna:

$$Z_{\text{NIC}}^{\text{an}} = Z_0 \cdot \left(\frac{S_{22} \cdot S_{11} - S_{12} \cdot S_{21} + S_{11}}{S_{22} \cdot S_{11} - S_{12} \cdot S_{21} - S_{11}} \right). \tag{4.2}$$

The *Sens* parameter has to be calculated for different potential positions for the second port of the antenna, where the NIC is to be loaded.

The optimal choice is that at which the sensitivity is minimized, which implies that changes in the NIC will not greatly affect the input impedance. Otherwise, any small change in the impedance provided by the NIC will dramatically affect the antenna performance in terms of the overall matching bandwidth. This step is critical since not all the antennas neither the positions in them are suitable for including non-Foster matching networks.

4.2.2 Step 2: NIC Topology Considerations

The NIC selection comprises not only the frequency range of operation of transistors but the type of circuit connection (grounded or floating) and the fabrication technology as well. The non-Foster behavior of a NIC is usually expected to be a small fraction of the high-frequency parameter, f_{T} [23,67] —the gain bandwidth product defined as that frequency at which $h_{\mathrm{fe}} = 1$ (0 dB) [92]. This, in turn, allow keeping low the influence of internal capacitances (C_π, C_μ in the BJT or C_{gs} in the FET) on the NIC impedance response, as shown before in Section 2.7.2. On the other hand, especially in balanced-NIC configurations, a transistor with a f_{T} lower than the frequency of possible oscillations predicted for the manufactured circuit is preferred [93]. Such oscillation can result from currents in the even mode, operating across the feedback paths between the transistors. As a general rule, short feedback path-lengths should be implemented to bring the potential oscillations into higher frequencies, out of the working range of the transistors [93].

In addition, floating or grounded NIC configurations may be selected depending on the sensitivity analysis results. Then, if the lowest sensitivity point in the antenna is found to be near the ground plane (if it exists), a grounded configuration will be easier to build, especially for the DC return path from the bias network. Nevertheless, grounded configuration produces important changes in the current distribution of the antenna, especially in planar structures, as it was shown in the previous chapter. This implies that for antennas such as patches or printed monopoles, undesired changes in the radiation pattern of the actively matched antenna can arise. Among these changes, it could be mentioned additional lobes or nulls, or even an entire different radiation mode. This phenomenon is due to the presence of an additional path to ground for the currents at

frequencies where the NIC is working.

Additionally, it is necessary to decide which port of the NIC itself is appropriate to be connected inside the antenna. Since the embedded negative capacitor/inductor circuit is intended to compensate the effective capacitance/inductance of the corresponding ESA, the impedance seen by the NIC at certain port-2 location (Z_s in Fig. 4.7a) must satisfy the first necessary condition for stability, accordingly to the Linvill criteria [19].

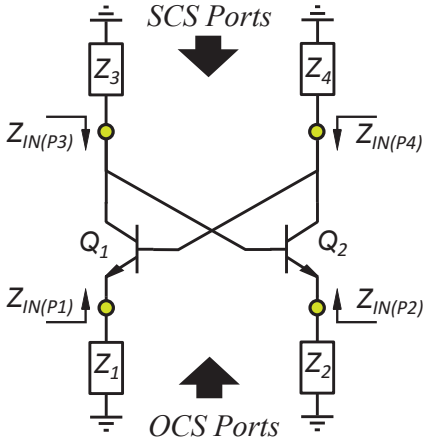

Figure 4.6: General topology of a NIC circuit with the input impedances when looking into each of the four ports

These criteria state the classification of the NIC ports in two types: Open Circuit Stable (OCS) or Short Circuit Stable (SCS). Each one of these types states a condition on the external loading impedance/admittance magnitude to avoid any pole of the system lying in the complex Right Half-Plane (RHP). The system results of connecting the NIC with the antenna or with any other passive device. Figure 4.6 [70] shows a generalized and conventional NIC schematic consisting of two cross-coupled BJTs. The OCS or SCS classification at each port are shown as well. Then, both the stability condition and the input impedance can be calculated, as follows

$$\begin{array}{ll} \textbf{Stability Condition} & \textbf{Input Impedance} \\ |Z_{\text{IN(P1)}}| < |Z_1|; & Z_{\text{IN(P1)}} = -\dfrac{Z_3 \cdot Z_4}{Z_2}, \\ |Z_{\text{IN(P2)}}| < |Z_2|; & Z_{\text{IN(P2)}} = -\dfrac{Z_3 \cdot Z_4}{Z_1}, \\ |Z_{\text{IN(P3)}}| > |Z_3|; & Z_{\text{IN(P3)}} = -\dfrac{Z_1 \cdot Z_2}{Z_4}, \\ |Z_{\text{IN(P4)}}| > |Z_4|; & Z_{\text{IN(P4)}} = -\dfrac{Z_1 \cdot Z_2}{Z_3}. \end{array} \tag{4.3}$$

Is important to note that there are two different ways to connect a NIC into an active MN, depending on which ports are used to couple the signal. Thus, if the NIC is connected —or embedded— to the antenna through the ports 1 and 2, in Fig. 4.6, it is going to work in a balanced-OCS configuration. On the other hand, if ports 3 and 4 are selected, the NIC will work in a balanced-SCS configuration. For the case of a grounded active MN, if ports 1 or 2 are selected to act as Z_{NIC}, the NIC is going to work in an unbalanced-OCS configuration, while ports 3 and 4 will set the NIC in an unbalanced-SCS configuration.

Thus, deciding which port (or ports) to use to perform the NIC as an active MN is an important task. Conventionally, for example, in a series configuration where the NIC is connected at the feeding point of the ESA (as depicted in Fig. 2.18b), the antenna impedance nature have to be analyzed first. For instance, in a small monopole, whose impedance is highly capacitive at lower frequencies, a balanced-OCS NIC is used [39–41]. If the parallel connection of the NIC at the feeding point of the ESA is chosen, the unbalanced-SCS configuration is more appropriate [75]. In embedded active MNs, the magnitude of the analytic NIC impedance, $Z_{\text{NIC}}^{\text{an}}$, computed as (3.7), should be observed prior to choosing which port —or ports— of the NIC is going to be used either in the floating or in the grounded configuration. The concepts of OCS and SCS are further described in Step 3.

On the other hand, floating NIC configuration produces substantially lower changes in the radiation pattern, but with the drawback of higher values of sensitivity that implies, as aforementioned, poor impedance

matching performance. In addition, larger stability problems may also arise for floating structures, as mentioned in [19] and [39]. Then, a trade-off for the NIC selection has to be made to choose, both, the transistor (by considering its transition frequency) and the topology (grounded or floating) for the NIC, keeping in mind the location of the lowest sensitivity point in the antenna structure.

4.2.3 Step 3: Stability Analysis

It is well known that stability is a time-domain property of circuits [94], in such a way that every bounded input yields a bounded output as time approaches infinity. However, when the frequency of operation rises, the time-domain methods lack of practicality to be applied, thus, a frequency-domain technique is preferable, in order to account for dispersion of components, parasitics, and a very important parameter: the modeling of the inside active devices. In this sense, a number of reported works dealing with the circuit stability can be found [22, 95–100]. All these methods are based on the Nyquist criterion [101] to check if the corresponding network function does not have any poles lying in the RHP of the s-plane.

On the other hand, the stability analysis is critical when non-Foster circuits are present due to the positive feedback involved in the transistor-based realizations. The situation, when including the non-Foster circuit inside the antenna, is somewhat more critical than when considering the NIC itself as an outer part of a matching circuit. In this case, the antenna and the non-Foster circuit cannot be separated, in such a way that the simple analysis based on classical Linvill criteria [19], is no longer enough. However, the analysis on evaluating OCS or SCS constitute a necessary but non-sufficient condition for the stability verification.

To analyze the stability, Linvill used the equivalent circuit model of the BJT, and separate the analysis of the balanced topology he presented in two cases [19]. The first one accounts for the case when the input is taken from the emitter-terminals (ports 1 and 2 in Fig. 4.6). Then, the input impedance, Z_{NIC}, of this configuration is analyzed to verify the fact that it has no poles in the RHP, according to the reasoning presented

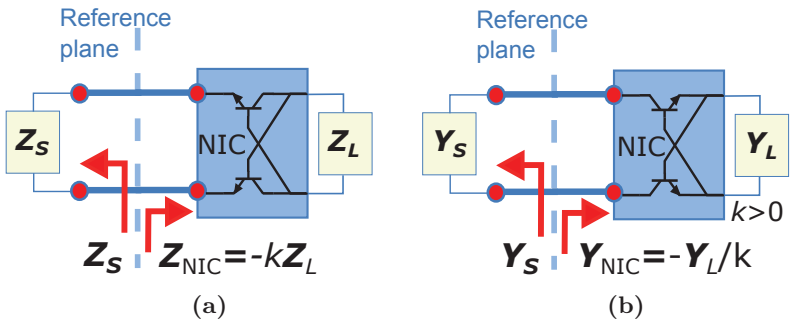

Figure 4.7: Ideal NIC diagram showing the reference plane for (a) open-circuit and (b) short-circuit stability verification.

by Merrill in [61]. Linvill concluded that, in this configuration, depicted in Fig. 4.7a, the open-circuit stability is verified. In other words, that an OCS-NIC will have all input impedance poles in the Left Half-Plane (LHP). This configuration leads to stability when the NIC is connected to an external impedance Z_s, providing $|Z_{\text{NIC}}| < |Z_s|$, which is the OCS condition. Likewise, in the second case, the input admittance of the NIC, Y_{NIC}, was analyzed when the input is taken from the collector-terminals (ports 3 and 4 in Fig. 4.6). In this case, the stability is verified as the fact that Y_{NIC} has no poles in the s-plane RHP. This configuration, depicted in Fig. 4.7b, leads to stability when the NIC is connected to a source admittance Y_s, providing $|Y_{\text{NIC}}| < |Y_s|$: the SCS condition. Then, a SCS-NIC will have all input admittance poles in the LHP. These two conditions are described in more detail below.

Let us particularize these criteria for the current situation where the non-Foster circuit is embedded in the antenna itself. For this situation, the block diagram in Fig. 4.3 is modified to see what is the impedance seen at the reference plane, between the NIC circuit and the analytical two-port network of the antenna (extracted in Step 1). This can be seen in Fig. 4.8 where the actual antenna input port (P1) is loaded with the receiver impedance that is transformed by a bilinear S-parameter transformation in a new Z_s impedance at port-2 (P2). Z_{RX} is the impedance of the receptor —or the subsequent stage in the reception system— assumed to equal, by simplicity, the reference impedance of the system, Z_0.

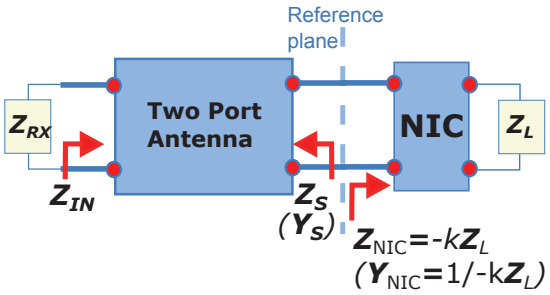

Figure 4.8: Reference plane in the two-port antenna approach for evaluating the classical Linvill stability analysis.

The so-called OCS condition states that the stability of the NIC is that the absolute value of the impedance at the left side of the reference plane (Z_S), should satisfy the following condition for all frequencies at which the NIC can effectively negate Z_L:

$$|Z_s| \geq |Z_{\text{NIC}}| \ \textit{or} \ |Y_s| \leq |Y_{\text{NIC}}| \quad \text{OCS port.} \tag{4.4}$$

If we consider the circuit mesh formed around reference plane (slotted line in Fig. 4.8), it is possible to observe that the total impedance is $Z_s - Z_{\text{NIC}}$. If the NIC impedance should equals Z_s, a voltage source would call for infinite current, an impossible condition [61]. The negative difference between the magnitude of those impedances ($|Z_s| - |Z_{\text{NIC}}| < 0$) can lead to oscillation, so the inequities in (4.4) are valid to describe the OCS condition.

For the short-circuit stability, a necessary condition for the NIC to be stable is that the absolute value of the admittance at the reference plane (Y_s), should satisfy the following condition for all frequencies at which the NIC can effectively negate Z_L:

$$|Y_s| \geq |Y_{\text{NIC}}| \ \textit{or} \ |Z_s| \leq |Z_{\text{NIC}}| \quad \text{SCS port.} \tag{4.5}$$

In this case, by considering the node currents flowing from the reference plane in Fig. 4.8, if a SCS port is selected to be connected to

the two-port antenna block, the total admittance is $Y_s + Y_{\text{NIC}}$. Then, if the NIC admittance were equal to Y_s, a current source would produce an infinite voltage, an impossible condition. The negative difference between the magnitude of those admittances ($|Y_s| - |Y_{\text{NIC}}| < 0$) can lead to oscillation, so the inequities in (4.5) are valid to describe the SCS condition.

Previous analysis suffers from two drawbacks, first of all, the analysis on OCS or SCS criterion does not take into consideration important factors such as the reactive nature of the NIC load, the dispersion of the circuit components with frequency or the locus of the trace associated with the network function. Furthermore, as the non-Foster circuit is embedded in the antenna, there is no actual access to that point. Those are the reasons because of that the OCS-SCS validation constitutes a necessary but non-sufficient condition for stability in an actively loaded antenna system [102].

In addition, at microwave frequencies, besides the study of a corresponding transfer function, other parameters have to be used to predict stability since it is difficult to obtain the voltage or current transfer functions for applying to them the Nyquist criteria.

In this sense, other conventional parameters have been proposed to evaluate stability in microwave circuits such as Rollet [103] $K - \Delta_s$ pair (where Δ_s is the determinant of the system function in the s domain), or the μ factor. These parameters are functions of reduced two-port representations in terms of the S-parameters —but also applicable with z-, y or h-parameters— which look for unconditional stability by ensuring that the input/output impedances of the system are positive real. The K and the μ factors depend on which port (input or output) the analysis is carried out.

The K factor, proposed in [103], is a scalar dimensionless quantity that must be greater than 1, for all the frequencies at which the circuit is intended to work, provided $|\Delta_s| < 1$, to indicate that the loaded circuit is stable. It can be computed as follows

$$K = \frac{1 - |S_{11}|^2 - |S_{22}|^2 + |\Delta_s|^2}{2|S_{12}||S_{21}|}, \tag{4.6}$$

where

$$\Delta_s = |S_{11}S_{22} - S_{12}S_{21}|. \tag{4.7}$$

The μ parameter, proposed in [104], comprises a geometrical approach that represent the previous criteria by the single condition

$$\mu = \frac{1 - |S_{11}|}{|S_{22} - \Delta_s S_{11}^*| + |S_{12}S_{21}|} > 1. \tag{4.8}$$

The main drawback of these parameters is the fact that they disregard characteristics of more complex elements, as they are based on characterized devices (e.g. transistors) known to be stable under dedicated measurement fixtures [105]. In other words, these criteria fail due to the use of a reduced two-port version for predicting stability of an N-node network, disregarding some of the possible poles in the RHP loci of the antenna system.

Those tests (Rollet factor K or μ) are only valid provided that another condition —a proviso— is satisfied previously. That proviso comprises the evaluation of all the possibly hidden poles of the whole antenna system, including those from the active devices in the NFC, by evaluating the stability of the respective well-terminated model (e.g. S-parameters terminated at Z_0, or z-parameters terminated in opens) of each component in the system. In the early years of microwave circuits design, the mentioned proviso has often been ignored firstly because it is not easily evaluated, and secondly because its omission has not been typically a problem for circuits with only a single active device (e.g. single stage amplifiers) [105]. This is acceptable if the S-parameter used in the analysis come from measurement and the basic device (the transistor) is known to be stable in the 50 Ω system. This is not the case of a non-Foster circuit NFC loading an antenna, where the two-port parameters of the active components are often extracted from Electronic Design Automation (EDA) circuit software, and the antenna two-port network model is extracted from an electromagnetic CAD software.

It is possible to devise many lists containing the complete conditions for unconditional stability in two-port networks, based on the immittance

parameters (z, y, g, or h) or the S-parameters, all of them equivalent to each other under the same Nyquist criterion, as reported in [105]. If the analysis is based on the S-parameters of a terminated two-port network —e.g. the NIC shown in Fig. 4.7a— the set of necessary and sufficient conditions for unconditional stability can be list as follows

- No RHP poles in the network terminated with Z_0.
- $|\Delta_s| < 1$ for all ω.
- $K > 1$ for all ω.

If all the system poles are observable, the condition (1) corresponds to the proviso, thus the S-parameters having no RHP poles. Is precisely this first condition the one in which the stability analysis of actively loaded ESAs should pay more attention, in order not to obviate the effect of those possible *hidden* RHP poles.

Consequently, the stability analysis of the antenna, loaded with a non-Foster network, requires the use of methods that does not only include a reduced two-port version of the N-node network, but all the possible poles of the whole antenna system [106]. Such an N-node network can be described by a matrix equation in the frequency domain: $s = \sigma + j\omega$ [107]:

$$\mathbf{Y}(s) \cdot \mathbf{V}(s) = \mathbf{I}(s), \tag{4.9}$$

where $\mathbf{Y}(s)$ is an NxN square matrix and $\mathbf{V}(s)$ and $\mathbf{I}(s)$ are respectively the excitation and response column vectors of size N. The whole circuit (antenna+NIC) will be stable if and only if all the poles of the system (roots of $|\mathbf{Y}(s)|$) lie in the LHP. Otherwise, the transient response will exhibit an exponential growth leading to instability [87]. This analysis is also valid for the impedance ($\mathbf{Z}(s)$) or the S-parameters representation of the system. In mathematical terms, the stability of the system can be computed as the roots of the determinant of $|\mathbf{Y}(s)|$, Δ_s. The designer should be able to algebraically extract all the zeros of Δ_s (the

poles of the complete system) to validate they lie on the LHP. To illustrate the procedure, let's take the circuit in Fig. 4.9, which depicts a simplified version of a ring oscillator presented in [107] and [105], as an example to carry out the stability analysis. The circuit consist of the small-signal model of two FETs connected in a ring, and observed from ports 1 and 2 through resistors R.

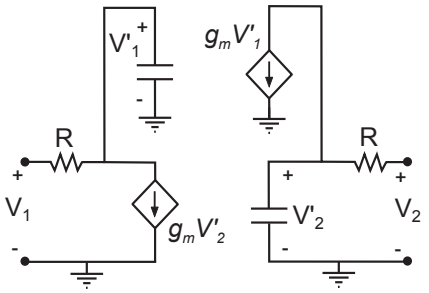

Figure 4.9: Simplified version of a ring oscillator using the small signal model of two FETs [105].

If we use the S-parameters to analyze the circuit, the circuit model must be terminated in the characteristic impedance that define the S-parameters, Z_0. Then, the network determinant can be expressed as the determinant of the $[S]$ matrix, as follows

$$\Delta_s = \left(sC_g + \frac{1}{R + Z_0} \right)^2 - g_m^2. \tag{4.10}$$

After some algebra to calculate the roots of Δ_s, the system poles of the Z_0-terminated network are found not to lie on the RHP as long as $R + Z_0 < 1/g_m$. For values of R in that range, the system is stable and the proviso is satisfied.

Note that, since the circuit is terminated in Z_0, the roots of the determinant of Δ_s will give us the poles of the system itself, thus, possibly without the loads of interest for the designer. Hence, the remaining conditions in the list ((2) and (3)) shall be checked to find the set of loads for stability, making the process even more complicated.

Furthermore, in most cases, the appropriate network determinant is too complicated to be easily determined or factorized. Moreover, we only want to know whether there are any RHP zeros of Δ_s rather than their exact location in the complex plane. Then, it is possible to make use of the Nyquist test. Therefore, according to the Nyquist test, by tracing the locus of Δ_s as s travels clockwise around the RHP s-plane, the number of times the locus encircles the origin, in such clockwise direction, equals the difference between the number of zeros and poles of Δ_s lying on the RHP. It is necessary to assume that the network matrix is formed by components such that none of them have RHP poles. As a result, the network determinant, Δ_s, has no RHP poles, and the number of Nyquist encirclements indicates the number of RHP zeros —the unstable poles of the system— [105].

Further, for convenience, instead of testing Δ_s, an alternative is to evaluate the Normalized Determinant Function (NDF), first devised by Platzker et al. in [107]. The NDF is defined as the quotient Δ_s/Δ_{s0}, where Δ_{s0} is the network determinant when all dependent sources are turned off [108]. Since Δ_{s0} is the determinant of a passive network, it has no RHP zeros and, thus, it does not introduce any RHP poles to Δ_s/Δ_{s0}. By normalizing the network determinant in this way, we force Δ_s/Δ_{s0} to reach 1 along the semicircular part of the s contour —in the right-half of the s-plane— where $|s|$ is infinite, and the circuit is assumed passive. In consequence, Δ_s/Δ_{s0} only needs to be evaluated along the imaginary axis, $s = j\omega$. A more detailed description of these properties are shown in Appendix A. A further theoretical discussion is presented in [11].

Then, following the nomenclature presented in (4.9), the NDF can be defined as (4.11) if the admittance parameters are used to describe the system.

$$NDF(s) = |\mathbf{Y}(s)| \,/\, |\mathbf{Y}_0(s)| = \Delta_s/\Delta_{s0}, \tag{4.11}$$

where $|\mathbf{Y}(s)|$ is the determinant of the studied system, and $|\mathbf{Y}_0(s)|$ is the determinant of the same circuit but with all the dependent generators (associated to active elements in the NIC) switched off. As mentioned

above, it is possible to determine the number of zeros of the NDF in the RHP as the number of encirclements of the NDF around the origin in the complex plot. The system will be stable if the NDF does not encircle the origin when it is evaluated from $\omega = -\infty$ to $\omega = \infty$ [107].

The NDF can be easily calculated as (4.12) for the ring oscillator shown in Fig. 4.9, the condition of stability has been infringed by setting $R + Z_0 = 1.5/g_m$. Note that, for this example, it is easier to directly compute the roots of the network determinant by solving $\Delta_s = 0$, rather than calculate the two-stage NDF function. Nonetheless, in practical problems, where the designer is interested in including parasitics in devices, deviations from nominal values of components, manufacturing tolerances, arbitrary terminations (other than Z_0), and so on, this algebraic calculation becomes in a cumbersome —perhaps impossible— task.

$$NDF = \frac{\Delta_s}{\Delta_{s0}} = 1 - \frac{g_m^2}{[(R + Z_0)^{-}1 + j\omega C_g]}. \tag{4.12}$$

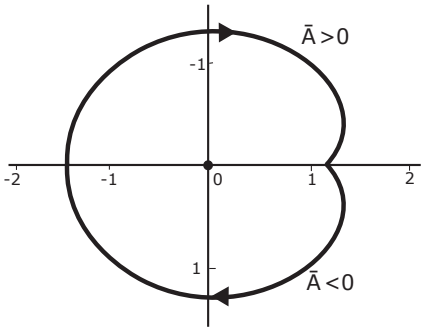

Figure 4.10: Nyquist plot of the NDF, for the ring oscillator in Fig. 4.9, once set the relation $R + Z_0 = 1.5/g_m$.

Figure 4.10 show the Nyquist trace of the NDF in (4.12). Since the NDF encircles the origin, the complete circuit is unstable for that particular terminations.

Struble and Platzker went beyond on this method in [108] and [109], and devised an outstanding technique that takes advantage of

EDA/CAD software to plot the Nyquist test of the NDF. Thus, by using any software for circuit analysis, it is possible to evaluate the NDF through the called Return Ratio (RR). The concept of *return ratio* was first discussed by Bode [11], and after by Maclean [110], and others [111], and was used to assess the stability of feed-back amplifiers. This concept can be related to the NDF of a network containing linear models of its active devices. The RR of an active element, which is embedded into a network, is defined as the response developed across its dependent nodes by an external excitation of magnitude 1.

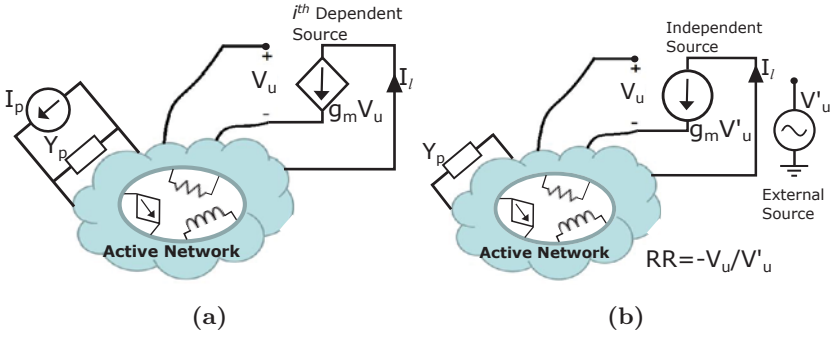

Figure 4.11: Sketch for the calculus of RR_i where: a) the i^{th} dependent source is replaced for (b) an independent source of arbitrary amplitude $V'_u = 1$. All others external excitations (I_p) are also removed.

To find a RR, let's suppose a network with M active devices, all modeled with dependent current sources, as depicted in Figs. 4.11(a and b). First, remove all external excitations while retaining their associated impedances (see Fig. 4.11a). Then, select one of these sources, say, $I_l = g_m V_u$, where I_l is dependent on the voltage V_u. Make this source independent by redefining it as $I_l = g_m V'_u$, where V'_u is an external unconnected ideal source (for convenience, of magnitude 1), as it is shown in Fig. 4.11b. Finally, the response of the independent node, V_u, can be evaluated leading to the RR be defined as

$$RR_1 \equiv -\frac{V_u}{V'_u}. \tag{4.13}$$

This RR_1 is related with the network determinant by (see Appendix A and [11])

$$\frac{\Delta_s}{\Delta_{s01}} = RR_1 + 1. \tag{4.14}$$

This relation is not the NDF since Δ_{s01} is the network determinant with just one dependent source set to zero, whereas the denominator of the NDF, Δ_{s0}, has all sources set to zero. Δ_{s01} may have RHP zeros, while Δ_{s0} has none. In order to obtain Δ_{s0} in this process, all the remaining RRs must be computed by maintaining the already evaluated dependent sources turned off. Hence, the NDF can be calculated as follows:

$$NDF = \prod_{i=1}^{M} (RR_i + 1) = \frac{\Delta_s}{\Delta_{s0M}} = \frac{\Delta_s}{\Delta_{s0}}, \tag{4.15}$$

where RR_i is the return ratio for the i^{th} dependent source; M is the total number of active elements of the network, thus, RR_1 is the return ratio of the source $i = 1$, when the sources $i = 2, 3...M$ are switched on. In the same way, RR_k is the return ratio of the source $i = k$, when the sources, $i = 1, ..., (k-1)$, are switched off.

In practical designs, the symmetry property in the NDF polar plot around the horizontal (x) axis, between the positive and the negative frequencies (see Fig. 4.10) can be used for simplification of the analysis. Such property can be expressed as the relation: $NDF(-\omega) = NDF^*(\omega)$. Thus, it is usually enough to compute NDF along the range $[0, \omega)$ only, and afterwards, calculating the complex conjugate of $NDF(\omega > 0)$. This procedure allows the use of almost any type of modern circuit simulators, and at the same time, reduces the processing time.

It is important to note that it is necessary to extract the linear model for each active device in the non-Foster network, around its bias point, prior to carrying out the NDF calculation. The more accurate the linear models are the more reliable the NDF is for predicting stability. A more detailed description of the NDF, comprising its properties and algebraic deduction is presented in Appendix A.

A remarkable advantage of using an EDA circuit simulator to compute the NDF is the possibility of including the two-port network sub-circuit in the same schematic containing the NIC. That sub-circuit can be either the simulated or the measured S-parameter matrix of the ESA whose port-2 is located in a low sensitivity position. Moreover, other parameters like package parasitics, lossy transmission lines, etc. can also be included. This fact allows us to carry out the stability analysis of the whole antenna system (antenna + NIC) at once, and accounting for several parameters effects related with a realistic application.

4.2.4 Step 4: Radiation Considerations

According to the antenna structure and the selected NIC topology, the current distributions can change, and different modes can be excited once a non-Foster network is placed. This phenomenon is more significant for planar structures, as shown in the previous chapter. In a linear structure, (e.g. dipoles and loops) the currents along the antenna do not change when an ideal purely reactive implementation of $Z_{\mathrm{NIC}}^{\mathrm{an}}$ is placed along the antenna. Nevertheless, the resistive part of a real non-Foster network, unavoidable in practice, will produce some changes in the radiation pattern that must be considered in the design process.

In this sense, testing the real part of the implemented NIC impedance is crucial. If the resistive part of the needed analytical impedance $Z_{\mathrm{NIC}}^{\mathrm{an}}$ (4.2), is far from zero and, at the same time, the *Sens* value is not low enough, poor impedance performance can be expected in the evaluating location of the port-2.

4.2.5 Step 5: Components' Tolerance Effects

Additionally, and complementary to sensitivity and stability analysis, a study about the influence of the tolerance of components (i.e. resistors, capacitors, and inductors) in the impedance response of the NIC, and in the stability of the antenna system is profitable. The easiest way to do that is through a CAD circuit software with the option of statistical analysis, in order to study the effects of possible variations on circuit performance, where a confidence interval around the nominal values of each

component (e.g. normal distribution for the nominal values in lumped elements with some tolerance percentage given by the manufacturer) can be set up. Moreover, it is possible to include parameters of the transistor linear model, physical lengths of the layout and package parasitics.

There are two steps that must be performed before analyzing the deviation of a circuit response, associated to the tolerance of its components. The first step is setting up the statistical properties of each parameter value to be analyzed. The second one is the specification of the goals that are used to determine if the circuit has an acceptable or unacceptable performance. Then, iterative simulations take place automatically, and the results can be evaluated by graphic inspection or by numeric calculation of the deviation from some interval of interest, e.g. the S_{11} parameter over the intended bandwidth.

Figure 4.12a shows a typical graphical result of a tolerance analysis, carried out in the commercial software Applied Wave Research (AWR)® for FET-based NII circuit, shown in Fig. 4.12b, previously described in Section 2.7.2, when it is embedded into a small antenna. In this example, the effects on the NDF plot are observed as the result or applying a statistical analysis —called *yielding analysis* in AWR— around the nominal values of the NIC components, such as the transconductance g_m of transistors, the microstrip paths size, the DC-biasing elements, etc.

The importance of tolerance analysis does not rely on the statistic calculation around nominal values; but in the identification of those parameters that have the most influence on the expected performance of the whole antenna system, providing reliability and higher control for the designer. For the case of the NII in Fig. 4.12b, a tolerance of 10% in the analysis shows that the circuit remains stable, as the NDF plot does not encircle de origin.

4.3 Noise Considerations

Noise can be understood as any disturbing influences on the signal of interest. It is one of those factors that is either difficult to analyze and measure in practical applications. There is a number of noise sources involved in any communication system, some of them are part

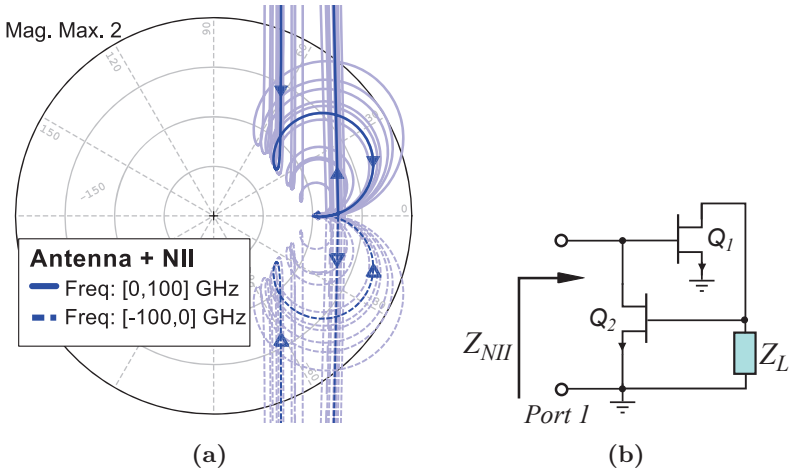

Figure 4.12: (a) Typical tolerance analysis outcome over the NDF computation from the MOSFET-based NII circuit sketched in (b), when it is embedded in an ESA.

of the propagation media itself, and others are consequence of electronic phenomena inherent to the circuitry composing the transmitters and receivers. Among the first category of noise sources, it is worth mentioning those that are present in the propagation media of radio signals: the noise in the atmosphere.

Since the atmosphere is not composed of air only, a significant interaction between it and the electromagnetic radiation has been verified throughout the development of radio communications [112]. It is possible to say that the behavior of the atmosphere against the propagation of electromagnetic waves is determined mainly by two major components: oxygen and water vapor. These elements show states of vibration and rotation of their molecules. In turn, these states exhibit absorption peaks corresponding to the points with greater attenuation of a wave traveling through the atmosphere. Those peaks are located at frequencies around 24 GHz and 185 GHz, associated with the water vapor, and at 60 GHz and 118 GHz, in the case of oxygen, as can be observed in Fig. 4.13.

Under the 3 GHz or 4 GHz, other factors come into play, such as the atmospheric noise. This type of noise can be described as a natural process primarily caused by lightning discharges in thunderstorms, es-

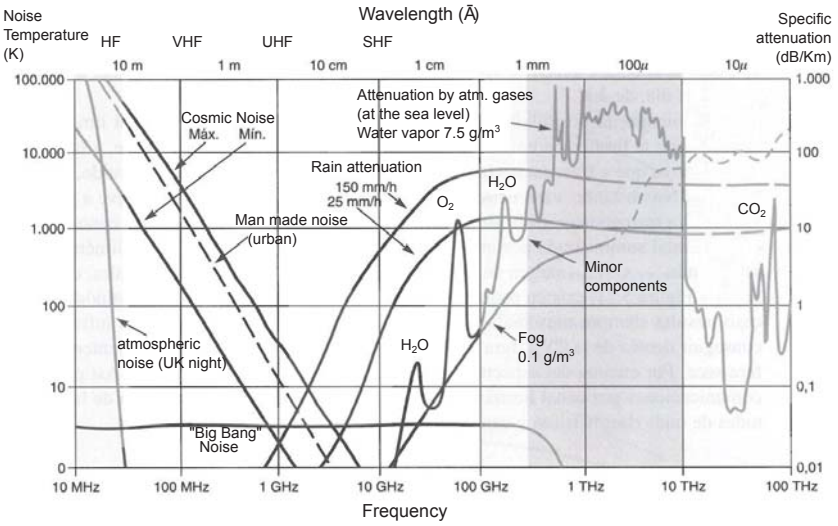

Figure 4.13: Atmospheric noise contributions [112]. The background intensity indicates the atmospheric opacity level.

pecially in the ionosphere, and whose influence is greater at frequencies below 30 MHz. In this interval, the attenuation is such high that the ionosphere can be treated as a reflector. The receiving systems designed to operate in this frequency region are called natural-noise limited [75]. Another contribution to the noise in the atmosphere is the cosmic noise, associated with all the astronomical bodies surrounding the earth in our galaxy, as depicted in the right side of Fig. 4.13.

Finally, the *man made noise* appears as the result of all the electric machinery, hand-held devices, other radio communication systems, among others, especially in urban areas. Summarizing, the best choice for the propagation of electromagnetic waves through the atmosphere, is the microwave band, thus, for wavelengths in the order of centimeters or tenths of a meter. At lower frequency bands, however, several applications have been possible due to the engineering of other alternatives aiming at compensating the signal degradation caused by the noise and the low gain of the small antennas involved (repeater stations, high power at the radiation stage, among others). It is possible to list some of those applications as aeronautical communications (ground-to-aircraft and aircraft-to-aircraft), Frequency Modulation (FM) broadcasting, ana-

log television, over-the-horizon radar, TETRA links, etc. Nevertheless, the noise and its effects are always present in the communications systems, and its analysis and measurement are of capital importance for obtaining reliable and controlled designs.

On the other hand, internal electronic noise in transistors and resistors results of physical phenomena, associated with the natural granularity of charge in electronic devices. Thus, current consist of a very large number of individual charge quanta. Hence, at the junction of a diode, for example, the current resulting of injecting charge is not purely constant. It still exhibits some random variations, which are called *shot noise*. Also, associated with the shot noise, it has to be mentioned other electronic noise sources: the *flicker* and the *burst* noise, also known as the low-frequency noise forms, or the $1/f$, $1/f^2$ *noise*, respectively. Another important source of electronic noise is due to the random motion of charges in lossy elements, at temperatures above absolute zero. This type of noise is called *thermal noise*, and as it can be predicted from fundamental physics principles, is used as a standard for describing other types of noise [113].

In any case, noise has been, and continues to be, a fundamental limitation to the capabilities and performance of communication systems. In fact, information and communication theory are almost entirely formulated around the problem of obtaining reliable communication in a noisy environment.

Therefore, it is possible to describe the quality of a communication system, especially in the receiving side, by measuring the signal-to-noise parameter (SNR). The SNR appears as an important parameter in such a way it describes the strength of a signal in relation to the noise accompanying it. The output SNR is dependent on the receiver input SNR and the Noise Figure (NF) of the receiver chain, understood as the degradation of the SNR between its input and output ports. Input SNR is a function of the power transmitted, transmitter antenna gain, atmospheric transmission coefficient, temperature, receiver antenna gain, and receiver NF. The reduction of the receiver NF enhances the output SNR.

On the other hand, for cases when embedded devices are present in the receiving chain, it is no possible to access all the points that would

be of interest to measure the SNR parameter. The characterization of the noise in a noisy device is commonly carried out by measuring its noise figure, computed as the *noise factor*, F, expressed in decibels, as follows

$$\begin{aligned} &F = \frac{S_i/N_i}{S_o/N_o} = \frac{SNR_i}{SNR_o},\ and \\ &F \geq 1, \end{aligned} \tag{4.16}$$

$$\begin{aligned} &NF = 10\log(F)\ \text{(dB)},\ and \\ &NF \geq 0\ \text{(dB)}. \end{aligned} \tag{4.17}$$

That is the case when an ESA is designed to contain an active non-Foster MN, the noise figure measurement becomes a challenging task. Additional considerations have to be addressed in order to estimate if the inclusion of an active MN to the antenna structure represents an advantage or an issue for the merit NF of the global antenna system. Thus, a primary circuital parameter should be used to estimate the SNR degradation (or advantage). This parameter can be the figure-of-merit G/T, where G is the antenna gain and T stands for the equivalent noise temperature of the receiving system, as it will be described below.

In active-loaded receiving antennas, as it is the case of an ESA with an embedded non-Foster MN, the parameter that contains all the information on the performance of the active antenna is the figure-of-merit G/T. This parameter remains constant along the entire receiver, and comprises an interesting alternative when its components (G or T) cannot be separately measured. Thus, G/T is the only parameter that can be directly measured by applying a conventional on–off method [114]. A discussion on the G/T-parameter in actively loaded antennas (oscillator, amplifier, mixer or impedance-converter types) has been made in [115] and [116]. The underlying idea is that as the active element is directly connected to the antenna, the losses between the active-MN and the antenna are mainly due to the radiation efficiency. These losses can be included in a new loss factor $L_e > 1$. It must also be noted that the actual actively matched antenna temperature T_a (not physically available) is not the same as the one in the passive system counterpart. T_a depends on the overall antenna pattern which, for the actively matched antenna, is not exactly the same as that for the passive one. The figure-of-merit, G/T, in an actively matched antenna is then given as (4.18),

where F_{opt} is the optimum noise factor, and T_{rec} is the receiver equivalent noise temperature.

$$\frac{G}{T} = \frac{\frac{G_{\text{ACT}}}{\Delta G}}{T_a + T_0(L_e - 1) + T_0(F_{\text{opt}} - 1)L_e + T_0(L-1) \cdot \frac{L_e}{\Delta G \cdot L} + \frac{T_{\text{rec}} \cdot L_e}{\Delta G}}. \tag{4.18}$$

ΔG accounts for the potential increase in gain once the active device is added (e.g. in the amplifier-type active antenna). For the case of an actively matched antenna, since the non-Foster MN is not aimed at providing power gain across its ports, ΔG should be ideally computed as 1. Hence, in theory, once the NIC is added no insertion losses should be expected either. T_0 is the room temperature and L stands for the losses associated to the NIC components. Finally, G_{ACT} is the *effective gain*, a parameter that can result in a value larger than the directivity of the corresponding passive (unloaded) antenna, as it is the case of amplifier-type active antennas. For an actively matched antenna, the maximal effective gain value is the maximal directivity itself, because of the improvement in the overall reflection coefficient, $|\Gamma_{\text{IN}}|$ (neglecting the ohmic losses of the radiating element), result of adding the active MN. An expression for the effective gain, as a function of the observing direction, is given as [114]

$$G_{\text{ACT}} = D_{\text{MAX}}(\theta, \phi)\Delta G \frac{(1 - |\Gamma|^2_{\text{IN}})}{L}, \tag{4.19}$$

where L is a factor that accounts for losses in the active non-Foster MN. Then, once measured the G/T parameter, the overall noise contribution from the actively matched antenna can be extracted as in (4.20), provided standard anechoic chamber conditions ($T_a = T_0$).

$$F_{\text{ACT}} = \left.\frac{kT_{\text{ACT}}B}{kT_0B}\right|_{T_a = T_0} = F_{\text{opt}}L_e + \frac{(L-1)L_e}{L\Delta G}, \tag{4.20}$$

where T_{ACT} is the equivalent noise temperature for the system (antenna + NIC). As ΔG is not large enough, the terms on the right side in (4.20) have comparable magnitudes.

For frequencies at which an anechoic chamber is not a viable option (e.g. at the VHF band), most of the authors in the reported work —with practical implementations— have followed a conventional on–off method [39] to characterize the noise performance in the actively matched ESA. This method comprises two stages. First, the *gain advantage* measurement, which accounts for the improvement in the realized gain between the NIC-loaded ESA and the unloaded (unmatched) ESA. The scheme of this measurement is shown in Fig. 4.14a (previously described and depicted in Fig. 2.27b, Section 2.8). Second, the output *SNR advantage* measurement, in which some additional steps are needed according to the scheme shown in Fig. 4.14b. The complete method steps can be listed as follows:

1. Unloaded Receiving ESA with the transmitter OFF: for measuring the noise floor (unmatched case), N_0 (dBm).
2. NIC-loaded Receiving ESA with the transmitter OFF: for measuring the noise floor, N_1 (dBm).
3. Unloaded Receiving ESA with the transmitter ON: for measuring the signal level (unmatched case), S_0 (dBm).
4. NIC-loaded Receiving ESA with the transmitter ON: for measuring the signal level, S_1 (dBm).

As a result of the listed procedure, the possible advantage in SNR for the actively-loaded antenna can be computed as

$$\begin{aligned} SNR_{\text{adv:dB}} &= Gain_{\text{adv}} - Noise_{\text{added}}, \\ SNR_{\text{adv:dB}} &= (S_1 - S_0) - (N_1 - N_0). \end{aligned} \tag{4.21}$$

In addition, some analytical treatment, reported in [117], identified the non-Foster matching approach for ESAs as advantageous for noisy receivers only (i.e. $NF_{\text{receiver}} > 6$ dB). This, along with the simulation-based analysis presented in [118], leads us to the assumption that the inclusion of non-Foster elements in an antenna does not imply an obvious advantage in the output SNR of the global system.

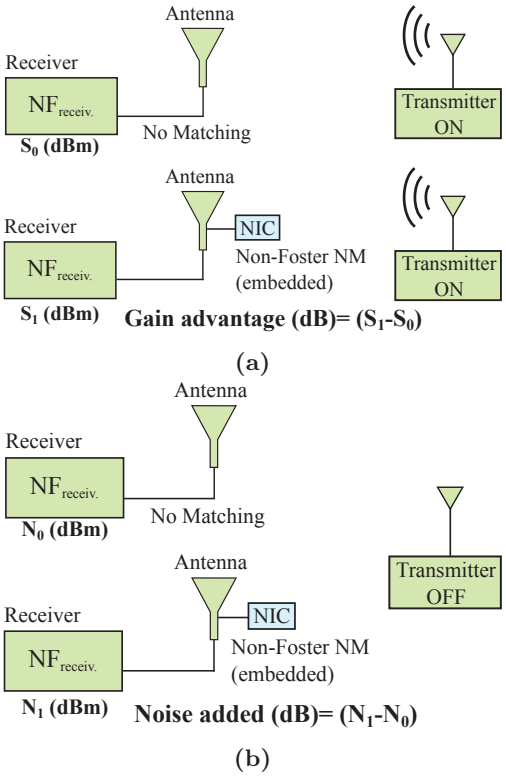

Figure 4.14: Scheme used for measuring the SNR advantage in actively-loaded ESAs, as the difference between (a) the gain advantage and (b) the added noise.

Nevertheless, the results from the noise characterization reported thus far allow concluding that for rigorous design of actively-matched ESAs, loaded with NIC-based non-Foster MNs, a careful noise investigation should always be performed.

4.4 Design Examples

In the following sections, some design examples applying the described methodology are presented. The first example comprises a printed semiloop set in a ground plane of similar size. The active matching network is intended to be located embedded into the semiloop struc-

ture itself in order to set a bidirectional antenna, with an engineered impedance bandwidth at Very High Frequency (VHF) frequencies, without affecting its natural resonant band.

The second example accounts for a printed blade-type monopole, whose natural resonant frequency is at the lower part of the Ultra High Frequency (UHF) band, loaded with an embedded non-Foster circuit. In this case, an impedance matching bandwidth over a frequency range in the lower part of the VHF band is intended. The monopole is electrically small across the interest band. The involved application is the aircraft radio communication systems, in response to the continuous changes and demanding requirements on aerodynamic drag in airplanes, which implies the need for miniaturization of the antennas involved in such an airborne systems.

4.4.1 Small Printed Semiloop Actively Matched with an Embedded NIC

A printed small semiloop, with a radius $R = 40$ mm in an FR4 substrate of 0.5 mm thick, $\epsilon_r = 4.4$, and loss tangent $Tan\delta = 0.02$, has been built. The objective is to obtain an impedance matched dual-band small antenna, with a monopole-like radiation pattern at the lower band (i.e. VHF-band up to 200 MHz) as well as a simple and low-cost fabrication (see Fig. 4.15a).

Sensitivity Analysis

The proposed antenna is an ESA for frequencies up to 450 MHz since the factor $ka < 0.5$, where a is the radius of the smallest sphere enclosing the antenna system ($1.3 * R$ in the current design) at the resonance frequency, $f_0 = 1.2$ GHz, and k is the free-space wavenumber (i.e. $k = \omega_0/c$). The antenna and the embedded non-Foster circuit are first modeled in a CAD full-wave simulator and in an EDA circuit simulator, respectively, prior to be manufactured. As claimed before, according to the proposed methodology, the first instance of the design process consists of checking the suitability of this structure to be actively matched. Thus, to obtain the *Sens* parameter, a sweep of the port-2 location is

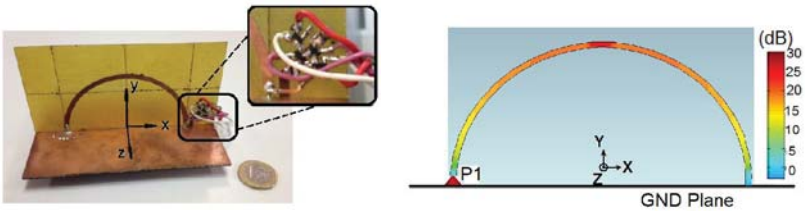

(a) **(b)**

Figure 4.15: (a) Proposed prototyped small semiloop antenna with the embedded NIC. (b) The averaged sensitivity $\overline{Sens}$ over the antenna structure.

made using the Computer Simulation Technology (CST)® software, by including a gap in the semiloop at different angles to connect the analytical port-2, and extracting a two-port S-parameter matrix each time. A region with low sensitivity ($|Sens| < 10$ dB) is found on the opposite side of the input port, near to the ground plane, as depicted in Fig. 4.15b. *Sens* parameter was computed as the average of (4.9) over a frequency range from 10 to 300 MHz (VHF band).

NIC Topology and Components Selection

Since the best location is near the ground plane, a grounded NIC topology will be easy to implement. In previous efforts, in the seeking for alternatives to achieve stable and easy-to-build grounded NICs, a grounded NII topology, first proposed by Kolev [67], was found. This topology is selected as active MN for the semiloop antenna in this design example. The circuit consists of two BF998 MOSFETs connected in the way shown in Fig. 4.17a. There is a strong dependence of Z_{NII} on the squared transfer-conductance $(g_m)^2$; as shown in the equation in Fig. 4.17a. Since the NII property used here is its negative-slope reactance, the terms NIC and NII can be interchanged, as mentioned before in Chapter 2. The choice of the transistor and its bias conditions constitute a trade-off between the stability of the NII and the maximum frequency of non-Foster response. Increasing the working frequency implies choosing a transistor with higher transient frequency. However, higher transient frequencies imply higher transfer conductance, and therefore, higher levels of feed-back currents. This fact results in potentially higher

instability problems. For this reason, a transistor with a moderate transient frequency and with a stable transfer admittance, over a bandwidth as large as possible, is welcome. The proposed transistor presents a constant forward transfer admittance up to 1 GHz (see Fig. 4.16) and a transient frequency $f_T = 1.9$ GHz.

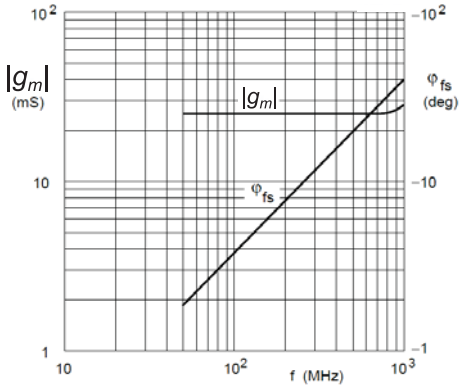

Figure 4.16: Forward conductance parameter vs. frequency in the BF998 MOSFET, taken from the datasheet [119].

NIC Impedance Performance

The non-Foster behavior in the NII impedance (Z_{NII}) should be expected at frequencies up to 200 MHz (approximately $f_T/10$, as mentioned in Section 4.2.2). It is confirmed by the negative slope in the imaginary part of the simulated NII impedance in Fig. 4.17c. The change in the slope of the NII reactance indicates those frequencies after which the gate-source internal capacitance, C_{gs}, dominates the impedance response at the NII input port. This frequency approximately corresponds to the maximum range of impedance matching at the added lower band, as it will be shown below. In addition, the sharply change in slope of $Z_{\text{NIC}}^{\text{an}}$, at frequencies above 400 MHz, makes this analytical impedance difficult to fit even with a NIC (or a NII) working at higher frequencies, as it can be seen in Fig. 4.17c. Thus, a practical NIC (or NII) will not fit the required $Z_{\text{NIC}}^{\text{an}}$. This condition explains the dual-band response of the antenna, and limits the performance of an ultra-wide-band actively matched semiloop. A series LC-tank ($L_L = 15$ nH, $C_L = 55$ pF) is

connected to act as the load (Z_L) of the NII (see Fig. 4.17a). This is an alternative for implementing a single-NII active non-Foster MN, whose input impedance (Z_{NII}) closely fits the analytical one ($Z_{\text{NIC}}^{\text{an}}$).

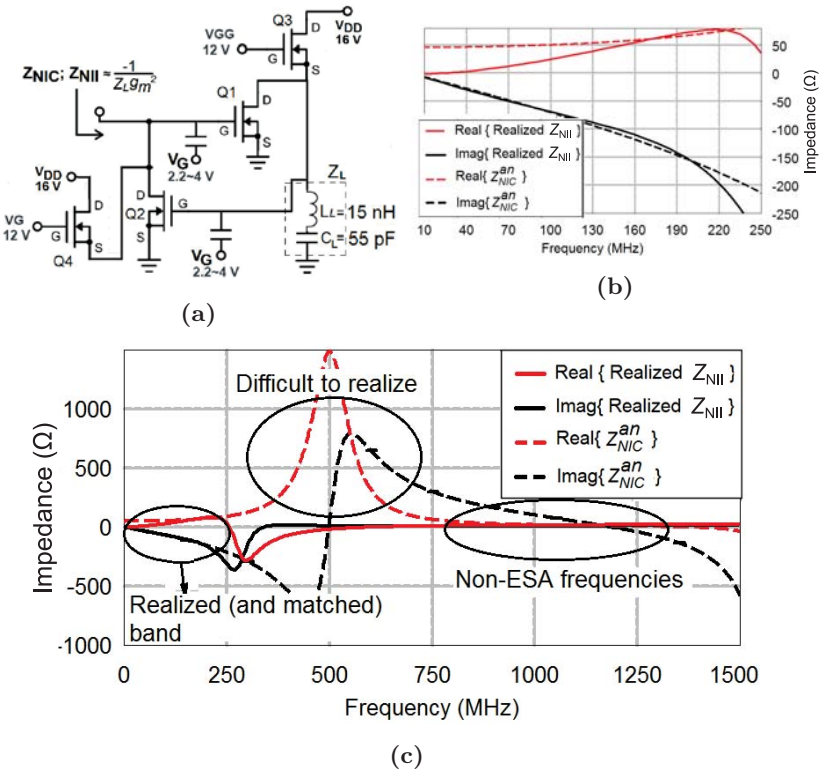

Figure 4.17: a) Kolev's grounded NII topology with MOSFETs, where Q_3 and Q_4 are acting as current sources. (b) Impedance response of the designed NII vs. the analytic one, computed as in (4.4), when port-2 is placed at the opposite point from port-1. (c) A wider span comparing both impedances.

Those values of Z_L for the NII are found through visual comparison with the response of $Z_{\text{NIC}}^{\text{an}}$ at the selected port-2 location, as it is shown in Fig. 4.17b. Although the real and imaginary parts are not identical respectively, it is possible to obtain significant impedance bandwidths, as the inductive behavior of the semiloop impedance is effectively compensated by that from the NII. This is the benefit of loading the antenna with the NII in a low sensitivity location. In order not to degrade the

radiation efficiency, a NIC circuit with a low real part (ideally zero) in its input impedance must be connected. The bias circuit consists of another two BF998 connected as current sources to provide the drain current to the NII's FETs.

Stability and Components' Tolerance Analysis

The results, in terms of impedance matching, are shown in Fig. 4.18. The blurred red lines indicate the effects in the S_{11} parameter due to a tolerance of 10%. Over a bandwidth of 140 MHz centered at 117 MHz (i.e. $FBW = 119\%$) an acceptable matching level is measured (i.e. $|S_{11}| < -8$ dB). The natural band of the unloaded antenna is not greatly degraded. In terms of miniaturization, values in the range 0.04 to 0.17 for the ka-factor are reached at frequencies from 47 MHz to 187 MHz.

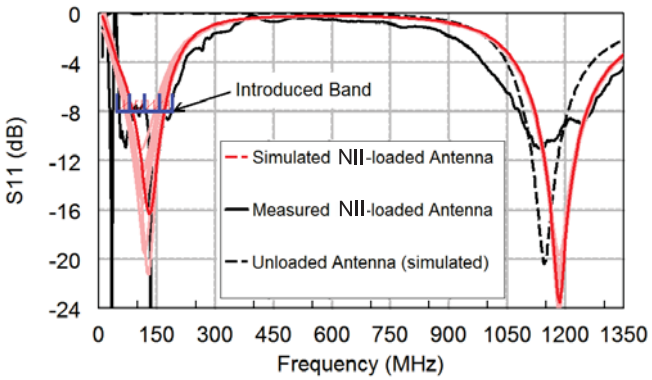

Figure 4.18: $|S_{11}|$ response for the manufactured actively matched semiloop.

The stability test was performed using the AWR Microwave Office® suite to calculate the NDF and, at the same time, statistical analysis with a tolerance of 10% around the nominal values for all the components and transistor linear model parameters. The S-parameter model of the antenna was included in the calculus of the NDF. Figure 4.19 shows that the NDF, calculated for the whole system, does not encircle the origin of the root-locus plane, nor for the nominal values neither for the worst tolerance case (blurred lines). The NDF was computed within the interval [-100, 100] GHz. Since no encirclements are observed, a

stable condition for the design can be expected. However, low tolerance in NIC's (or NII's) components is preferable in a non-Foster approach. It was found that due to the strong relation between the impedance response and the bias point of the MOSFETs (through the parameter g_m^2), small changes in DC biasing, especially in the gate-source voltage, produces more significant changes in antenna performance and stability than tolerance in lumped components.

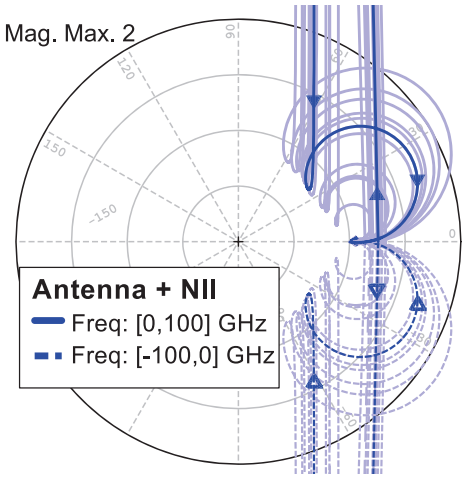

Figure 4.19: NDF loci for the entire system: antenna + NII.

Radiation Performance

It is worth noting that, at frequencies near the semiloop resonance (around 1200 MHz), the current distributions over the antenna, depicted in Figs. 4.20 (a and b), do not have significant changes. A counter-phase current, flowing from the ground plane through the NIC and from the input port, generates a double-lobe pattern along the polar axis of the loop, as expected for the wavelength loop antenna [26], as can be seen in the measured results in Fig. 4.20c. This condition corresponds to the fact that, at higher frequencies, the magnitude of the realized NIC impedance $|Z_{\text{NIC}}|$, decreases greatly, as the current flowing through the NIC (NII in this case) does. However, at 1200 MHz, the measured received power, for the NIC-loaded case, is 1.4 dB lower than the unloaded antenna, indicating a moderate effect in the antenna gain.

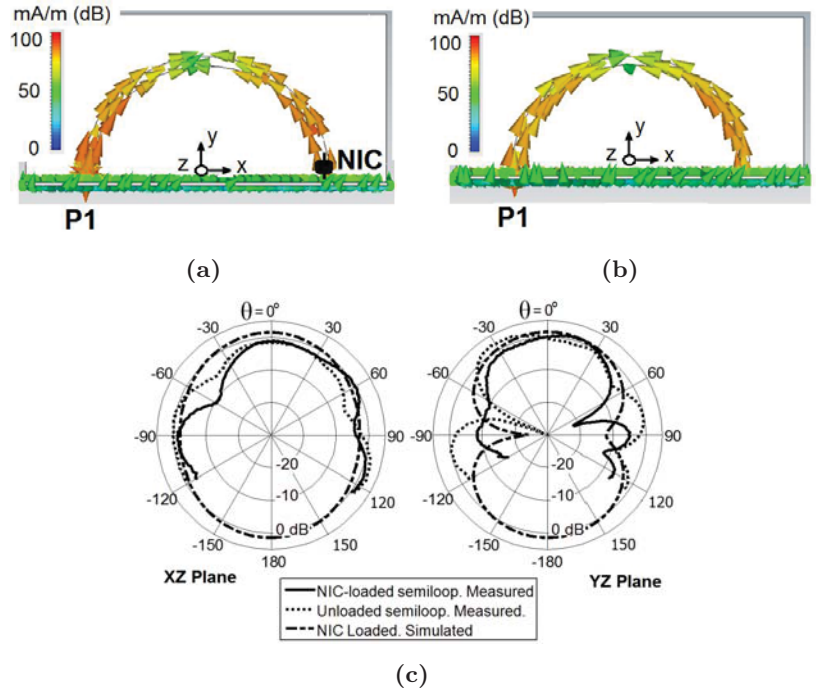

Figure 4.20: Sketch of the current distributions at 1200 MHz for (a) the loaded and (b) the unloaded semiloop. (c) Measured radiation plot for both cases. In both planes the point $\theta = 0^{\circ}$ agrees with the polar axis of the semiloop (z-axis).

For frequencies in the new lower band, where the NIC is acting as an active MN, a radiation pattern without significant changes should be expected. However, the unavoidable condition of nonzero real part in the implementation of $Z_{\mathrm{NIC}}^{\mathrm{an}}$, produces a slight increase in the current over the semiloop at the input port side (Fig. 4.21a). This leads to a lobe centered at the negative part of the x-axis ($\Phi = 180^{\circ}$), in comparison with the unloaded case in Fig 4.21b, as can be seen in the simulated radiation pattern in Fig. 4.21c. This condition can be considered as a design constraint and it cannot be omitted in the design process.

With the aim to complement the radiation considerations, the simulated directivity patterns, for frequencies within the introduced lower band, that is 100 MHz and the edge frequencies (50 MHz and 200 MHz)

are depicted in Fig. 4.22. For those frequencies, the actively matched loaded semiloop shows similar radiation patterns. However, higher values of the resistive part of the NIC impedance may imply a more influenced radiation pattern at frequencies where the NIC is working as an active MN.

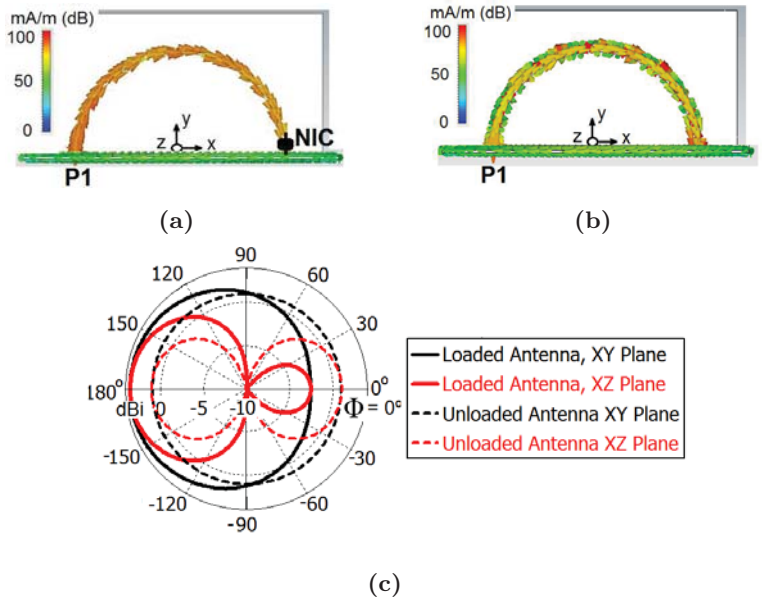

Figure 4.21: Sketch of the current distributions at 125 MHz for (a) the loaded semiloop and (b) the unloaded semiloop. (c) Simulated directivity plot for both cases.

Finally, a power-budget in the VHF-band at 125 MHz has been undertaken. At this frequency, the semiloop is around $\lambda_0/10$ and its ka factor is 0.15. A known reference antenna is used as a transmitter, Tx, while the antenna under test is located for receiving at $\theta = -90$, $\Phi = 180$, that is, in a direction parallel to the semiloop ground plane. A comment on the parameters to be measured should be made in advance. As the antenna is fully integrated with the NIC, the transmitting measured parameter would inherently include the joint effect of the antenna+NIC system. This results in a so-called *effective gain* parameter (see [114] and [120]). For the NIC-loaded antenna, this effective gain, $G_{NIC-loaded}$ is -6.88 dB. When we repeat the measurement for the

unloaded semiloop, the so-called effective gain results in the actual antenna gain, $G_{unloaded}$, of -28.1 dB. These two measurements show us the actual improvement between the NIC-loaded and the unloaded case.

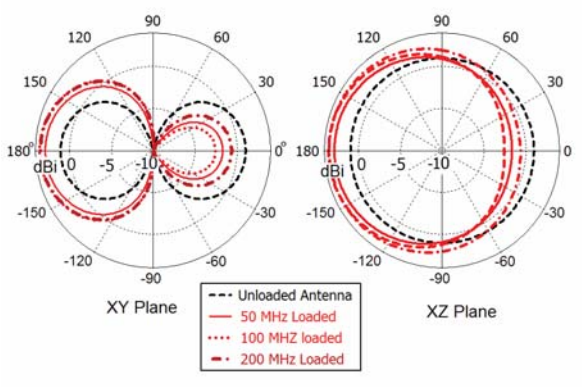

Figure 4.22: Simulated directivity plot for the active matched semiloop at different frequencies in the introduced lower band.

In addition to the previous measurement, for comparison purposes, an estimation of the radiation efficiencies can be extracted. Then, as it can be inferred from Fig. 4.21c, the presence of the NIC has slightly changed the current distribution in the original unloaded semiloop antenna. This new current distribution yields to a directivity in the direction of measurement, $D_{\max}$, of 2.7 dBi (continuous line in Fig. 4.21c). This change has to be accounted for to have a suitable comparison of the radiation parameter in both cases. The estimated radiation efficiency (η_{rad}) is 10.91%, for the loaded case, calculated from the relation $G = \eta_{\text{rad}} \cdot D_{\max}$. For the unloaded antenna, where the simulated $D_{\max}$ is 1.45 dBi (dashed line in Fig. 4.21c), the calculated radiation efficiency, η_{rad}, is 0.1%. If we now include the mismatching losses, we can calculate the total efficiency as $\eta_{\text{total}} = \eta_{\text{rad}} \cdot (1 - |\Gamma_{\text{IN}}|^2)$. For the NIC-loaded case it results in $\eta_{\text{total\_NIC}} = 0.109 \cdot (1 - 0.35^2) = 9.6\%$, while for the unloaded case it results in $\eta_{\text{total\_unloaded}} = 0.001 \cdot (1 - 0.98^2) = 0.004\%$.

Added Noise Measurement

The noise performance of the actively matched small semiloop is evaluated by computing the difference between the *gain advantage* and

the *added noise* quantities, according to (4.21). The measurement procedure described in Fig. 4.14 is set up for measuring the noise performance of the NIC-loaded antenna, with respect to the same antenna without any impedance matching. The transmitter comprises a signal generator, whose output impedance is 50 Ω, driving a 60 cm height blade-monopole, working across the upper VHF band (from 100 to 300 MHz), set over a ground plane of 1 m side. The receiver consist of the Antenna Under Test (AUT) —either the NIC-loaded and the unloaded semiloop— followed by the Spectrum Analyzer (SA), the Agilent N1996A. In order to reduce the noise figure of the instrument, and hence its sensitivity, an external preamplifier is used (Agilet LNA-87405B), whose gain and NF are 26 dB and 3 dB, respectively. The experiment was conducted from 110 MHz to 250 MHz.

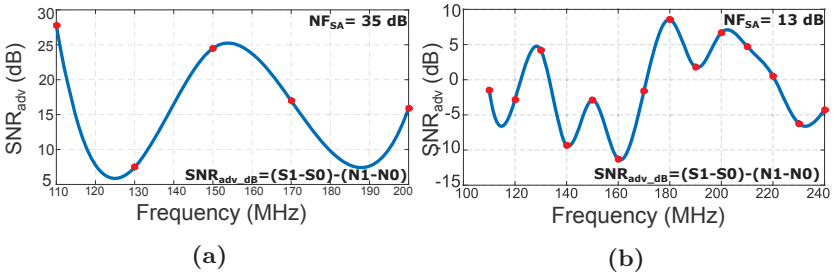

Figure 4.23: Added noise of the actively matched small semiloop, measured as the SNR_{adv} according to (4.21), with respect to the unloaded semiloop. (a) For a $NF_{\mathrm{SA}} = 38$ dB (no preamp). (b) For a $NF_{\mathrm{SA}} = 13$ dB (with the Agilent 87405B preamp).

The obtained SNR_{adv} is depicted in Fig. 4.23, for two different noise figures at the receiver, NF_{SA}, depending on whether the preamplifier was used or not. The red points represents the calculated SNR_{adv} while the curves corresponds to an interpolation made in the post-processing stage. It can be observed that the NIC-loaded semiloop effectively enhances the output SNR for a noisy receiver, as it is the case shown in Fig. 4.23a. For a less noisy receiver, as with the reduced-NF instrument situation, the actively matched antenna shows a SNR improvement only at certain frequencies, especially those above 190 MHz, where the active MN does not match the semiloop anymore (see Fig. 4.18). Additional parameters regarding the active devices involved (i.e. the MOSFETs) such as its biasing levels and topology should be considered in an optimization pro-

cess, comprising a future line of work in active non-Foster MNs applied to antennas.

4.4.2 Blade-type Monopole Actively Matched with an Embedded NIC

In this section, a blade-type small monopole of 22 cm by 25 cm over a substrate of 1.6 mm thick, and a permittivity $\epsilon_r = 4.35$, is matched over a 50-90 MHz range using an active non-Foster MN in two different configurations: floating-MN and grounded-MN. At the frequency interval of design, the ka factor is within 0.26 and 0.47 if the image of the monopole (beneath the ground plate) is accounted in the computation of the radius a. To alleviate the highly reactive response of the monopole impedance at lower impedances, a rectangular slot is placed along the blade (see inset sketch in Fig. 4.24), to give a longer path for currents, thus, an inductive compensation. This response is confirmed by simulation, as depicted in Fig. 4.24.

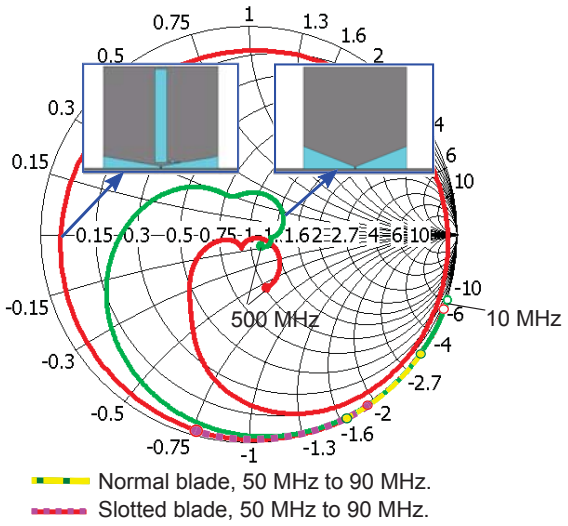

Figure 4.24: Antenna impedance response, in the Smith chart, of a 25 cm by 22 cm blade monopole. The inclusion of the longitudinal slot slightly compensates the reactive nature of the normal monopole, as the 50 to 90 MHz range is closer to the horizontal axis.

The intended impedance matching level is such that $|S_{11}| < -6$ dB. The design strategy developed along this chapter is applied. Therefore, the *Sens* parameter is used to find out two capital answers at the starting point of the design. First, the confirmation of the suitability of a blade-type monopole to be matched with an active embedded non-Foster MN and, second, only in the case of an affirmative outcome in the sensitivity analysis, to find out the best location for the active matching network over the monopole structure itself, through the sensitivity analysis.

Sensitivity analysis

The first studied configuration is the grounded one. Then, once an analytical port-2 is inserted in the antenna, through a CAD software for full wave simulation, a sufficient number of locations for the port-2 should be set, all over the monopole structure, for extracting the same number of S-parameters matrices. It is worth noting that in all the situations, in the grounded configuration, the port-2 is grounded. Then, by computing the *Sens* parameter applying (4.1), it is possible to plot the behavior of the frequency-averaged $\overline{Sens}$. The sweep result shows the bottom corner area as the lowest sensitivity point, as it is shown in Fig. 4.25. This is the most feasible point to connect the non-Foster matching network.

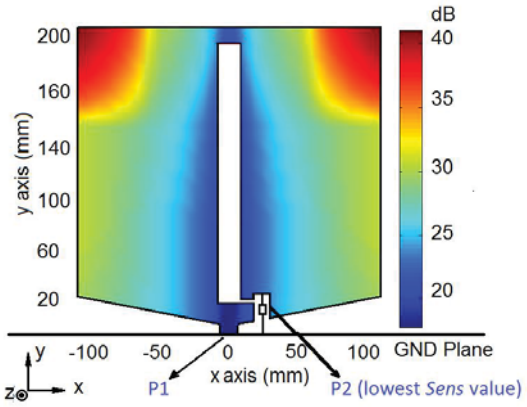

Figure 4.25: $\overline{Sens}$ parameter over the monopole structure, averaged from 10 MHz to 500 MHz, for the grounded-MN configuration.

In order to find alternatives for a variety of NIC topologies, a floating configuration for the port-2 is explored. In this sense, a gap in the blade is inserted to place the port-2 and to analyze the *Sens* parameter. The frequency-averaged magnitude of $\overline{Sens}$ for the floating case is depicted in Fig. 4.26. The averaged *Sens* shows again the central bottom corner area as the point of lowest sensitivity. However, the averaged $\overline{Sens}$ does not let us to observe how the behavior of this parameter over a specific frequency range is, in this case, for frequencies lower than 90 MHz. In other words, once the variation of the *Sens* parameter over the structure is checked, its behavior in the frequency domain, at a certain point, must be observed.

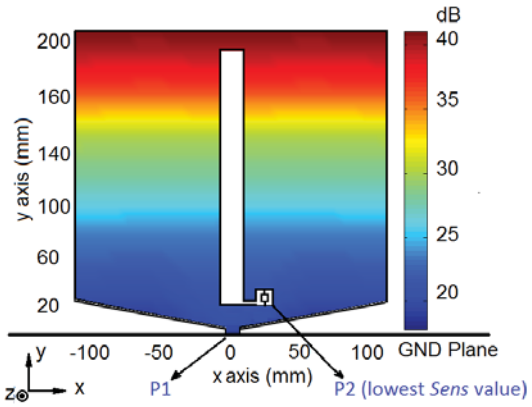

Figure 4.26: $\overline{Sens}$ parameter over the monopole structure, averaged from 10 MHz to 500 MHz, for the floating-MN configuration.

For the blade-type monopole, an important difference in the *Sens* parameter for both floating and grounded configurations is identified and shown in Fig. 4.27. The curves are depicted for the same frequency interval as the one used to compute the $\overline{Sens}$ parameter in the structure-based sweet, in Figs. 4.25 and 4.26.

Since the difference in the *Sens* parameter for both floating-MN and grounded-MN configurations is over than 25 dB, within the design interval (see Fig. 4.27), an important difference is expected between the impedance matching performance obtained by certain active non-Foster network connected at port-2, in each case. Even small differences between the realized (Z_{NIC}) and the analytical ($Z_{\mathrm{NIC}}^{\mathrm{an}}$) impedances will result

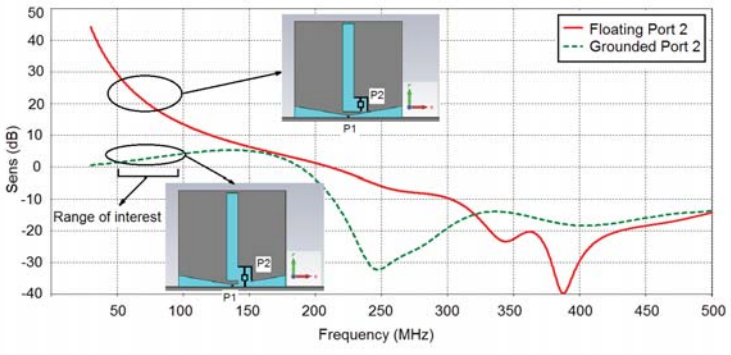

Figure 4.27: *Sens* parameter vs frequency in a blade-type printed monopole for two different configurations: floating MN and Grounded MN.

in greatly narrowed lower band. The obtained impedance bandwidth for the grounded-MN case is going to be much wider than the floating case, as it will be shown later.

Once the lowest *Sens* point and the most suitable configuration have been found, the analytical impedance, $Z_{\mathrm{NIC}}^{\mathrm{an}}$, derived from the ideal $\Gamma_{\mathrm{NIC}}^{\mathrm{an}}$, can be computed as (4.2) for the S-parameter matrix extracted when the port-2 is located in that position (the lowest *Sens* point). The continuous lines in Fig. 4.28 show the real and the imaginary parts of the analytical $Z_{\mathrm{NIC}}^{\mathrm{an}}$, for the grounded-MN case.

The behavior and the negative slope with frequency of the imaginary part of $Z_{\mathrm{NIC}}^{\mathrm{an}}$ ($X_{\mathrm{NIC}}^{\mathrm{an}}$), which indicates the non-Foster behavior needed to be fulfilled with the MN, also gives us an idea of what kind of load impedance we have to convert with the NIC (or the NII). In this case, since the analytical reactance reaches negative values over an almost straight line "going down", in the frequency range of interest, the more agreeable MN would be an ideal negative inductor, connected between the monopole and its ground plane, in shunt with the feeding port.

Transistor and NIC topology selection

Since the grounded configuration is the most suitable for broadband matching of this kind of monopole antenna, and the nature of the computed non-Foster reactance ($X^{\text{an}}_{\text{NIC}}$), the implementation of the active-MN can be carried out by means of the same NIC (strictly a NII) as in the previous design example. Moreover, the bottom corner location facilitates the biasing network for the active devices (transistors in this case) that compose the NIC.

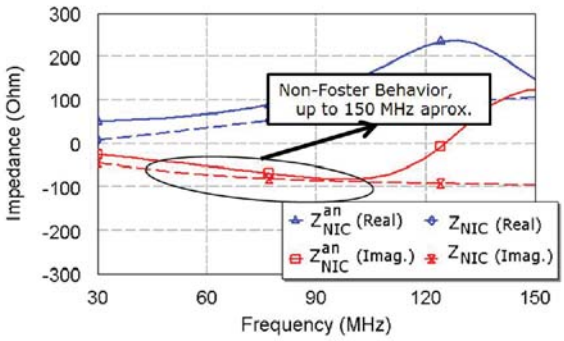

Figure 4.28: Analytical $Z^{\text{an}}_{\text{NIC}}$ compared with a simulated implementation of it with a real NIC (lowest Sensitivity case)

Figure 4.28 depicts the real and the imaginary parts of both the analytical $Z^{\text{an}}_{\text{NIC}}$ and the proposed MOSFET-based Z_{NIC}, looking into the port $P2$ in the inset NIC schematic of Fig. 4.29. For convenience, the same NIC topology as that in the previous design example is used here to act as non-Foster MN. Four BF998 transistors are used, two of them acting as the actual NIC and the remaining two acting as current sources. The impedance to be negated, and inverted since this NIC is actually a NII, consist of a series LC-tank. A surface mounting (SMD) multilayer inductor, L_L, of 4 nH and a SMD ceramic capacitor, C_L, of 300 pF compose the NIC load.

As a consequence of the higher value of *Sens* parameter for the floating configuration compared to the grounded one, when locating the port-2 close to the feeding port (port-1), the S_{11} response at the input port of the antenna is quite different, as it can be seen in Fig. 4.29, once the

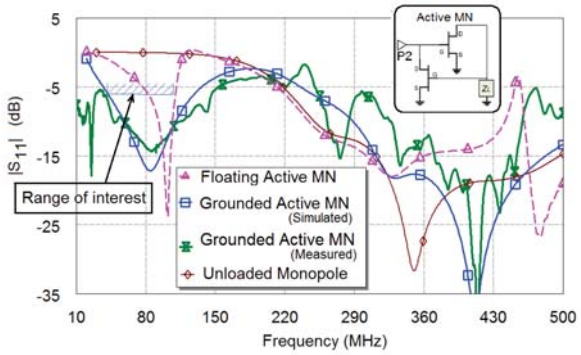

Figure 4.29: S_{11} parameter for both floating and grounded configurations, when a non-Foster circuit is loaded at port-2 of the antenna.

MOSFET-based NIC circuit is loaded at port-2 of the antenna.

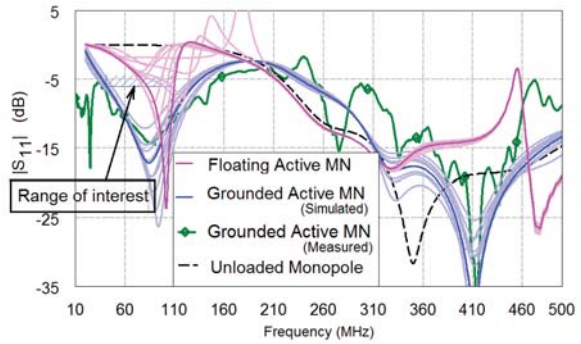

Figure 4.30: S_{11} parameter for both floating and grounded configurations, when a non-Foster circuit is loaded at port-2 of the antenna, including the tolerance analysis of the NIC components.

The intended matching level ($|S_{11}| \leq -6$ dB) is achieved for the grounded configuration only. The measured $|S_{11}|$ (green line in Fig. 4.29) corresponds to the grounded NIC configuration and agrees satisfactorily with the simulation.

The prototyped antenna with the embedded non-Foster MN is shown in Figs. 4.31 (a and b). The NIC has been mounted in the back of the radiating element to facilitate the biasing connection and measurement.

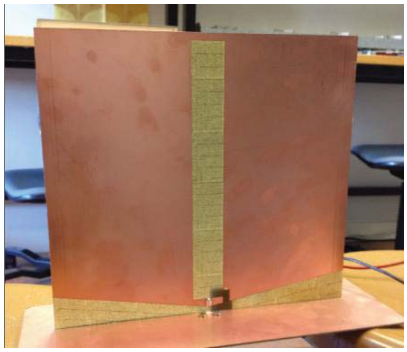

(a)

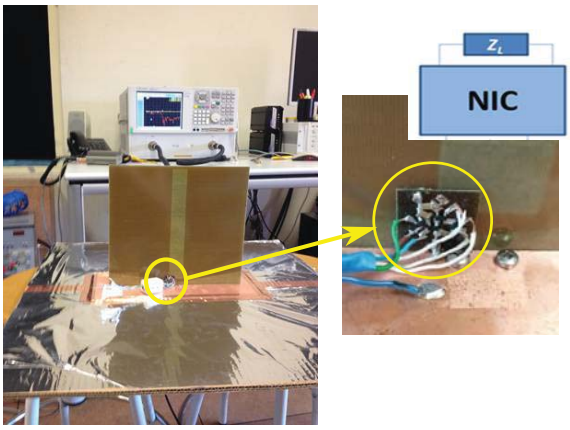

(b)

Figure 4.31: Prototyped antenna with the embedded non-Foster MN. (a) Frontal view. (b) Rear view of the actively matched blade-monopole, mounted on a 1 m X 1 m ground plate for S_{11} measurement.

Stability Analysis

The stability is also checked, by applying the NDF for the whole antenna system (blade-monopole + NIC). Thus, the influence of the two-port antenna (through its simulated or measured S-parameters) and all the components in the active-MN are considered. With the aim of observing the robustness of the design, the component's tolerance analysis tool, available in AWR® circuit simulator, is also computed besides the NDF. Two different percentages of tolerance are shown in Figs. 4.32a

and 4.32b, both of them following a normal distribution of probability.

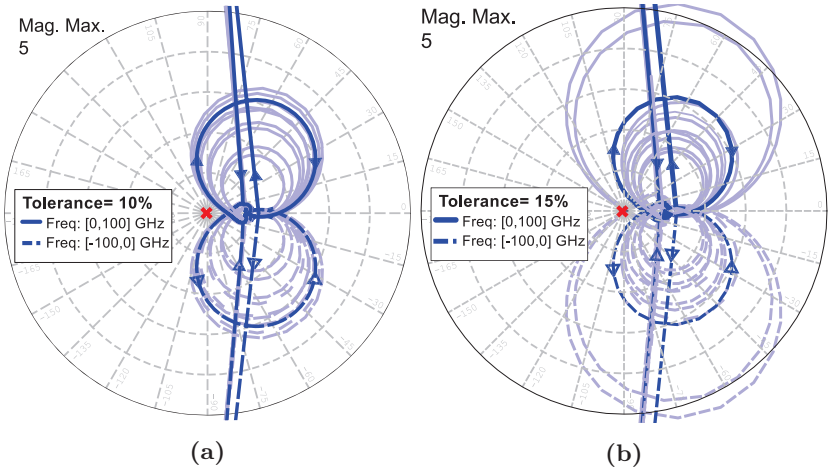

Figure 4.32: Polar plot of the NDF computed to check the stability of the NIC-loaded blade-monopole, in grounded configuration, for a component tolerance of (a) 10% and (b) 15%.

The risk of instabilities increases as the tolerance in components and microstrip paths do. Thus, it is desirable to choose low tolerance SMD elements as well as high resolution manufacturing process to implement the embedded active-MN. Such risk is deduced, in this case, from how much the NDF curve gets close to the polar origin, according to the NDF theory mentioned above and described in Appendix A. The NDF is computed up to 100 GHz, for both tolerances, along with its correspondent values for the negative frequencies ($\omega < 0$). It is observed no origin encirclements (i.e. the instabilities of the system) for the 10% tolerance. However, a potential risk of instability can be expected if the tolerance reaches 15%.

Passive vs. Active Impedance Matching Exploration

A typical question that arises from the active matching design for ESAs is if there is no way to obtain a similar impedance bandwidth by connecting a passive-MN, instead of an active one. In this sense, a passive MN based on lumped-reactive elements is designed and optimized

through the AWR circuit simulator software, to match the blade-type monopole along the intended frequency band. The passive-MN comprises two *L*-sections, composed of two capacitors in series and two inductors in shunt, as depicted in Fig. 4.33. The result of connecting such a passive-reactive network to the feed point of the antenna is depicted in 4.34, in terms of the $|S_{11}|$ magnitude, and compared with the grounded-NIC selected for this design.

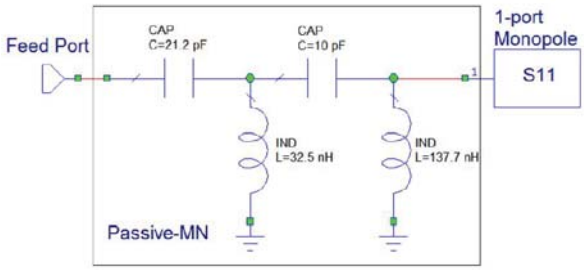

Figure 4.33: Schematic of the passive-MN, connected to a measured S_{11} parameter block from the one-port unloaded blade-monopole.

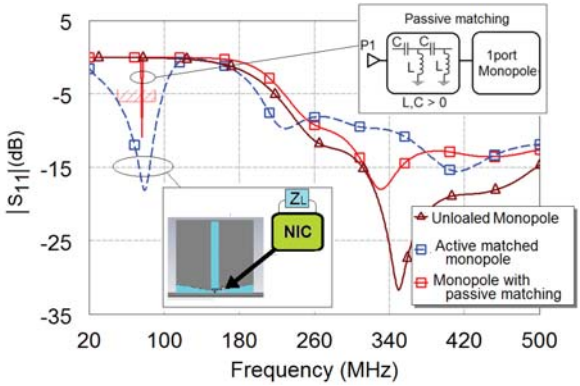

Figure 4.34: Passive MN vs. active MN (grounded configuration).

It can be seen the advantage that the active MN represent, even over a automatically optimized passive MN by a simulator. Nonetheless, in real applications, an important miniaturization level in ESAs is performed by adding toroidal coils with ferrites cores to match the antenna [121]. This approach is widely used in airborne antennas, at the expense of weight increase and gain reduction, this latter associated with losses in

ferrites at radiofrequency (RF) bands, that is, at VHF or higher.

Radiation considerations

When loading an ESA with any kind of circuit, composed well of lumped elements well of distributed ones, some change in the current distribution is expected, and therefore, some change in the radiation pattern or the radiated power has to be checked. By means of full wave simulation, it is possible to observe the current distributions for the antenna when loaded with the NIC acting as the active-MN. Figure 4.35 shows the current distributions for the NIC-loaded blade-type monopole, working at 50 MHz.

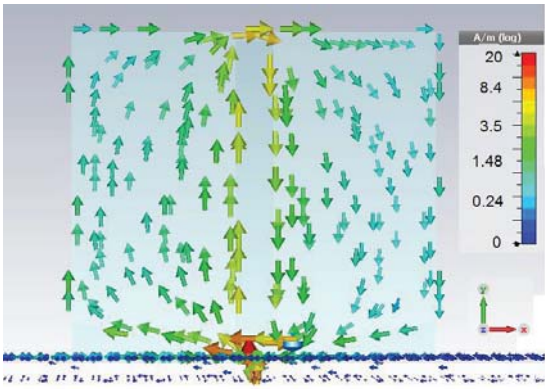

Figure 4.35: Current distributions for the actively matched monopole, at 50 MHz.

As expected, and according to the considerations discussed in Chapter 3, in antennas with planar structures, there is a substantial change in the net current distribution along the antenna, when the NIC is inserted, in comparison when there is no NIC (unloaded one-Port antenna). In this way, changes in the radiation pattern are expected and have to be considered in every situation of the application.

For comparison purposes, the current distributions of the same monopole, but without non-Foster MN (unloaded case), is depicted in Fig. 4.36. In this case, the intensity of the current is clearly higher in the bottom edge of the monopole, as the strength of the arrows shows.

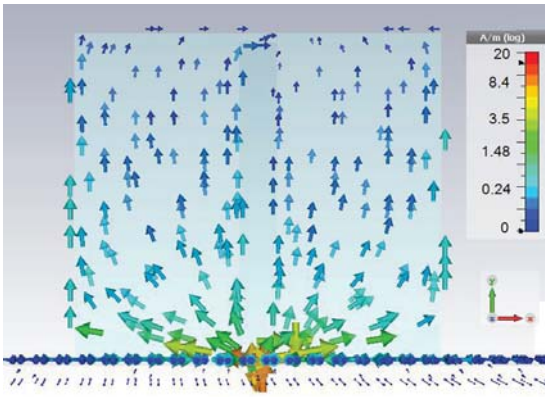

Figure 4.36: Current distribution for the unloaded case, at 50 MHz.

In order not to affect the radiation efficiency, just the imaginary part of the $Z_{\mathrm{NIC}}^{\mathrm{an}}$ should be loaded at port-2, as mentioned in the previous chapter. However, the fact of placing circuitry in the antenna structure implies unavoidable resistive responses which produces such changes, in the radiation pattern.

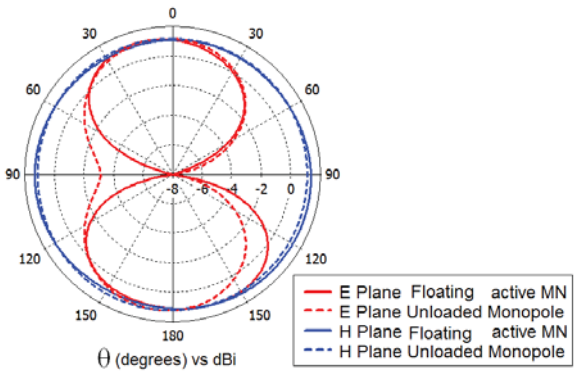

Figure 4.37: Radiation pattern of the simulated directivity for the unloaded case.

In this sense, Figs. 4.37 and 4.38 shows a comparative result in terms of directivity for both the floating and the grounded non-Foster MN loading the antenna. It can be observed an important difference in the radiation pattern, respect to an unloaded blade-monopole with

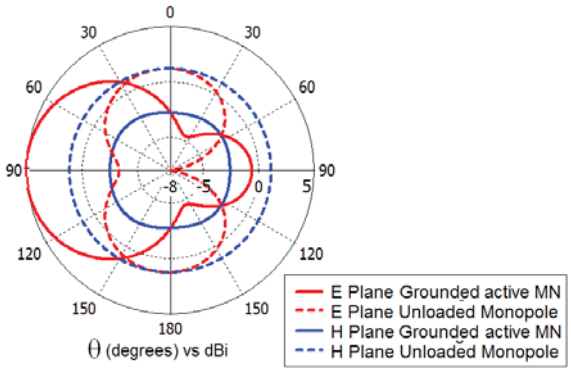

Figure 4.38: Radiation pattern of the simulated directivity for the NIC-loaded case.

its structure slotted in the same way. The grounded-MN configuration changes the current distribution in a way that the radiation response is a directional pattern with the main lobe perpendicular to the ground plane. This radiation pattern differs substantially with respect to the monopole-like pattern in the floating-MN case.

For a better understanding of the radiation effects of loading the monopole with a grounded NIC, with non-zero resistive part ($\mathrm{Re}\{Z_{\mathrm{NIC}}\} \neq 0$), the 3D-plot of the directivity pattern is shown in Figs. 4.39a and 4.39b. Unquestionably, there is an important change in the radiation response when the blade-monopole is loaded with an active non-Foster MN, for frequencies at which the host antenna behaves as an ESA. This changes are intimately related with the resistive part of the NIC impedance, even when some compensation is used to reduce the NIC resistive part, which is usually made by means of inductors and resistors connected in the feedback branches of the NIC. As the radiation resistance of an ESA is of the order of some ohms, it is possible to state that any small resistive part in the connected MN affects not only the radiation efficiency (by applying (2.33)) but also the radiation pattern, in such a way that a different mode can be radiated.

Finally, and similarly to the previous design example, a power-budget in the VHF-band at 110 MHz has been undertaken to avoid the FM broadcasting band. A known reference antenna is used as a transmitter,

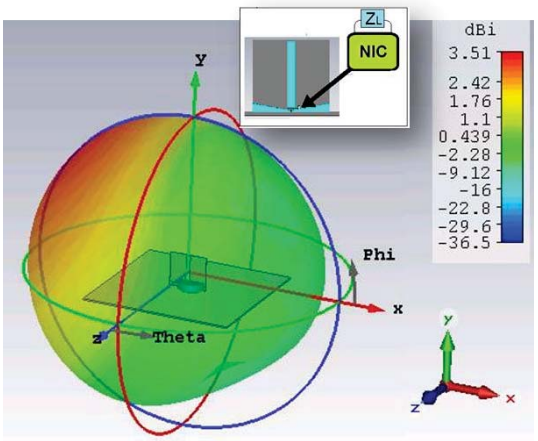

(a)

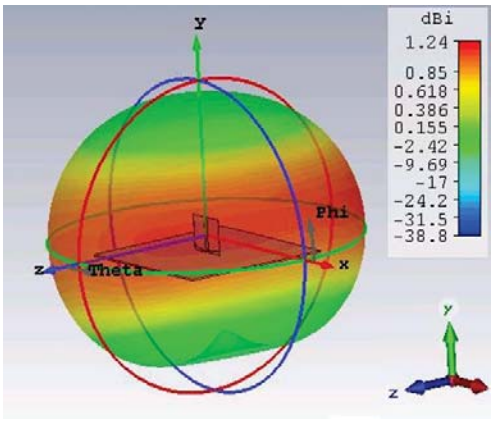

(b)

Figure 4.39: Simulated 3D directivity pattern, at 90 MHz for the blade-monopole when it is (a) loaded with the designed Z_{NIC}, and (b) a conventional unloaded one-port ESA.

Tx, while the antenna under test is located for receiving at $\theta = -90$, $\Phi = 180$, that is, in a direction parallel to the blade-monopole ground plane, and on the opposite side of the NIC. As the antenna is fully integrated with the NIC, the transmitting measured parameter would inherently include the joint effect of the antenna+NIC system. This results in a so-called *effective gain* parameter (see [114] and [120]). For

the NIC-loaded antenna, this effective gain, $G_{\text{NIC-loaded}}$ is -1.24 dB. When we repeat the measurement for the unloaded blade-monopole, the so-called effective gain results in the actual antenna gain, G_{unloaded}, of -6.46 dB. These two measurements show us the actual improvement between the NIC-loaded and the unloaded case, at least for the direction of the expected higher directivity.

4.5 Conclusion

In this chapter, a design methodology for actively matched ESAs, with some additional criteria to the conventional process has been proposed and described. With the purpose of complementing the sensitivity analysis presented in the Chapter 3, which aims at locating, in a smart an automated way, the most suitable location for an active non-Foster MN in the radiating structure. Then, by means of two different design examples, the steps of the methodology have been explained and illustrated.

It is worth pointing out that any antenna structure can be studied under this strategy previously to be prototyped, saving time and effort. Antennas that are not electrically small can also be designed following the proposed strategy. Additionally, considerations about tolerance in components have been shown to be profitable to identify sensitive parameters, not only in lumped components values but in manufacturing and set-up stages in the antenna plus MN system, which are studied as a unique entity. The NDF has been used to complement the methodology with a remarkable and easy to calculate alternative to predict the stability of the whole antenna system.

On the other hand, in terms of radiation performance considerations —one of the most challenging topics in embedded active matching design— important changes in the radiation pattern have been found. There are unavoidable responses in real non-Foster networks that produce changes in the current distributions, worthy of consideration, with respect to the case of the single-port unloaded antenna. In general, the directivity pattern, which is expected to be omnidirectional in some plane —depending on the nature of the ESA: electric or magnetic— results in a more directive pattern, especially in the direction opposite to

the point where the NIC is connected. Understood as a non-controllable condition, this fact can be seen as a drawback if the application requires an omnidirectional actively-matched ESA. However, in a different scenario, those changes have simply to be taken into consideration in order to reach some other application specifications.

The added noise in a receiving NIC-loaded semiloop, while good in a noisy receiver, was found to be an issue when a low-noise receiver is involved, as the SNR_{adv} resulted negative, at some frequencies in the lower band, with respect to the unloaded-unmatched case. These results agree with the analytical ones presented in [117]. This fact suggest that the internal noise of the NFC should be minimalized by optimizing well the biasing topology well the biasing levels.

The improvement in the antenna effective gain is the more remarkable advantage, in terms or radiation performance. As it was measured in both design examples, the NIC-loaded ESA overcome their passive counterpart, in 21 dB for the semiloop and 6.3 dB for the blade-monopole. In both cases, the receiving angle agreed with the region of greater directivity, for the NIC-loaded antenna case.

CHAPTER 5

NON-FOSTER NETWORKS IN ANTENNA ARRAYS

Once the performance of individual radiating structures (single ESAs) when loaded with non-Foster networks for impedance matching has been described, it is interesting to observe the response of multiple radiators —an antenna array— under the same approach. First, a brief introduction to the antenna array theory is presented and, then, the active non-Foster impedance matching technique applied to simple antenna arrays is presented.

5.1 Antenna Arrays Basics

Since there is no ability to control the radiation patterns of the individual element antennas, an alternative arises as combining the outputs of multiple antenna elements. This widely studied approach allows us to significantly change the pattern, including pattern adjustment in response to time changing requirements, or the overall gain in the radiator [25]. In general, an antenna array, often called a *phased array*, can be defined as a set of N antennas spatially separated, designed to improve one or more performance characteristics of a radiating element. In other words, an antenna array can be used to:

- increase the overall gain
- provide diversity reception
- cancel out interference from given directions
- "steer" the radiation pattern of the array to make it more sensitive in a particular direction
- determine the direction of arrival of incoming signals (scanning)
- to maximize the Signal to Interference plus Noise Ratio (SINR)

According to the geometric arrangement of the elements in space, an antenna array can be classified in three different types: *linear array*, *planar array*, and *conformal array*. In a linear array, the elements are arranged on a straight line in one dimension. The planar array presents its elements arranged on a plane in two dimensions (rectangular, square or circular aperture). Finally, in the conformal array the elements are distributed on a non-planar surface (conical, semi-spherical, etc.).

The basic antenna array model consists of two parts: the *element pattern*, the pattern of one of the elements, when isolated, and the *array factor*, the pattern of the array with the actual elements replaced with isotropic sources. Figure 5.1 shows a linear array with isotropic sources equally spaced along the z-axis. The individual element behaves identically in response to a plane wave coming from any direction. However, when this plane wave is received by the array and coupled to a common receiver, the global isotropic array response will show constructive and destructive interference at certain directions. Thus, the array pattern will be a function of the angle, θ, which is the angle with respect to the line of elements [25].

Then, the array factor can be understood as a representation of the directivity response of an antenna array, only due to the spatial distribution of the elements and its excitation (magnitude and relative phase) [122]. It can be computed as

$$AF(\Psi) = \sum_{n=0}^{N-1} A_n \cdot e^{jn\Psi}, \tag{5.1}$$

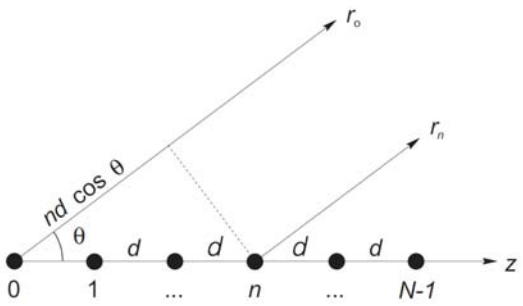

Figure 5.1: Linear array of equally spaced isotropic point sources [25].

defining

$$\Psi = kd\cos\theta + \alpha, \tag{5.2}$$

where N is the number of elements, d is the distance between them, k is the wavenumber $(2\pi/\lambda)$, A_n is the amplitude factor, and α is the phase difference between the excitation of adjacent elements. When the elements are fixed positioned, A_n and α are the parameters modified by the designer to steer the main lobe of the array. The array factor is a function of Ψ and can be understood as a Fourier series. Note that Ψ is an electrical and a spatial variable at the same time.

Actual arrays have radiating elements that, of course, are not isotropic. These elements may have a different orientation, current distributions, amplitudes and relative phases with respect to each other. In practical arrays, for the sake of simplicity in design and analysis stages, the elements are chosen to be similar, meaning that the currents of each element are in the same direction, of the same length, and have the same distribution. There may be different current amplitudes and phases for each element, to keep control on the beamforming property of the array. This fact allows the total array pattern to be written as a product of a single element antenna (the element pattern), $g_a(\theta, \phi)$, and an array factor, $f(\theta, \phi)$ (i.e. a normalized version of (5.1)). The process of factoring the pattern of an array into an element pattern and an array factor is referred to as the *principle of pattern multiplication* [25]. Then, the complete pattern of an array is

$$F(\theta, \phi) = g_a(\theta, \phi) f(\theta, \phi). \tag{5.3}$$

Mutual Coupling

So far, the arrays have been treated as an arrangement of non interacting elements being perfectly matched in impedance to the feed points. This fact allows further assumptions: the element terminal currents are proportional to their incident signals, the relative current distributions on each element of the array are identical (although their levels can be different), and finally, the pattern multiplication is valid [25]. As expected, in a real array the elements interact with each other and alter the currents (and thus impedances) from that which would exist if the elements were isolated. This interaction, called *mutual coupling*, changes the current magnitude, phase, and distribution on each element from their free-space values. As a consequence, the total array pattern changes in comparison to the no-coupling approach. Furthermore, these changes are functions of the frequency and the scan angle, as it will be described later.

The three mechanisms responsible for mutual coupling are depicted in Fig. 5.2a. First, the direct space coupling occurs between array elements. Second, indirect coupling can occur by scattering from adjacent elements. Third, the feed network interconnecting the elements leads to additional coupling path. This last contribution to the mutual coupling is mitigated by means of proper impedance matching networks (MNs) at each element. It is possible to model each element in the array as an independent voltage generator with its terminal impedance, the impedance of the actual element and the resulting current through them, as depicted in Fig. 5.2b [25]. V_m^g and Z_m^g represent the voltage generator at the m^{th} element. The voltage and current at the element terminals, V_m and I_m, include all coupling effects. Then, an array of N elements can be treated as an N-port network using conventional circuit analysis, as follows:

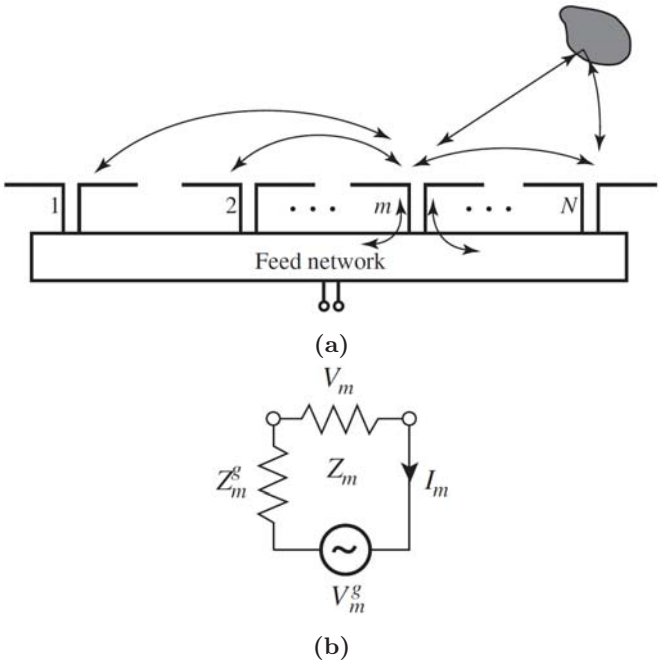

Figure 5.2: (a) Mechanisms that contribute to mutual coupling in an array. (b) Independent voltage generator model of the m^{th} element, proposed in [25].

$$\begin{bmatrix} V_1 \\ V_2 \\ \vdots \\ V_N \end{bmatrix} = \begin{bmatrix} Z_{11} & Z_{12} & \cdots & Z_{1N} \\ Z_{12} & Z_{22} & \cdots & Z_{2N} \\ \vdots & & & \\ Z_{1N} & Z_{2N} & \cdots & Z_{NN} \end{bmatrix} \cdot \begin{bmatrix} I_1 \\ I_2 \\ \vdots \\ I_N \end{bmatrix} \tag{5.4}$$

where V_n and I_n are the voltage and current across the n^{th} element. Z_{nn} is the *self-impedance* of the n^{th} element when all other elements are open-circuited. Thus, the *mutual impedance*, Z_{mn} (=Z_{nm} by reciprocity) between the two terminal pairs of elements m and n is the open circuit voltage produced at the first terminal pair divided by the current supplied to the second when all other terminals are open-circuited; that is,

$$Z_{mn} = \left.\frac{V_m}{I_n}\right|_{I_i=0} \quad for\ all\ i \neq n. \tag{5.5}$$

Mutual coupling in arrays can be described by means of some general trends, that can be listed as follows [25, 123]:

- The magnitude of mutual impedance decreases with spacing distance d, in many cases decaying as $1/d^2$ [124].
- The far field pattern is an indicator of coupling between elements, although the coupling mechanism is a near-field, not far-field, effect. Coupling is proportional to the element pattern level in the array plane (or surface).
- Elements with a narrow pattern will have lower coupling than a elements with a broad beam.
- Elements with polarizations (i.e. electric field orientations) that are parallel couple more than when collinear.
- Larger elements have smaller coupling.

An additional way to quantify coupled arrays, in addition to the mutual impedance analysis, is by using the S-parameters matrix describing the array as an N-port network. As the S-parameters are commonly used in full-wave simulations, and measured in any commercial Vector Network Analyzer (VNA), they are convenient for applying the design methodology, described in previous chapters, in order to embed active non-Foster MNs in antenna arrays.

The scattering matrix entries can be related with impedance matrix entries, Z_{mn}. For the first element of a two-element array with every connecting transmission line of characteristic impedance Z_0:

$$S_{11} = \frac{(Z_{11} - Z_0)(Z_{22} + Z_0) - Z_{12}^2}{(Z_{11} + Z_0)(Z_{22} + Z_0) - Z_{12}^2}, \tag{5.6}$$

$$S_{12} = \frac{2Z_0 Z_{12}}{(Z_{11} + Z_0)(Z_{22} + Z_0) - Z_{12}^2}. \tag{5.7}$$

The input impedance of an element in the array can now be computed using the mutual impedance values. For the m^{th} element, the input impedance can be found by using (5.4) as [25]

$$Z_m = \frac{V_m}{I_m} = Z_{m1}\frac{I_1}{I_m} + Z_{m2}\frac{I_2}{I_m} + \cdots + Z_{mN}\frac{I_N}{I_m}. \tag{5.8}$$

This is the input impedance of an element of the array when all the others are fully excited. It is referred as the *scan impedance* (formerly called *active impedance*) [124]. This formula shows the dependence of the impedance response of one element on not only the mutual impedances, but also on the terminal currents of the other elements. This is a significant result, as the phase of the terminal currents is modified by the designer (or by a beamforming control unit) to steer the beam of the array, the input impedance (scan impedance) of all the elements will also change with the scan angle.

Array Pattern Including Mutual Coupling

The mutual coupling effect not only affects the impedance response of a radiating element in an array, but also influences its complete radiation properties such as gain, polarization and the radiation pattern. Complete analysis using full-wave simulations or measuring the parameters of each radiating element can be used to completely characterize the array, However, this task is cumbersome and rarely done, even in few-element arrays.

In this sense, an additional array performance expression that combines the isolated element pattern and the impedance mismatch factor (directly related with the *scan impedance*) into one parameter called the Scan Element Pattern (SEP), has been defined [124]. The SEP account for all coupling effects and it is easier to measure than other approaches (e.g. the mutual impedance). It can be understood as the envelope of the array beam gain versus the scan angle, and can be computed as

$$g_s(\theta) = \frac{R_s(0) g_{\text{iso}}(\theta)}{R_s(\theta) g_{\text{iso}}(0)} \left[1 - |\Gamma_*(\theta)|^2\right], \tag{5.9}$$

where $g_{\text{iso}}(\theta)$ is the isolated element power pattern, calculated with all the other elements open circuited. $R_s(\theta)$ is the scan resistance, and $\Gamma_*(\theta)$ is the conjugate scan reflection coefficient. $\Gamma_*(\theta)$ is used for the general case when the generator reactance is not zero, and can be defined as

$$\Gamma_*(\theta) = \frac{Z_s^*(\theta) - Z_g}{Z_s(\theta) + Z_g}, \tag{5.10}$$

where $Z_s(\theta)$ is the *scan impedance* of the array, which is difficult to measure in practice since all the elements must be properly excited. The measurement process of the SEP parameter ($g_s(\theta, \phi)$) is easier to carry out by exciting one of the elements while all other elements are terminated with Z_0. Figure 5.3 depicts the measure approach of both the SEP and the scan impedance.

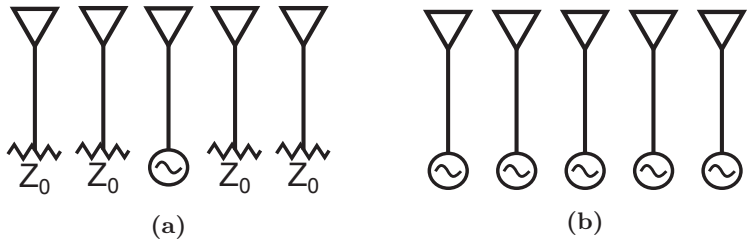

Figure 5.3: Array gain measurement by (a) SEP and (b) scan impedance methods [124].

This quite simple performance expression allows the designer to discern the contribution of the array lattice and element spacing, element type, and mutual coupling. It is worth noting that after computing, simulating or measuring the SEP of a central element of an array, the complete array pattern can be expressed in a similar form as in (5.3). Finally, a global expression for the array response can be extracted as

$$F(\theta,\phi) = g_s(\theta,\phi) \cdot \sum_{n=0}^{N-1} A_n \cdot e^{\Psi}. \tag{5.11}$$

Figure 5.4 illustrates the coupling effect in radiation for a linear array of eight microstrip patches [25] by measuring the SEP of some elements. Each sketched SEP was measured with the actual element excited and the others terminated in Z_0. Those elements in the edges of the array present a distorted pattern on the side away from the array, due to the asymmetry condition. Hence, the use of the SEP of central elements, and applying them to (5.11), will result in a more accurate characterization of the total array pattern.

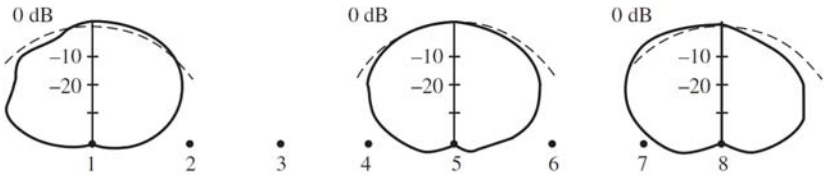

Figure 5.4: Measured SEP of some elements in a linear array of microstrip patch antennas [25].

The most common applications of antenna arrays are related with satellite communications, remote sensing, airborne radar for surveillance, ground based multi-function radar for military or navigation control — Surface Movement Radar (SMR)— and, recently, radio astronomy. The most representative properties of array antennas are the high directivity obtained by arranging several radiating elements and the possibility of steering the beam of the total pattern, at the expense of increasing the size and the manufacturing cost. All of these systems use antenna arrays working at frequencies where the elements within the array are resonant, or a number or electrically small antennas (ESAs), passively matched with reactive MNs, at the expense of their inherent narrowband response.

5.2 Antenna Arrays with non-Foster Forms

After the brief introduction to the basics on antenna array properties and its characterization, a recently introduced approach involving

antenna arrays is described in this section. This is the case of the antenna arrays containing active non-Foster forms, added to enhance certain parameters of the array performance. The limited number of reported work in literature indicates that this approach, while not popular, constitutes an open topic for contributing to the antenna community. Nevertheless, some alternatives have been explored and reported so far in which few-element arrays has been integrated with NICs, most of them using linear-array geometries at frequencies close to the resonance of the radiating elements, as it will be described below. These alternative solutions have mostly been focused on certain parameters related to the radiation performance of the array rather than in engineering an additional frequency band of matched impedance.

In this sense, the complexity of adding non-Foster circuits to obtain broadband impedance matching lies on the sensitivity of the array to changes (in amplitude or phase) of the signal feeding each element of the array. Moreover, adding one active MN to each element of the array is a very difficult task due to the necessity of fine tuning the NIC, once it is connected to a variable load. This is the case of a radiating element in an array, whose impedance changes not only with frequency but with the scan angle and with its position within the array, as mentioned before. Additionally, when the lower bound of the intended frequency band is such that the electrical size of the elements in the array is around 0.1λ, the designer must deal with additional constraints. These are the high reactance value and a strongly frequency dependent resistance presented by ESAs, related to the well-known high quality factor Q of these structures [15]. This condition transfers the difficulty of broadband impedance matching also for antenna arrays composed of ESAs.

As mentioned above, few-element active loaded antenna arrays have been previously reported in the literature. These approaches can be classified according to the goal. First, by adding non-Foster elements it is possible to increase the realized gain over a broadband, as it is described by C. White in [125], giving continuity to the currents at lower frequencies. Furthermore, it is possible to improve the SEP using passive and active reactive elements, well connected between the array elements (coupling configuration) well connected at each element input port (matching configuration) [126, 127]. Those reactive elements would be lumped inductors or capacitors in the passive case, and negative en-

gineered capacitors or inductors implemented by means of NICs for the active ones.

Second, by including Negative Group Delay (NGD) networks (to obtain fast-wave propagation) in the feed network of a linear array, as proposed by H. Mirzaei and G. Eleftheriades in [73]. This approach looks for reducing the inherent beam-squinting of a linear array of tapered-slot antennas, over a FBW of 40%, by loading the transmission lines in the feed-network with non-Foster circuits. Additionally, a parasitic two-element monopole array loaded with a NIC is proposed by M. Jacob et al. in [128]. In this approach, the total array pattern takes advantage of the property of increasing phase-response (i.e. another behavior inherent to non-Foster circuits) of the NICs with frequency, looking for a broadband squint-free and steerable pattern. The broadband pattern steered is reported in a band (180 to 350 MHz) over which the impedance matching is provided by the natural response of the driving element, a printed elliptical monopole, 45 cm in length, whose resonant frequency ($\lambda_0/4$) is close to 330 MHz. Third, a more specific approach has been recently reported by A. Elfrgani and R. Rojas in [129], in which an active non-Foster coupling network is implemented to improve the direction-finding capability of a Biomimetic Antenna Array (BMAA) —a two-element antenna array inspired on the hearing mechanism of insects— over a wide band. In this approach, BJT-based NIC is used as the main part of a external coupling network, added to increase the output phase response, relative to the incident signal angle (input phase), measured in the element terminals of the array. The elements consist of two wire-type monopoles, 7.5 cm in length, spaced 4 cm to each other (0.13 λ_0). The reported results show an improvement in the output phase response in the range from 420 to 550 MHz ($f_0 = 1$ GHz).

For the sake of completeness, the alternative of embedding an active non-Foster MN into a few-element array is explored in the subsequent sections of this chapter. The design methodology developed throughout this work is applied to a couple of design examples, looking for broadband impedance matching at a new lower band. The goal is to observe the performance of antenna arrays when loaded with an embedded active non-Foster MN. In response to the difficulties lying on this purpose, as described before, the design examples that will be presented here are simple structures of few radiating elements which meet the ESA

definition ($ka < 0.5$).

5.3 Design Examples

The first design example presented here comprises a two-element linear array composed of two printed semiloops, arranged in a coplanar configuration. This array is intended to be matched at the VHF band through a NIC, once the sensitivity analysis takes place. In the second design example, a small printed log-periodic array is involved in the same active matching process, aided by the proposed *Sens* parameter, in order to add a new working frequency interval at the lower part of the UHF band. Some considerations are also described in terms of NIC selection, radiation performance and stability.

5.3.1 Active Matching of a Two-Element Semiloop Array

A linear array, composed of two coplanar semiloops as it is shown in Fig. 5.5, connected through a non-Foster MN in a coupling configuration, is presented as a comparative design between two cases: an ideal non-Foster MN (a series negative inductor, $L < 0$) and a BJT based balanced NIC acting as the active-MN. A FR4 slab, with $\epsilon_r = 4.3$ and 1.5 mm thick, contains the coplanar array elements. The design aims at matching the array at the VHF band (under 300 MHz). The natural frequency for the array ($\lambda_0 = 2\pi R$) is about 1200 MHz, where the typical double lobe (i.e. along the $+z$ and $-z$ axis) is observed for a $\lambda_0/2$ separation between elements.

The multi-port antenna approach, presented in Chapter 3, is used to deduce the analytical impedance, $Z_{\mathrm{MN}}^{\mathrm{an}}$, that has to be implemented either with an ideal non-Foster MN or with a transistorized circuit (a NIC) for broadband impedance matching. The *Sens* parameter plays again an important role in the design process. As it was shown in Chapter 4, the most suitable location for an active-MN in a single semiloop was found by introducing an analytical second port. Such location is on the opposite side from the input port. In this case, the analytical port is a third one (see Fig. 5.5), added for full-wave simulation to extract a 3-port S-parameter matrix for each port-3 position. Due to the

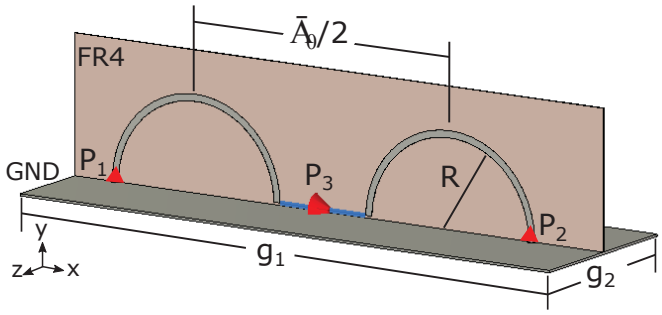

Figure 5.5: Sketch of the two elements array. All dimensions in mm: $R = 40$, $g_1 = 80$, $g_2 = 260$.

symmetry of the two-element array here, it is possible to calculate the *Sens* parameter by terminating the port-2 (Fig. 5.5) with Z_0. Thus, both the sensitivity analysis and the analytical $Z_{\text{MN}}^{\text{an}}$ can be carried out by using the S-parameter matrix of a two-port structure, as depicted in Fig. 5.6, computed with any EDA circuit software. Then, we can start the analysis, as in the case of a single antenna, by computing the *Sens* parameter and the analytical $Z_{\text{MN}}^{\text{an}}$, as previously described in Chapter 3. In this chapter, Γ_{NIC} is threated in a generalized way as Γ_{MN}. The most relevant expressions are shown below again, as follows:

$$\Gamma_{\text{IN}} = S_{11} + \frac{S_{12} \cdot S_{21} \cdot \Gamma_{\text{MN}}}{1 - S_{22} \cdot \Gamma_{\text{MN}}} = 0, \tag{5.12}$$

which leads to

$$\Gamma_{\text{MN}}^{\text{an}} = \frac{S_{11}}{S_{22} \cdot S_{11} - S_{12} \cdot S_{21}}, \tag{5.13}$$

directly related to the analytical impedance

$$Z_{\text{MN}}^{\text{an}} = Z_0 \cdot \left(\frac{S_{22} \cdot S_{11} - S_{12} \cdot S_{21} + S_{11}}{S_{22} \cdot S_{11} - S_{12} \cdot S_{21} - S_{11}} \right), \tag{5.14}$$

which has to be implemented, as accurate as possible, with the active non-Foster MN.

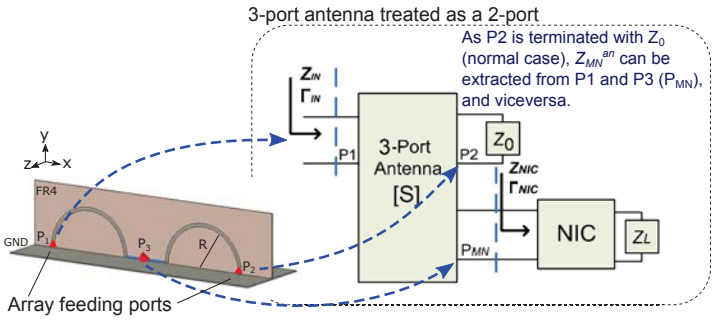

Figure 5.6: Two-port network obtained for symmetry of the 3-port one, extracted in the sensitivity analysis of the semiloop array.

Sensitivity Analysis Over the Array Structure

If $Z_{\mathrm{MN}}^{\mathrm{an}}$ is placed between the semiloops, the reflection coefficient at ports 1 and 2, $\Gamma_{IN:1,2}$, ideally equals 0 in the design band. However, in real designs, the impedance shown by the NIC does not equal $Z_{\mathrm{MN}}^{\mathrm{an}}$ precisely. In this point of the design, the *Sens* parameter, derived from (5.15) and (5.16), emerges to indicate us how the changes in the MN impedance, affect the input impedance in the array ports. In other words, *Sens* parameter says how convenient is to place a MN (active or passive one) in the analyzed position of port-3.

$$\Delta\Gamma_{\mathrm{IN}} = \underbrace{\left.\frac{\partial\Gamma_{\mathrm{IN}}}{\partial\Gamma_{\mathrm{MN}}}\right|_{\Gamma_{MN}=\Gamma_{MN}^{an}}}_{Sensitivity:\ Sens} \cdot\Delta\Gamma_{\mathrm{MN}} = Sens\cdot\Delta\Gamma_{\mathrm{MN}}, \tag{5.15}$$

$$Sens = \left|\frac{S_{21}S_{12}}{\left(1-S_{22}\Gamma_{\mathrm{MN}}\right)^2}\right|\Bigg|_{\Gamma_{\mathrm{MN}}=\Gamma_{\mathrm{MN}}^{\mathrm{an}}} = \left|\frac{\left(S_{11}S_{22}-S_{21}S_{12}\right)^2}{S_{21}S_{12}}\right|. \tag{5.16}$$

Figure 5.7 shows the parameter *Sens*, averaged over the intended lower band (below 300 MHz), and swept over the array structure. The port-3 is a floating one, placed vertically to connect the elements. A similar response to that in the single semiloop antenna is observed, where the lowest *Sens* value was reached close to the ground plate. For practicality of the active MN, the two points opposite to the feed point of each element are chosen, that is, in the actual position of P_3 in Fig. 5.7.

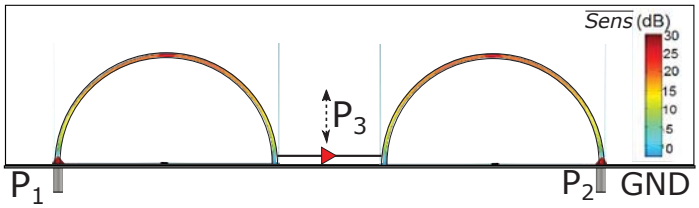

Figure 5.7: $\overline{Sens}$ over the elements of the array when P_3 is swept vertically, connecting different points between them.

Figure 5.8 shows the *Sens* parameter versus frequency, computed at the lowest sensitivity point found in the previous step, for the proposed two-element array. For comparison purposes, the same curve computed at the lowest *Sens* point for the single two-port semiloop is also shown. Values near 10 dB or lower can be treated as low sensitivity. Acceptable levels of impedance matching, once the array is loaded with the non-Foster MN, should be expected if we take the single semiloop case (developed in Chapter 4) as reference.

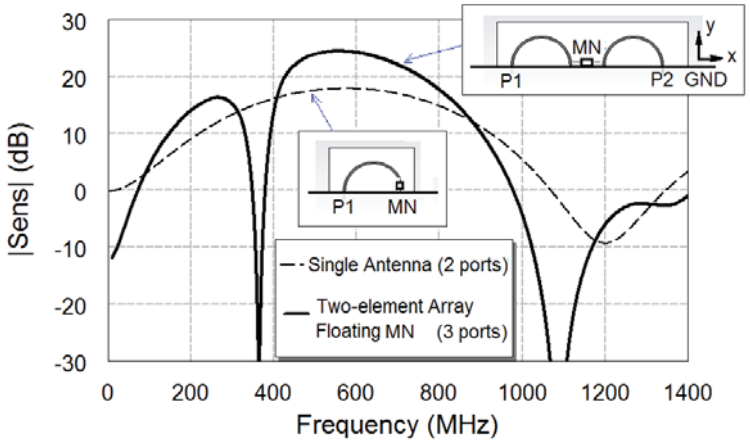

Figure 5.8: Magnitude of the *Sens* parameter vs frequency.

Once a suitable position for the non-Foster MN is found, the impedance Z_{NIC} —to be place in there— must be set up, following as much as possible the shape of the analytical one, $Z_{\text{MN}}^{\text{an}}$, especially the imaginary (reactive) part. As in the case of a single ESA, the real part of the intended NIC impedance should be kept low, in order not to affect the

radiation efficiency.

The small semiloop impedance is often modeled as an inductor in series with a resistor. That model is confirmed as the magnitude of the semiloop impedance starts as a short-circuit at 0 Hz and shows a quasi-inductive response in the Smith chart at lower frequencies ($f < f_0/2$, or $f < 500$ MHz in this design). Thus, over the band intended to be added (i.e. VHF), the magnitude of the input impedance at each port in this semiloop array is low. Moreover, due to the symmetry condition of the semiloops, the magnitude of the impedance that the NIC is going to "see," when connected to the array at the lowest sensitivity point, is also small. Then, the SCS ports of the NIC should be chosen to fulfill $Z_{\mathrm{MN}}^{\mathrm{an}}$, as described in Section 4.2.3. This, in addition to the floating configuration of the non-Foster network needed at the lowest *Sens* point (port P3 in Fig. 5.5), suggest us that a balanced-SCS NIC topology is the most suitable for this case. The BFG410W wideband BJT, whose f_T is 22 GHz, is selected to be connected into a classic Linvill topology, as depicted in Fig. 5.9. The load impedance consists of an inductor (L) of 250 nH. R_{comp} is a compensation resistor of 5 Ω, used to set the real part of the NIC impedance close to zero. The biasing collector current is set at 5 mA, as well as the collector-emitter voltage at 2 V. All other elements in the biasing network have been omitted for simplicity.

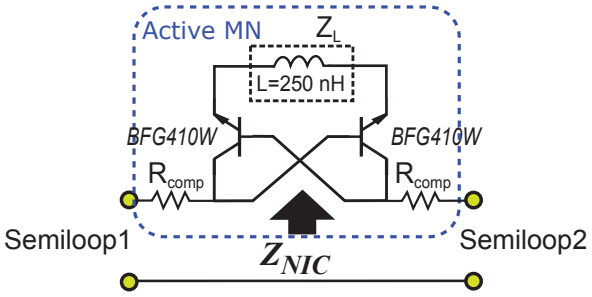

Figure 5.9: Balanced SCS-NIC, acting as the active MN; replacing the port-3 in Fig. 5.7.

With the aim of illustrating and comparing, an alternative ideal network is connected as MN, instead of the NIC, also at the lowest *Sens* point. It is an ideal non-Foster inductor ($L_{\mathrm{neg}} = -248$ nH) connected in series, whose impedance response acceptably fits the analytical one.

This fact confirms the simplicity of the needed non-Foster network for this design, even though it is an idealized case. Figure 5.10 shows the behavior of $Z_{\mathrm{MN}}^{\mathrm{an}}$ versus frequency, as well as the ideal series negative inductor and the BJT-based NIC.

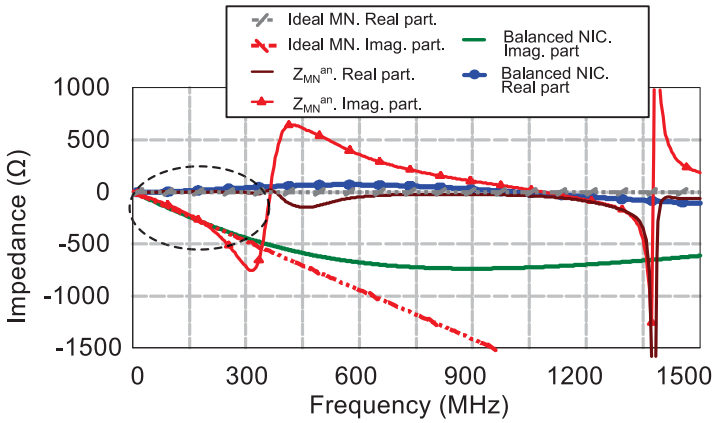

Figure 5.10: Impedance response of $Z_{\mathrm{MN}}^{\mathrm{an}}$, the ideal negative inductor, and the balanced BJT-based NIC.

For frequencies above 300 MHz, the array shall be difficult to match because of the resonant-like response of $Z_{\mathrm{MN}}^{\mathrm{an}}$. A reduced span in the previous figure let us to observe how much the NIC impedance fits the analytical one, as shown in Fig. 5.11. In the proposed design strategy, a visual inspection aided by the EDA software reduces greatly the complexity of fitting the actual NIC impedance to the analytical $Z_{\mathrm{MN}}^{\mathrm{an}}$.

It is worth noting that the maximum frequency at which the NIC acts as an active MN is expected to be around 300 MHz. Above this frequency, the reactance of $Z_{\mathrm{MN}}^{\mathrm{an}}$ changes abruptly, being impossible to follow with a single NIC. That frequency corresponds to the upper bound of the lower band obtained ($S_{11} < -10dB$), as the S_{11} parameter, computed when the other element of the array is Z_0 terminated, shows in Fig. 5.12.

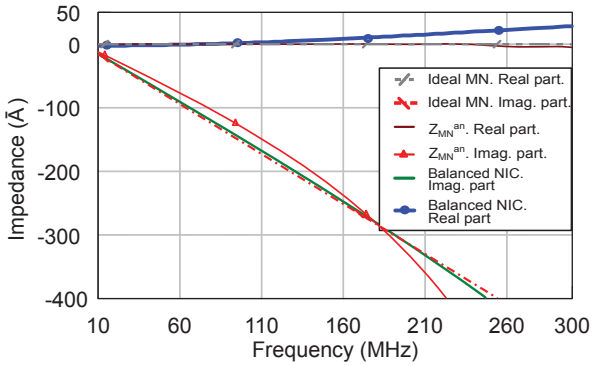

Figure 5.11: Reduced span for the impedance response of $Z_{\mathrm{MN}}^{\mathrm{an}}$, the ideal negative inductor, and the balanced BJT-based NIC.

Stability Analysis

Following the design method presented in Chapter 4, the stability of the complete actively matched array (array + NIC) is checked. The NDF is computed in the AWR design software, by using the linear small-signal model of the transistors at the selected biasing point, including package effects and the transmission lines. The S-parameters matrix of the 3-port array, extracted in the sensitivity analysis step, is also included in the NDF calculation. The NDF is calculated along the interval from -300 GHz to 300 GHz, as shown in Fig. 5.13. A zoom-in around the origin is also shown. Since the f_T parameter of the used BJT is 22 GHz, computing the NDF up to 300 GHz is a reasonable decision to look for oscillations or any other instability phenomenon. It can be observed that there are no origin encirclements. This fact predicts stability in the overall design, as mentioned earlier.

Radiation performance

In terms of radiation performance, an omnidirectional response in the plane containing the elements, in the lower VHF band (at 100 MHz), is found for both the NIC-loaded array, and the unloaded array, as can be seen in the upper row of Fig. 5.14. This pattern is the one expected from a small loop antenna, which is often referred as the "magnetic

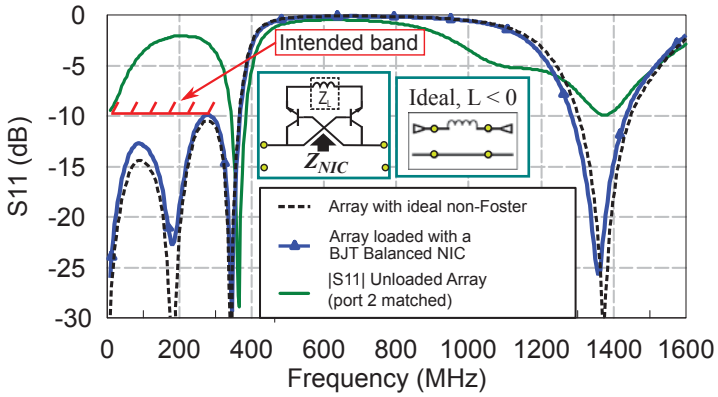

Figure 5.12: S_{11} and S_{22} response of the array for both cases: Ideal and implemented non-Foster MN.

dipole," because at lower frequencies the distance between the elements ($\lambda_0/2 = 0.125$ m) is small compared to the wavelength at 100 MHz($\lambda = 3$ m). The fact that the feeding points at each semiloop within the array are in opposite positions with respect to each other (see Fig. 5.7), implies the need of setting a phase difference of 180° between the feeding signals. However, for two in-phase signals exciting the elements, the pattern of the NIC-loaded array is quasi omnidirectional in the horizontal plane (i.e. parallel to the ground plate). This response can represent an advantage for some applications like airborne communications, ATC systems, and so on. The response of the unloaded array for an in-phase excitation corresponds to the expected pattern of two loops fed in opposite points, showing two main lobes pointing to each side from the feed. At 1.2 GHz, the obtained pattern remains basically unchanged, compared with the unloaded array when two in-phase signals are applied at the input of each element. For the series negative-inductor case, the simulated radiation response in both frequencies is practically the same as the one with a transistorized MN.

In short, it is possible to claim that an important advantage in loading symmetric array structures, comprising electrically small radiating elements, with active MNs. The design method presented in previous chapters enables the option to include, in a systematic way, a new low working band. Two-element semiloop array appears to be a suitable choice for broadband impedance matching. An important miniaturiza-

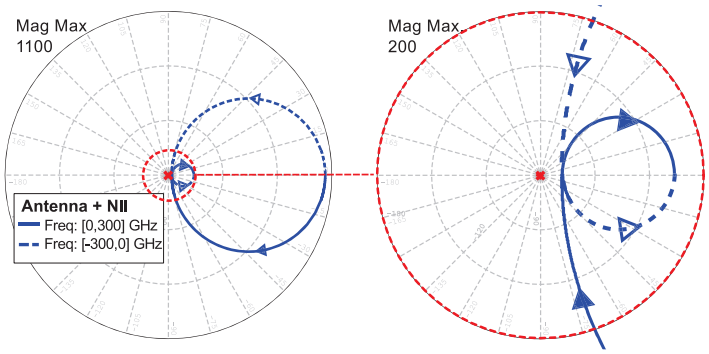

Figure 5.13: NDF plotted up to 300 GHz to check the stability of the actively matched semiloop array.

tion level can be obtained in a low-cost and easy-to-manufacture array. Even though there are changes in the radiation pattern in the engineered lower band, the antenna system can still be attractive for some applications.

5.3.2 Small Printed Log-Periodic Array, Matched with an Active non-Foster Network

In order to show a different design example, the design of a small printed-log-periodic antenna loaded with an active MN for multi-band applications is presented in this section. A well-known, low-cost, and low-profile antenna is re-engineered for including an additional broad impedance band in the upper VHF- and the lower UHF-band (from 30 to 720 MHz), maintaining its natural broadband response (around 2.3 GHz). The design method involves again the methodology described in Chapter 4, by means of the sensitivity parameter *Sens*, to find a suitable location for a transistor-based non-Foster network (a NIC). A BJT-based balanced NIC is selected to act as active MN, after an impedance analysis that will be shown below.

A log-periodic array of printed dipoles consists of a group of dipoles which follows a logarithmic relation with frequency [24]. This configuration is well-known for broadband applications in frequencies at which the length of the array elements is around half-wavelength ($\lambda/2$), that is,

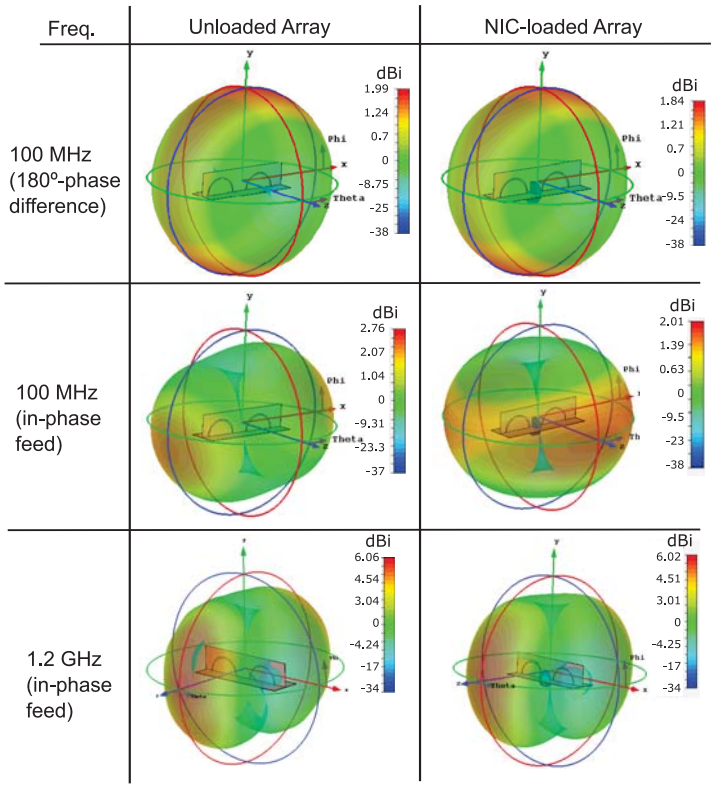

Figure 5.14: 3D plot of the radiation response for a two-element semiloop array, at different frequencies for both the unloaded and NIC-loaded cases.

from 1.8 to 2.7 GHz for this case ($FBW = 40\%$). However, at lower frequencies, important constraints arise in terms of gain-bandwidth when the intended operating band is designed to include a passive network, as the Bode-Fano criteria states [11]. An additional design constraint arises from the high-Q condition of ESAs, described before.

The antenna under study is composed of two dipoles (see Fig. 5.15). These dipoles are implemented by using an antipodal configuration (each branch of the dipole is printed on one side of a dielectric substrate). Each element is fed through a parallel plate line, so the array has just one physical feeding port (P1 in Fig. 5.15), and can be treated as a single antenna for the active matching procedure. In this case, a slab of FR4

with 0.5 mm thick, $\epsilon_r = 4.4$, and $tan\delta = 0.015$ is used. All dimensions of the array are in mm: $L_s = 65$, $W_s = 60$, $L_{d1} = 28.5$, $L_{d2} = 32$, $W_{d1} = 3$, $W_{d2} = 4$, $d_1 = 19 : 75$, $d_2 = 25$, $W_f = 1$. The resonance frequency of the structure is expected to be around 2.3 GHz ($\lambda_0 = 0.13$ m). The complete structure can be classified as an ESA ($ka < 0.5$, with $a = L_s$) at frequencies up to 720 MHz, this is the upper bound of the interval of interest.

The design procedure follows the two-port antenna approach as the starting point, previously described and depicted in Fig. 5.17a. To do so, the array is modeled using CST in order to add the analytical port-2, as it is shown in Fig. 5.16. Then, the sensitivity analysis takes place. As mentioned before, this analysis aims at explaining and analytically finding a suitable location for the non-Foster circuit in between of some elements of the array. This step is critical since neither all the elements nor their possible positions are suitable for using non-Foster matching networks, as mentioned earlier. For this goal, the *Sens* parameter is computed at different positions of the port-2, which is swept from the feeding line to the tip of the dipole branches.

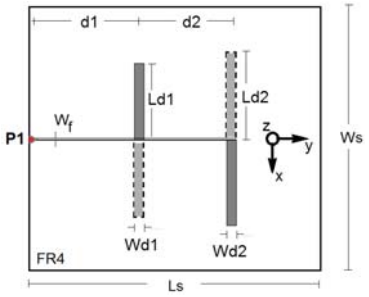

Figure 5.15: Small log-periodic array sketch.

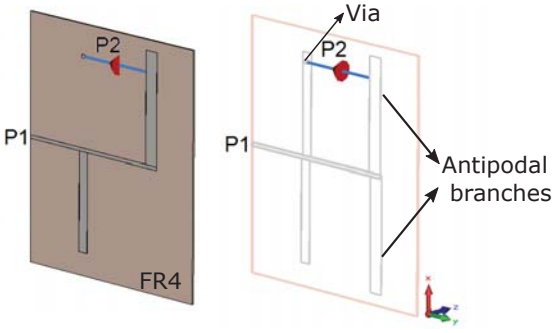

Figure 5.16: CAD model of the small log-periodic array with the analytical second port (P2) added to carry out the sensitivity analysis.

As a result of the sensitivity analysis, a convenient location for the second port is found to be close to the dipoles' axis (y-axis), between the same side branches, as the lower value of the *Sens* parameter indicates in Fig. 5.17b. The *Sens* parameter was computed as the average value, in dB, of (5.16) from 10 MHz to 600 MHz at each port-2 location.

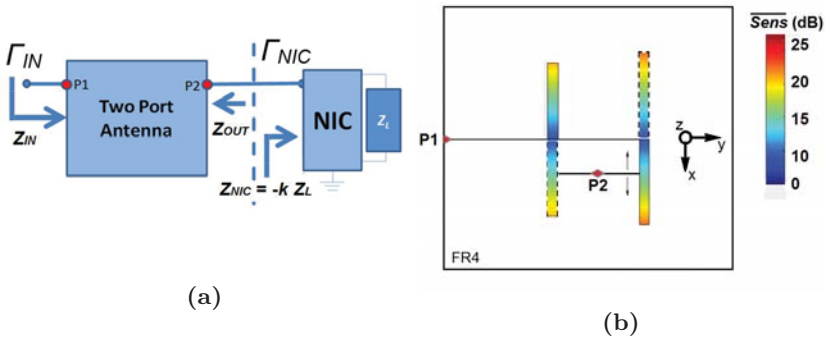

Figure 5.17: (a) Scheme of the two-port antenna approach. (b) Averaged parameter $\overline{Sens}$ between the antipodal dipoles.

The behavior of the *Sens* parameter versus the frequency is shown in Fig. 5.18 for different positions of port-2. This is a less-graphic way of observing the sensitivity in a structure, but still helps to confirm in which frequency ranges the sensitivity is low.

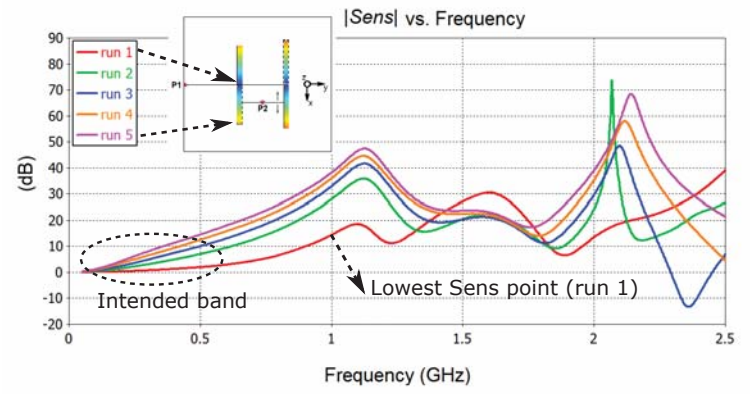

Figure 5.18: $|Sens|$ versus frequency for different positions of port-2.

It is worth having a look at the S-parameters of the two-port network

extracted in the sensitivity process. Figure 5.19 depicts the magnitude of the S-parameters at the point of the lowest *Sens*. The high magnitude of the S_{21}, along the intended lower band (below 600 MHz), indicates high coupling between ports, which derives in low sensitivity.

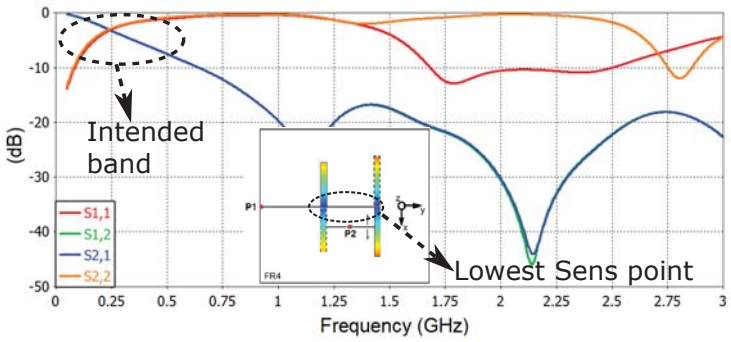

Figure 5.19: S-parameters of the 2-port array approach, when the analytical port is placed close to the feeding line (lowest *Sens* value).

Impedance analysis

As the elements involved in this log-periodic array are dipoles (whose impedance starts as an open circuit at 0 Hz), a quasi-capacitive response in the Smith chart at lower frequencies ($f < f_0/2$, or $f < 1,1$ GHz in this design) is expected. Thus, over the band intended to be added (i.e. lower part of the UHF), the magnitude of the input impedance at the input port in this log-periodic array is high. In addition, as the most suitable point in terms of *Sens* magnitude is close to the central point of each dipole, the magnitude of the impedance that the NIC is going to "see," when connected to the array at the lowest sensitivity point, is also high. Then, the OCS ports of such a NIC should be chosen to fulfill $Z_{\mathrm{MN}}^{\mathrm{an}}$. In this sense, there is a duality respect to the design example described in the previous section.

Furthermore, since the lowest *Sens* point was found between branches of different elements, the most suitable NIC topology is the balanced one. Thus, a balanced-OCS NIC should be selected. A modified version of the BJT-based NIC used in the previous design example is chosen and shown in Fig. 5.20. In this version, the non-Foster impedance is observed

looking inside from the emitter of each BJT. The R_{comp}, whose value is 9.6 Ω, is now located in series with the load inductor (L = 17 nH).

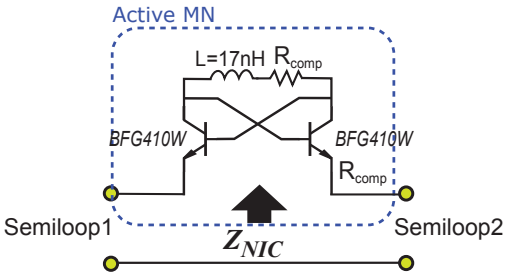

Figure 5.20: Balanced BJT-based OCS NIC topology used to actively match the log-periodic array.

The NIC impedance of the BJT-based network is analyzed to fit the analytical impedance derived from the S-parameters in the lowest *Sens* point (2 mm above the feeding line in Fig. 5.17b). The AWR software is used to carry out the impedance analysis.

Figure 5.21 shows the impedance behavior of the NICs, in simulation, compared to the analytical $Z_{\text{MN}}^{\text{an}}$. The impedance implemented with the BJT-based NIC, $Z_{\text{NIC-BJT}}$, offers the possibility of compensating the resistive part, letting us to control the tradeoff between impedance bandwidth and radiation efficiency of the loaded array. The reactive response of the NIC impedance agrees successfully with the analytical one.

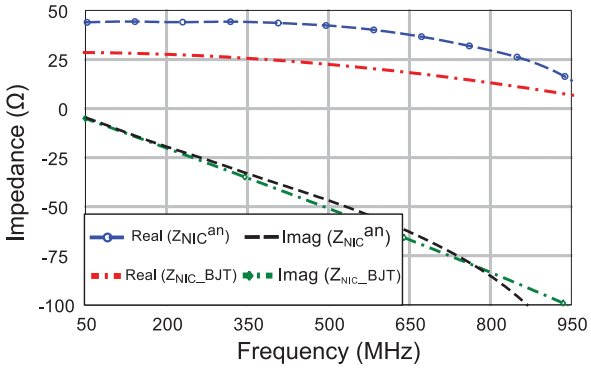

Figure 5.21: Computed $Z_{\text{MN}}^{\text{an}}$ versus the simulated NIC impedance for the BJT-based NIC.

The simulated S_{11} parameter for the NIC-loaded case is depicted in Fig. 5.22. Once loaded, the log-periodic array still presents an impedance FBW of over 40% ($S_{11} < -10$ dB) in its natural band (centered at 2.25 GHz). In the new VHF-UHF engineered band, the targeted matching level ($S_{11} < -8$ dB) is obtained over the entire range of interest. In fact, the resulting lower band is from 0 MHz to 900 MHz. It is an encouraging result, at least in simulation, for such an electrically small printed structure. One advantageous property of this NIC topology is the capability of adjusting the matching level within the added band. This is made by changing the R_{comp} value, as mentioned before, in case of experimenting a substantial reduction in the overall gain.

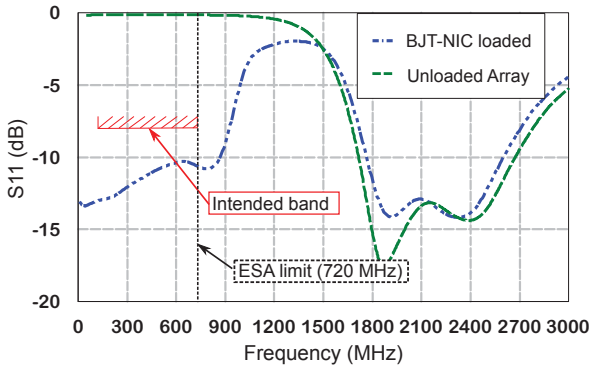

Figure 5.22: S_{11} parameter of the log-periodic array when loaded with a balanced-OCS BJT-based NIC.

Radiation considerations

The radiation response is studied for the NIC loading the small log-periodic array in comparison with the unloaded case. At the engineered lower band, it can be observed the quasi-omnidirectional pattern in the xz-plane (i.e. orthogonal to both the substrate and the dipoles) for the NIC-loaded antenna, depicted in Fig. 5.23. Similar directivity values compared to the unloaded case are obtained, but without the characteristic nulls on the "doughnut-like" pattern of a small dipole. This fact indicates a slight modification in the current distribution across the array by introducing an active MN. Nonetheless, the obtained radiation pattern is still attractive for some applications, as it was claimed in the small semiloop array example.

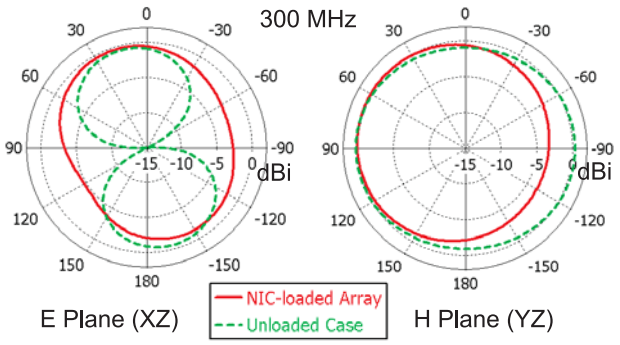

Figure 5.23: Directivity pattern of the small log-periodic array at 300 MHz.

On the other hand, at the natural frequency band of the antenna (around 2 GHz), the NIC-loaded array does not show a greatly disturbed pattern, as shown in Fig. 5.24, despite of the slight decrease in the maximum directivity.

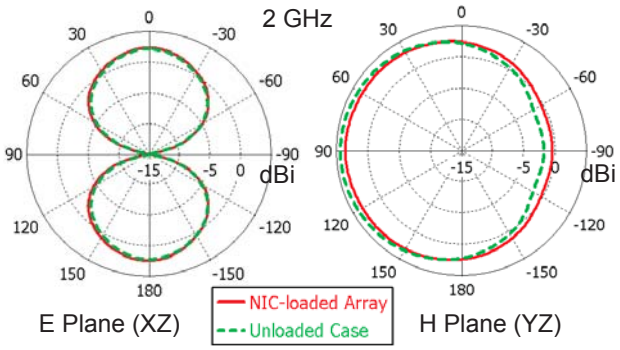

Figure 5.24: Directivity pattern of the small log-periodic array at 2 GHz.

A 3D plot of the pattern for both the unloaded and the NIC-loaded cases is presented in Fig. 5.25. It gives us a more graphic idea of the changes in the radiation pattern once the array is actively matched. One frequency from each working band is shown (300 MHz and 2 GHz). At 300, a lobe is obtained, for the NIC-loaded case, while the nulls disappear, in comparison to the unloaded array. At 2 GHz, no substantial changes are observed since the NIC impedance is small compared with

the array impedance.

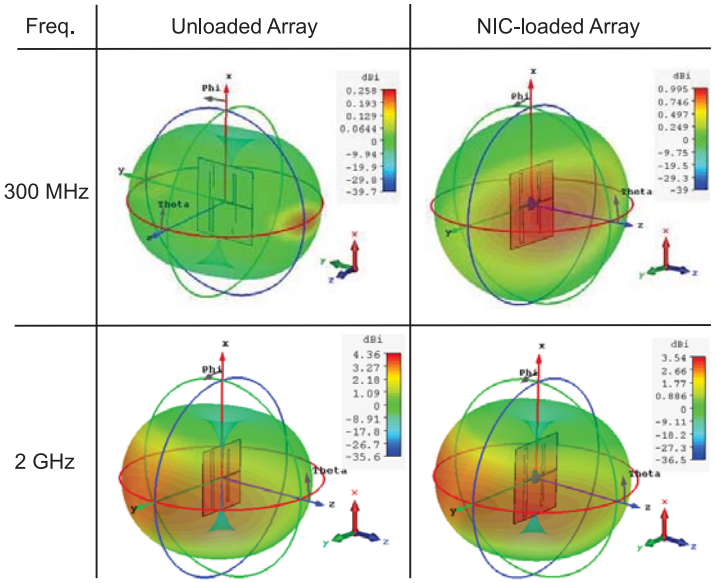

Figure 5.25: 3D plot of the simulated directivity pattern of the small log-periodic array.

5.4 Conclusion

The embedded active matching network (MN) is an interesting option to manage an additional working band at frequencies where the array is electrically small. The design strategy presented in Chapter 4 appears to be an interesting way to face the impedance matching limitations of such electrically small structures. Similarly, this method let us to make use of the available computational power through the use of electromagnetic full-wave and the EDA circuit simulators. The *Sens* parameters provide the designer with additional considerations related to the most suitable location to add an active non-Foster MN. The easy-to-compute impedance $Z_{\mathrm{MN}}^{\mathrm{an}}$ enables a fitting process of the active MN performance at any EDA software, besides the possibility of comparing several NIC topologies for the same radiating structure.

Nevertheless, due to the non-zero resistive part of the NIC, the radiation efficiency at the lower band is expected to be low. Thus, further

efforts have to be made to compensate its effect and mitigate this drawback, based on the tradeoff between radiation efficiency and matching level. Then, an active non-Foster MN in which the resistive part can be controlled or compensated is advantageous for the active impedance matching approach for arrays containing ESAs.

CHAPTER 6

CONCLUSIONS AND FUTURE WORK

6.1 Summary and Conclusion

The main goal of this thesis has been the development of multiband antennas with an engineered lower broadband obtained by embedding an active non-Foster matching network (MN).

It is not easy to summarize in a few paragraphs all the work undertaken and the observations collected in these last years of realization of this doctoral thesis. However, in the following lines, the most relevant conclusions are presented. The major difficulties observed throughout this work, that arise when the antenna engineer attempts to design actively-matched electrically small antennas (ESAs) loaded with non-Foster matching networks (MNs) are also described.

In Chapter 2 the background and the most relevant work related to ESAs, its classification, its performance limitations, and the evolution of the techniques to overcome such limitations were presented. The high-quality factor Q of the ESAs —and the gain-bandwidth limitations inherent to it— represents one of the most challenging tasks to be addressed when any type of impedance MN is to be included in the antenna system. Among the alternatives to enhance the ESAs performance, the non-Foster showed up as an interesting and effective way

to obtain broad-instantaneous impedance bandwidth. Those techniques and results became the cornerstone of the work developed and presented afterward in this document.

A novel parameter, called *Sens*, was introduced in Chapter 3 as an easy-to-calculate and versatile S-parameter based tool which is useful to analyze the feasibility of the embedding non-Foster MNs approach for the actual antenna. Thus, *Sens* parameter let us know whether the antenna under study is suitable to be loaded with an active non-Foster MN and, if so, it tells us what is the best location to place the MN. The breakthrough with the *Sens* parameter is its property of easily be computed in any full-wave CAD software, as well as, that it can be used with any other type of antenna disregarding its electrical size.

Chapter 4 presented another contribution of this dissertation: the design method for designing electrically small antennas actively matched with embedded non-Foster forms. It can be said that any compendium of considerations, presented as a to-do list of steps, gives to the engineer an additional discernment and decision tool. This design strategy aims at contributing with additional considerations, organized in an integral methodology, to reduce as much as possible the percentage of failure when a design is taken from the simulation and the calculations stage to the practice.

The strategy of embedding the active matching network is presented as an interesting alternative, especially for those applications where the space occupied by the antenna and all its circuitry is limited and comprises a determining factor in their design. In this sense, two different structures: a printed small semiloop antenna and a printed small blade-type monopole were presented as design examples applying the proposed method. An important miniaturization level was reached in both antennas at the lower bound of the engineered lower band (up to 90% and 95% in the semiloop and the blade-monopole respectively), compared to the full-size resonant antenna of each type. Besides the miniaturization level, the impedance FBW obtained at the added band were 119%, centered at 117 MHz, for the semiloop (ka factor from 0.04 to 0.17), and over 82%, centered at 85 MHz, for the blade-monopole (ka factor from 0.26 to 0.56). It is worth mentioning that the natural impedance response of each antenna was not affected once the active-MN was embedded. The

notable impedance bandwidth performance reached in both structures encouraged us to keep seeking solutions to the changes in the radiation pattern, which resulted after adding the active non-Foster MN into the antennas.

Regarding the selection of the active element involved in the active non-Foster network, it is important to point out the need to use a transistor with a constant transconductance (g_m) response up to the highest possible frequency. In addition, its transition frequency (f_T) should also be high, since the non-Foster behavior of the associated NIC impedance is expected to be a fraction of this value. Short feedback path-lengths are preferred to reduce the associated inductive effect, that can lead to oscillations in the manufactured non-Foster network. In this line, the proposed design methodology make use of the tolerance analysis, available in many commercial circuit simulators, which give us an additional view on those specific parameters to which the system overall performance (antenna + NIC) is more sensitive.

The stability of the antenna system is also addressed in Chapter 4. The NDF is used as a very interesting alternative as well as easy to calculate and rigorous for the evaluation of the stability of linear systems. Again, by using any commercial circuit design software, the stability analysis can be generalized to include the simulated or measured S-parameters of the antenna into the NDF computation. The parasitic or packaging effects of the components, as well as edge effects on the microstrip or strip-line that connect the components, can also be considered when computing the NDF. This fact makes the NDF be one of the most versatile stability analysis method reported to date.

It is important to note that this methodology may be used directly in any type of antenna, besides in a single ESA. It can be used in antennas of any electrical size, even in presence of other radiating elements in the near field. In this sense, Chapter 5 presented the proposed design methodology applied to antenna arrays, in order to add an additional lower working band. A couple of few-element arrays were presented as design examples to illustrate the approach.

One of the facts that perhaps most discourages antennas engineers from including active elements in their designs is the high level of effort

and laboratory work involved in the fine tuning of the devices, in this case the NICs. In the clear majority of cases, as actually occurred with the design examples shown throughout this thesis, it spends hours adjusting and testing before achieving a successful result that fits the expected performance.

Perhaps this last fact is one of the reasons why, for many research groups around the world, the use of negative impedance converters, NICs, as antenna impedance MNs, has reached the final phase of its life-time in the research and development field. Proof of this is the small number of teams that report contributions today. Nonetheless, it should be noted that much work remains to be done in the realization of ESAs, actively-matched with non-Foster networks, for them to be attractive to the industry and the academy.

6.2 Future Lines

Arising from the research carried out during this work, areas of potential further research could include the topics mentioned below.

First, parasitic effects and other inaccuracies associated with the fabrication of NICs on a Printed Circuit Board (PCB) board can be overcome by means of the monolithic technology (MMICs). Although some works have been reported as successful, it has not been possible to explore that approach in this work. Nonetheless, this is an interesting alternative for implementing more reliable non-Foster devices to be integrated into an ESA.

Second, the use of other active devices to realize non-Foster circuits, such as the resonant tunneling diodes (RTD) operating in a Negative Differential Resistance (NDR) region, has been recently reported in [60, 130, 131]. This approach represents an encouraging alternative to mitigate the limited frequency problem, and the associated tradeoff between this limitation and potential instability issues in non-Foster circuits, as reported so far. This is perhaps one of the most interesting future lines of work that the author wants to point out.

On the other hand, the noise performance of the receiving antennas, represented by the noise figure (NF), is a fundamental figure of merit

especially when active devices are integrated into the receiver chain. Estimating the added noise in an actively matched ESA is not an easy task, even less when the active-MN is embedded into the radiating structure. Then, a quantification technique for added noise estimation is welcome and stands for a line of future work. An interesting approach in this area has been recently reported by M. Jacob and D. Sievenpiper in [117]. In their work, the noise model of a BJT-based NIC, around its biasing point, is used to estimate the added noise when connected to the feeding port of an ESA. A comparative analysis is done for the case of a single-stage amplifier connected directly to the feeding point (instead of the NIC) of the same antenna.

Estimation and measurement of the actively loaded antenna performance in transmitting mode, comprise another important topic to be addressed in actively matched antennas area. To the best of our knowledge, by embedding the non-Foster elements into the antenna, the antenna system (ESA + NIC) can be used either in transmitting or receiving mode. Nonetheless, the non-linear phenomena effects, related to the power compression and saturation of the active devices (e.g. transistors), in presence of high voltages and currents driving the antenna, are still a significant constraint, especially at practical transmitting power levels (i.e. greater than 100 mW).

Finally, the manufacture of a few-element array loaded with a non-Foster MN is a task ahead in the seeking for extending the reported enhanced performance down in frequency. Thus, obtaining an actively matched electrically small array with additional enhanced parameters would be possible. Among these additional parameters it can be mentioned a high scan element pattern (SEP) level —a challenging task since the coupling effects between elements increase at lower frequencies— or an enhanced direction finding sensitivity, as it was recently proposed by A. Elfrgani et al. in [129].

CONCLUSIONES Y TRABAJO FUTURO

Resumen y Conclusiones

El objetivo principal de esta tesis ha sido el desarrollo de antenas multibanda que presenten una banda adicional de trabajo a bajas frecuencias, obtenida mediante la incorporación de una red de adaptación de impedancia —MN, de *Matching Network*— activa, de tipo non-Foster.

No es fácil resumir en unos pocos párrafos todo el trabajo realizado y las observaciones recogidas en estos últimos años de realización de esta tesis doctoral. Sin embargo, en las líneas siguientes, se presentan las conclusiones más relevantes. De igual modo, se describen las mayores dificultades experimentadas a lo largo de este trabajo, que surgen cuando se intenta diseñar antenas eléctricamente pequeñas (ESAs) adaptadas con redes activas tipo non-Foster.

En el Capítulo 2 se presentan los antecedentes y el trabajo previo más relevante relacionado con las ESAs, su clasificación, sus limitaciones de funcionamiento y la evolución de las técnicas para superar tales limitaciones. El alto factor de calidad (Q) que presentan las ESAs, sumado

las limitaciones de ancho de banda y de ganancia asociados a esta característica, representan una de las tareas más difíciles de tratar al incluir cualquier tipo de red de adaptación de impedancia en el sub-sistema radiante (antena). Entre las alternativas para mejorar el desempeño de las ESAs, los circuitos tipo non-Foster surgen como una alternativa interesante y efectiva de obtener un ancho de banda —de impedancia— instantáneo amplio. Esas técnicas y resultados se convirtieron en la piedra angular del trabajo desarrollado, y posteriormente presentado, en este documento.

Un nuevo parámetro, denominado *Sens* por el autor, fue introducido y desarrollado en el Capítulo 3 como una herramienta versátil y fácil de calcular, basada en los parámetros S del modelo de dos puertos de la antena misma, que es útil para analizar la viabilidad de la integración de una MN tipo non-Foster en la estructura de la antena. Por lo tanto, el parámetro *Sens* nos permite saber si la antena estudiada es adecuada para ser integrada a una MN activa, tipo non-Foster y, de ser así, nos indica también cuál es la mejor ubicación para colocar tal MN. El avance que representa el parámetro *Sens* radica en su propiedad de ser fácilmente calculado por medio de cualquier software de simulación electromagnética, siempre que éste tenga la opción de diseño asistido por computadora (CAD). Una propiedad adicional y no menos importante del parámetro *Sens* es que puede ser utilizado con cualquier otro tipo de antena sin tener en cuenta su tamaño eléctrico o su estructura.

En el Capítulo 4 fue presentada otra de las contribuciones de esta tesis: el método para el diseño de antenas eléctricamente pequeñas, adaptadas con formas activas incorporadas tipo non-Foster. Se puede decir que cualquier compendio de consideraciones prácticas da al ingeniero una herramienta adicional de discernimiento y decisión. Esta estrategia de diseño pretende contribuir con consideraciones adicionales, organizadas en una metodología integral, para reducir, tanto como sea posible, el porcentaje de fallas al abordar el diseño, desde la etapa de cálculo y simulación, hasta la práctica.

La estrategia de incorporar —embeber— la red de adaptación activa de impedancias, se presenta como una alternativa interesante, especialmente para aquellas aplicaciones en las que el espacio ocupado por la antena, y todos sus circuitos, es limitado y constituye un fac-

tor determinante en su diseño. En este sentido, fueron presentadas dos estructuras distintas: una antena impresa, eléctricamente pequeña, de tipo lazo (*semiloop*), y un monopolo impreso tipo aleta (*blade*), también eléctricamente pequeño, como ejemplos de diseño aplicando el método propuesto. Un importante nivel de miniaturización en ambas antenas fue obtenido en la banda baja incorporada, de entre 90% y 95% a la frecuencia más baja, en el semiloop y el monopolo de aleta, respectivamente. Este nivel de miniaturización fue calculado, en cada caso, con respecto a una antena resonante, de igual naturaleza (magnética o eléctrica), es decir, de tamaño eléctrico completo a dicha frecuencia.

Además del grado de miniaturización conseguido, el ancho de banda relativo (FBW) medido, en la banda baja añadida, fue del 119% (centrado en 117 MHz) para el semiloop (factor ka entre 0,04 y 0,17), y de más del 82% (centrado en 85 MHz) para el monopolo de aleta (factor ka entre 0,26 y 0,56). Cabe señalar que la respuesta natural de impedancia de cada antena no fue afectada una vez que la red de adaptación activa es incorporada. El notable ancho de banda de impedancia, alcanzado en ambas estructuras, nos alentó a continuar en la búsqueda de soluciones a los cambios en el diagrama de radiación, experimentados después de añadir la red activa non-Foster en la estructura de la antena.

Con respecto a la selección del dispositivo activo a ser utilizado en la red activa non-Foster, es importante señalar la necesidad de utilizar un transistor con una respuesta de transconductancia (g_m) constante, hasta la máxima frecuencia posible. Además, su frecuencia de transición (f_{T}) también debe ser alta, ya que se espera que el comportamiento non-Foster de la impedancia de entrada del NIC sea una pequeña fracción de dicha frecuencia f_{T}. En este sentido, la metodología de diseño propuesta utiliza el análisis de tolerancia, disponible en muchos simuladores de circuitos comerciales, que nos da una visión adicional sobre los parámetros específicos a los que el rendimiento general del sistema (antena + NIC) es más sensible.

La estabilidad del sistema de antena también se aborda en el Capítulo 4. La función del determinante normalizado (NDF) se muestra como una herramienta tan interesante como fácil de calcular, al mismo tiempo que rigurosa, para la evaluación de la estabilidad de sistemas lineales. De nuevo, utilizando cualquier software de diseño y simulación de circuitos

comercial, el análisis de estabilidad puede generalizarse para incluir los parámetros S (simulados o medidos) de la antena misma en el cálculo de la NDF. Los efectos parásitos o del empaquetado de los componentes, así como los efectos de borde en las conexiones *microstrip* o *strip-line* que sirven de conexión, también pueden ser considerados al calcular la NDF. Este hecho hace que la NDF sea uno de los métodos de análisis de estabilidad más versátiles reportados hasta la fecha.

Es importante destacar que esta metodología puede ser utilizada directamente en cualquier tipo de antena. Se puede utilizar, además, en antenas de cualquier tamaño eléctrico, incluso en presencia de otros elementos radiantes en campo cercano. En este sentido, en el Capítulo 5 fue presentada la metodología de diseño propuesta aplicada a los arreglos *(arrays)* de antenas, con el fin de agregar una banda de frecuencia de trabajo a bajas frecuencias. Un par de arreglos de antenas de pocos elementos han sido presentados como ejemplos de diseño para ilustrar este enfoque.

Uno de los hechos que quizás más desalienta a los ingenieros de antenas para incluir elementos activos en sus diseños, es el alto nivel de esfuerzo y trabajo de laboratorio involucrados en el ajuste fino de los dispositivos, en este caso los NICs. En la mayoría de los casos, como en efecto ocurrió con los ejemplos de diseño mostrados a lo largo de esta tesis, es necesario dedicar horas al ajuste y a las pruebas preliminares, antes de lograr un resultado exitoso que se ajuste al desempeño esperado.

Tal vez este último hecho es una de las razones por las que, para muchos grupos de investigación alrededor del mundo, el uso de convertidores de impedancia negativa, NICs, utilizados como redes de adaptación de impedancia para antenas, ha llegado a la fase final de su vida en el campo de la investigación y el desarrollo. Prueba de ello es el reducido número de equipos de trabajo que reportan contribuciones en la actualidad. No obstante, cabe señalar que aún queda mucho trabajo por hacer en la realización de las ESAs, adaptadas con redes activas tipo non-Foster, que podría enfocarse a convertirlas en una alternativa atractiva para la industria y la academia.

Prospectiva de Trabajo Futuro

A partir de la investigación realizada durante este trabajo, las áreas con mayor potencial, y de las que puede esperarse un desarrollo adicional, son descritas continuación.

En primer lugar, los efectos parásitos y otras imprecisiones asociadas con la fabricación de un NIC en una placa de circuito impreso (PCB) se pueden mitigar por medio de la tecnología monolítica (MMIC). Aunque algunos trabajos han sido reportados como exitosos, no ha sido posible explorar dicha alternativa en este trabajo. Sin embargo, esta es una opción interesante y de muy alto nivel tecnológico para implementar dispositivos tipo non-Foster más confiables, que puedan ser integrados en antenas eléctricamente pequeñas.

En segundo lugar, el uso de otros dispositivos activos para implementar redes non-Foster, como los diodos de efecto túnel (RTD), operados en una región de resistencia diferencial negativa (NDR), ha sido reportado recientemente en [60, 130, 131]. Este enfoque representa una alternativa alentadora para mitigar tanto el problema de frecuencia limitada como la situación de compromiso entre dicha limitación y los problemas de inestabilidad en los circuitos non-Foster, tal y como se ha demostrado hasta ahora. Esta es, quizás, una de las líneas de trabajo futuras más interesantes, desde el punto de vista del autor.

Por otra parte, el desempeño en términos del ruido añadido en las antenas receptoras adaptadas con redes non-Foster, representado por la figura de ruido (NF), es una figura de mérito fundamental, en especial cuando se integran dispositivos activos en la cadena receptora.

Sin embargo, la estimación del ruido añadido en una ESA adaptada con circuitos activos no es una tarea fácil, menos aún cuando la red activa está embebida en la estructura de radiación. Por ende, una técnica de cuantificación para la estimación del ruido añadido es siempre bienvenida, y representa una línea de trabajo futuro. Un enfoque interesante en esta área ha sido recientemente reportado por M. Jacob y D. Sievenpiper en [117]. En su trabajo, el modelo de ruido de un NIC basado en BJTs, alrededor de su punto de polarización, se utiliza para estimar

el ruido añadido cuando se conecta al puerto de alimentación de una ESA. Posteriormente, se realiza un análisis comparativo para el caso de un amplificador, de una sola etapa, conectado directamente al punto de alimentación (en lugar del NIC) de la misma antena.

La estimación y medición del desempeño de la antena adaptada con elementos activos en modo de transmisión, comprenden otro tema importante que debe abordarse en ésta área. Hasta donde ha sido posible experimentar con los prototipos presentados aquí, el embeber los elementos non-Foster en la estructura de la antena permite al conjunto (antena + NIC) ser usado tanto en recepción como en transmisión. Sin embargo, los fenómenos no lineales (reportados en la literatura) que están relacionados con la compresión de potencia, la saturación y la inestabilidad de los dispositivos activos (e.g. los transistores), en presencia de altos voltajes y corrientes a través de la antena, siguen siendo un inconveniente significativo, especialmente a potencias de transmisión prácticas (mayores a 100 mW en onda continua).

Para terminar, la fabricación de un arreglo de antenas de pocos elementos, cargado con una red de adaptación tipo non-Foster, es una tarea pendiente en aras de extender, hacia frecuencias más bajas, la mejora en el desempeño general observada a nivel de simulación. Por lo tanto, sería posible obtener un arreglo de antenas eléctricamente pequeñas adaptado con redes non-Foster y que presente ciertos parámetros adicionales de radiación deseados. Entre dichos parámetros se puede mencionar un alto nivel del diagrama del elemento de escaneo (*scan element pattern*, SEP) —una tarea desafiante puesto que los efectos de acoplamiento entre elementos aumentan a frecuencias más bajas— o un factor de sensibilidad direccional mejorado, tal como ha sido propuesto recientemente por A. Elfrgani et al. en [129].

Appendices

APPENDIX A

STABILITY OF LINEAR SYSTEMS THROUGH THE NDF

As mentioned before, the dynamic response for any N-node network containing linear elements can be derived from vector equations —in the frequency domain $s = \sigma + \mathrm{j}\omega$— comprising an admittance $\mathbf{Y}(s)$ (or impedance $\mathbf{Z}(s)$) representation of the system. Among those linear elements we find: resistors, inductors, capacitors, distributed transmission lines, active devices such as transistors, whose currents or voltages depend on node voltages or loop currents. Hence, a vector equation describing the system can be stated as $\mathbf{Y}(s) \cdot \mathbf{V}(s) = \mathbf{I}(s)$, where $\mathbf{I}(s)$ and $\mathbf{V}(s)$ are respectively the excitation and the response column vectors of size N [109].

In presence of any steady excitation, the general solution of the system is composed of a linear superposition of the transient and the steady state responses. The transient response is determined by the roots (poles) of the system which are, in turn, the zeros of its determinant. The transient response is given as

$$\sum_{k=1}^{p} a_k \cdot t^{(m_k-1)} \cdot e^{(\sigma_k \pm j \cdot \omega_k)}, \tag{A.1}$$

where $\sigma_k \pm j \cdot \omega_k$ is the k^{th} root of the system (zero of its determinant) with multiplicity m_k, and p is the total number of roots. These roots always appear in complex conjugate pairs since the system response is a real function of time. By direct inspection of the transient response, it is possible to claim that it will be diminished, allowing the system to reach its steady state, if and only if all $\sigma_k < 0$. Thus, if none of the individual elements has poles in the RHP, a linear system is stable if and only if all the zeros of its determinant lie in the LHP. This last statement is also widely used in dynamic systems theory, and well-known by control systems engineers.

It is reasonable to believe that a complete evaluation of the zeros of the circuit determinant is the most comprehensive and direct way to determine its stability. Nonetheless, in realistic systems containing several nodes and active devices, such calculation might be cumbersome and impractical, even when powerful computers are available today.

Since the real circuits and systems are usually analyzed along the imaginary axis only (i.e. in terms of ω), one can ask whether a frequency-domain-technique might be reliable to determine if some zero of the circuit determinant lies in the RHP —predicting instability— and the answer is affirmative. This is when the Normalized Determinant Function (NDF) shows up.

A.1 Determination of the RHP-Poles of the System

The NDF was devised by A. Platzker and W. Struble in 1993 [107,108] as well as its properties and methodology to be applied through any EDA circuit simulator in [109]. It arises as a rigorous way to check the stability of linear systems since it accounts for all the possible *hidden* poles, disregarded in conventional stability analysis techniques. In microwave circuits, the NDF ascertain the Rollet's proviso, stated in Section 4.2.3 as the condition of having no RHP poles when the network is terminated with the system reference impedance. This proviso has been systematically disregarded in the stability analysis of typical microwave devices, such as filters and amplifiers, due to the use of reduced two-port versions of the active components [105].

The *Principle of the Argument* theorem of complex theory can be

quoted as: "the total change of the argument (phase) of a function $F(s)$ along a closed contour C, on which the function has no zeros and inside which it is analytic except for poles, is equal to $2\pi(N_z - N_p)$, where N_z is the number of zeros and N_p is the number of poles of the function $F(s)$ inside C." Nyquist has used the same theorem for his stability analysis [101], and the plots used for the NDF are related to his.

To make use of the theorem, we define the NDF as

$$NDF = \frac{\Delta(s)}{\Delta_0(s)}, \tag{A.2}$$

where $\Delta(s)$ is the determinant of the circuit under investigation and $\Delta_0(s)$ is the determinant of a companion identical circuit in which all the dependent active generators have been set to zero.

Some important properties of the NDF can be summarized as [109]:

(a) The denominators of $\Delta(s)$ and $\Delta_0(s)$ are equal and therefore cancel out.

(b) NDF has not poles in the RHP ($\Delta_0(s)$ is passive, then, it has no zeros in the RHP)

(c) The $\lim_{\omega\to\infty} NDF = 1$ since the active networks $\Delta(s)$ tends to the passive one $\Delta_0(s)$ as $s \to \infty$. Thus, both the circuit under investigation and its passive companion are of the same order of s.

(d) The NDF reduces to $\Delta(j\omega)/\Delta_0(j\omega)$ when evaluated along the imaginary axis.

(e) NDF $(-\omega) =$ NDF$^*(\omega)$ since the system response is a real function of time.

Making use of these properties and the principle of the argument theorem, the evaluation of the NDF along the closed contour shown in Fig. A.1, give us an important result. The total change in the argument (phase) of $\Delta_0(j\omega)/\Delta_0(j\omega)$ as ω varies from ∞ to $-\infty$, i.e. the number

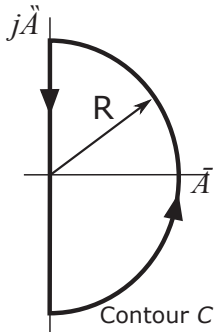

Figure A.1: Contour for evaluating the NDF.

of times the NDF contour encircles the origin counterclockwise, is equal to the number of zeros of the circuit determinant.

As mentioned in Section 4.2.3, in practical designs, the symmetry property of the NDF between the positive and the negative frequencies —(e) in the list above— can be used. Then, the possible origin encirclements can be found by post-processing the NDF, computed along the interval $[0, \omega)$ only. This simplifies the calculation of the NDF and enables a wider range of circuit simulators to be used.

The actual breakthrough in the stability analysis by using the NDF lies on the possibility of easy computing it by applying the so-called Return Ratios (RRs). As mentioned in Chapter 4, the concept of *return ratio* was first discussed by Bode [11], and after by Maclean [110], and others [111], and was used to assess the stability of feed-back amplifiers with single- or multi-loop circuits.

A.2 Relation between the NDF and Return Ratios (RR)

In cases where a multi-device circuit is modeled in detail in a CAD/EDA software, it is not practical to determine the NDF algebraically. Besides the NDF basics, Struble and Platzker also devised a CAD method for creating a Nyquist plot of the NDF [108]. RRs are commonly used in the analysis of stability in single-loop feedback circuits. The procedure to calculate those RRs was described before in

Section (4.2.3). In this section the relation between the RR and the NDF is further described.

The circuit previously illustrated in Chapter 4, in Fig. 4.11a, is shown again, for convenience, in Fig. A.2(a and b). It contains M dependent sources. One of them, I_l, is explicitly labeled and depends on node voltage V_u. If I_l is made independent by redefining V_u to be an ancillary (and arbitrary) voltage V'_u, the node voltage equations for the resultant circuit can be written as

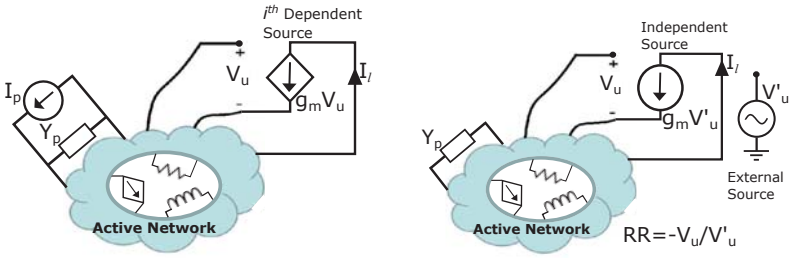

Figure A.2: Sketch for the calculus of RR_i. (a) Before, and (b) after the replacement of the i^{th} dependent source for an independent source of arbitrary amplitude $V'_u = 1$. All others external excitations (I_p) are also removed.

$$[\mathbf{Y_{01}}] \begin{bmatrix} V_1 \\ V_2 \\ \vdots \\ V_u \\ \vdots \\ V_M \end{bmatrix} = \begin{bmatrix} 0 \\ \vdots \\ -g_m \cdot V'_u \\ 0 \\ \vdots \\ 0 \end{bmatrix} \tag{A.3}$$

where $\mathbf{Y_{01}}$ is the node admittance matrix of the network when g_m is set to zero. Solving for V_x, it gives

$$V_x = \frac{-g_m V'_u C_{01lx}}{\Delta_{01}} = \frac{-g_m V'_u C_{lx}}{\Delta_{01}}, \tag{A.4}$$

where C_{01lu} is the co-factor of the element y_{01lu} in $\mathbf{Y_{01}}$, and C_{lu} is the co-factor of the element y_{lu} in the full admittance matrix, $\mathbf{Y}$. $C_{01lu} = C_{lu}$ since the only difference between $\mathbf{Y}$ and $\mathbf{Y_{01}}$ is the l, u element, which does not contribute to either co-factor. Thus, it is possible to associate a RR with the dependent source as

$$RR_1 = -\frac{V_u}{V_u'} = g_m \frac{C_{lu}}{\Delta_{01}}, \tag{A.5}$$

where Δ_{01} is the determinant of $\mathbf{Y_{01}}$. By applying the Laplace expansion of $\mathbf{Y}$ along the row or the column that contains y_{lu}, and observing that $y_{lu} = y_{01lu} + g_m$, it is possible to claim that

$$\Delta = \Delta_{01} + g_m C_{lu}. \tag{A.6}$$

Then, by replacing (A.5) into (A.6), we obtain the expression that relates the RR with the NDF.

$$\frac{\Delta}{\Delta_{01}} = 1 + RR_1. \tag{A.7}$$

In circuits with several dependent sources, it is possible to use a straightforward extension of the above procedure for calculating the NDF [108]:

$$\begin{aligned} NDF = \frac{\Delta}{\Delta_{0(1,2,\cdots,M)}} &= \frac{\Delta}{\Delta_{0(1)}} \cdot \frac{\Delta_{0(1)}}{\Delta_{0(2)}} \cdot \frac{\Delta_{0(2)}}{\Delta_{0(3)}} \cdots \frac{\Delta_{0(M-1)}}{\Delta_{0(M)}} \\ &= (1 + RR_1)(1 + RR_2) \cdots (1 + RR_M), \end{aligned} \tag{A.8}$$

and finally, the expression shown before in (4.15):

$$NDF = \prod_{i=1}^{M} (RR_i + 1). \tag{A.9}$$

APPENDIX B

DESIGN AND NOISE FIGURE MEASUREMENT OF A BALANCED NON-FOSTER IMPEDANCE

The noise added by a transistor-based non-Foster circuits to a host structure (e.g. a filter or an antenna) is a factor of growing interest in the microwave and antenna community. Even when such non-Foster element is embedded into a distributed-elements circuit or in a radiating structure, doing impossible the access to its input-output ports, the noise characterization of the added noise is welcome. This appendix contains the design process of a two-port balanced NIC, manufactured as a stand-alone device, with the aim of measuring its Noise Figure (NF). The most part of the work presented in this appendix was carried out during a research stage at the Queen Mary University of London (QMUL), in collaboration with members of the Antennas and Electromagnetics Research Group, lead by Prof. Yang Hao.

B.1 NIC Topology

With the purpose of characterizing the noise performance of a standalone NIC, a couple of previous one-port prototypes, previously developed to be embedded into an antenna, are re-designed to implement

a two-port device whose NF can be measured. A conventional topology, first proposed by Linvill [19], is used because of its suitability for two-port noise characterization. This NIC topology consists of two cross-coupled BJT-transistors, configured in such a way a signal can be coupled through the two-port network. Figure B.1 shows a simplified schematic of the described NIC topology, modeled in the AWR® software. The two resistors R_2 are included to bias the BJTs and, at the same time, to make the equivalent negative capacitance of the NIC less sensitive to variations and parasitics in the lumped elements, as proposed in [70].

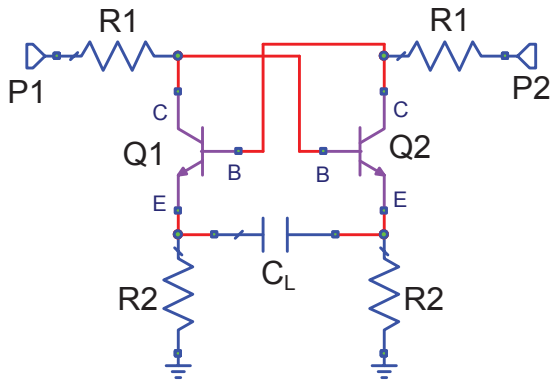

Figure B.1: Simplified NIC schematic for the noise figure characterization.

An FR4 slab, with 1.5 mm thick and a relative permittivity (ϵ_r) of 4.3, is used as substrate. Two BFG410W BJT-transistors, manufactured by NXP® semiconductors, are used to act as active devices. The manufactured prototype is shown in Fig. B.2a. A touchstone file containing the S-parameters is extracted from the network analyzer. After post-processing, it is possible to extract the equivalent non-Foster impedance, seen across the two-port network, as it is shown in Fig. B.2b.

As a result, the NIC impedance is no longer a constant (frequency independent) negative capacitance but instead is a bandwidth-limited non-constant negative capacitance, even with a negative resistive part. Parasitics and possible differences between the active devices might be the origin of the differences between the measured and the simulated NIC impedance response.

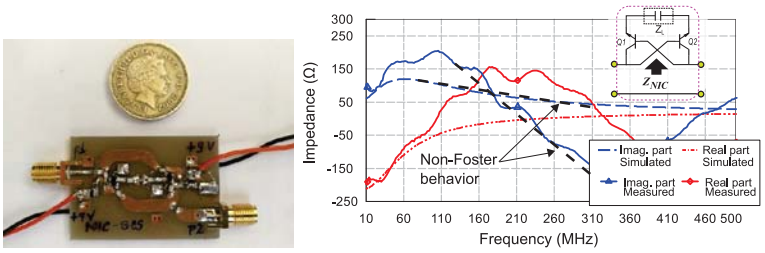

(a) **(b)**

Figure B.2: (a) Prototyped 2-port NIC on a PCB. (b) Simulated and measured response of the NIC impedance (Z_{NIC}) showing the negative slope of the imaginary part, proof of the non-Foster behavior.

Figure B.3 depicts the equivalent negative capacitance implemented with the NIC, which can be computed once the measured Y_{21} parameter is extracted, as in (B.1).

$$Z_{\mathrm{NIC}} = -1/Y_{21}. \tag{B.1}$$

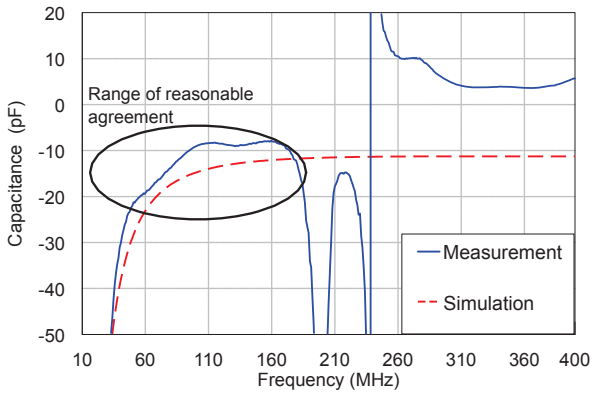

Figure B.3: Equivalent capacitance that shows an acceptable agreement between measurement and simulation up to 200 MHz.

A negative capacitor is obtained as far as the reactive part of the NIC impedance (continuous blue line in Fig. B.2b) cross the zero ($X_{\mathrm{NIC}} = 0\,\Omega$), that is, up to about 200 MHz.

B.2 Noise Performance Modeling

The noise contributions in the NIC can be modeled by including the main noise sources: the shot-, the ficker-, and the burst- noise in the BJTs, and the thermal noise associated with the lossy components. A reasonable model for the noise in a BJT is depicted in Fig. B.4. It includes a thermal noise voltage source associated to the resistive component of the base; a current noise source in shunt with the junction base-emitter, accounting for the shot noise accompanying the base current (the flicker and the burst noise are very low in bipolar transistors [132]). Finally, a noise current source associated to the shot noise in the collector. The detailed analytical noise modeling of the transistor has been reported in [133–135].

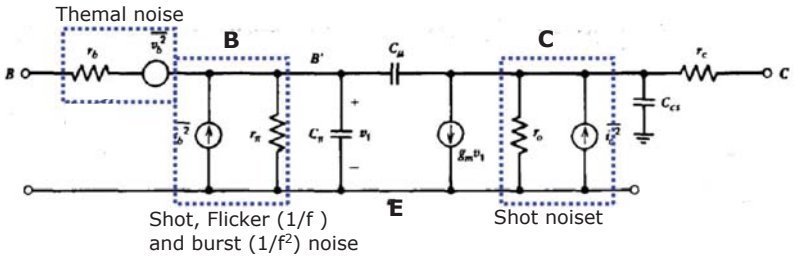

Figure B.4: Small signal model of a BJT, including the main noise contributions [135].

Once those noise sources are included in the small signal model of the transistors, it is possible to obtain a complete noise circuital model of the NIC, as the one depicted in Fig. B.5. By means of a circuit simulator with the harmonic balance simulation capability, it is possible to analyze the NF of the NIC across its working band, in order to compare it with the measurement, as it will be shown in the section below.

B.3 Measurements

Among the techniques for measuring noise in two-port devices, the Y-factor is one of the most used due to its capabilities of wide frequency range as well as the wider availability of Spectrum Analyzers (SA) as compared to a noise figure meter. In addition, nowadays, many Noise

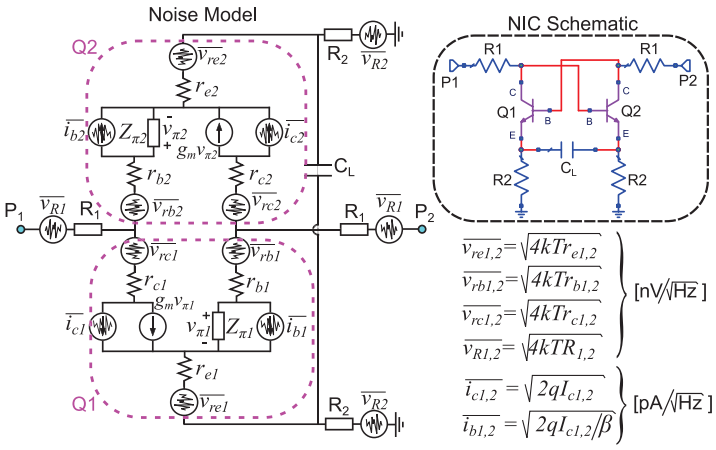

Figure B.5: Representation of the current and voltage noise sources in the balanced SCS-NIC [117] used for simulating the NF response in the AWR software. k is the Boltzmann constant ($1.38 \cdot 10^{-23}$ J/K). The inset on the right shows the NIC schematic of Fig. B.1.

Figure Analyzers (NFA) implements this technique in an automated way and let us account for the effects due to losses in connectors, attenuators, matching pads, and so on, involved in the test fixture. Figure B.6 depicts the Y-factor strategy. The Device Under Test (DUT), and any other coupling device, have to be removed at the calibration stage. In this technique, a calibrated noise source with a known output noise level must be available. It is represented by the Excess Noise Ratio (ENR). The ENR value is expressed in dB as a difference between hot temperature (T_h when noise source ON) and cold temperature (T_c when noise source OFF), divided by the room temperature, T_0, as follows

$$ENR_{\mathrm{DB}} = 10 \log \left(\frac{T_h - T_c}{T_0} \right). \tag{B.2}$$

As the instrument (NFA or SA) itself contributes to the overall noise result, a calibration (or second stage correction) is needed. Then, by applying the Friis formula, the Noise Factor (F) —linear scaled noise figure— of the cascaded system, NFA + DUT is given as:

$$F_{\text{total}} = F_{\text{DUT}} + \frac{F_{\text{instrument}} - 1}{G_{\text{A:DUT}}}, \tag{B.3}$$

thus, the F_{DUT} can be extracted as

$$F_{\text{DUT}} = F_{\text{total}} - \frac{F_{\text{instrument}} - 1}{G_{\text{A:DUT}}}. \tag{B.4}$$

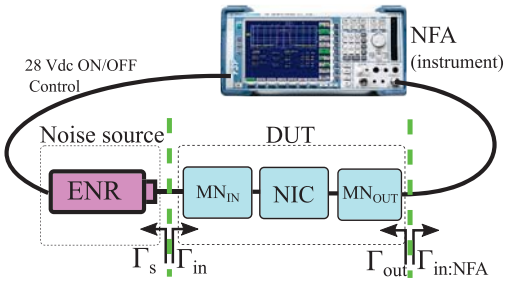

Figure B.6: Scheme of the Y-factor technique for noise figure measurement [131].

In order to set adequate deltas between the ON and OFF states during the calibration and measurement stages [136], three guidelines can be summarized as follows:

- The difference between the noise source ON and OFF measurements (no DUT) should be at least 3 dB: $ENR_{\text{dB}} > NF^{\text{NFA}} + 3$ dB.
- The difference between the noise source ON and OFF measurements (including the DUT) should be at least 5 dB: $ENR_{\text{dB}} > NF_{\text{dB}}^{\text{DUT}} + 5$ dB.
- The difference between measurement and calibrations should be at least 1 dB. This is done by choosing the NFA, and possibly a preamp, such that the noise figure of the DUT + the available gain of the DUT is at least 1 dB greater than the noise figure of the NFA: $NF_{\text{dB}}^{\text{DUT}} + G_{\text{A:dB}}^{\text{DUT}} > NF_{\text{dB}}^{\text{NFA}} + 1$ dB.

In addition, as a rule of thumb, a low ENR noise source has advantages if the noise figure of the DUT is very low. Otherwise, as for the case of a two-port balanced-NIC, a high ENR is preferred [136]. Minimal VSWR changes between the the noise source and DUT, when the source is toggled between ON and OFF states is a key factor to obtain accurate results. Commercial ENR sources meet this condition nowadays. A low ENR source usually contains an in-built attenuator which limits the ENR and reduces the sensitivity in reflection coefficient between both states. In our case, the gain and the output noise of the BJT-based NIC are sensitive to changes in input impedance. Furthermore, the VSWR in both the input and the output DUT ports should be kept at the minimum since reflected signals can be coupled with the one from the ENR and the estimation of NF_{DUT} can be flawed. For this case, as the NIC is designed to implement a floating negative reactance, a poor matching level is expected. Thus, an additional matching network (MN) is needed for the sake of accuracy in the noise characterization. A poor matching level can lead to errors in both gain and noise figure measurements.

In order to obtain a 50-Ω-terminated NIC across the band, two impedance MNs, comprising three lumped-reactive elements each, are connected in series at the input and output ports, respectively. The input impedance response of both the matched and the unmatched NIC is shown in Fig. B.7.

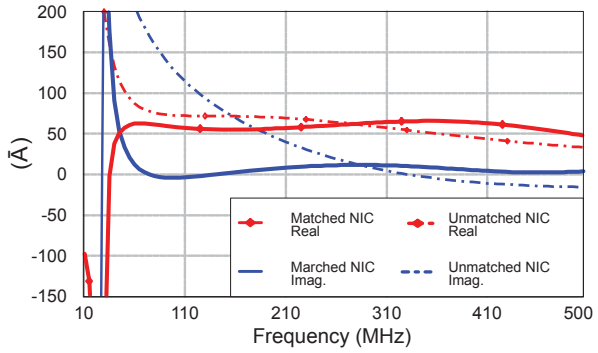

Figure B.7: Input impedance response of the two-port NIC in simulation. By the reciprocity ($S_{12} = S_{21}$) and symmetry ($S_{11} = S_{22}$) property of the balanced-NIC, the output impedance is expected to be the same.

The measurements were carried out following the test fixture depicted in Fig. B.8a. A mini-anechoic chamber is used to act as a Faraday cage, and was exclusively designed by the QMUL laboratory staff to avoid the interference of surrounding noise. The ENR, shown in Fig. B.8b, is an Agilent-346B with a NF of around 15 dB, characterized up to 18 GHz. A Rohde and Schwarz FSP40 spectrum analyzer is used as instrument. An application firmware (FSV-K30) installed in the SA provides an enormous reduction in instrument noise figure (NF_{NFA}). Such a reduction in the instrument NF let us to avoid the use of a preamplifier to compensate possible $G_{\text{A:DUT}}$ issues. Corrections are also applied for losses of connectors between devices.

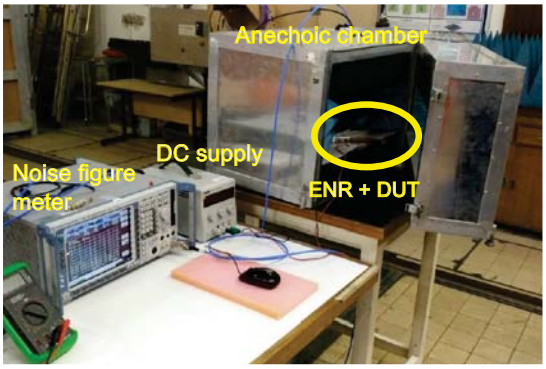

(a)

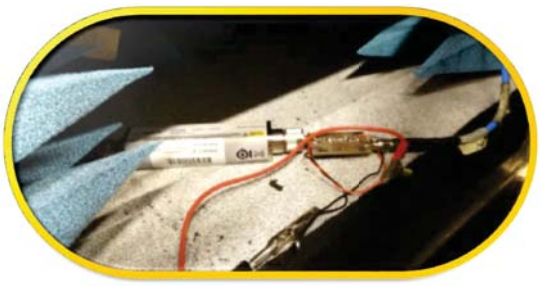

(b)

Figure B.8: (a) Noise figure measurement setup and (b) a zoom showing the ENR and the NIC.

The measured NF along with the simulated results are shown in Fig. B.9. A difference within the range 5 dB to 9 dB is observed, being

the measured NF values higher. This result allow us to infer that the uncertainty in the measurement is high, and that the noise model is not accurate enough to predict the noise figure in a circuit simulator. The low gain condition of a balanced-NIC —since it is not intended to act as an amplifier— makes the situation worse as it rise up the second stage contribution, given as in (B.3). The measured available gain $G_{\text{A:DUT}}$ is around -5 dB across the measured band for this NIC. A preamplifier was added as an attempt to mitigate the low-gain effect, but the results remained similar to those in Fig. B.9.

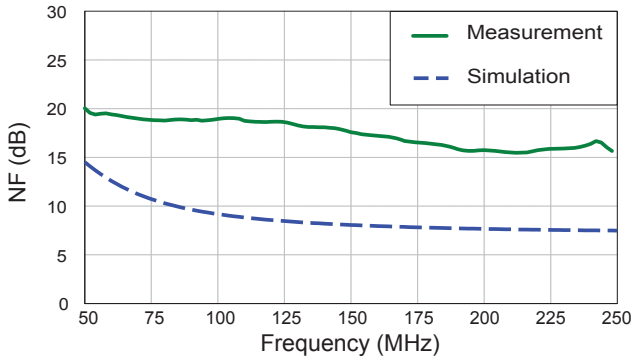

Figure B.9: Simulated and measured Noise figure (NF) of the proposed NIC.

There are several factors which contribute to noise figure measurement uncertainty. Those with the most significant impact are the noise figure of the instrument (NFA or the SA), uncertainty of ENR value, and gain of the DUT. An estimation of the noise figure uncertainty can be computed by using the Taylor expansion of (B.4) and applying the Root of the Sum of Squares (RSS) approach, as follows [136]:

$$\Delta NF_{\text{DUT}} = \sqrt{A^2 + B^2 + C^2 + D^2}, \tag{B.5}$$

where

$$\begin{aligned} A =& \frac{F_{\text{total}}}{F_{\text{DUT}}} \Delta NF_{\text{total,dB}}, \\ B =& \frac{F_{\text{NFA}}}{F_{\text{DUT}} G_{\text{A:DUT}}} \Delta NF_{\text{NFA,dB}}, \\ C =& \frac{F_{\text{total}} - 1}{F_{\text{DUT}} G_{\text{A:DUT}}} \Delta G_{\text{A:DUT,dB}}, \\ D =& \left(\frac{F_{\text{total}}}{F_{\text{DUT}}} - \frac{F_{\text{NFA}}}{F_{\text{DUT}} G_{\text{A:DUT}}} \right) \Delta ENR_{\text{dB}}. \end{aligned} \tag{B.6}$$

The four delta terms in the previous equations accounts for the four "primary contributions" of measurement uncertainty. The ΔENR_{dB} is specified by the manufacturer and is around 0.2 dB for this case. The remaining three delta terms are strong functions of the reflection coefficients at both the DUT input (Γ_{in}) and output (Γ_{out}) ports, at the NFA/SA input ($\Gamma_{\text{in:NFA}}$), and at the ENR port (Γ_{s}). The $NFA_{\text{uncert:dB}}$ values are typically around 0.05 dB in commercial instruments. The three remaining delta terms can be computed as

$$\Delta NF_{\text{total,dB}} = \sqrt{\left(20 \log(1 - \Gamma_{\text{s}} \Gamma_{\text{in}})\right)^2 + \left(NFA_{\text{uncert:dB}}\right)^2}, \tag{B.7}$$

$$\Delta NF_{\text{NFA,dB}} = \sqrt{\left(20 \log(1 - \Gamma_{\text{s}} \Gamma_{\text{in:NFA}})\right)^2 + \left(NFA_{\text{uncert:dB}}\right)^2}, \tag{B.8}$$

$$\Delta G_{\text{A:DUT,dB}} = \sqrt{\begin{array}{l} \left(20 \log(1 - \Gamma_{\text{s}} \Gamma_{\text{in:NFA}})\right)^2 + \left(20 \log(1 - \Gamma_{\text{s}} \Gamma_{\text{in}})\right)^2 \\ + \left(20 \log(1 - \Gamma_{\text{out}} \Gamma_{\text{NFA:in}})\right)^2 + \left(NFA_{\text{uncert:dB}}\right)^2 . \end{array}} \tag{B.9}$$

Some manufacturers provide designers with open-access applets specifically devoted to calculate the uncertainty in the noise figure measurement. Figures B.10(a, b) shows a theoretical analysis of the measurement uncertainty for the used equipment, as a function of the NF_{DUT} and its gain, according to (B.5). It is assumed that the cascaded noise figure (NF_{total}) equals NF_{DUT} as the firmware FSV-K30 reduces the noise figure of the SA to a very low value across the working band. Two different matching levels at the DUT ports were analyzed. Even with an acceptable matching level ($VSWR = 2$), at each DUT port, the noise

figure uncertainty reach high values. For lower impedance matching levels ($VSWR > 5$), the uncertainty becomes a serious issue, leading to a considerable error in measuring the noise figure of this kind of low-gain devices. Since the available gain in this balanced-NIC is low (≈ -5 dB), and the measured NF_{NIC} is greater than 15 dB, the uncertainty is expected to be close to 4 dB (see Fig. B.10b).

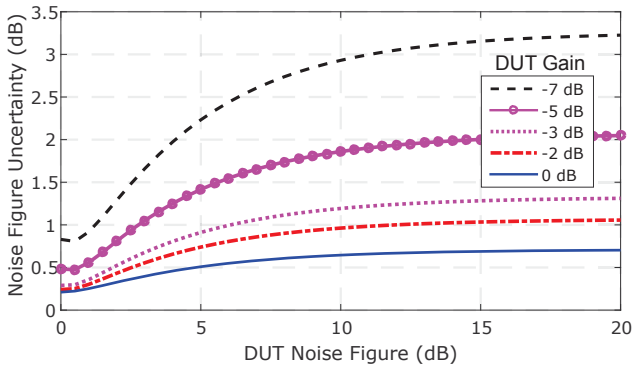

(a)

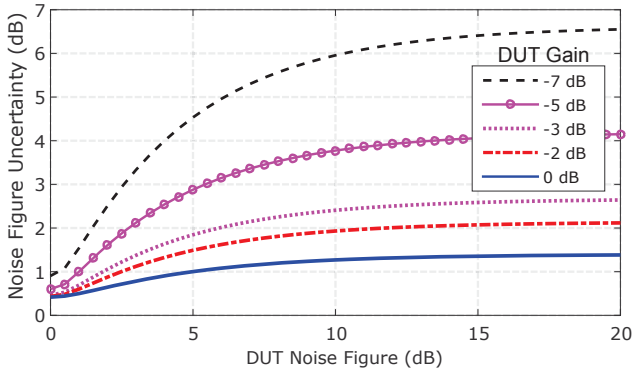

(b)

Figure B.10: Variation of the uncertainty vs. DUT noise figure for different DUT gain values, at two matching levels: (a) $VSWR = 2$, and (b) $VSWR = 5$. Lower G_{DUT} values result in higher uncertainties.

Even in the worst case of uncertainty (NF_{NIC} ± 4 dB), the measured NF is still far from its simulated values (see Fig. B.9). This can be due to the poor matching level at the NIC ports, even after including the tuning networks. Another possible reason might be the high level in

noise figure of the proposed two-port NIC, whose value is close to that of the ENR level itself. This is not an advisable condition for the Y-factor technique to be applied, as mentioned before. Further considerations on the accuracy in noise figure evaluation of low-gain mismatched devices through the Y-factor approach are presented in [137]. It was found that errors in the noise are mainly related to the fact of neglecting the DUT mismatch effect on the noise figure of the instrument (NFA or SA). Furthermore, the use of the available gain, $G_{\mathrm{A:DUT}}$, instead of insertion gain does not necessarily provide more accurate results for high values of DUT return losses.

B.4 Conclusion

A two-port non-Foster impedance implemented with a balanced BJT-based NIC has been shown. It has been measured and reported to work from 50 MHz to 200 MHz, acting as a negative capacitor. The noise figure measurement has been done by applying the Y-factor technique. An additional input-output MNs were included to obtain a 50-Ω-terminated two-port network, as necessary for the Y-factor approach. The device noise figure is between 15 to 20 dB, across the band 50 MHz to 250 MHz. The noise figure uncertainty has been also estimated. This specific NIC circuit has been found to be a "noisy" device. Thus, more efforts have to be made to reduce its noise figure of merit to lower values, as they has been found by other authors, whose measured NF_{DUT} is between 10 to 15 dB [138].

In addition, from the actively matched ESA point of view, in spite that the non-Foster MNs have provided enormous bandwidth improvements, their significantly high noise figure —as for the BJT-based NIC shown here— indicates a source for degradation in the receiving mode. Thus, an additional tradeoff between the output SNR and the impedance bandwidth is also present in the actively matched ESA design, loaded with non-Foster elements.

PUBLICATIONS

The work developed in this Ph.D. thesis has led to journal and conference contributions. The complete list is detailed below.

Journals

Related with Chapter 3:

- F. Albarracín-Vargas, E. Ugarte Muñoz, and D. Segovia Vargas, "Sensitivity analysis for active matched antennas with non-Foster elements," *IEEE Transactions on Antennas and Propagation*, vol. 62, no. 12, pp. 6040–6048, Dec. 2014.

Related with Chapter 4:

- F. Albarracín-Vargas, V. G. Posadas, F. J. Herraiz-Martinez, and D. Segovia-Vargas, "Design Method for Actively Matched Antennas with Non-Foster Elements," *IEEE Transactions on Antennas and Propagation*, vol. PP, no. 99, pp. 1–1, Jun. 2016.
- D. Segovia-Vargas, J. L. Jimenez-Martin, A. Parra-Cerrada, E. Ugarte-Muñoz, L. F. Albarracín-Vargas, and V. Gonzalez-Posadas, "Stability Analysis and Design of Negative Impedance Converters: application to circuit and small antennas," *Radioengineering*, vol. 25, no. 3, pp. 409–418, Sep. 2016.

Related with Chapter 5:

- F. Albarracín-Vargas and D. Segovia-Vargas, "Active Non-Foster Matching Network for a Small Printed Antenna Array," *IEEE Antennas and Wireless Propagation Letters*, no. submitted, 2017.

Related with Appendix B:

- F. Albarracín-Vargas, D. S. Nagarkoti, and D. Segovia-Vargas, "Noise Measurements in a Balanced Two-Port Negative Impedance Converter," *IEEE Transactions on Microwave Theory and Techniques*, no. submitted, 2017.

Conferences

Related with Chapter 3:

- F. Albarracín-Vargas, E. Ugarte Muñoz, V. Gonzlez Posadas, and D. Segovia Vargas, "Consideraciones de diseo de adaptacin activa para antenas cargadas con circuitos non-Foster," in *XXIX Simposium nacional de la URSI, Valencia 2014*, Valencia, 2014, pp. 1–4.
- E. Ugarte-Muñoz, F. Albarracín-Vargas, F. Herraiz-Martinez, and D. Segovia-Vargas, "Sensitivity and stability analysis of non-foster matched two-port antennas," in *2013 7th European Conference on Antennas and Propagation (EuCAP)*, Apr. 2013, pp. 3006–3009.
- E. Ugarte Muñoz, F. Albarracín-Vargas, and D. Segovia Vargas, "Anlisis de Sensibilidad de Antenas Adaptadas con Redes de Adaptacin non-Foster," in *XXVIII Symposium of the International Union of Radio Science, URSI 2013*, Spain, Sep. 2013.
- F. Albarracín-Vargas, E. Ugarte Muñoz, and D. Segovia Vargas, "Design Considerations on Active Matching for Small Antennas with Non-Foster Forms," in *2014 8th International Congress on Advanced Electromagnetic Materials in Microwaves and Optics (METAMATERIALS)*, Aug. 2014.

- A. Lopez-Yela, F. Albarracín-Vargas, and D. Segovia Vargas, "Passive Matching Networks for Electrically Small Antennas," in *XXX Symposium of the International Union of Radio Science, URSI 2015*, Spain, Sep. 2015.

related with Chapter 4

- F. Albarracín-Vargas and D. Segovia-Vargas, "A printed monopole loaded with a non-Foster matching network in the VHF band; radiation considerations," in *2015 9th International Congress on Advanced Electromagnetic Materials in Microwaves and Optics (METAMATERIALS)*, Sep. 2015, pp. 7–9.
- F. Albarracín-Vargas, E. Ugarte-Muñoz, V. Gonzalez-Posadas, and D. Segovia-Vargas, "A design strategy of active matched small-antennas with non-Foster elements," in *2015 9th European Conference on Antennas and Propagation (EuCAP)*, Apr. 2015, pp. 1–4.
- F. Albarracín-Vargas, D. Segovia-Vargas, and V. Gonzalez-Posadas, "Non-Foster matching network for a small, bladetype monopole in the VHF band," in *2015 IEEE International Symposium on Antennas and Propagation USNC/URSI National Radio Science Meeting*, Jul. 2015, pp. 1396–1397.
- A. Lopez-Yela, F. Albarracín-Vargas, F. Herraiz-Martinez, D. Segovia-Vargas, and V. Gonzalez-Posadas, "Embedded matching networks for electrically small antennas," in *2016 10th European Conference on Antennas and Propagation (EuCAP)*, Apr. 2016, pp. 1–4.

related with Chapter 5

- F. Albarracín-Vargas, D. Segovia-Vargas, and V. Gonzalez-Posadas, "Design considerations in an active matched semiloop array with non-foster networks," in *2016 IEEE International Symposium on Antennas and Propagation (APSURSI)*, Jun. 2016, pp. 925–926.

- F. Albarracín-Vargas, F. J. Herraiz-Martinez, and D. Segovia-Vargas, "Small Printed Log-Periodic Array, Matched with an Active non-Foster Network," in *2017 11th European Conference on Antennas and Propagation (EuCAP)*, Apr. 2017, pp. 1–4.
- E. Ugarte-Muñoz, S. Hrabar, D. Segovia-Vargas, and A. Kiricenko, "Stability of Non-Foster Reactive Elements for Use in Active Metamaterials and Antennas," *IEEE Transactions on Antennas and Propagation*, vol. 60, no. 7, pp. 3490–3494, Jul. 2012.

BIBLIOGRAPHY

[1] C. A. Balanis, *Modern Antenna Handbook*. John Wiley & Sons, Sep. 2011.

[2] R. C. Hansen and R. E. Collin, *Small Antenna Handbook*. John Wiley & Sons, Aug. 2011.

[3] K. Fujimoto and H. Morishita, *Modern Small Antennas*. Cambridge University Press, Jan. 2014.

[4] J. Volakis, C.-C. Chen, and K. Fujimoto, *Small Antennas: Miniaturization Techniques & Applications*, ser. pp. 361-388. McGraw Hill Professional, Dec. 2009.

[5] R. C. Hansen, "Fundamental limitations in antennas," *Proceedings of the IEEE*, vol. 69, no. 2, pp. 170–182, Feb. 1981.

[6] Halton_Company, "Halton Garage Door Opener," http://www.haltongaragedoors.ca/, Apr. 2017.

[7] 3M_Company, "RFID Products," http://solutions.3m.com/wps/portal/3M/en_WW/Track_Trace/home/Products/one/one/, Apr. 2017.

[8] B. D. Pell, E. Sulic, W. S. Rowe, K. Ghorbani, and S. John, "Advancements in automotive antennas," *New Trends and Developments in Automotive System Engineering*, 2011.

[9] Cobham_Company, "UHF/L Band Communication Antenna," http://www.cobham.com/communications-and-connectivity/antenna-systems/, Apr. 2016.

[10] H. A. Wheeler, "Fundamental limitations of small antennas," *Proceedings of the IRE*, vol. 35, no. 12, pp. 1479–1484, Dec. 1947.

[11] H. W. Bode, *Network Analysis and Feedback Amplifier Design*. Van Nostrand, 1945.

[12] R. M. Fano, *Theoretical Limitations on the Broadband Matching of Arbitrary Impedances*. MIT Res. Lab. of Electronics, 1947.

[13] L. J. Chu, "Physical limitations of omni-directional antennas," *Journal of applied physics*, vol. 19, no. 12, pp. 1163–1175, Dec. 1948.

[14] R. F. Harrington, "Effect of antenna size on gain, bandwidth, and efficiency," *J. Res. Nat. Bur. Stand*, vol. 64, no. 1, pp. 1–12, 1960.

[15] S. Best, "Low Q electrically small linear and elliptical polarized spherical dipole antennas," *IEEE Transactions on Antennas and Propagation*, vol. 53, no. 3, pp. 1047–1053, Mar. 2005.

[16] D. Youla, "A New Theory of Broad-band Matching," *IEEE Transactions on Circuit Theory*, vol. 11, no. 1, pp. 30–50, Mar. 1964.

[17] H. L. Thal, "New Radiation Limits for Spherical Wire Antennas," *IEEE Transactions on Antennas and Propagation*, vol. 54, no. 10, pp. 2757–2763, Oct. 2006.

[18] R. M. Foster, "A reactance theorem," *Bell System Technical Journal, The*, vol. 3, no. 2, pp. 259–267, Apr. 1924.

[19] J. Linvill, "Transistor Negative-Impedance Converters," *Proceedings of the IRE*, vol. 41, no. 6, pp. 725–729, Jun. 1953.

[20] K. L. Su, "A Method for Realizing the Negative-Impedance Inverter," *IEEE Journal of Solid-State Circuits*, vol. 2, no. 1, pp. 22–25, Mar. 1967.

[21] T. Yanagisawa, "RC Active Networks Using Current Inversion Type Negative Impedance Converters," *IRE Transactions on Circuit Theory*, vol. 4, no. 3, pp. 140–144, Sep. 1957.

[22] A. Davies, "Stability Properties of a Negative Immittance Converter," *IEEE Transactions on Circuit Theory*, vol. 15, no. 1, pp. 80–81, Mar. 1968.

[23] S. Kolev, B. Delacressonniere, and J.-L. Gautier, "Using a negative capacitance to increase the tuning range of a varactor diode in MMIC technology," *Microwave Theory and Techniques, IEEE Transactions on*, vol. 49, no. 12, pp. 2425–2430, 2001.

[24] C. A. Balanis, *Antenna theory: analysis and design*, 3rd ed. Hoboken, NJ: John Wiley, 2005.

[25] W. L. Stutzman and G. A. Thiele, *Antenna Theory and Design*, 3rd ed. John Wiley & Sons, May 2012.

[26] J. D. Kraus and R. J. Marhefka, *Antennas for all applications*. McGraw-Hill, 2002.

[27] P.-S. Kildal, *Foundations of Antenna Engineering: A Unified Approach for Line-of-sight and Multipath*. Artech House Publishers, 2015.

[28] R. W. P. King, *The theory of linear antennas: with charts and tables for practical applications*. Harvard University Press, 1956.

[29] O. Lodge, *Signalling Across Space Without Wires: Being a Description of the Work of Hertz and His Successors*. Cambridge University Press, Mar. 2013.

[30] D. F. Sievenpiper, D. C. Dawson, M. M. Jacob, T. Kanar, S. Kim, J. Long, and R. G. Quarfoth, "Experimental Validation of Performance Limits and Design Guidelines for Small Antennas," *IEEE Transactions on Antennas and Propagation*, vol. 60, no. 1, pp. 8–19, Jan. 2012.

[31] J. S. McLean, "A re-examination of the fundamental limits on the radiation Q of electrically small antennas," *IEEE Transactions on Antennas and Propagation*, vol. 44, no. 5, pp. 672–, May 1996.

[32] R. Collin and S. Rothschild, "Evaluation of antenna Q," *IEEE Transactions on Antennas and Propagation*, vol. 12, no. 1, pp. 23–27, Jan. 1964.

[33] W. Geyi, P. Jarmuszewski, and Y. Qi, "The Foster reactance theorem for antennas and radiation Q," *IEEE Transactions on Antennas and Propagation*, vol. 48, no. 3, pp. 401–408, Mar. 2000.

[34] D. M. Pozar, *Microwave Engineering*, 2nd ed. Wiley, Aug. 1998.

[35] R. C. Hansen, "Bode and Fano impedance matching," *Microwave and Optical Technology Letters*, vol. 50, no. 4, pp. 875–877, Apr. 2008.

[36] H. Mirzaei and G. V. Eleftheriades, "A Compact Frequency-Reconfigurable Metamaterial-Inspired Antenna," *IEEE Antennas and Wireless Propagation Letters*, vol. 10, pp. 1154–1157, 2011.

[37] M. C. Tang, R. W. Ziolkowski, S. Xiao, M. Li, and J. Zhang, "Frequency-Agile, Efficient, Near-Field Resonant Parasitic Monopole Antenna," *IEEE Transactions on Antennas and Propagation*, vol. 62, no. 3, pp. 1479–1483, Mar. 2014.

[38] N. Zhu and R. W. Ziolkowski, "Active Metamaterial-Inspired Broad-Bandwidth, Efficient, Electrically Small Antennas," *IEEE Antennas and Wireless Propagation Letters*, vol. 10, pp. 1582–1585, 2011.

[39] S. E. Sussman-Fort and R. M. Rudish, "Non-Foster Impedance Matching of Electrically-Small Antennas," *IEEE Transactions on Antennas and Propagation*, vol. 57, no. 8, pp. 2230–2241, Aug. 2009.

[40] D. S. Nagarkoti, K. Z. Rajab, and Y. Hao, "Design and stability of negative impedance circuits for non-foster matching of a monopole antenna," in *The 8th European Conference on Antennas and Propagation (EuCAP 2014)*, Apr. 2014, pp. 2707–2709.

[41] C. R. White, J. S. Colburn, and R. G. Nagele, "A Non-Foster VHF Monopole Antenna," *IEEE Antennas and Wireless Propagation Letters*, vol. 11, pp. 584–587, 2012.

[42] H. Mirzaei and G. V. Eleftheriades, "A Resonant Printed Monopole Antenna With an Embedded Non-Foster Matching Network," *IEEE Transactions on Antennas and Propagation*, vol. 61, no. 11, pp. 5363–5371, Nov. 2013.

[43] W. Wang, J. Geng, R. Jin, X. Liang, and R. Ziolkowski, "Design of a 600 MHz non-Foster dipole," in *2014 International Workshop on Antenna Technology: "Small Antennas, Novel EM Structures and Materials, and Applications" (iWAT)*, Mar. 2014, pp. 351–354.

[44] M. Barbuto, A. Monti, F. Bilotti, and A. Toscano, "Design of a Non-Foster Actively Loaded SRR and Application in Metamaterial-Inspired Components," *IEEE Transactions on Antennas and Propagation*, vol. 61, no. 3, pp. 1219–1227, Mar. 2013.

[45] O. O. Tade, P. Gardner, and P. S. Hall, "Antenna bandwidth broadening with a negative impedance converter," *International Journal of Microwave and Wireless Technologies*, vol. 5, no. Special Issue 03, pp. 249–260, Jun. 2013.

[46] C. D. Nallo, G. Bit-Babik, and A. Faraone, "Wideband antenna using non-foster loading elements," in *2007 IEEE Antennas and Propagation Society International Symposium*, Jun. 2007, pp. 4501–4504.

[47] M. C. Tang, H. Wang, T. Deng, and R. Ziolkowski, "Compact Planar Ultra-wideband Antennas with Continuously Tunable, Independent Band-Notched Filters," *IEEE Transactions on Antennas and Propagation*, vol. PP, no. 99, pp. 1–1, 2016.

[48] F. J. Herraiz-Martinez, P. S. Hall, Q. Liu, and D. Segovia-Vargas, "Left-Handed Wire Antennas Over Ground Plane With Wideband Tuning," *IEEE Transactions on Antennas and Propagation*, vol. 59, no. 5, pp. 1460–1471, May 2011.

[49] S. k. Oh, Y. s. Shin, and S. o. Park, "A novel PIFA type varactor tunable antenna with U-shaped slot," in *2006 7th International Symposium on Antennas, Propagation EM Theory*, Oct. 2006, pp. 1–3.

[50] M. Berg, M. Komulainen, V. Palukuru, H. Jantunen, and E. Salonen, "Frequency-tunable DVB-H antenna for mobile terminals," in

2007 IEEE Antennas and Propagation Society International Symposium, Jun. 2007, pp. 1072–1075.

[51] V. A. Nguyen, R. A. Bhatti, and S. O. Park, "A Simple PIFA-Based Tunable Internal Antenna for Personal Communication Handsets," *IEEE Antennas and Wireless Propagation Letters*, vol. 7, pp. 130–133, 2008.

[52] N. Behdad and K. Sarabandi, "Dual-band reconfigurable antenna with a very wide tunability range," *IEEE Transactions on Antennas and Propagation*, vol. 54, no. 2, pp. 409–416, Feb. 2006.

[53] I. Carrasquillo-Rivera, R. A. R. Solis, and J. G. Colom-Ustariz, "Tunable and dual-band rectangular slot-ring antenna," in *IEEE Antennas and Propagation Society Symposium, 2004.*, vol. 4, Jun. 2004, pp. 4308–4311 Vol.4.

[54] F. Costa, A. Monorchio, S. Talarico, and F. M. Valeri, "An Active High-Impedance Surface for Low-Profile Tunable and Steerable Antennas," *IEEE Antennas and Wireless Propagation Letters*, vol. 7, pp. 676–680, 2008.

[55] Y. Cai, Y. J. Guo, and A. R. Weily, "A Frequency-Reconfigurable Quasi-Yagi Dipole Antenna," *IEEE Antennas and Wireless Propagation Letters*, vol. 9, pp. 883–886, 2010.

[56] M. Fallahpour, M. T. Ghasr, and R. Zoughi, "Miniaturized Reconfigurable Multiband Antenna For Multiradio Wireless Communication," *IEEE Transactions on Antennas and Propagation*, vol. 62, no. 12, pp. 6049–6059, Dec. 2014.

[57] A. Petosa, "Frequency agile antennas for wireless communications - A survey," in *2010 14th International Symposium on Antenna Technology and Applied Electromagnetics the American Electromagnetics Conference*, Jul. 2010, pp. 1–4.

[58] J. T. Aberle and R. Loepsinger-Romak, *Antennas with Non-Foster Matching Networks*. Morgan & Claypool Publishers, 2007.

[59] M. E. Pedinoff, "The Negative-Conductance Slot Amplifier," *IRE Transactions on Microwave Theory and Techniques*, vol. 9, no. 6, pp. 557–566, Nov. 1961.

[60] D. S. Nagarkoti, Y. Hao, D. P. Steenson, L. Li, E. H. Linfield, and K. Z. Rajab, "Design of Broadband Non-Foster Circuits Based on Resonant Tunneling Diodes," *IEEE Antennas and Wireless Propagation Letters*, vol. 15, pp. 1398–1401, 2016.

[61] J. L. Merrill, "Theory of the negative impedance converter," *The Bell System Technical Journal*, vol. 30, no. 1, pp. 88–109, Jan. 1951.

[62] A. Larky, "Negative-Impedance Converters," *IRE Transactions on Circuit Theory*, vol. 4, no. 3, pp. 124–131, Sep. 1957.

[63] C.-K. Kuo and K. Su, "Some New Four-Terminal NIC Circuits," *IEEE Transactions on Circuit Theory*, vol. 16, no. 3, pp. 379–381, Aug. 1969.

[64] S. E. Sussman-Fort, "Gyrator-based biquad filters and negative impedance converters for microwaves," *International Journal of RF and Microwave Computer-Aided Engineering*, vol. 8, no. 2, pp. 86–101, Mar. 1998.

[65] A. K. Perry, "Broadband Antenna Systems Realized from Active Circuit Conjugate Impedance Matching," Naval Postgraduate School Monterrey CA, Tech. Rep., Sep. 1973.

[66] E. A. Gonzalez, L. Dorčák, I. Petráš, and J. Terpák, "On the mathematical properties of generalized fractional-order two-port networks using hybrid parameters," in *Proceedings of the 14th International Carpathian Control Conference (ICCC)*, May 2013, pp. 88–93.

[67] S. Kolev, B. Delacressonniere, and J. L. Gautier, "Novel Microwave Negative Capacitance. Application to a Wide-Range Tunable Capacitance," in *Microwave Conference, 2000. 30th European*, Oct. 2000, pp. 1–3.

[68] S. K. Mitra, "Alternate realizations of four-terminal and three-terminal negative-impedance inverters," *Proceedings of the IEEE*, vol. 56, no. 3, pp. 368–368, Mar. 1968.

[69] S. Hrabar, I. Krois, and A. Kiricenko, "Towards active dispersionless ENZ metamaterial for cloaking applications," *Metamaterials*, vol. 4, no. 2–3, pp. 89–97, Aug. 2010.

[70] J. Long, M. M. Jacob, and D. F. Sievenpiper, "Broadband Fast-Wave Propagation in a Non-Foster Circuit Loaded Waveguide," *IEEE Transactions on Microwave Theory and Techniques*, vol. 62, no. 4, pp. 789–798, Apr. 2014.

[71] J. Long and D. F. Sievenpiper, "Low-Profile and Low-Dispersion Artificial Impedance Surface in the UHF Band Based on Non-Foster Circuit Loading," *IEEE Transactions on Antennas and Propagation*, vol. 64, no. 7, pp. 3003–3010, Jul. 2016.

[72] S. Hrabar, I. Krois, I. Bonic, and A. Kiricenko, "Basic concepts of active dispersionless metamaterial based on non-foster elements," in *ICECom, 2010 Conference Proceedings*, Sep. 2010, pp. 1–4.

[73] H. Mirzaei and G. Eleftheriades, "Arbitrary-Angle Squint-Free Beamforming in Series-Fed Antenna Arrays Using Non-Foster Elements Synthesized by Negative-Group-Delay Networks," *IEEE Transactions on Antennas and Propagation*, vol. 63, no. 5, pp. 1997–2010, May 2015.

[74] T. P. Weldon, J. M. C. Covington, K. L. Smith, and R. S. Adams, "Performance of digital discrete-time implementations of non-Foster circuit elements," in *2015 IEEE International Symposium on Circuits and Systems (ISCAS)*, May 2015, pp. 2169–2172.

[75] A. D. Harris and G. A. Myers, *An Investigation of Broadband Miniature Antennas*. Defense Technical Information Center, 1968.

[76] G. Skahill, R. M. Rudish, and J. A. Pierro, "Apparatus and method for broadband matching of electrically small antennas," U.S. Patent US6 121 940 A, Sep., 2000.

[77] S. E. Sussman-Fort and R. Rudish, "Progress in use of non-Foster impedances to match electrically-small antennas and arrays," in *29th Antenna Application Symposium*, Allerton Park, IL, Sep. 2005.

[78] R. M. Rudish and S. E. Sussman-Fort, "Non-foster impedance matching improves S/N of wideband electrically-small VHF antennas and arrays," in *Antenna Applications Symposium*, M. H. Hamza, Ed. Anaheim: Acta Press Anaheim, Sep. 2005.

[79] S. E. Sussman-Fort, "Matching network design using non-Foster impedances," *International Journal of RF and Microwave Computer-Aided Engineering*, vol. 16, no. 2, pp. 135–142, Mar. 2006.

[80] S. E. Sussman-Fort and R. M. Rudish, "Non-Foster matching of a lossy electrically-small antenna over an extended frequency range," in *Antenna Applications Symposium*, Allerton Park, IL, Sep. 2007.

[81] S. E. Sussman-Fort and R. Rudish, "Non-Foster Impedance Matching for Transmit Applications," in *IEEE International Workshop on Antenna Technology Small Antennas and Novel Metamaterials, 2006.*, White Plains, NY, Mar. 2006, pp. 53–56.

[82] Y. Fan, K. Rajab, M. Muñoz, and Y. Hao, "Electrically small half-loop antenna design with non-foster matching networks," in *2012 6th European Conference on Antennas and Propagation (EUCAP)*, Mar. 2012, pp. 126–129.

[83] K.-S. Song and R. Rojas, "Non-Foster impedance matching of electrically small antennas," in *2010 IEEE Antennas and Propagation Society International Symposium (APSURSI)*, Jul. 2010, pp. 1–4.

[84] N. Zhu and R. W. Ziolkowski, "Broad-Bandwidth, Electrically Small Antenna Augmented With an Internal Non-Foster Element," *IEEE Antennas and Wireless Propagation Letters*, vol. 11, pp. 1116–1120, 2012.

[85] J. Volakis, C.-C. Chen, and K. Fujimoto, "Chapter 8," in *Small Antennas: Miniaturization Techniques & Applications.* McGraw Hill Professional, Dec. 2009, pp. 361–388.

[86] S. Koulouridis, "Non - foster circuitry design for antennas," in *Proceedings of the 5th European Conference on Antennas and Propagation (EUCAP)*, Apr. 2011, pp. 237–239.

[87] E. Ugarte-Muñoz, S. Hrabar, D. Segovia-Vargas, and A. Kiricenko, "Stability of Non-Foster Reactive Elements for Use in Active Metamaterials and Antennas," *IEEE Transactions on Antennas and Propagation*, vol. 60, no. 7, pp. 3490–3494, Jul. 2012.

[88] A. D. Yaghjian and S. R. Best, "Impedance, bandwidth, and Q of antennas," *IEEE Transactions on Antennas and Propagation*, vol. 53, no. 4, pp. 1298–1324, Apr. 2005.

[89] W. L. Langston and D. R. Jackson, "Impedance, axial-ratio, and receive-power bandwidths of microstrip antennas," in *IEEE Antennas and Propagation Society International Symposium, 2002*, vol. 2, 2002, pp. 882–885 vol.2.

[90] F. J. Herraiz-Martinez, V. Gonzalez-Posadas, L. E. Garcia-Muñoz, and D. Segovia-Vargas, "Multifrequency and Dual-Mode Patch Antennas Partially Filled With Left-Handed Structures," *IEEE Transactions on Antennas and Propagation*, vol. 56, no. 8, pp. 2527–2539, Aug. 2008.

[91] M. M. Jacob, J. Long, and D. F. Sievenpiper, "Broadband non-Foster matching of an electrically small loop antenna," in *Proceedings of the 2012 IEEE International Symposium on Antennas and Propagation*, Jul. 2012, pp. 1–2.

[92] A. Sedra and K. Smith, *Microelectronic Circuits*. Oxford University Press, Incorporated, Sep. 1998.

[93] O. O. Tade, "Negative impedance converter for antenna matching," Thesis, University of Birmingham, Jul. 2014.

[94] S. D. Stearns, "Stable band-pass non-Foster circuits," in *2015 IEEE International Symposium on Antennas and Propagation USNC/URSI National Radio Science Meeting*, Jul. 2015, pp. 1386–1387.

[95] A. Suárez and R. Quéré, *Stability Analysis of Nonlinear Microwave Circuits*. Artech House, 2003.

[96] J. Brownlie, "On the Stability Properties of a Negative Impedance Converter," *IEEE Transactions on Circuit Theory*, vol. 13, no. 1, pp. 98–99, Mar. 1966.

[97] R. F. Hoskins, "Stability of negative-impedance convertors," *Electronics Letters*, vol. 2, no. 9, pp. 341–341, Sep. 1966.

[98] J. D. Brownlie, "Small-signal responses realizable from d.c.-biased devices," *Proceedings of the Institution of Electrical Engineers*, vol. 110, no. 5, pp. 823–829, May 1963.

[99] A. P. Stern, "Stability and Power Gain of Tuned Transistor Amplifiers," *Proceedings of the IRE*, vol. 45, no. 3, pp. 335–343, Mar. 1957.

[100] R. D. Middlebrook, "Measurement of loop gain in feedback systems†," *International Journal of Electronics Theoretical and Experimental*, vol. 38, no. 4, pp. 485–512, 1975.

[101] H. Nyquist, "Regeneration theory," *The Bell System Technical Journal*, vol. 11, no. 1, pp. 126–147, 1932.

[102] S. D. Stearns, "Circuit stability theory for non-Foster circuits," in *Microwave Symposium Digest (IMS), 2013 IEEE MTT-S International*. IEEE, 2013, pp. 1–3.

[103] J. Rollett, "Stability and Power-Gain Invariants of Linear Twoports," *IRE Transactions on Circuit Theory*, vol. 9, no. 1, pp. 29–32, Mar. 1962.

[104] M. L. Edwards and J. H. Sinsky, "A new criterion for linear 2-port stability using a single geometrically derived parameter," *IEEE Transactions on Microwave Theory and Techniques*, vol. 40, no. 12, pp. 2303–2311, 1992.

[105] R. W. Jackson, "Rollett proviso in the stability of linear microwave circuits-a tutorial," *IEEE Transactions on Microwave Theory and Techniques*, vol. 54, no. 3, pp. 993–1000, Mar. 2006.

[106] E. Ugarte-Muñoz, D. Segovia-Vargas, V. Gonzalez-Posadas, and J. Jimenez-Martin, "Non-Foster matching of Electrically Small Antennas. Stability considerations," in *2012 IEEE Antennas and Propagation Society International Symposium (APSURSI)*, Jul. 2012, pp. 1–2.

[107] A. Platzker, W. Struble, and K. T. Hetzler, "Instabilities diagnosis and the role of K in microwave circuits," in *1993 IEEE MTT-S International Microwave Symposium Digest*, Jun. 1993, pp. 1185–1188 vol.3.

[108] W. Struble and A. Platzker, "A rigorous yet simple method for determining stability of linear N-port networks [and MMIC application]," in *15th Annual GaAs IC Symposium*, Oct. 1993, pp. 251–254.

[109] A. Platzker and W. Struble, "Rigorous determination of the stability of linear n-node circuits from network determinants and the appropriate role of the stability factor K of their reduced two-ports," in *Third International Workshop on Integrated Nonlinear Microwave and Millimeterwave Circuits*, Oct. 1994, pp. 93–107.

[110] D. Maclean, "Improved methods of assessing feedback in wide-band multiloop amplifiers," *IEEE Transactions on Circuits and Systems*, vol. 27, no. 9, pp. 779–792, Sep. 1980.

[111] R. F. Hoskins, "Definition of loop gain and return difference in transistor feedback amplifiers," *Proceedings of the Institution of Electrical Engineers*, vol. 112, no. 11, pp. 1995–2001, Nov. 1965.

[112] A. R. Figueiras, *Una panorámica de las telecomunicaciones*. Pearson Educación, 2002.

[113] S. A. Maas, *Noise in Linear and Nonlinear Circuits*. Artech House, 2005.

[114] D. Segovia-Vargas, D. Castro-Galan, L. E. Garcia-Munoz, and V. Gonzalez-Posadas, "Broadband Active Receiving Patch With Resistive Equalization," *IEEE Transactions on Microwave Theory and Techniques*, vol. 56, no. 1, pp. 56–64, Jan. 2008.

[115] J. J. Lee, "G/T and noise figure of active array antennas," *IEEE Transactions on Antennas and Propagation*, vol. 41, no. 2, pp. 241–244, Feb. 1993.

[116] U. R. Kraft, "Gain and G/T of multielement receive antennas with active beamforming networks," *IEEE Transactions on Antennas and Propagation*, vol. 48, no. 12, pp. 1818–1829, 2000.

[117] M. M. Jacob and D. F. Sievenpiper, "Gain and Noise Analysis of Non-Foster Matched Antennas," *IEEE Transactions on Antennas and Propagation*, vol. 64, no. 12, pp. 4993–5004, 2016.

[118] C. Stedler, V. Wienstroer, and R. Kronberger, "Noise investigation of an active non-foster matching network for small antennas," in *2014 International Symposium on Antennas and Propagation (ISAP)*, 2014, pp. 237–238.

[119] NXP_Semiconductors, "BF998 Datasheet," http://www.nxp.com/documents/data_sheet/BF998.pdf, Apr. 2017.

[120] A. J. Simmons and D. G. Bodnar, "Gain of active Antenna Systems: Antenna Standards committee requests input," *IEEE Antennas and Propagation Society Newsletter*, vol. 31, no. 5, pp. 62–62, Oct. 1989.

[121] S. D. Ahirwar, C. Sairam, and A. Kumar, "Broadband blade monopole antenna covering 100-2000 MHz frequency band," in *2009 Applied Electromagnetics Conference (AEMC)*, Dec. 2009, pp. 1–4.

[122] n. Cardama Aznar, L. J. Roca, and S. B. Boris, *Antenas*. Univ. Politèc. de Catalunya, 2002.

[123] A. W. Rudge, *The Handbook of Antenna Design*. Peregrinus ; Institution of electrical engineers, 1986.

[124] R. C. Hansen, *Phased Array Antennas*. John Wiley & Sons, Nov. 2009.

[125] C. White, "A non-foster monopole array," in *2012 IEEE Antennas and Propagation Society International Symposium (APSURSI)*, Jul. 2012, pp. 1–2.

[126] R. Hansen, "Dipole arrays with non-foster circuits," in *IEEE International Symposium on Phased Array Systems and Technology, 2003*, Oct. 2003, pp. 40–44.

[127] R. C. Hansen, "Non-Foster and connected planar arrays," *Radio Science*, vol. 39, no. 4, pp. 1–14, Aug. 2004.

[128] M. Jacob, J. Long, and D. Sievenpiper, "Non-Foster Loaded Parasitic Array for Broadband Steerable Patterns," *IEEE Transactions on Antennas and Propagation*, vol. 62, no. 12, pp. 6081–6090, 2014.

[129] A. M. Elfrgani and R. G. Rojas, "Biomimetic Antenna Array Using Non-Foster Network to Enhance Directional Sensitivity Over Broad Frequency Band," *IEEE Transactions on Antennas and Propagation*, vol. 64, no. 10, pp. 4297–4305, Oct. 2016.

[130] D. S. Nagarkoti, Y. Hao, and K. Z. Rajab, "Q-bandwidth enhancement of an antenna using non-Foster circuit based on negative differential resistance devices," in *2016 10th European Conference on Antennas and Propagation (EuCAP)*, Apr. 2016, pp. 1–2.

[131] D. S. Nagarkoti, "Characterisation and design of novel non-Foster circuits for electrically small antennas," Thesis, Queen Mary University, Nov. 2016.

[132] M. Stoisiek and D. Wolf, "Origin of 1/f noise in bipolar transistors," *IEEE Transactions on Electron Devices*, vol. 27, no. 9, pp. 1753–1757, Sep. 1980.

[133] A. V. D. Ziel, "Theory of Shot Noise in Junction Diodes and Junction Transistors," *Proceedings of the IRE*, vol. 43, no. 11, pp. 1639–1646, Nov. 1955.

[134] E. R. Chenette and A. v. d. Ziel, "Accurate noise measurements on transistors," *IRE Transactions on Electron Devices*, vol. 9, no. 2, pp. 123–128, Mar. 1962.

[135] A. V. D. Ziel, "Noise in Junction Transistors," *Proceedings of the IRE*, vol. 46, no. 6, pp. 1019–1038, Jun. 1958.

[136] R. Leffel, "The Y Factor Technique for Noise Figure Measurements Application Note," Rhode&Schwarz, Tech. Rep., Jan. 2015.

[137] J. M. Collantes, R. D. Pollard, and M. Sayed, "Effects of DUT mismatch on the noise figure characterization: a comparative analysis of two Y-factor techniques," *IEEE Transactions on Instrumentation and Measurement*, vol. 51, no. 6, pp. 1150–1156, Dec. 2002.

[138] D. Nagarkoti, Y. Hao, and K. Rajab, "Noise measurements of a non-Foster circuit for matching of a receiver antenna," in *2015 9th European Conference on Antennas and Propagation (EuCAP)*, Apr. 2015, pp. 1–3.

About the Author

Fernando Albarracín-Vargas was born in Bogotá, Colombia, on September 11, 1985. He received the Engineering degree in Electronics from the National University of Colombia, in 2008, and the Masters' degree in Multimedia and Communications from the Charles III University of Madrid, Spain, in 2014.

He is currently working with the Group of Radiofrequency, Electromagnetism, Microwaves, and Antennas (GREMA), at the Charles III University of Madrid. His present research interests include metamaterials based structures, non-Foster elements, ultra-wideband antennas, active-matching and miniaturization of antennas. For the author, it has always been a pleasure working as a researcher. His first steps took place in Bogotá (Colombia), in the Open-Area Test Site (OATS) seminar, associated to the National University of Colombia in 2007. From 2010 to 2011, he was a Research Assistant, for the development of equipment for soil moisture and concentration measurement, at the International Center for Physics (CIF), in Bogotá, Colombia. Then, through his affiliation with the Charles III University of Madrid, with the GREMA research group in 2012, he started working with actively matched ESAs, as part of his Masters' course, and afterward, his Ph.D.